COMMUNAUTÉ FRANÇAISE DE BELGIQUE

UNIVERSITÉ DE LIÈGE – GEMBLOUX AGRO-BIO TECH

Soil-plant silicon dynamics in natural ecosystems and agroecosystems

Félix de Tombeur

Dissertation originale présentée en vue de l'obtention du grade de docteur en sciences agronomiques et ingénierie biologique

Promoteurs : Jean-Thomas Cornélis, Grégory Mahy

2021

Deep in the human unconscious is a pervasive need for a logical universe that makes sense. But the real universe is always one step beyond logic.

From « The Sayings of Muad'Dib » by the Princess Irulan

Frank Herbert, Dune, 1965

Abstract

Silicon (Si) is widely recognized as an important regulator of the global carbon (C) cycle via its effect on diatom productivity in oceans, and as a beneficial plant nutrient, improving resistance to herbivory and pathogens and mitigating the negative effects of several abiotic stresses. This thesis explores the long-term dynamics of Si in terrestrial ecosystems, and investigates some factors driving soil-plant Si dynamics in agroecosystems. The main study sites are three 2-million-years dune chronosequences located on a climatic gradient in southwestern Australia. Within a chronosequence, plant productivity is limited by nitrogen (N), then by phosphorus (P), as soils age.

We show that soil Si dynamics is primarily driven by geochemical processes in young and middle-aged soils (carbonates dissolution, clay formation, quartz enrichment), but increasingly by biological processes (silica formation in plants followed by its dissolution in soils) in old and highly-weathered soils. A climate-driven increase in biomass production along the climatic gradient seems to enhance this biological Si feedback loop. Besides, the continuous increase in community-level leaf Si concentrations with increasing soil age and P depletion might reflect the importance of silica-based defenses in P-poor environments. This increase is associated with a decrease in leaf total phenol concentrations, suggesting a tradeoff between both defense strategies along N-P gradients. We also propose that the increase in nutrient-acquisition carboxylate-releasing strategies with increasing soil age might explain the increase in leaf Si concentrations, with carboxylates not only mobilizing rhizosphere P, but also Si. Based on the above results and a literature review, we then summarized the biotic and abiotic controls on soil Si dynamics, and wondered whether they could be exploited in agroecosystems. We particularly stress the importance of mycorrhizal associations, silicate-solubilizing bacteria, soil macrofauna, root exudates and large herbivores on soil-plant Si dynamics. These ecological processes might in turn be exploited in cereal-legume intercropping, cover crops implementation, or integrated crop-livestock systems. We finally demonstrate that soil properties and recycling crop residues strongly influence the foliar silicification and its beneficial effects for two crop species (rice and sugarcane) through two case studies in Burkina Faso and Guadeloupe, respectively.

This thesis highlights the major influence of soil age and weathering degree on soil-plant Si dynamics, from both a biogeochemical and ecological perspective, and demonstrate that knowledge from complex natural systems might help to improve the Si-use efficiency and subsequent sustainability of modern agroecosystems. Besides, this thesis stresses the need to develop multidisciplinary approaches to better understand elements mobility in natural ecosystems and agroecosystems.

Résumé

Le silicium (Si) est largement reconnu comme un régulateur majeur du cycle global du carbone (C) via son effet sur la productivité des diatomées dans les océans, et comme un nutriment bénéfique pour les plantes, qui augmente la résistance contre les herbivores et les pathogènes et réduit les effets négatifs de nombreux stress abiotiques. Cette thèse explore la dynamique à long terme du Si en écosystèmes terrestres, et étudie certains facteurs contrôlant la dynamique sol-plante du Si dans les agroécosystèmes. Les principaux sites d'étude sont trois chronoséquences de 2 millions d'années situées le long d'un gradient climatique en Australie. La croissance des plantes est limitée par l'azote (N), puis par le phosphore (P), avec l'âge croissant du sol dans une séquence.

La dynamique du Si est contrôlée principalement par des processus géochimiques dans les sols jeunes et d'âges moyens (dissolution des carbonates, formation d'argiles, enrichissement en quartz), mais de manière croissante par des processus biologiques (formation de silice biogénique dans les plantes, suivie de sa dissolution dans les sols) avec le vieillissement des sols. L'augmentation de production de biomasse végétale le long du gradient climatique semble renforcer cette boucle de rétroaction biologique sur la dynamique du Si. Par ailleurs, l'augmentation continue des concentrations en Si foliaire dans les communautés végétales avec l'augmentation de l'âge du sol et la diminution du P pourrait refléter l'importance des défenses à base de silice dans les environnements pauvres en P. Cette augmentation est associée à une diminution des concentrations en phénols totaux dans les feuilles, suggérant un compromis entre ces deux stratégies de défenses le long de gradients N-P. L'augmentation des stratégies de libération de carboxylates par les racines pour acquérir les nutriments dans les sols anciens pourrait expliquer l'augmentation des concentrations de Si dans les feuilles, les carboxylates mobilisant non seulement le P de la rhizosphère, mais aussi le Si. Les facteurs biotiques et abiotiques contrôlant la dynamique du Si sont ensuite synthétisés. L'importance des associations mycorhiziennes, des bactéries solubilisatrices de silicates, de la macrofaune du sol, des exsudats racinaires et des grands herbivores sur la dynamique sol-plante du Si est particulièrement soulignée. Ces processus écologiques pourraient être exploités dans les cultures intercalaires céréale/légume, les cultures de couverture, ou les systèmes culture/élevage. Enfin, nous démontrons la forte influence des propriétés du sol et du recyclage de résidus de cultures sur la silicification foliaire et ses effets bénéfiques pour deux cultures (riz et canne à sucre) via deux études de cas au Burkina Faso et en Guadeloupe, respectivement.

Cette thèse souligne l'influence majeure de l'âge et du degré d'altération du sol sur la dynamique sol-plante du Si, d'un point de vue à la fois biogéochimique et écologique, et démontre que les connaissances acquises de systèmes naturels complexes peuvent aider à améliorer la nutrition en Si des cultures et la durabilité des agroécosystèmes. Elle démontre aussi le besoin de développer des approches multidisciplinaires pour mieux comprendre la mobilité des éléments dans les écosystèmes naturels et les agroécosystèmes.

Graphical Abstract

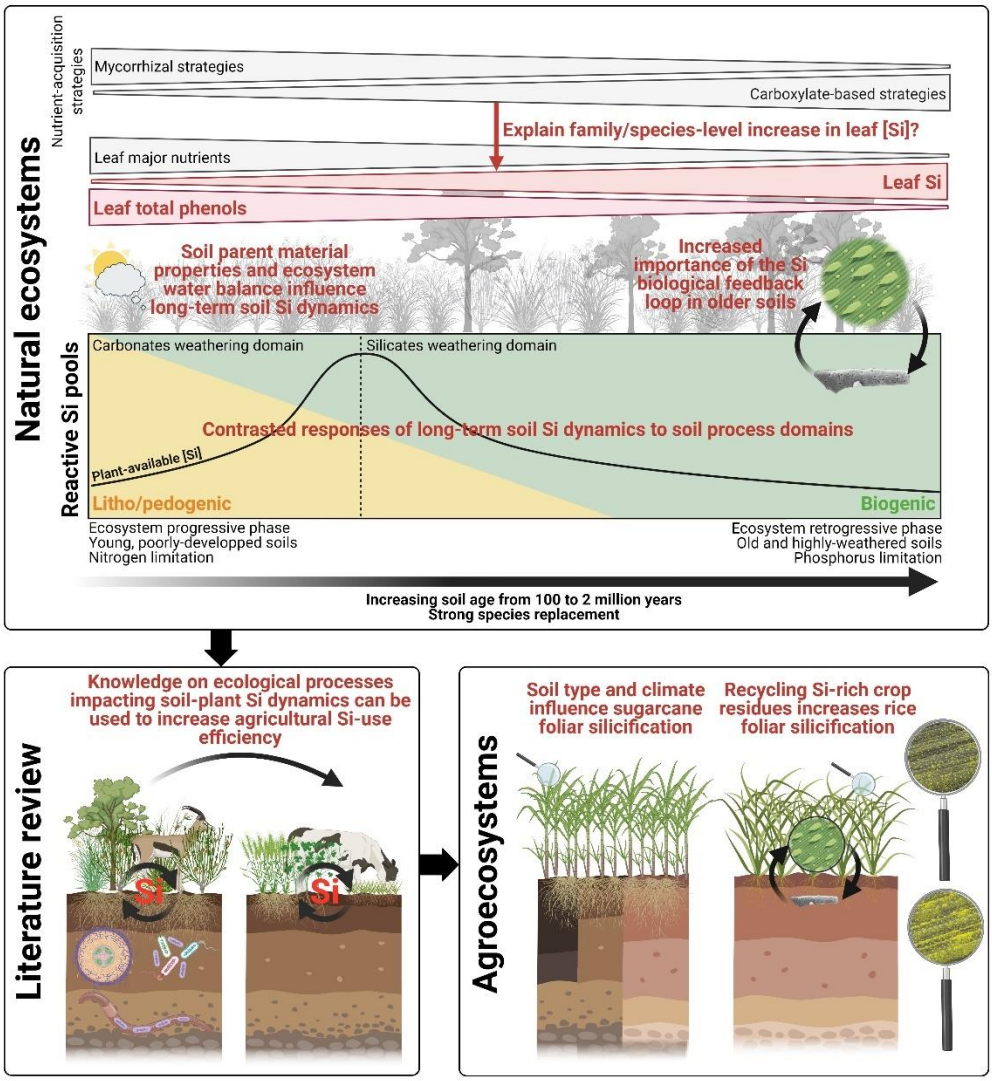

Remerciements

Car nous ne sommes finalement que bien peu sans les autres, je tiens à remercier du fond du cœur de nombreuses personnes avant de commencer ce document.

Mes premières pensées vont à *Jean-Thomas Cornélis*, sans qui ce travail de thèse n'aurait pas vu le jour. Je te dis merci mille fois, mon cher J-T, de m'avoir fait confiance pour assurer ce travail d'assistant de recherche à Gembloux, et pour m'avoir si bien encadré pendant ce travail de thèse. Tu as su me laisser une grande liberté de choix et d'actions, tout en répondant toujours présent à mes questionnements et inquiétudes. Ce fut également un immense bonheur de t'accompagner dans l'enseignement des sciences du sol et d'avoir essayé ensemble de passionner les étudiants pour cette magnifique discipline. Merci aussi pour ces longues discussions, qu'elles fussent légères ou profondes, au fond d'une fosse pédo ou dans un bar, qui ont su forger une belle amitié.

Je tiens aussi à remercier chaleureusement mon co-promoteur de thèse, *Grégory Mahy*. Si je ne suis toujours pas écologue, je peux au moins me targuer d'en être un en devenir, et tu y as évidemment contribué. Je te remercie donc pour ces discussions et conseils tout au long de ma thèse sur ces questions d'écologie végétale, qui me fascinent un peu plus chaque jour et vers lesquelles je désire maintenant me tourner.

J'adresse aussi mes sincères remerciements à mon jury de thèse, *Anne Alexandre*, *Marie-Pierre Turpault*, *Gilles Colinet*, *Cyrille Violle*, pour avoir pris le temps de lire mon travail, et au président du jury, *Jérôme Bindelle*. Vos commentaires et suggestions m'ont été précieux, et ont su me pousser plus loin dans la maturation de cette thèse et de mes futures recherches.

Même si l'image du chercheur geek seul devant son ordinateur ne doit pas être tout à fait erronée, la recherche scientifique reste avant tout une belle histoire d'interactions entre êtres vivants ! Je me dois donc ici d'exprimer ma gratitude envers les collaborateurs ayant contribué à ce document. Je commencerai par *Michel-Pierre Faucon*, que je remercie pour nos discussions sur les traits fonctionnels des plantes qui ont tout de suite suscité mon intérêt au balbutiement de ma thèse. Je remercie également *Benjamin L. Turner*, *Étienne Laliberté*, *Hans Lambers* et *Graham Zemunik* pour m'avoir donné accès à ces magnifiques chronoséquences du sud-ouest australien, et pour tous les apports et réflexions sur mes premières versions de manuscrits, ce travail n'aurait pas vu le jour sans eux. Je tiens à remercier tout particulièrement *Hans Lambers* pour tous ses conseils et suggestions, sa très grande disponibilité, et pour avoir accepté de continuer notre collaboration au-delà de ma thèse. Mes pensées vont aussi à l'équipe de l'Université Catholique de Louvain : *Bruno Delvaux* pour m'avoir accueilli en Guadeloupe et guidé dans mes questions scientifiques, *Charles Vander Linden* pour nos discussions sur nos sujets de thèse respectifs et cette superbe campagne d'échantillonnage sous les tropiques, et *Zimin Li* pour ces riches échanges scientifiques. Je remercie également *Philippe Compère* de l'ULiège pour m'avoir guidé dans l'utilisation de la microscopie à balayage, tant sur la pratique que

l'interprétation des images. Un grand merci également à *Bruno Godin*, avec qui j'ai beaucoup appris sur les composants structurels des feuilles de cannes à sucre ! Je pense aussi à mes collègues 'entomo' *François Verheggen* et *Nicolas Leroy* avec qui j'ai beaucoup appris sur les interactions plante-herbivore, à *Ryosuke Nakamura* pour ces supers échanges lors de son séjour en Belgique, à *David Lefebvre* pour ses connaissances sur le biochar, et à *Julia Cooke* pour ses réflexions éclairées sur la silicification foliaire. Je remercie aussi *Monique Carnol* et *Jean-Dominique Meunier*, membres de mon comité de thèse, qui m'ont apporté conseils et suggestions lors de la réalisation de ce travail. Je remercie enfin mes collègues burkinabés *Drissa Cissé*, *Saba Fatimata*, et *Hassan Bismarck Nacro* pour leur accueil chaleureux au Burkina Faso, et les riches échanges scientifiques que nous avons eus, ici ou là-bas !

Quelle magnifique démarche que de se poser des questions scientifiques et d'émettre des hypothèses… Mais encore faut-il être en moyen de les tester ! J'adresse mes plus sincères remerciements à toutes les personnes m'ayant aidé dans les analyses fastidieuses de mes échantillons de sols et de plantes, ils se reconnaitront. J'adresse une mention toute spéciale à *Émilie Marit* pour toutes ses analyses 'ICP' qui n'ont pas toujours été simples (c'est le moins qu'on puisse dire !), à *Jean-Charles Bergen* pour avoir passé des semaines (des mois ?) dans le labo pour ma thèse, et à *Françoise Toussaint* pour son aide précieuse (et recadrage !) au labo. Je ne saurais vous remercier suffisamment pour tout ça. Je pense aussi à *Raphaël Tarantino* qui a toujours su me simplifier différents aspects administratifs et techniques au labo, à *François Fontaine* pour les analyses de minéralogie, et à *Catherine Henrist* pour m'avoir formé au SEM-EDX à Liège. Pour finir, je suis grandement reconnaissant envers le Fonds de Recherche Scientifique (FRS-FNRS) d'avoir financé le projet de recherche SiCliNG que nous avons écrit avec *Jean-Thomas*, et qui a grandement contribué à cette thèse.

J'adresse également mes plus sincères remerciements à *Marie Davin* et *Amandine Liénard*, qui m'ont toutes deux énormément guidé lors de mon arrivée à Gembloux. Je peux difficilement estimer le nombre de questions que je leur ai adressées, et auxquelles elles ont toujours su répondre. Merci aussi pour la super ambiance qui régnait dans notre petit bureau malgré une certaine promiscuité physique, c'est le moins qu'on puisse dire !

Malgré ma présence "aléatoire" au labo, je tiens à adresser un immense merci à toute l'équipe du GP, présente ou passée, où règne toujours une super ambiance. Je pense ici à *Gilles* & *Gilles*, *Marie* & *Marie*, *Amandine*, *Mathilde*, *Jonas*, *Sébastien*, *Brieuc*, *Daphné*, *Émilie*, *Kevin*, *Clémence*, *Catherine*, *Pauline*, *Christophe*, *Sibylle*, *Florent*, *Aurore*, *Jean-Charles*, *Béatrice*, *Raphaël*, *Françoise*, *Oriane*… Et une spéciale dédicace à mon doctorant et mes deux postdocs préférés, *Victor*, *Julien* et *Philippe* ! Merci à vous trois pour tous ces beaux moments de vie et échanges passionnés, tant au labo que dans des bars plus ou moins louches de Namur ou de Bruxelles.

Je ne pourrais commencer ce document sans une pensée pour *Jérôme Poulenard*, qui m'a transmis sa passion. Il a su me faire découvrir le monde fascinant des sciences environnementales, et en particulier celui des sciences du sol, à une période de ma vie

un peu plus… confuse ! Je n'aurais pas continué dans cette direction sans sa passion (pas très éloigné de la folie, en réalité) pour les sols, les plantes et la montagne. Alors merci à toi, cher Jérôme. Je pense aussi ici à *Sophie Cornu*, avec qui mon travail de fin d'études m'a conforté dans mon intérêt pour le monde aventureux et passionnant de la recherche.

J'aimerais également lever ma tasse de café aux amis, qu'ils le soient depuis 25 ans ou depuis plus récemment. C'est bien avec cette seconde famille qu'on partage sa vie et que l'on se définit sans cesse, et je ne saurais leur être assez reconnaissant pour tout ce qu'ils m'ont apporté, m'apportent, et m'apporteront. Merci les copains !

On met toujours un peu de temps à comprendre la mission colossale que doit être celle d'être parent. Je veux ici remercier les miens du fond du cœur pour m'avoir toujours laissé une grande liberté dans mes choix de vie, et pour tout ce qu'ils ont pu m'apporter, de manière consciente ou non. Je pense aussi à mes deux *brodos* et à toutes ces années de folie, d'accrochage, d'amour, de conneries… Merci à vous deux.

Maëva, partager ma vie avec toi est un bonheur quotidien, et je te remercie de m'accompagner dans cette aventure et de savoir supporter mon panel d'émotions… Merci d'être là.

Table of Contents

List of Figures

List of Tables

1

Introduction

1.1 Thesis context

In 1935, Arthur Tansley suggested a definition of the ecosystem that already pointed out the complex interplay between biotic and abiotic factors (Arthur Tansley 1935, quoted from Richter & Billings 2015):

"the whole system (in the sense of physics), including not only the organism-complex, but also the whole complex of physical factors forming what we call the environment of the biome – the habitat factors in the widest sense. Though the organisms may claim our primary interest, when we are trying to think fundamentally we cannot separate them from their special environment, with which they form one physical system."

More than 80 years later, terrestrial ecosystems are more than ever recognized as complex systems where numerous biological and geochemical processes interplay, despite daily new findings that improve the understanding we have of them. This complexity pushes scientists towards interdisciplinary approach, as represented for instance by the 'critical zonists' who jointly study hydrology, geomorphology, geology, geochemistry, geophysics, pedology, and ecology in the Earth's Critical Zone (National Research Council 2001). At the very heart of terrestrial ecosystems, the soil constitutes a fascinating subject of interest because of its complexity and heterogeneity, where life meets mineral matter.

Soils play a pivotal role for numerous ecosystem processes and services (Jónsson & Davídsdóttir 2016), including nutrient cycling. They indeed continually provide nutrients to plants via mineral weathering and organic matter degradation after plant senescence (Vitousek 2004). Such soil-plant elemental cycling may in turn impact global biogeochemical cycles and their subsequent impact on Earth's climate (Berner *et al.* 1983; Gaillardet *et al.* 1999; Cornelis *et al.* 2010), as well as plant nutrition and growth (Vitousek & Howarth 1991; Vitousek *et al.* 2010). Now, and more than ever, better constrain how elements are cycled in soil-plant systems is fundamental to preserve Earth's climate and sustain global food production. Such considerations are particularly relevant today, when mankind shaped its own geological era: the Anthropocene (Crutzen 2002; Zalasiewicz *et al.* 2011).

Understanding terrestrial biogeochemical cycles and the factors that control them is also a prerequisite to develop sustainable agroecosystems (Mariotte *et al.* 2018). The world's population is rapidly growing (Tripathi *et al.* 2018), and we need to conceive agroecosystems with minimal impact on biogeochemical cycles (Altieri 2002). In this regard, knowledge about ecological processes influencing soil-plant elemental cycling in complex natural systems can be used to ameliorate the resource-use efficiency and productivity of agroecosystems (Faucon *et al.* 2017; Mariotte *et al.* 2018). Leverage such ecological processes for sustainable food production is timely since the current agriculture model has numerous negative impacts on the environment and human health (Horrigan *et al.* 2002; Stoate *et al.* 2009), and strongly interferes with global biogeochemical cycles (Quinton *et al.* 2010; Yuan *et al.* 2018).

One element on the periodic table that plays pivotal roles in both global biogeochemical cycles and agriculture is silicon (Si). The main theme of this thesis is to explore the long-term dynamics of Si in terrestrial ecosystems, and investigates some factors driving soil-plant Si dynamics in agroecosystems.

1.2 Thesis background

1.2.1 Global silicon cycle

Silicon is the second most abundant element of the Earth's crust (28.8 wt%) after oxygen (47.2 wt%), and before aluminum (8.0 wt%) (Wedepohl 1995). It occurs in a wide range of primary and secondary silicate minerals, which makes it ubiquitous in almost all rocks and soil-plant systems. On continents, the physical, chemical and biological weathering of rocks release dissolved Si, as monosilicic acid (H_4SiO_4). The chemical weathering of silicates is a key regulator of Earth's climate, because it consumes atmospheric carbon dioxide (CO_2) on geological time scales (Berner *et al.* 1983; Gaillardet *et al.* 1999). The equation below shows that atmospheric CO_2 is consumed and dissolved Si is released when a primary silicate mineral (orthoclase here) is converted to a secondary mineral (kaolinite here) through weathering:

$$2KAlSi_3O_8 + 2CO_2 + 11H_2O \leftrightarrow Al_2Si_2O_5(OH)_4 + 2K^+ + 2HCO_3^- + 4H_4SiO_4$$

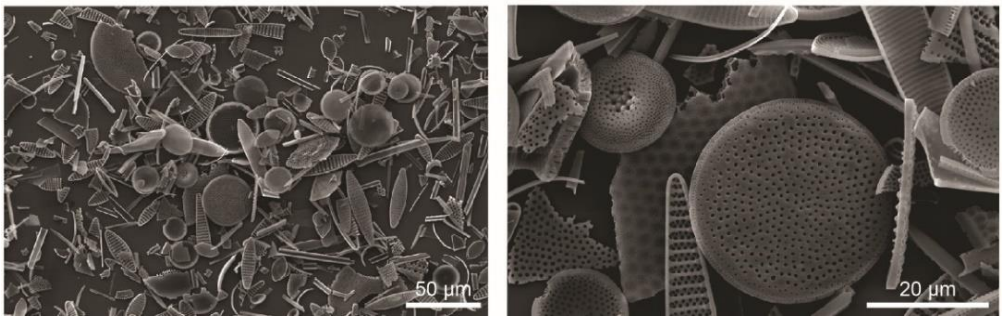

Figure 1-1: Scanning Electron Microscopic (SEM) images of diatoms, from Panizzo *et al.* (2014)

Silicon can be leached out from terrestrial ecosystems and transferred towards rivers and oceans (Struyf *et al.* 2010b; Conley & Carey 2015). Each year, about 9.4 ± 4.7 Tmol of Si reach the oceans, including 80% from terrestrial ecosystems as dissolved Si (6.2 ± 1.8 Tmol) and particulate Si (1.1 ± 0.2 Tmol) (Tréguer & De La Rocha 2013). In oceans, Si serves as an essential nutrient for microscopic phytoplankton, known as diatoms, who use it to build their cell frustules (Figure 1-1). The transfer of Si from land to oceans has a direct impact on the global C cycle since diatoms contribute to roughly half of oceanic carbon fixation, and about one fifth of Earth's photosynthesis

(Nelson *et al.* 1995; Nelson & Dortch 1996; Harrison 2000; Tréguer & Pondaven 2000; Armbrust 2009). Understanding the drivers of Si mobility from terrestrial to aquatic ecosystems is therefore pivotal for the oceanic carbon fixation and the global carbon cycle (Figure 1-2). In this regard, a thorough comprehension of Si dynamics in soil-plant systems where biotic and abiotic mineral weathering occur is required.

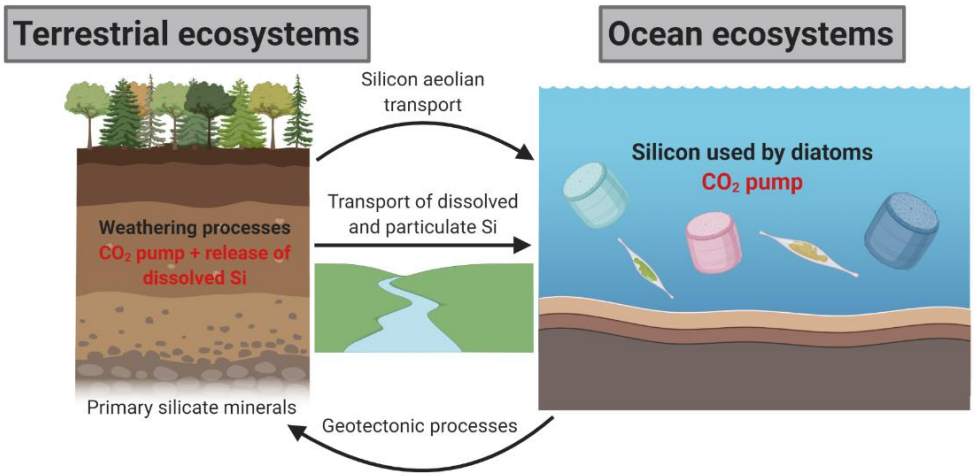

Figure 1-2: Simplified representation of the global silicon cycle.

1.2.2 Soil-plant silicon cycle

In soils, the first process mobilizing Si is the dissolution of primary silicate minerals. Chemical weathering involves the reaction of minerals with water/aqueous solution (as seen in the equation above), and each mineral has a solubility in water that strongly depends on temperature and pH (Palandri & Kharaka 2004; Wilson 2004; Churchman & Lowe 2012). More than 80 years ago, Goldich (1938) suggested a stability series for the major primary minerals (Figure 1-3), based on the rationale that the higher temperature at which a mineral crystallized from magma, the greater the extent to which it was out of equilibrium with the surface temperature of Earth, and therefore the more susceptible to dissolution it would be at the Earth's surface (Wilson 2004; Churchman & Lowe 2012). In this series, olivine is most easily weathered while the opposite is true for quartz (Figure 1-3), and more recent calculations of mineral dissolution rates generally confirm this series (Churchman & Lowe 2012). For instance, while quartz shows dissolution rates *log k* around -14/-13 mol m^{-2} s^{-1} at 25 °C, olivine shows higher values, around -8/-5 mol m^{-2} s^{-1} (Palandri & Kharaka 2004). According to Churchman & Lowe (2012), these important differences in the dissolution rates of silicate minerals depends on the strengths of the silica tetrahedra, which depends on (1) the nature of the links between tetrahedra, (2) the degree of

isomorphous substitution (substitution of 4-valency Si within tetrahedra by 3-valency Al and hence gain of negative charge, and (3) the extent of incorporation of charge-balancing cations, and their location in the structure.

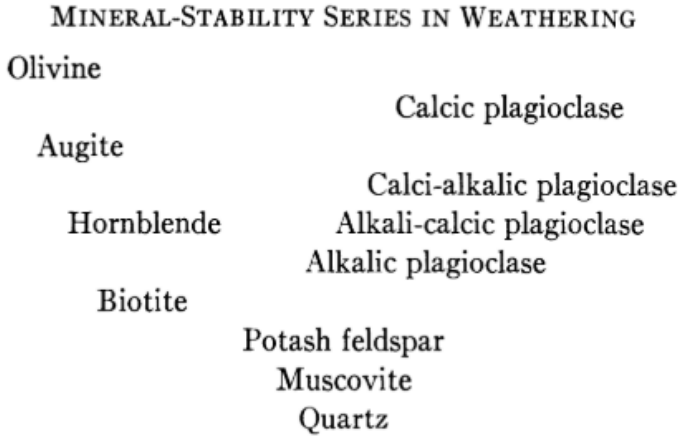

Figure 1-3: Stability series for the common primary minerals, from Goldich (1938).

Chemical weathering releases solutes in soil solution, which can recombine to synthesize pedogenic clay-sized minerals, which can in turn dissolve and contribute to dissolved Si (Figure 1-4). Both primary and secondary Si-bearing minerals can be physically transferred to the hydrosphere, by lessivage (Figure 1-4). Once in soil solution, Si can be adsorbed on reactive soil particles such as Fe and Al oxides, especially at alkaline pH (e.g., Hingston *et al.* 1972; Obihara & Russell 1972; Haynes & Zhou 2018) (Figure 1-4). Dissolved Si can also be transferred to the hydrosphere and be used by diatoms, but also be absorbed by terrestrial plants (Figure 1-4). Monosilicic acid is translocated to sites of rapid transpiration (Ma *et al.* 2006, 2007; Deshmukh *et al.* 2020), where it polymerizes as amorphous hydrated silica ($SiO_2.nH_2O$) between cell walls and the lumen, and in extracellular and intercellular spaces of plant epidermis (Kumar *et al.* 2017b). These mineral deposits within the plant organic matrix are called phytoliths, from Greek ‘Φύτον’ (plant) and ‘λίθος’ (stone), and they help plants to better resist to numerous biotic and abiotic stresses (Cooke & Leishman 2016; Debona *et al.* 2017; Coskun *et al.* 2019). Once returned to topsoil after plant shedding, phytoliths may dissolve and contribute to the dissolved Si pool, or be transferred to the hydrosphere by lessivage (Figure 1-4). Apart from plants, other living organisms use dissolved Si to synthesize amorphous silica, yielding to a zoogenic Si pool in soils (Sommer *et al.* 2013; Puppe 2020) (Figure 1-4).

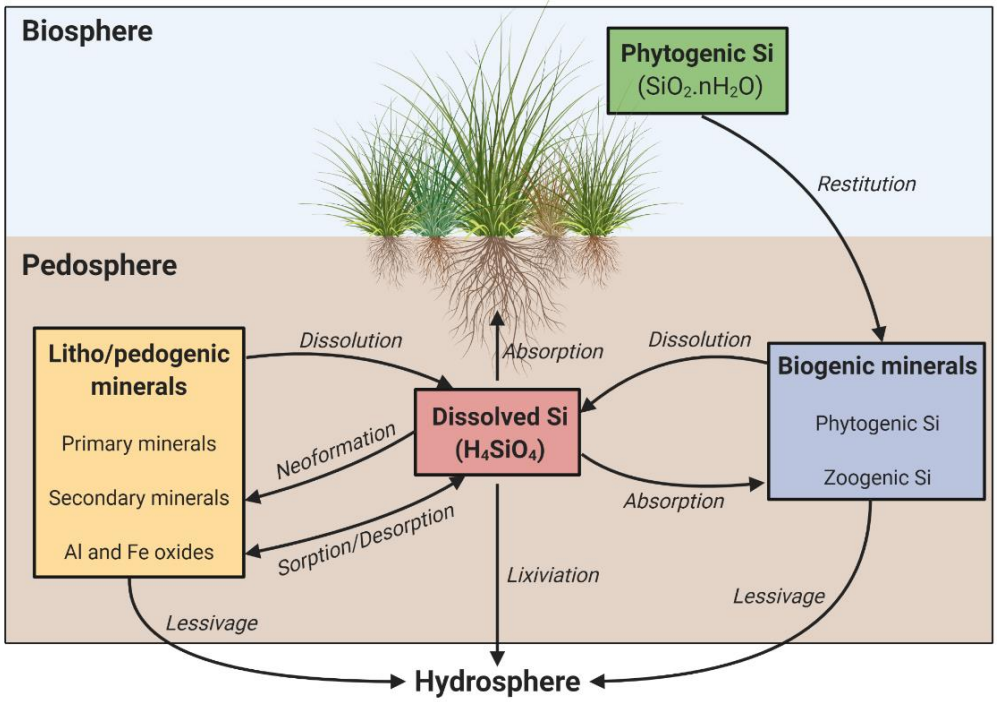

Figure 1-4: Schematic representation of the soil-plant silicon cycle, adapted from Cornelis & Delvaux (2016).

For years, scientists have attempted to better understand how soil processes controlled the dissolved Si pool given its importance for the global carbon cycle and plant stress alleviation. It is commonly admitted that dissolved Si primarily depends on soil parent material and weathering degree, and on their subsequent controls on soil texture and mineralogy (Savant *et al.* 1999; Cornelis & Delvaux 2016). If annual rainfall exceeds evapotranspiration, dissolved Si concentrations in soils decrease with increasing weathering degree and desilication (i.e. Si loss to hydrosphere by leaching or lessivage) (Chadwick & Chorover 2001; Sommer *et al.* 2006; Meunier *et al.* 2018). Therefore, dissolved Si concentrations decrease with the loss of primary Si-bearing minerals at early stages of pedogenesis, then with the loss of secondary 2:1, then 1:1, clay minerals at intermediate and advanced stages of soil weathering, respectively (Cornelis & Delvaux 2016). Moreover, the enrichment of minerals with low specific surface such as quartz during pedogenesis (Turner & Laliberté 2015) contribute to reducing dissolved Si concentrations in highly-weathered environments since particle-size also controls dissolved Si concentrations in soils (Drees *et al*. 1989).

Although this general pattern is well-established for the silicates weathering domain, the fate of dissolved Si in carbonate-rich soils having alkaline pH is still unclear. Alkaline pH could lead to increase dissolution rates of soil phytoliths (Fraysse *et al.* 2006b, 2009) and aluminosilicates (Drever 1994; Kelly *et al.* 1998), thus

increasing dissolved Si concentrations, but also to increase Si adsorption on soil colloids, thus decreasing dissolved Si concentrations (Jones & Handreck 1963; Beckwith & Reeve 1964; Hingston *et al.* 1972; Haynes & Zhou 2018). Studying soil Si pools during long-term soil formation from a carbonate-rich parent material could help to better understand these processes.

Dissolved Si concentration is not only controlled by geochemical processes (i.e., dissolution of rock and soil-derived minerals), but also by biological processes. In particular, the yearly return of phytoliths to topsoil after plant shedding build a pool of highly-reactive silicates that can also contribute to dissolved Si. In a pioneering work, Bartoli (1983) modeled the soil-plant Si cycle of two temperate forest ecosystems and showed that 85% of soil soluble Si was derived from phytolith dissolution. Later, Lucas *et al*. (1993) showed that Si biocycling in humid tropics had a direct influence on soil mineralogy by maintaining kaolinite stability on soil upper horizons. Since then, numerous mass-balance calculations of biogeochemical studies have also reported that a significant fraction of Si in soil solution derived from the dissolution of the phytogenic Si pool (Alexandre *et al.* 1997, 2011; Gérard *et al.* 2008; Sommer *et al.* 2013), because of its high solubility compared to crystalline Si-bearing minerals (Fraysse *et al.* 2006b, 2009; Sommer *et al.* 2013). As a consequence, the impact of human activities on biosphere has a direct influence on the soil-plant and global Si cycle (Struyf *et al.* 2010a; Clymans *et al.* 2011; Vandevenne *et al.* 2015; Carey & Fulweiler 2016).

The demonstration of vegetation impact on Si cycle challenged the common view that soluble Si concentrations were mainly driven by soil parent material, weathering degree, and subsequent soil mineralogy/texture. To reconcile both views, Cornelis & Delvaux (2016) proposed that, with increasing depletion of lithogenic and pedogenic silicates during prolonged desilication, the biological Si feedback loop progressively takes over the Si plant uptake from weatherable soil-derived minerals. From this theory, the silicon biological feedback loop would largely depend on soil weathering degree, with increased intensity in highly desilicated environments. Studying how long-term soil formation influence the control of both geochemical and biological processes on dissolved Si would allow to test this hypothesis.

Besides soil age and weathering degree, the impact of climate on the soil-plant Si dynamics remains poorly known. While a higher ecosystem water balance may increase the rate of chemical weathering and desilication (Chadwick *et al*. 2003), it may also increase annual Si pumping by vegetation due to greater biomass production (Autin 2002), increasing the input of highly-reactive phytoliths to soils (Blecker *et al*. 2006). As such, the control of climatic variables on the relative importance of geochemical and biological drivers on soil Si is unclear. Yet the global mean temperature and precipitation are expected to rise over the 21st century (Jia *et al*. 2019), with direct impacts on the C, N and P biogeochemical cycles (Delgado-Baquerizo *et al*. 2013; Geng *et al*. 2017; Hou *et al.* 2018; Nottingham *et al*. 2020).

Overall, understanding how soil age, weathering degree and mineralogy, and climate influence soil-plant Si dynamics is required since it underpins our

comprehension of Si-related functions in plants, fluxes to aquatic ecosystems, and ultimately the fixation of atmospheric C in terrestrial and oceanic ecosystems. However, Si dynamics in terrestrial ecosystems is also linked to many aspects of plant performance and ecology that still need to be elucidated.

1.2.3 Silicon in plant ecology

Biosilicification has occurred in land plants for over 500 million years (Trembath-Reichert *et al*. 2015; Deshmukh *et al*. 2020). Some plants can contain up to 15% of silica in their tissues (Hodson *et al.* 2005), which far exceeds those of macronutrients such as N and P (Epstein 1994), while others contain virtually none. Once deposited in plant tissues as amorphous silica, Si provides certain major plant functions such as the mitigation of a wide range of biotic and abiotic stress that have been extensively reviewed (e.g., Liang *et al.* 2007; Cooke & Leishman 2016; Hartley & DeGabriel 2016; Debona *et al*. 2017; Coskun *et al.* 2019), the mechanical strengthening of plant organs (Epstein 1999), and, eventually, the increase of growth rates and crop yields (Tubana *et al.* 2016). Despite these evidences, Si is still considered as a non-essential nutrient for plant growth (Coskun *et al.* 2019), even though the complexity of completely excluding Si from a growth media should be noted (Epstein 1994). On the one hand, Si has been extensively considered in agriculture studies given the importance of Si-accumulator species in the global food production (e.g., sugarcane, rice, wheat) (Savant *et al.* 1999; Datnoff *et al.* 2001; Liang *et al.* 2015b). Today, Si fertilization is routinely performed worldwide, which allows a significant increase in agriculture yields (Datnoff *et al.* 2001; Tubana *et al.* 2016). On the other hand, the last twenty years are characterized by a considerable increase of publications related to Si in plant biology (Coskun *et al.* 2019), which allowed to better discern its numerous positive functions in plants, and a better understanding of the underlying mechanisms (Frew *et al.* 2018; Coskun *et al.* 2019).

Silicon uptake in plants relies on both an active and passive processes (Liang *et al.* 2006). Regarding active uptake, Si enters the plant from the soil solution in the form of H_4SiO_4 through specific influx channels (Si transporters) encoded by a specific gene, *OsLSi1* in rice (*Oryza sativa*) where it is constitutively expressed in the roots (Ma *et al.* 2006). The gene *Lsi1* is expressed in a range of other plant species including maize (*Zea mays*), barley (*Hordeum vulgare*), wheat (*Triticum aestivum*), soybean (*Glycine max*), and tomato (*Solanum lycopersicum*) (Chiba *et al.* 2009; Mitani *et al.* 2009; Montpetit *et al.* 2012; Deshmukh *et al.* 2013; Sun *et al.* 2020a). In addition to actively taking up Si, plants acquire it passively (Liang *et al.* 2006). Active transport is the major mechanism in rice and maize (*Zea mays*), whereas passive uptake prevails in sunflower (*Helianthus annuus*) and wax gourd (*Benincase hispida*) at higher external Si concentrations (Liang *et al.* 2006). Even in these species active transport contributes to the total Si uptake, especially at lower external Si concentrations. Although active uptake and the expression of Si transporters seems to be key in driving the large variation of Si accumulation among vascular plants (Deshmukh *et*

al. 2020), the passive uptake reflects the importance of transpiration on leaf Si accumulation (e.g., Euliss *et al.* 2005; Henriet *et al.* 2006).

The great variation of leaf Si among vascular plants remains unresolved. In 2016, Strömberg *et al.* tested whether the evolutionary pattern of plant silica accumulation was consistent with adaptive hypotheses by mapping silica content onto time-calibrated land plant and grass phylogenies. The authors specifically considered three adaptive hypotheses: (1) when atmospheric carbon was scarce in Oligocene and where silica deposits could have been favored to over C-based compounds (2) times or habitats characterized by seasonal aridity (Coughenour 1985) (3) response to increased herbivore pressure (Katz 2015). The authors showed that active silica accumulation evolved numerous times rather than being ancestral in land plants, yet no clear evidence was found in support of any of the three 'functional demands'. In conclusion, although silica accumulation provides clear benefits to plants today and meet the criteria for adaptations (mainly structural support and herbivore deterrence), the adaptive origin of this trait remains actually unclear (Strömberg *et al.* 2016). More broadly, we tend to associate the expression of certain traits with the functions they play today, but silica accumulation could possibly be seen as an "exaptation" (that is, a shift in the function of a trait during evolution) rather than adaptation (Gould & Lewontin 1979). If so, seeking an adaptive origin for silica deposition based on the functions it plays today could not be appropriate and lead to bottlenecks (Katz 2020).

The research of Si in plant ecology was longer to initiate compared to agronomy, biogeochemistry, plant physiology or archeology (Cooke & Leishman 2011). In pioneering work conducted in the Serengeti National Park, McNaughton *et al.* showed that plants native to the more heavily grazed grasslands accumulate more Si than plants from less heavily grazed sites (McNaughton & Tarrants 1983). This pattern was confirmed by work conducted in North American grasslands (Brizuela *et al.* 1986), and biosilicification has demonstrated to reduce herbivory through an increase in leaf abrasiveness, which reduces penetration and chewing, and a decrease in the digestibility and palatability of leaves (Massey & Hartley 2006, 2009; Reynolds *et al.* 2009; Hartley & DeGabriel 2016; Johnson *et al.* 2021). Moreover, the induction of silica-based defense by herbivory has been demonstrated in both laboratory experiments (Massey *et al.* 2007b; McLarnon *et al.* 2017) and in the field (Huitu *et al.* 2014; Wieczorek *et al.* 2015; Ruffino *et al.* 2018). These works supported the hypothesis of an adaptive origin of silicification to periods of increased herbivory pressure. However, other factors influence Si uptake in natural ecosystems, including genotypic variation (Soininen *et al.* 2013) and variation in abiotic factors such as climate, nutrient limitation or Si availability (Henriet *et al.* 2008a; Ryalls *et al.* 2018; Johnson *et al.* 2019b; Minden *et al.* 2020; Quigley *et al.* 2020). In fact, some authors suggested that these environmental parameters may be more significant than herbivory in determining levels of Si in plants (Coughenour 1985; Cid *et al.* 1989; Quigley *et al.* 2016, 2020), and that the adaptive origin of silicification may not have been the defense against mammalian grazers (Strömberg *et al.* 2016).

In 1985, Coughenour hypothesized that grasses evolved firmer and more silicaceous leaves in drier and more open habitats rather than in response to grazers (Coughenour 1985), because of the positive effects of silica against cell collapse during droughts and, more generally, against water stress (Meunier *et al.* 2017). Such hypothesis received recent support in a study of Brightly *et al.* (2020). The authors tested the "C4-grazer hypothesis", which postulate that C4 grasses evolved stronger mechanical defenses than C3 grasses through increased phytolith deposition, in response to extensive ungulate herbivory. The authors found that C4 grasses did not show consistently high Si concentrations compared to C3 grasses, and that high temperature increased leaf Si, especially for species adapted to warm regions. Moreover, reduced water treatment promoted silica deposition, with a slightly stronger response for dry habitat species. These results allow to reject the C4-grazer hypothesis, and reinforce the key role of hot and dry conditions on plant Si accumulation (Brightly *et al.* 2020).

The role of environmental conditions other than grazing was further highlighted by a recent study of Quigley *et al*. who studied foliar chemistry of grasses from 17 globally distributed sites where nutrient inputs and grazing were manipulated (Quigley *et al.* 2020). They found that foliar Si concentration did not respond to large mammalian grazers exclusion, but that nutrient addition consistently reduced leaf Si. They also found negative relationships between Si and C, especially at arid sites compared to mesic sites. These results therefore suggest that soil nutrient and water limitation favor the investment in Si over C-based compounds. Indeed, given the defense and support roles of silicification, trade-offs between Si and C-based compounds with similar functions (phenolic compounds, lignin and cellulose) have been suggested (Schoelynck *et al.* 2010; Cooke & Leishman 2012; Frew *et al.* 2016; Klotzbücher *et al.* 2018c; Waterman *et al.* 2021). This could reflect a plant strategy to reduce C costs because silica-based compounds tend to be less costly than the synthesis of C-based compounds (Raven 1983). The role of soil nutrient limitation on plant Si accumulation was recently reinforced in a study where leaf Si concentrations of *Holcus lanatus* increased markedly in situation of P limitation (Minden *et al.* 2020). Overall, these studies highlight the key role of major abiotic factors in driving plant Si accumulation, and as potential driving forces for an adaptive origin.

Despite these evidences, the role of soil fertility on plant Si accumulation received only very little attention, yet Si has positive effects for plants growing under P stress (Hall & Morison 1906; Fisher 1929; Ma & Takahashi 1990b, 1991b; Kostic *et al.* 2017; Neu *et al.* 2017). Investing in silica rather than C-based components for leaf defense/support when P supply is low could indeed represent an energetic gain that would save resources for other key aspects of plant life. Moreover, prominent ecological theories, such as the resource availability hypothesis (RAH), predict that plant species adapted to resource-rich environments will have rapid growth rates and leaf turnover, high leaf nutrient concentrations, but low levels of anti-herbivore defenses (Coley *et al.* 1985; Endara & Coley 2011). By contrast, the benefits of allocating resources to anti-herbivore defenses become advantageous for species adapted to nutrient-poor environments, because biomass loss by herbivory represents

a significant loss of scarce nutrients (Coley *et al.* 1985; Endara & Coley 2011). Since silica is an efficient defense against herbivores, the RAH would predict a stronger investment in nutrient-depleted soils, but this has not received attention in the literature (but see Massey *et al.* 2007a). Exploring how plant Si and C-based compounds having similar functions evolve along soil fertility gradients could help to achieve this goal.

Moreover, a potential higher expression of silica-based defenses among plants growing on P-depleted environments could be linked to specific nutrient-acquisition strategies. In particular, the exudation of carboxylates in the rhizosphere is particularly widespread in plants that have evolved in old and highly-weathered environments, with low soil P concentrations (Lambers *et al.* 2008; Abrahão *et al.* 2014; Zemunik *et al.* 2015; Teodoro *et al.* 2019). However, their impact on Si mobilization from the rhizosphere and subsequent plant Si accumulation has received no attention to my knowledge. These carboxylates mobilize P from strongly sorbed forms by complexing metal cations that bind phosphates, and displace phosphates from the soil matrix by ligand exchange (Lambers *et al.* 2006). During this process, manganese (Mn) is also mobilized and leaf [Mn] can be used as a proxy for root-released rhizosphere carboxylates (Lambers *et al.* 2015; Pang *et al.* 2018). This nutrient-acquisition strategy is more prevalent on old and P-depleted soils (Zemunik *et al.* 2015), and it is important to study if it can mobilize Si for plant uptake, as for Mn.

1.2.4 Long-term soil chronosequences

Soils are at the core of the Earth's Critical Zone as an interface where geochemical and biological processes interact. Understanding their influence on the terrestrial biogeochemical cycling of elements is key for global cycles. The factors of soil formation have been established by Hans Jenny in 1941, and are still authoritative nowadays: time, parent material, vegetation, climate, and topography (Jenny 1941). Studying one of these factors alone and under natural conditions is complex, but allow to understand its effect on the process of interest. In particular, the impact of time and soil/ecosystem age always fascinated environmental scientists who aimed to study natural processes, despite the complexity of this independent factor in Jenny's equation (Phillips 1989). One way to study the effects of time on soil and ecological processes is the use of soil chronosequences, defined by *"sequences of related soils that differ, one from the other, in certain properties primarily as a result of time as a soil forming factor"* (Glossary of Soil Science Terms 1965 in Stevens & Walker 1970). In other words, four out five soil-forming factors must be constant, or vary ineffectively (Stevens & Walker 1970). When a soil chronosequence spans a wide range of soil age (i.e., long-term chronosequences), it has the advantage to embrace numerous *soil process domains* and *pedogenic thresholds*, to understand their influence on the process of interest (Chadwick *et al.* 1999; Chadwick & Chorover 2001; Vitousek & Chadwick 2013; Bateman *et al.* 2019).

Soil chronosequences are therefore valuable tools for environmental scientists (Walker *et al.* 2010). They have been used for decades to better understand processes

controlling cycling of nutrients and soil organic matter (Stevens & Walker 1970; Walker & Syers 1976; Elliott *et al.* 1991; Crews *et al.* 1995; Richardson *et al.* 2004; Laliberté *et al.* 2012; Hayes *et al.* 2014; Chen *et al.* 2015; Turner *et al.* 2018) and processes influencing plant diversity and ecological succession (Wardle *et al.* 2004, 2008; Walker *et al.* 2010; Turner *et al.* 2012; Zemunik *et al.* 2016; Chang & Turner 2019). However, the dynamics of Si in soil-plant systems, both in terms of ecological and biogeochemical considerations, still received very few attention in the context of soil chronosequences, where time can be isolated from the other major environmental factors. Yet, such study models have the potential to answer many questions related to soil-plant Si dynamics.

Better understanding the drivers of terrestrial biogeochemical cycles is not required only for a deeper appreciation of global cycles, but also to ameliorate our knowledge of nutrient cycling in agroecosystems. Similarly, knowledge on ecological processes influencing nutrient cycling learned from complex natural systems can help us to improve the resource-use efficiency and productivity of agroecosystems (Mariotte *et al.* 2018). For instance, research has long highlighted that P-use efficiency in agroecosystems could be significantly improved through knowledge of ecological processes occurring in natural systems (Lambers *et al.* 2011; Richardson *et al.* 2011). In this case, this is of special interest since global P reserves are being depleted (Lambers *et al.* 2006), and this nutrient limits plant productivity in many parts of the world (Du *et al.* 2020). Si plays a pivotal role in agroecosystems, and leverage ecological processes impacting soil-plant Si dynamics in alternative cropping systems could indeed ameliorate the Si status of crops, but this remains hypothetical to date.

1.2.5 Silicon in agriculture

The global food production heavily relies on Si-accumulating species such as wheat, maize, sugarcane, or rice (Figure 1-5) (Meyer & Keeping 2000; Datnoff *et al.* 2001a; Guntzer *et al.* 2012a; Liang *et al.* 2015b). Since Si has multiple beneficial effects for crop species and is ubiquitous in soils, it is crucial to discern the biotic and abiotic factors that drive its mobility in soil-plant systems. This is particularly important to understand these processes for tropical and subtropical agroecosystems supporting highly-weathered and desilicified soils with large total Si pools, but low plant-available Si concentrations. An optimal management of Si in agriculture would provide many benefits to crops and would contribute to the agriculture transition, towards a more sustainable model with less negative impacts on soil, water, air and biological diversity (Stoate *et al.* 2009). One way to increase foliar silicification is the application of Si fertilizers, such as wollastonite. However, the access to common Si fertilizers is low in developing countries, and the most accessible way to increase foliar silicification is to use amendments derived from organic products. In particular, the pyrolysis of Si-rich crop residues and the subsequent application of Si-rich biochar to soils is an efficient tool to increase Si availability (Houben *et al.* 2014; Li *et al.* 2018, 2019b; Li & Delvaux 2019). Evaluating if such practice can increase the degree

of foliar silicification and impact other leaf traits related to support/defense functions is now needed.

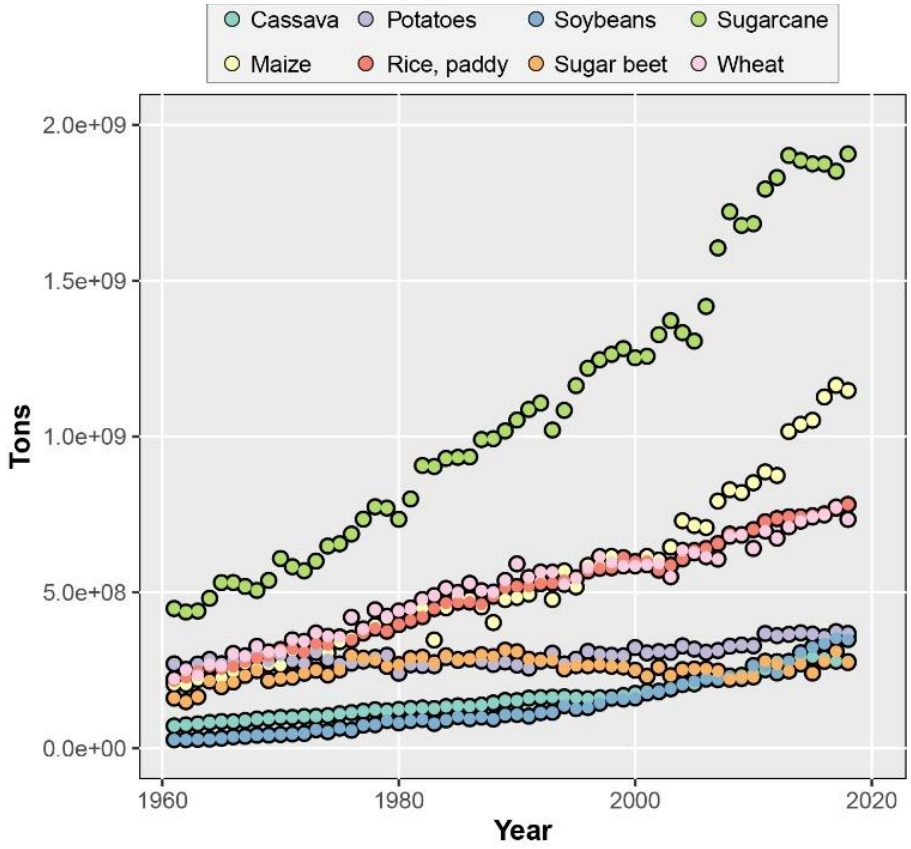

Figure 1-5: Global production of the 8 most important crops in 2018, from 1961 to 2018 (source = FAOSTAT).

1.3 Thesis objectives, scientific approaches and hypotheses

Silicon is involved in a number of key ecological and geochemical processes. It is widely recognized as an important regulator of the global carbon cycle via its effect on diatom productivity in oceans and the weathering of silicate minerals on continents, and as a beneficial plant nutrient improving resistance to herbivory and pathogens, and mitigating the negative effects of several abiotic stresses, including nutrient limitation. As described above, the main theme of this thesis is to explore the long-term dynamics of Si in terrestrial ecosystems, and investigates some factors driving soil-plant Si dynamics in agroecosystems. To do so, we will first study three long-

term soil chronosequences located on a climatic gradient in southwestern Australia (Jurien Bay, Guilderton, Warren). Each chronosequence consists of a series of coastal dunes within a global biodiversity hotspot, with a species-rich shrubland vegetation (Hopper & Gioia 2004). Within a chronosequence, soil ages range from 100 years to more than 2 million years, the parent material is marine sand and topography and climate are similar for all the stages. Each chronosequence exhibits extreme mineralogical changes – from carbonate-rich to quartz-rich soils – and an extreme gradient of nutrient availability, with shifts from N-limitation of plant productivity on young soils to P-limitation on old soils (Laliberté *et al.* 2012; Hayes *et al.* 2014). Along the three chronosequences, annual rainfall ranges from 533 to 1185 mm while potential evapotranspiration is rather similar, resulting in water balances ranging from -900 to +52 mm yr^{-1}. The study of these three chronosequences will allow to better discern the influence of soil weathering degree on long-term Si dynamics, and answer three compelling questions:

Q.1. How do soil Si dynamics evolve during long-term soil development, with strong mineralogical end-members?

Q.2. How does long-term weathering control the relative contribution of geochemical and biological processes on plant-available Si concentrations in soils?

Q.3. How do ecosystem water balance and soil parent material impact the long-term evolution of the pools of reactive Si-bearing minerals and plant-available Si in soils?

Better constraining the soil-plant Si dynamics as a function of soil weathering degree (questions **Q.1** to **Q.3**) can be achieved through complete mass-balance calculations following the determination of Si pools and fluxes at the ecosystem scale (e.g., Alexandre *et al.* 1997, 2011; Sommer *et al.* 2013). In particular, such approach allows to precisely determine the contribution of geochemical (i.e., litho/pedogenic silicates dissolution) versus biological (i.e., plant Si uptake followed by soil phytoliths dissolution) processes on the terrestrial Si cycle. However, an accurate determination of Si pools and fluxes at each stage of the three soil chronosequences was not possible in this thesis, for several reasons.

First and foremost, determining the annual Si uptake by vegetation within species-rich shrubland ecosystems is highly challenging. Some 10 x 10 m plots exhibit more than 70 different species, each having very different contribution to the overall relative cover (Zemunik et al. 2016). In addition, the strong phylogenetic diversity of these ecosystems suggests important variations in leaf Si (Hodson et al. 2005; Zemunik et al. 2016), and the annual net primary productivity has proven to be very difficult to determine in the field (personal communication). Moreover, all the Si taken up by vegetation is not yearly returned to topsoil, because some species exhibit leaf lifespan longer than one year. Therefore, estimating annual Si uptake along these chronosequences was not possible during this PhD. Instead, we chose to sample the

leaves of the 10 most-abundant species growing along the chronosequence of interest (Jurien Bay; see chapter 2), and to weight their leaf Si concentrations with their relative cover available from other studies (Zemunik et al. 2016). Since the leaf area index (LAI) does not vary much along the chronosequence in which we sampled plants (Jurien Bay; see chapter 2), such cover-weighted means gave us a rough proxy of the degree of Si biocycling as a function of soil age. Second, implementing each chronosequence stage with lysimeters to quantify dissolved Si concentrations in soil solution and annual Si output towards hydrosphere was not possible either, because of the high number of visited sites combined with challenging access. Instead, we chose to collect soil samples to perform specific extractions later. In particular, we performed $CaCl_2$ extractions to estimate the pool of so-called "plant-available Si", that is probably the closest to the pool of dissolved Si. Third, the determination of Si stocks and fluxes requires knowledge on the temporal stability of soil phytoliths (Alexandre et al. 1997, 2011). To do so, physical extractions of soil phytoliths have to be performed at several soil depth to know their distribution with accuracy. We performed such extractions within this work, but not at the same depth for all the soil profiles (because we sampled by pedogenic horizons), and probably not at enough soil depth sections to get an accurate depth distribution. Moreover, it should be combined with microscopic phytolith morphological analyses at each depth (Alexandre et al. 1997, 2011) , which could not be made for all the soil horizons sampled in this thesis, for technical reasons.

Overall, most accurate calculations of Si stocks and fluxes in soil-plant systems found in the literature focus on one single site (e.g., Bartoli 1983; Alexandre *et al.* 1997, 2011; Sommer *et al.* 2013). In this thesis, 6 or 7 sites have been visited along three soil chronosequences, for a total of 20 sites (see chapter 2 below). Therefore, the level of detail in the characterization of the soil-plant Si cycle is lower. Here, for the questions **Q.1** to **Q.3**, we mainly based our rationale on soil extractants as proxies of soil Si pools ($CaCl_2$, acetic acid, Na_2CO_3 and oxalate), and on cover-weighted means leaf Si concentration as proxies of Si biocycling. Our scientific approach was to trace the mineral source of "plant-available Si" as a function of soil processes and age, to better understand the importance of geochemical versus biological processes on soil-plant Si dynamics.

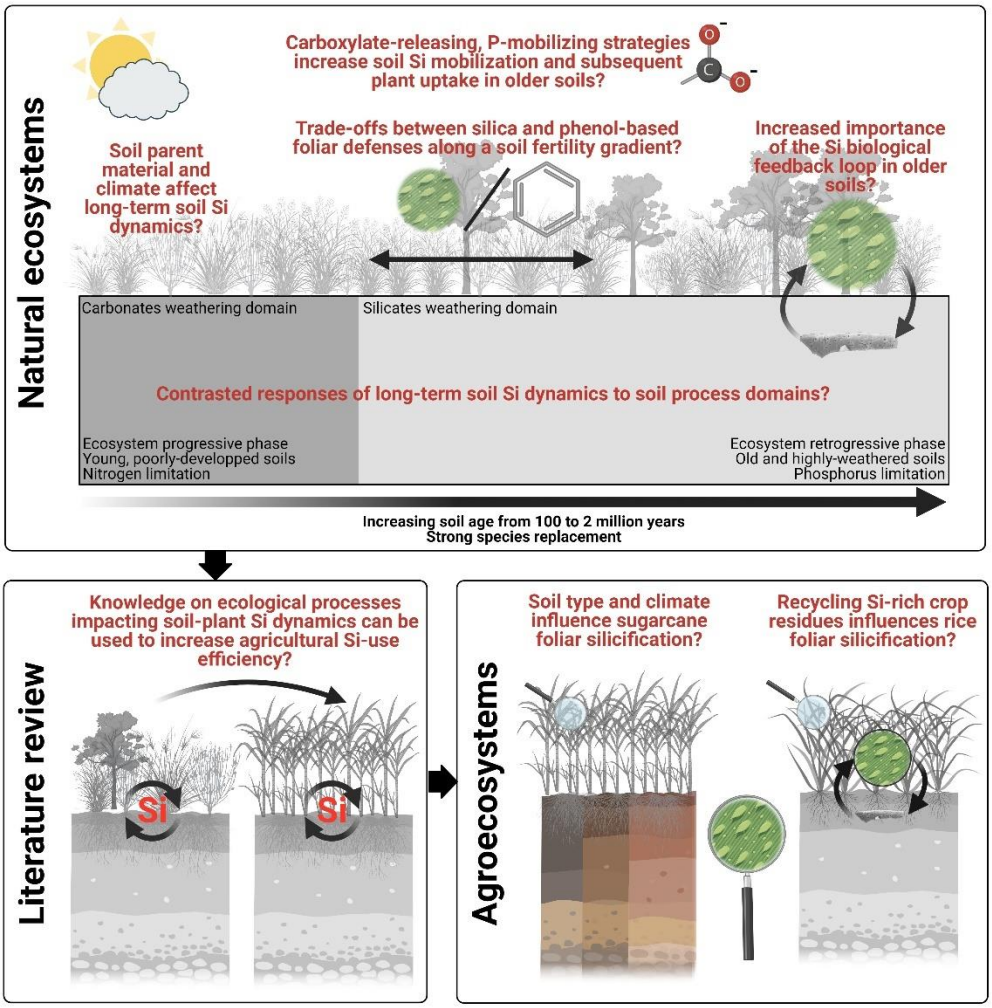

Figure 1-6: General overview of the thesis outline and hypotheses tested. Arrows indicate the order of the chapters.

With respect to **Q.1**, we hypothesized contrasting responses of soil Si dynamics (soil Si pools, including the pool of 'plant-available' Si) to the two main soil process domains that exhibit the chronosequences: carbonates weathering domain and silicates weathering domain (Figure 1-6). In particular, for the silicate-weathering domain, we hypothesized a decrease of the plant-available Si pool over time through desilication. We assumed Si release from carbonate-rich soils can be driven by contrasting processes for which the relative contribution is still unknown (Haynes 2019). For **Q.2**, we hypothesized that the reactive soil Si pools would be increasingly dominated by soil phytoliths as soils age, because of the continual loss of pedogenic reactive Si pools following desilication and the continuous supply of phytoliths by

vegetation. We also hypothesized that phytoliths would be the main source of plant-available Si in the older desilicated soils, due to their greater reactivity compared to most litho/pedogenic Si-bearing minerals (Fraysse *et al.* 2009), especially quartz that is abundant in the oldest soils. Such pattern would bring support for an increased importance of the biological feedback loop (plant Si uptake followed by phytoliths dissolution in soils) in old and desilicated soils (Cornelis & Delvaux 2016), as observed for instance for P (Walker & Syers 1976; Turner *et al.* 2007) (Figure 1-6). Regarding **Q.3**, we predicted that ecosystem water balance and soil parent material properties (that differ among the three chronosequences) would influence markedly long-term soil Si dynamics (Figure 1-6).

After having highlighted the long-term soil Si dynamics in these soil chronosequences, we will try to leverage ecological approaches to understand some of the results acquired in the first chapters. As described above, Si is involved in numerous ecological processes, and long-term chronosequences might help to better discern its functional role in plant ecology. Moreover, ecological approaches might be useful to better understand terrestrial elemental biogeochemistry, in particular the degree of elemental biocycling. Specifically, two questions based on one chronosequence and related to Si in plant ecology emerged from the first three questions:

Q.4. How do phenol and silica-based defenses evolve along a strong gradient of nutrient availability shifting from N to P-limitation in species-rich shrubland ecosystems?

Q.5. Do root-released carboxylates by plants adapted to P-poor environments mobilize Si from the rhizosphere for plant uptake?

With respect to **Q.4**, we hypothesized a greater expression of anti-herbivore defenses in plants growing on the oldest (P-limiting) and the very youngest (N-limiting) soils, compared with the intermediate-aged and most fertile soils where plant productivity, N and P availability peak (Laliberté *et al.* 2012, 2014), in accordance with the RAH. Yet we further hypothesized the existence of tradeoffs between both foliar defense strategies along the resource gradient, as shown elsewhere (Cooke & Leishman 2012; Moles *et al.* 2013; Frew *et al.* 2016; Simpson *et al.* 2017; Waterman *et al.* 2021) (Figure 1-6). Finally, we expect the community-level patterns to be mostly driven by changes in plant species composition since the Jurien Bay chronosequence is characterized by a strong species turnover (Zemunik et al. 2016), which reflects the expression of selective edaphic forces acting on a species-rich regional flora over an ecological time scale (Laliberté *et al.* 2014). In **Q.5**, we discuss the potential of root-released carboxylates by plants adapted to P-poor environments to co-mobilize Si from the rhizosphere for plant uptake, in the form of an opinion article (Figure 1-6).

Following this, we will try to understand how knowledge on soil-plant Si dynamics learned from complex natural systems can help us to improve Si-use efficiency in

agroecosystems. This is particularly important because Si is involved in a wide range of functions that contribute to plant performance and stress regulation, which can ultimately lead to increase plant productivity and crop yields, especially in desilicated environments with low plant-available Si. To do so, we will review the biotic and abiotic processes influencing soil-plant Si dynamics – including some highlighted in the first chapters – to determine if they could be leveraged in alternative cropping systems to ameliorate crops Si status:

Q.6. What are the main biotic and abiotic factors controlling soil-plant Si dynamics, and how can they be exploited in alternative cropping systems to ameliorate crop Si status?

We hypothesized that numerous biotic factors influencing soil-plant Si mobility but that are often overlooked (mycorrhizal associations, root exudates, silicate-solubilizing bacteria, soil macrofauna, large herbivores) could improve Si-use efficiency in agricultural systems, in particular through the implementation of cover crops, cereal-legume intercropping and integrated crop-livestock systems (Figure 1-6).

Finally, we propose to consider two aspects highlighted in Q.6 through two case studies about Si in agriculture. In particular, we will first test if one of the factors highlighted in the first chapters of the thesis and in Q.6, namely soil weathering degree, will influence foliar silicification of sugarcane leaves. Sugarcane is an important crop worldwide, and silicification is now seen as the main mechanism explaining the Si-related functions in plants. Understanding how soil weathering degree and its subsequent control on plant-available Si influence foliar silicification patterns at the cellular level of this important crop is therefore needed. This study will be carried out in the island of Guadeloupe, in the Caribbean Sea, where three contrasted soil types under sugarcane crops will be studied. Secondly, we will test if one of the agriculture practices highlighted in Q.6, namely recycling crop residues, affects foliar silicification of upland rice grown in an agricultural, desilicated soil from Burkina Faso, where access to common Si fertilizers is low. Assessing if sustainable agriculture practices might improve crop Si status in developing countries is timely in the face of global changes and resource depletion. These two case studies will allow to answer two final questions:

Q.7. How does soil weathering degree influence the silicification patterns of sugarcane (*Saccharum officinarum*) leaves?

Q.8. Does the application of biochar on a highly desilicated soil increase the silicification of rice (*Oryza sativa*) leaves?

Regarding **Q.7**, we hypothesized that the degree of soil weathering/desilication and evapotranspiration potential will be key drivers of the magnitude of silica deposits on leaf epidermis, via contrasted level of Si accumulation (Figure 1-6). We further

hypothesized that leaves with low foliar Si concentration will have higher cellulose concentrations as a mechanical compensatory role, as hypothesized elsewhere (Yamamoto *et al.* 2012; Guerriero *et al.* 2016). With respect to **Q.8**, we hypothesized that biochar produced from high-Si accumulating rice would result in higher degree of foliar silicification of the rice cropped compared to low-Si accumulating cotton-based biochar (Figure 1-6). We further hypothesized that a higher degree foliar silicification will result in straighter leaves. We further hypothesized that a higher degree of leaf silicification could affect foliar traits linked to structural/defense functions, namely leaf mass per area and force required to punch leaves, but without conjecture on the direction of the response.

1.4 Thesis outline

The research results (Chapters 3 to 10) are presented in a succession of articles either published or submitted to peer review journals. As such, each chapter can be read and understood independently. All chapters were written by the PhD student, even though modifications were made by co-authors while working on the articles. The succession of chapters is coherent for a continuous reading, although some information and results will sometimes be repeated. I apologize for any inconvenience. A foreword is presented at the beginning of each chapter to summarize the results and advances made in the previous chapters, and to outline the logical continuation that constitutes the new chapter.

The ***Chapter 2*** presents the environmental settings of the study sites in southwestern Australia, because five of the eight questions outlined above are based on these study systems (Q.2 to Q5). The environmental settings related to the questions Q.7 and Q.8 will be presented in the corresponding chapters (see below).

The ***Chapter 3*** is related to the question Q.1, and analyzes soil Si pools along one of the soil chronosequences: the Guilderton chronosequence. At the end, this chapter opens the question of the main source of Si in old and highly-desilicated soils, where litho- and pedogenic Si reserves are depleted, which will be addressed in the next chapter.

In ***Chapter 4***, the question Q.2. is tested by analyzing different soil Si pools, including the biogenic Si pool, along two chronosequences (Jurien Bay and Guilderton). In addition, Si and major nutrients in mature leaves of the most abundant plants growing along the Jurien Bay chronosequence were quantified to roughly indicate the degree of elemental biocycling.

The question Q.3. is addressed in the ***Chapter 5***, where major Si pools were quantified along the three soil chronosequences (Jurien Bay, Guilderton and Warren).

For these first three chapters, soil descriptions and basic properties (*i.e.*, soil pH, carbonates content and texture) were already available from other studies (Turner & Laliberté 2015; Turner *et al.* 2018). Vegetation survey to estimate the relative canopy cover of each species in different plots along one of the chronosequences (Jurien Bay)

were also available (Hayes *et al.* 2014; Zemunik *et al.* 2016). However, the determination of soil Si pools, total elemental concentrations, pedogenic oxide concentrations, phytolith concentrations and microscopic analyses, soil mineralogy and plant total elemental concentrations has been achieved within the framework of this thesis. To do so, two field campaigns were conducted in Australia to collect soil and plant samples.

The question Q.4. is addressed in the ***Chapter 6*** where Si and total phenols were quantified in the leaves of plants growing along the Jurien Bay chronosequence. These two compounds were then linked to the major leaf nutrients and soil properties to study how plant defense mechanisms are expressed as a function of soil fertility, in the RAH framework. For this chapter, vegetation survey and soil total P and N concentrations were already available from other studies (Hayes *et al.* 2014; Turner & Laliberté 2015; Zemunik *et al.* 2016), but leaf Si, total phenol, and major nutrient concentrations were quantified within the framework of this thesis.

The ***Chapter 7*** is based on Q.5, and presents evidence for the mobilization of Si by root-released carboxylates into the rhizosphere, in the form of an opinion article entirely based on the literature and on results obtained during this thesis.

The ***Chapter 8*** is related to Q.6, and is presented in the form of a literature review.

The ***Chapters 9 and 10*** are related to the questions Q.7 and Q.8, respectively. They consider whether knowledge on factors controlling soil-plant Si dynamics learned from the previous chapters, mainly at the ecosystem/soil-plant scale, could influence the foliar silicification at the cellular level of two important crop species. This shift in scale study is fundamental to understand whether some of the factors highlighted earlier in the thesis can induce beneficial effects for crops. The chapter 9 presents results on soil basic properties, soil Si pools, leaf Si concentrations, leaf C-based structural components, and detailed analyses of foliar silicification patterns at the cellular level for three sugarcane cultivation sites. The results presented in this chapter were gathered by the PhD student in the framework of this thesis, with the exception of soil basic properties (*e.g.*, soil total elemental concentrations, cation exchange capacity) and concentrations of C-based compounds, gathered by co-authors. The chapter 10 presents results on soil basic properties, soil Si pools, leaf Si concentrations, leaf physical traits, and detailed analyses of foliar silicification patterns of upland rice. These results were gathered by a Master student co-supervised by the PhD student.

Finally, ***Chapter 11*** summarizes the findings from all chapters and highlights some directions for future research.

2

Environmental settings

2.1 Study sites

The core of the present thesis is based on three 2-million-years dune chronosequences located on a climatic gradient in southwestern Australia: the Jurien Bay, Guilderton and Warren chronosequences (Figure 2-1). The first sequence that has received attention in the literature is the Jurien Bay chronosequence (Laliberté *et al.* 2012; Hayes *et al.* 2014), which is described in details in Turner & Laliberté (2015). Later, the Guilderton and Warren chronosequences have been characterized and extensively described in Laliberté *et al.* (2017) and Turner *et al.* (2018).

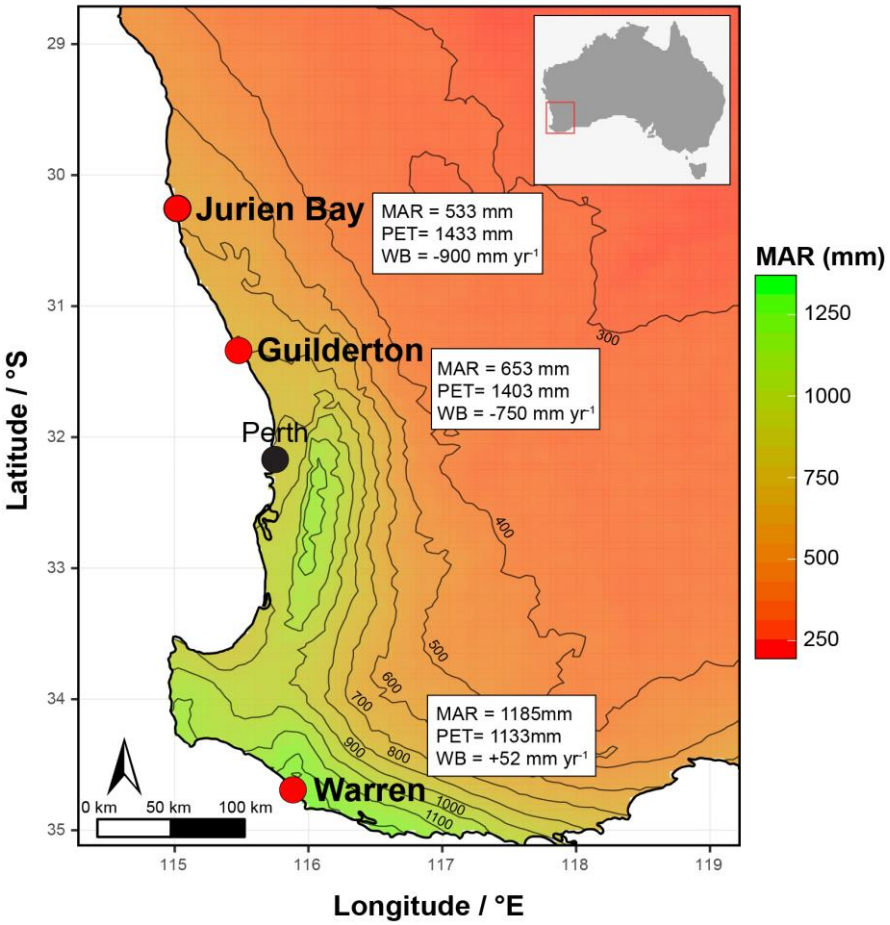

Figure 2-1: Location of the three soil chronosequences in southwestern Australia. The gradient of mean annual rainfall (MAR) and rainfall isolines result from 30 years of data (1961-1990) gathered by the Bureau of Meteorology of the Australian Government. The potential evapotranspiration (PET) and water balance (WB) data comes from Turner *et al.* (2018).

2.1.1 Ages of dune formation

The Jurien Bay and Guilderton chronosequences are part of the Swan Coastal Plain, a series of dunes that run parallel to the coast for 400 km from Geraldton (28.7774◦S, 114.6150◦E) in the north to Dunsborough (33.6082◦S, 115.0940◦E) in the south. The dunes have been formed by periodic interglacial sea-level high-stands since the Early Pleistocene or Late Pleistocene (i.e. 2.59 million years ago) (Kendrick *et al.* 1991). The dunes and their associated soil types are grouped into three main units according to the underlying parent sand deposits (McArthur & Bettenay 1974; Playford *et al.* 1976): the Quindalup dunes date from the Holocene (up to 6500 years old), the Spearwood dunes date from the Middle Pleistocene (120,000 to 500,000 years old) and the Bassendean dunes date from the Early Pleistocene (approximately 2 million years old) (Figure 2-2). The Warren chronosequence is part of the Scott Coastal Plain, where the dune units are assumed to correspond to those of the Swan Coastal Plain (Playford *et al.* 1976) (Figure 2-2). The dunes have not been buried by younger sediments, and have therefore undergone active weathering since their deposition, creating a clear gradient of soil age by increasing distance from the Indian Ocean (Turner *et al.* 2018).

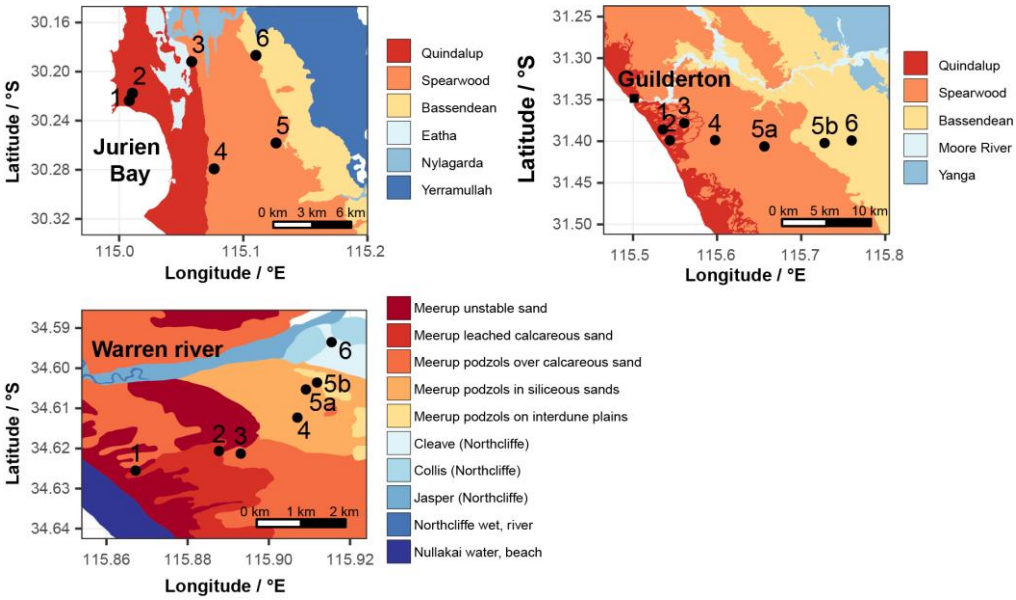

Figure 2-2 : Detailed maps of the Jurien Bay, Guilderton and Warren area, showing the main dune systems (Quindalup, Spearwood, and Bassendean for Guilderton and Jurien Bay and Meerup sand, and Cleave series for Warren) and the locations of the six (Jurien Bay) and seven (Guilderton and Warren) profile pits. Mapping of soil systems and subsystems is based on the Western Australian Department of Agriculture soil classification. Adapted from Turner *et al.* (2018).

Along the three chronosequences, six or seven locations were defined as chronosequence stages by previous studies (Turner & Laliberté 2015; Turner *et al.* 2018), and are represented in Figure 2-2. These six (Jurien Bay) and seven (Guilderton and Warren) chronosequence stages will be at the basis of the present thesis.

The age of dune formation, and therefore soil ages, are not precisely known, but relatively well constrained by previous studies (Turner & Laliberté 2015; Turner *et al.* 2018). The Quindalup dunes have been formed in the last 6500 years since the Holocene post-glacial sea level high stand. Four phases of Quindalup development have been identified in areas of the Swan Coastal Plain, but past studies grouped the Quindalup dunes into three chronosequence stages based on the degree of soil development and landscpae position (Hayes *et al.* 2014). The younger Quindalup dunes have been very recently stabilized by vegetation, show almost no pedogenic development, and are no more than 100 years old (Turner & Laliberté 2015). The medium-aged Quidanlup dunes are around 1000 years old, and show an onset of pedogenic development (Turner & Laliberté 2015). The oldest Quidnalup dunes are approximately 6500 years old, and occur inland at the Holocene-Pleistocene transition (Turner & Laliberté 2015).

Five Spearwood dune sub-systems have been identified in the Perth area, based on heavy mineral assemblages (Bastian 1996), yet they are difficult to precisely date (Turner & Laliberté 2015). However, the youngest Spearwood dune system most likely corresponds to the last interglacial sea level high stand, around 116,000-128,000 years ago (Stirling *et al.* 1998), and the increasing age of dune systems with moving away from the Indian Ocean is supported by several evidence, including heavy mineral assemblages and dating by different methods (Turner & Laliberté 2015). Older Spearwood dunes presumably corresponds to earlier major sea level high stands, which occurred around 220,000 years, 330,000 years, 410,000 years and 480,000 years ago (Turner & Laliberté 2015), and the upper age is constrained at about 500,000 years (Brooke *et al.* 2014). Based on this information, past studies determined two and three chronosequence stages in the Spearwood system along the Jurien Bay and Guilderton chronosequences respectively, and gave rough soil ages: ~120.000, ~250,000 and ~400,000 years for stage 4, 5A and 5B, respectively, at Guilderton; ~120,000 and ~400,000-500,000 years for stages 4 and 5, respectively, at Jurien Bay (Turner & Laliberté 2015; Turner *et al.* 2018).

The oldest sand deposits along the Jurien Bay and Guilderton chronosequences are the Bassendean dunes. They are assumed to be of Early Pleistocene age (> 2,000,000 years) based on dating with marine fossil assemblage (Kendrick *et al.* 1991; Turner & Laliberté 2015).

Overall, although there may be differences in soil ages for the Spearwood dunes (stages 4 and 5 at Jurien Bay and 4, 5A and 5B at Guilderton) and that the precise age of dunes formation is hard to determine, the broad chronology of dune formation is consistent for both chronosequences (Turner *et al.* 2018). In addition, given that the formation of the main costal dunes in the region relates to sea levels during interglacial periods throughout the Pleistocene (Kendrick *et al.* 1991), it is assumed that the

chronology of the Swan Coastal Plain is comparable to the main stages of dune formation along the Warren chronosequence on the Scott Coastal Plain (Playford *et al.* 1976; Turner *et al.* 2018).

2.1.2 Climate along the chronosequences

Climatic variables across the three chronosequences are described in detail in Turner *et al.* (2018), and summarized in Figure 2-1. Mean annual rainfall is 533, 653 and 1185 mm, at the Jurien Bay, Guilderton and Warren chronosequences, respectively (Figure 2-1). The dry season lasts only 2 months at Warren, but 6-7 months at Jurien Bay and Guilderton. Mean annual temperature is 19.0, 18.4 and 15.5 °C at the Jurien Bay, Guilderton and Warren chronosequences, respectively. Annual potential evapotranspiration is 1433, 1403 and 1133 mm at the Jurien Bay, Guilderton and Warren chronosequences, respectively, yielding water balances of -900, -750 and +52 mm yr^{-1} (Figure 2-1).

There is little if any variation in climate along each chronosequence, which extends only an approximate 15 km inland from the coastline (Turner & Laliberté 2015; Turner *et al.* 2018). However, we have little information on paleoclimate for the three chronosequences. There are evidence suggesting an increased aridity in central and Western Australia in the Miocene, but the Swan Coastal Plain appears to have been buffered climatically during the Quaternary, with a hydrological regime similar to the present (Turner & Laliberté 2015; Turner *et al.* 2018). Therefore, although historical climate changes almost certainly occurred during the development of the three chronosequences, this was relatively moderate compared to inland variation and the climatic ranking of the three sequences has been generally maintained throughout their geological history (Wyrwoll *et al.* 2014; Turner & Laliberté 2015; Turner *et al.* 2018).

Past studies estimated the soil moisture and temperature regimes along the three chronosequences, based on the USDA Soil Taxonomy system (Turner & Laliberté 2015; Turner *et al.* 2018). Since soil temperature data are not available, they have been estimated from air temperature at nearby stations. The soil temperature regime is classified as thermic for all the three chronosequences (that is, mean annual air temperature between 15°C and 22°C and the difference between the minimum and maximum mean monthly temperature is >6°C) (Turner *et al.* 2018). Similarly, the moisture regime is similar across the three chronosequences and classified as xeric (that is, the soil is dry for at least 45 days in the winter and moist for more than half the year in total) (Turner *et al.* 2018).

2.1.3 Soil parent materials

The parent materials are calcareous sand from the nearshore coastal environment for the three chronosequences (Turner & Laliberté 2015; Turner *et al.* 2018). However, while the texture of the parent sand is similar among the three sequences (>98% sand), the carbonate content of the modern parent material significantly decreases from north to south: ~80% at Jurien Bay, ~45% at Guilderton, <5% at

Warren (Turner *et al.* 2018). This regional variation may reflect differences in off-shore productivity, but it is unknown whether the pattern in modern sand composition also occurred historically (Turner *et al.* 2018).

It is also likely that the original Bassendean sand of the Jurien Bay and Guilderton chronosequences (stage 6) contained a lower carbonate content compared to the Spearwood and Quindalup sands (Turner & Laliberté 2015). It has indeed been difficult to precisely quantify its origin because of the extremely weathered nature of the present Bassendean sand. However, carbonates are rapidly lost during the early stages of pedogenesis and the Bassendean dunes still represents the endpoint of an exceptional mineral gradient where slight differences in parent material can be neglected (Laliberté *et al.* 2013; Turner & Laliberté 2015). Indeed, soil formation patterns along each chronosequence is consistent with well-known soil process domains: carbonates leaching, mineral neoformation, and quartz enrichment.

2.1.4 Vegetation along the chronosequences

The three chronosequenes are located in the Southwest Australian Floristic Region (Hopper & Gioia 2004) which is listed as a global biodiversity hotspot (Lambers 2014). Plant communities are dominated by schlerophyllous shrubs and trees with remarkably high species richness and endemism (Hopper & Gioia 2004), and there is a marked increase in plant species diversity with increasing soil age (at least at Jurien Bay ; Zemunik *et al.* 2015, 2016). Along the Jurien Bay and Guilderton chronosequences, Fabaceae and Myrtaceae are common on younger dune systems, while Proteaceae become common on older dunes (Zemunik *et al.* 2015, 2016). The species turnover is very high along the Jurien Bay chronosequence (Zemunik *et al.* 2016), and there is a strong increase in the diversity of nutrient-acquistion strategies with increasing soil age and decreasing soil fertility (Zemunik *et al.* 2015). In particular, older soils are characterized by an increase in non-mycorrhizal, carboxylate-exuding species that 'mine' P from the soil (Zemunik *et al.* 2015).

While the vegetation at Jurien Bay and Guilderton is dominated by low stature shrubland known as kwongan, the vegetation at Warren is relatively tall forest dominated by eucalyptus and Western Australian peppermint forests (*Agonis flexuosa*) (Figure 2-3a). The Leaf Area Index (LAI in $m^2\ m^{-2}$) was reported in Laliberté *et al.* (2017) and is presented in Figure 2-3b. The net increase between Jurien Bay/Guilderton (between 0.5 and 0.7 $m^2\ m^{-2}$) and Warren (around 1.5 $m^2\ m^{-2}$) indicates the change of vegetation structure and the greater Annual Net Primary Production (ANPP) in the wetter Warren chronosequence.

In agreement with a relatively stable climate along the coastal margins of southwestern Australia (see above), shrublands may have persisted in the region throughout the Last Glacial Maximum whereas changes in vegetation and climate could have been more pronounced in other regions of Australia (Turner & Laliberté 2015). In fact, it has been suggested that the relative climate stability along the coastline of southwestern Australia may explain why this region has a hyperdiverse sclerophyll flora whereas sclerophyll diversity was reduced in southeastern Australia

due to climate fluctuations during the Pleistocene (Turner & Laliberté 2015). Despite this evidence, we cannot rule out the possibility of significant vegetation changes throughout the formation of these soil chronosequences.

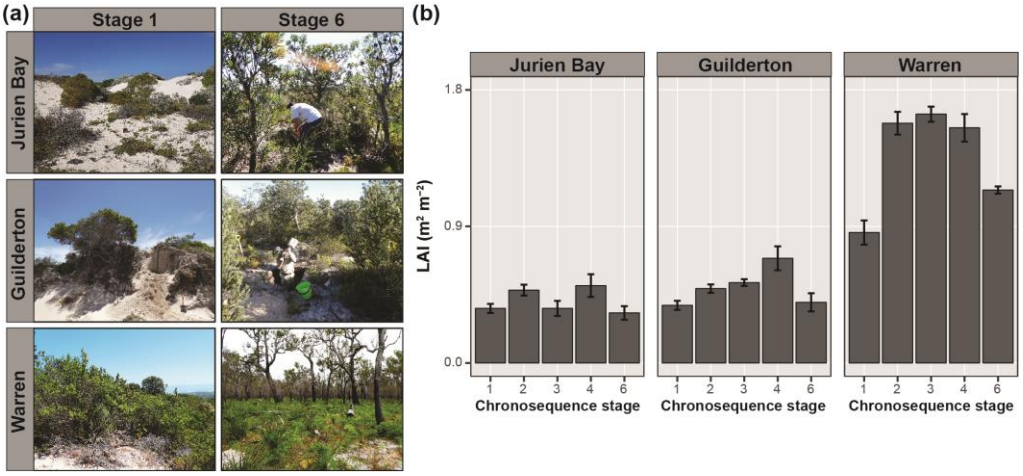

Figure 2-3 : Changes in vegetation structure across the three chronosequences for the first and last stage of soil development (a). Mean Leaf Area Index (LAI in m^2 m^{-2}) from Laliberté *et al.* (2017) across the three chronosequences (b).

2.1.5 Disturbances

Southwestern Australia is stable geologically (Wyrwoll *et al.* 2014), and had not been glaciated since the Permian (Turner & Laliberté 2015). Therefore, the dunes have remained relatively undisturbed throughout their history, and have not been buried by younger sediments (Turner & Laliberté 2015). Fire is probably the most important disturbance to vegetation in these ecosystems (Turner & Laliberté 2015). Seedlings recruitment occur indeed almost only after fire in these shrublands ecosystems. Finally, although dust deposition along the chronosequences could have occurred, past studies showed no evidence for this (Turner & Laliberté 2015). Limited dust deposits could be explained by the prevailing westerly air flow from the Indian Ocean (Turner & Laliberté 2015).

2.2 Soil development across the chronosequences and basic soil properties

Along the three chronosequences, soil development consists of carbonate leaching in Holocene dunes (stages 1 to 3), formation of clay minerals and iron (Fe) oxides from medium Holocene (stage 2) to young Middle Pleistocene stages (stage 4), followed by clay dissolution, Fe cheluviation and quartz enrichment from Middle

Pleistocene dunes (stages 4-5), resulting in bleached quartz sand profiles of several meters deep on Early Pleistocene dunes (stage 6). This results in the following sequence of soil horizons: C – Bw – BE – E (Figure 2-4 for soil profiles of the Guilderton chronosequence; Figure A-1 and C-1 in the Appendix for Jurien Bay and Warren, respectively). As a consequence, soils of stages 1-3 have alkaline pH, which decreases towards acidic values from stage 4 (Table 2-1). The clay + silt fraction increases from stage 1 to stages 3-4, and then decreases from stage 4 to stage 6 (Table 2-1). Analytical bulletins comprising soil particle-size distribution, carbonate concentrations, pH-$CaCl_2$, effective cation exchange capacity and OC concentrations for each soil horizon can be found in the Appendix (Tables A-1, B-1 and C-1 for Jurien Bay, Guilderton and Warren, respectively).

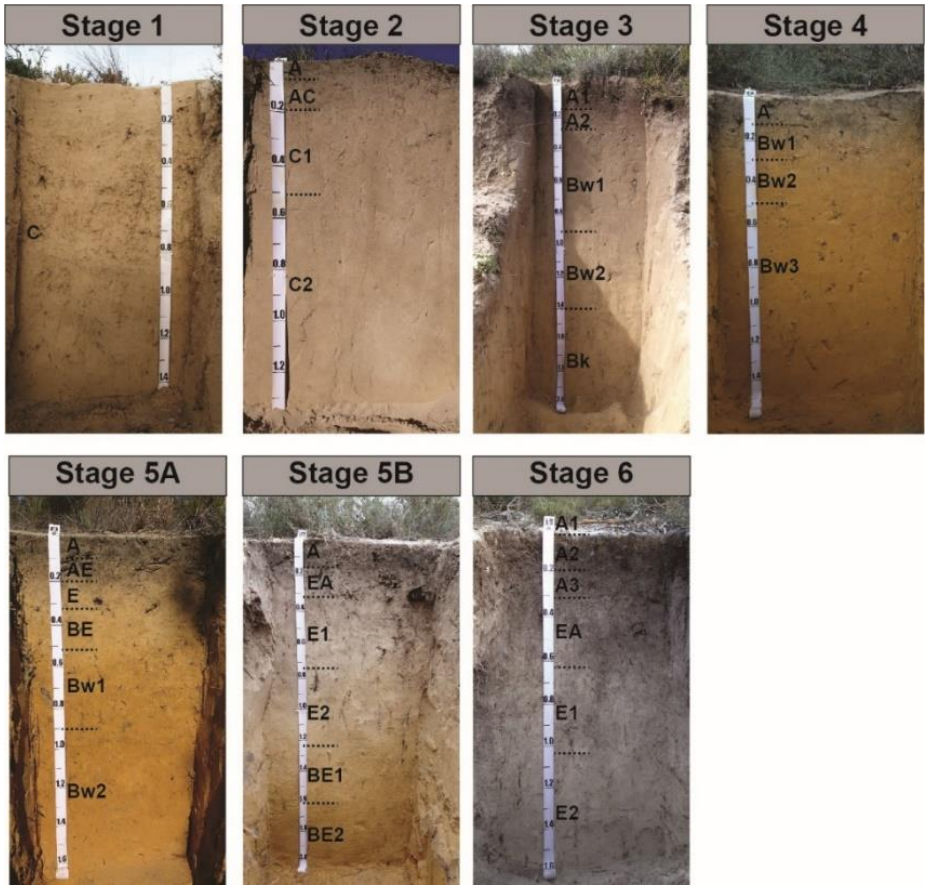

Figure 2-4 : Soil profiles of the Guilderton chronosequence, from Turner *et al.* (2018)

Table 2-1 : Texture and pH-water across the chronosequence stages from previous studies (Turner & Laliberté 2015; Turner *et al.* 2018). Analytical bulletins comprising soil particle-size distribution, carbonate concentrations, pH-$CaCl_2$, effective cation exchange capacity and OC concentration for each soil horizons can be found in the Appendix (Tables A-1, B-1 and C-1 for Jurien Bay, Guilderton and Warren, respectively).

Stages	pH-water[a]			Sand (%)[b]			Clay + silt (%)[b]		
	Jur.	Gui.	War.	Jur.	Gui.	War.	Jur.	Gui.	War.
1	8.7-9.2	9.0	9.2-9.3	97-99	99	≥99	2-3	1	1
2	8.8-9.3	8.6-9.3	8.1-9.3	92-98	95-98	≥99	3-8	2-5	1
3	8.3-9.2	8.4-9.1	6.0-6.2	93-98	89-96	95-99	2-7	4-11	1-5
4	6.4-7.0	5-8-6.0	5.7-5.9	93-95	93-96	≥98	5-7	4-7	1-2
5	6.1-6.7	-	-	97-98	-	-	3	-	-
5A	-	5.7-5.8	5.7-5.9	-	92-97	≥99	-	3-6	1-2
5B	-	5.4-5.7	5.2-5.6	-	96-99	≥99	-	1-3	0-2
6	4.7-5.8	5.5-6.3	5.0-6.3	96-99	97-99	≥99	1-4	1-3	1-2

[a]Determined in distilled water in a 1 :2 soil to solution ratio.
[b]Pipette method with further separation of sand fractions by manual dry sieving.

2.3 Soil and plant sampling design

The chapters 3, 4, 5, 6 and 7 of this thesis are based on these soil chronosequences. Two distinct sampling designs were established.

A first sampling design focused on the 20 profile pits already characterized by previous studies (one for each of the six chronosequence stages at Jurien Bay and the seven chronosequence stages at Guilderton and Warren) (Figure 2-2). In each location, a new soil profile pit was excavated for this thesis, being careful not to dig at the previously disturbed location, and pedogenic horizons were sampled. These samples will be used in the Chapters 3, 4 and 5.

A second sampling design focused on vegetation plots across the Jurien Bay chronosequence. For each chronosequence stage except for stage 5, five plots within 10 plots previously characterized (Hayes *et al.* 2014; Laliberté *et al.* 2014; Zemunik *et al.* 2016) were selected (Figure 2-5). These plots were therefore not at the exact same location as the soil pits, but always on the same dune and pedological context, with similar age (Figure 2-5). In a first plant sampling design, we sampled leaves from one individual plant for each of the 10 most-abundant species of each of the 25 plots as defined in Zemunik *et al.* (2016). We sampled leaves because they accumulate more Si than stems, and sampling aboveground organs is more achievable. The 250 species sampled with this first procedure accounted for 57% to 88% of the total cover of each plot, allowing us to have a representative view of the evolution of leaf Si concentrations at the ecosystem scale. However, no replicates by species/plot combination were taken, due to the subsequent number of analyses. Similarly, this sampling design was not adapted to studying intraspecific variations in leaf Si concentrations. This sampling design will be used in the Chapters 4, 6 and 7. In addition to this first plant sampling design, we systematically sampled the species belonging to nine families, even if they were not included in the 10 most-abundant species, in order to study family-level variation in leaf [Si] and [phenols], following

the same sampling procedure: Asparagaceae, Cyperaceae, Ericaceae, Fabaceae, Haemodoraceae, Myrtaceae, Poaceae, Restionaceae and Rhamnaceae. These families were selected because they were well represented and found at all stages of the chronosequence (Zemunik *et al.* 2016), and likely had contrasting [Si] based on known phylogenetic patterns (Hodson *et al.* 2005). This second plant sampling design will be used in the Chapters 6 and 7.

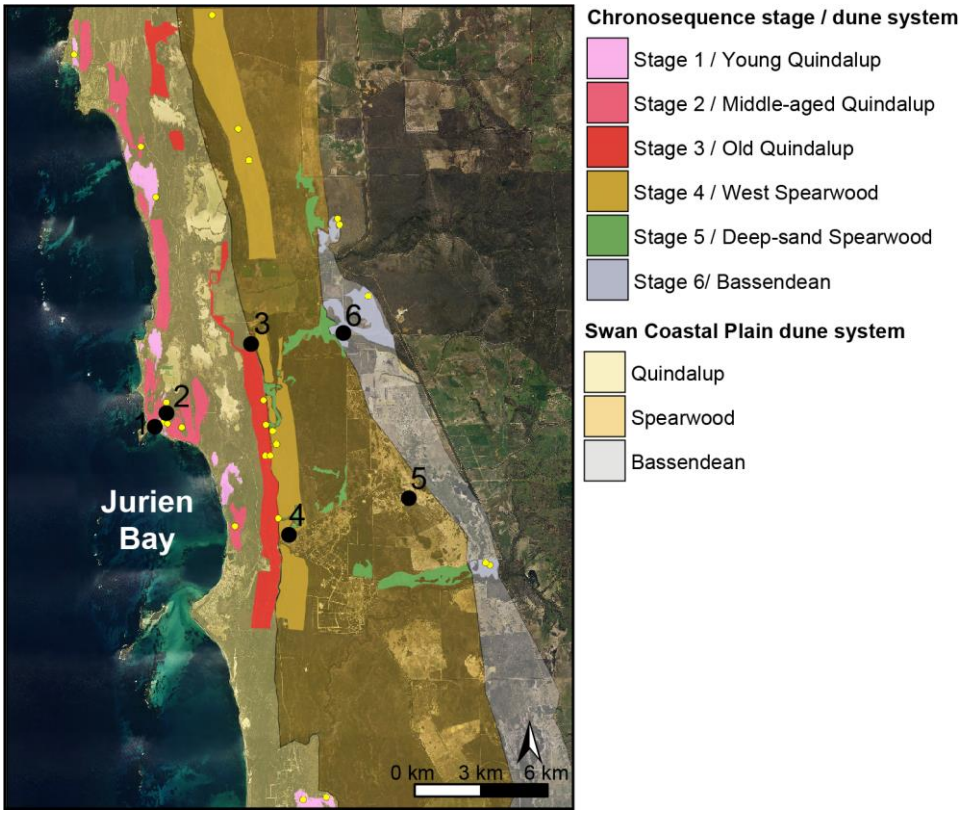

Figure 2-5 : Location of the 25 sampling plots along the Jurien Bay chronosequence (five plots by chronosequence stage; yellow points). Note that no plots were selected at stage 5. The black points indicate the locations of the soil profile pits (see Figure 2-2).

These long-term chronosequences and the associated sampling designs constitute the core of this thesis, but two additional studies in a different setting were conducted. The associated study sites and sampling designs will be presented in the Materials & Methods section of the corresponding chapters (Chapters 9 and 10).

3

Silicon dynamics during 2 million years of soil development in a coastal dune chronosequence under a Mediterranean climate*

*This Chapter is adapted from

de Tombeur, F., Turner, B.L., Laliberté, E., Lambers, H., Cornélis, J-T. (2020). Silicon dynamics during 2 million years of soil development in a coastal dune chronosequence under a Mediterranean climate. *Ecosystems*

Rhazès dit, dans son livre Physica auscultatione, qu'avec le temps, la pierre passe à l'état argileux par suite de l'action du soleil de la pluie.

Ibn-al-Awam - ابن العوام, Le Livre de l'agriculture - كتاب الفلاحة, XII^e siècle

3.1 Summary

Silicon (Si) in plants confers a number of benefits, including resistance to herbivores and water or nutrient stress. However, the dynamics of Si during long-term ecosystem development remain poorly documented, especially the changes in soils in terms of plant availability. We studied a 2-million-year soil chronosequence to examine how long-term changes in soil properties influence soil Si pools. The chronosequence exhibits extreme mineralogical changes – from carbonate-rich to quartz-rich soils – where a carbonate weathering domain is succeeded by a silicate weathering domain. Plant-available Si concentrations were lowest in young soils (Holocene, < 6.5 ka), increased in intermediate soils (Middle Pleistocene, 120 ka), and finally decreased toward the oldest, quartz-rich soil (Early Pleistocene, 2 Ma). Silicon availability is likely low and relatively constant in the young soils because (1) carbonate weathering consumes protons and therefore reduces weathering of silicate minerals and (2) Si adsorption by secondary minerals is high in alkaline soils. In the middle-aged sites, Si availability rises with the loss of carbonates and the formation of kaolinite that appears to drive its concentration, and then falls in the oldest sites with quartz enrichment. The increasing accumulation of biogenic silica following carbonate depletion indicates stronger soil–plant Si cycling as ecosystem development proceeds. A literature analysis confirms the shift in processes controlling Si availability between the carbonate and silicate weathering domains. Overall, our results show a nonlinear response of plant-available Si to long-term pedogenesis, with likely important implications for the Si-related functioning of terrestrial ecosystems.

3.2 Introduction

The global importance of the silicon (Si) cycle lies in its interaction with the global carbon cycle and its influence on plant performance. Silicon is a beneficial nutrient for vascular plants (Epstein 2009) and an essential nutrient for diatoms, which account for about 50% of the oceanic carbon fixation (Harrison 2000; Tréguer & Pondaven 2000; Conley & Carey 2015). The weathering of Si-bearing minerals consumes CO_2 on geological timescales (Berner *et al.* 1983), and Si has numerous functions in plant biology, including defense against biotic and abiotic stresses (Epstein 1994; Ma & Yamaji 2008; Cooke & Leishman 2016; Coskun *et al.* 2019; Leroy *et al.* 2019 for reviews). Plants take up monosilicic acid and produce amorphous silica in leaves, stems, and roots (Exley 2015). Biosilicification can reduce water, nutrient, salinity and metal stresses (Ma & Takahashi 1990b; Schaller *et al.* 2012b; Wu *et al.* 2013; Coskun *et al.* 2016; Meunier *et al.* 2017) as well as protect against herbivory (Massey & Hartley 2006) and fungal attacks (Fauteux *et al.* 2005). In this regard, providing data and information on Si availability to plants over long-term pedogenesis is important for our understanding of the biogeochemistry and ecology of terrestrial ecosystems.

The cycling of Si in terrestrial biomes is controlled by soil processes that drive the release of Si into soil solution as monosilicic acid (Bartoli 1983; Alexandre *et al.*

1997; Sommer *et al.* 2006). The 'plant-available Si' is directly available for plant uptake and is commonly quantified by extraction in dilute $CaCl_2$ (Sauer *et al.* 2006). Biocycling of Si in turn influences the distribution of Si in soils between pedogenic and biogenic pools through the return of phytoliths during litter decomposition (Alexandre *et al.* 1997; Lucas 2001; Cornelis *et al.* 2011b). Silicon can also leach from soil to hydrosphere which contributes about 80% of the input of Si to oceans (Treguer *et al.* 1995; Tréguer & De La Rocha 2013). The understanding of soil processes is therefore central to better decipher the dynamics of Si in terrestrial biomes and leaching to the hydrosphere (Cornelis *et al.* 2011a; Vander Linden & Delvaux 2019).

The chemical weathering rate of silicate minerals depends on their nature and particle-size, and the pH of the soil. During long-term pedogenesis under a humid climate, weathering acidifies the soil and alters its texture and mineralogy, possibly yielding different soil process domains (Vitousek & Chadwick 2013) according to the mineralogical context. For instance, soil formation can include a carbonate weathering domain followed by a silicate weathering domain, after the exhaustion of carbonate minerals (Chadwick & Chorover 2001). It is generally recognized that plant-available Si in soils decreases during pedogenesis due to desilication (i.e. Si loss; Savant *et al.* 1999; Chadwick & Chorover 2001; Lucas 2001). Yet how non-linear variation in soil properties affects plant-available Si remains poorly understood, although it is key to identify critical thresholds controlling Si cycling (Kreyling *et al.* 2018). In particular, studying variation in the plant-available Si concentrations across contrasted soil process domains occurring in similar climatic conditions is an ideal opportunity to address this gap. Here, we studied the 2-million-year Guilderton dune chronosequence in southwestern Australia, which is characterized by contrasting end-members of pedogenesis, to better understand how marked changes in soil mineralogy and pH drive changes in plant-available Si. Previous work on this chronosequence have identified the following soil processes: (1) carbonate weathering, (2) formation of iron (Fe) oxides and clay minerals, and (3) clay dissolution, Fe cheluviation, and quartz enrichment (Turner *et al.* 2018). Therefore, a carbonate weathering domain is followed by a silicate weathering domain. We hypothesized contrasting responses of the plant-available Si pool to these two process domains. In particular, for the silicate-weathering domain, we hypothesized a decrease of the plant-available Si pool over time through desilication. We assume Si release from carbonate-rich soils can be driven by contrasting processes for which the relative contribution is still unknown (Haynes 2019). We compared our results with literature data and discuss the implications for ecosystem processes.

3.3 Materials and methods

3.3.1 Experimental design

This chapter is based on the > 2-million-years Guilderton dune chronosequence and the first sampling design (see Chapter 2 for details). We selected the seven

chronosequence stages described by Turner *et al.* (2018) (Figure 2-2 in Chapter 2): three Holocene stages in the Quindalup system (stages 1-3), three Middle Pleistocene stages in the Spearwood system (stages 4, 5 and 6) and one Early Pleistocene stage in the Bassendean system (stage 7). For this Chapter, the original stages 5A, 5B and 6 (see Chapter 2) will be referred as stages 5, 6 and 7 respectively.

3.3.2 Soil sampling

We excavated one soil profile pit for each chronosequence stage (at least 1.5 m deep and 1 m^2 in area) at the same locations of soils sampled in the study carried out by Turner *et al.* (2018), taking care not to dig at the previously disturbed location (Figure 2-2 in Chapter 2). We then sampled the same pedogenic horizons, at the same depth as Turner *et al.* (2018). Each four sides of soil pits were sampled for soil horizons and then merged to get a composite soil sample for each soil horizon at each soil chronosequence stage.

3.3.3 Soil analysis

For each pedogenic horizon, texture, pH-$CaCl_2$ (pH_{CC}) and the concentrations of carbonate were published previously (Turner *et al.* 2018). Texture was determined by the pipette method following pretreatment to remove organic matter, with further separation of sand fractions by manual dry sieving. Carbonates were not destroyed prior to texture measurements. Soil pH was determined in 0.01 M $CaCl_2$ in a 1:2 soil to solution ratio. Carbonate concentrations were determined by mass loss after addition of 3 M HCl. The concentration of total free Fe (Fe_{DCB}), which comprises amorphous and crystalline Fe oxides, was determined after the dissolution in a Na-dithionite-citrate-bicarbonate (DCB) extract (Mehra & Jackson 1960), with Fe detection by ICP-AES.

We assessed mineralogy in bulk soil horizons representative of the three soil process domains identified by previous work, based on diagnostic horizons (Turner *et al.* 2018): carbonate weathering (C horizon of stage 1 and AC for stage 2), clay and Fe oxide formation (Bw1 for stage 3, Bw2 for stage 4), clay dissolution and Fe cheluviation (BE for stage 5, E1 for stage 6 and E1 for stage 7). The analysis was performed on the bulk soil without orientation. Analyses were done using a Bruker D8-Advance Eco diffractometer with a Cu-anode (University of Liège). Minerals were first identified using EVA v.3.2 (software of Bruker AXS GmbH) and the Crystallography Open Database (COD). Quantitative phase analysis was performed using Rietveld refinement with the TOPAS code and the graphical user interface Profex v.3.13.0.

Soil total aluminum (Al), calcium (Ca), Fe, potassium (K), magnesium (Mg), manganese (Mn), and sodium (Na) concentrations were determined by inductively coupled plasma spectrometry (ICP-AES) after calcination at 450 °C followed by a HF-$HClO_4$ digestion (Ciesielski *et al.* 1997). Soil total Si concentration was determined by ICP-AES after calcination at 450 °C followed by fusion at 1100 °C in a Pt/Rh crucible with 0.2 g of Li-tetraborate and 0.8 g Li-metaborate (Voinovitch *et*

al. 1962). The fusion bead was dissolved in diluted HNO_3 prior to analysis. We then calculated a modified mafic index of alteration (MIA; Babechuk *et al.* 2014). Silicate-bound CaO was not considered in the formula, because of the very high content of calcium carbonates in the first stages of soil development:

$$MIA_{modified} = 100 * \left[\frac{(Al_2O_3 + Fe_2O_3)}{Al_2O_3 + Fe_2O_3 + MgO + Na_2O + K_2O}\right]$$

where all the major elements are expressed in mole kg^{-1}.

Figure 3-1 describes the extractions for assessing the various Si forms in soil. This includes Si released from solution, adsorbed, amorphous and poorly crystalline forms. Si was quantified in all extracts by ICP-AES. The pool of so-called "plant-available" Si was determined by extraction in 0.01 M CaCl2 (Si_{iCC}; Haymsom & Chapman 1975; Sauer *et al*. 2006; Cornelis *et al.* 2011b; Georgiadis *et al.* 2013). The pool of "adsorbed" Si was determined by extraction in 0.5 M acetic acid (SiAA; Snyder 2001; Georgiadis *et al.* 2013). For both extractions, soil was shaken for 5 h at a 1:10 soil-to-solution ratio (Henriet *et al.* 2008b, a) before it was filtered (cellulose filter, pore size < 2 µm, Healthcare Whatman™). Carbonates were not destroyed prior to extraction, to preserve natural soil conditions and avoid alteration of other soil properties that might influence the dissolution of Si-bearing minerals.

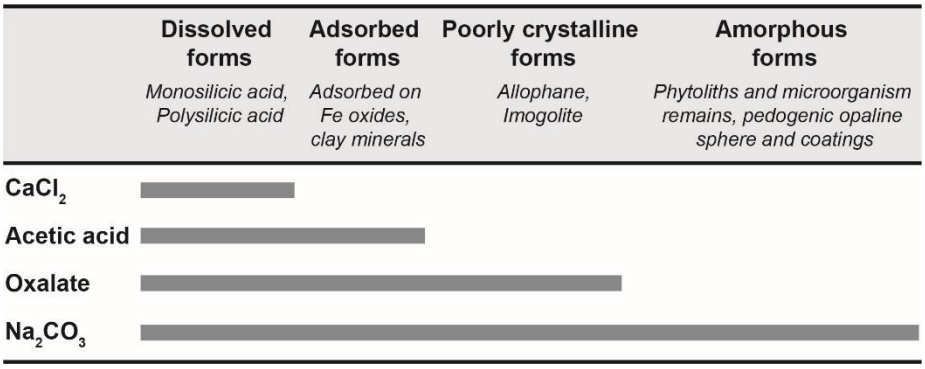

Figure 3-1 : Classification of silicon (Si) released from different forms using $CaCl_2$, acetic acid, oxalate and Na_2CO_3 extractions, adapted from Cornelis and others (2011b).

Silicon associated with poorly crystalline constituents and/or adsorbed onto weakly ordered sesquioxides (Si_{ox}) was estimated by extraction with ammonium oxalate-oxalic acid at pH 3 (Tamm 1922; de Endredy 1963; Duchaufour & Souchier 1966),. This extractant does not dissolve Si from amorphous silica (Wada 1989; Kodama & Ross 1991).

We used a kinetic Na_2CO_3 extraction (Saccone *et al.* 2007) to estimate a pool of Si (Si_{alk}) that includes biogenic opal (phytoliths) as well as pedogenic opal and Si sorbed onto mineral phases (DeMaster 1981; Clymans *et al.* 2011; Cornelis *et al.* 2011b, 2014). Briefly, 150 mg of soil was extracted in 40 mL of 0.1 M Na_2CO_3 for 5 h at 85

°C. Subsamples (1 mL) of solution were taken after 15, 60, 120, 180, 240 and 300 min, neutralized with 0.022 M HCl and quantified for Si. The concentration of Si_{alk} was estimated by extrapolating the linear part of the plot to zero (intercept value on Y-axis) (De Master 1981) to isolate the biogenic pool (i.e. mainly phytoliths) from litho-pedogenic silicate minerals.

3.4 Results

3.4.1 Soil physico-chemical properties

In the stages 1 to 3, the soils were carbonaceous (29-50% carbonate) and alkaline (pH_{CC} from 7.1 to 7.8; Table B-1). The clay fraction increased from 1.3% in stage 1 to 3.5-6.7% in stage 3 (Table B-1). Total depletion of carbonates occurred from stages 3 to 4, and the clay fraction decreased from stage 2.5-4.9% in stage 4 to <1% in stage 7 (Table B-1). The stages 4 to 7 were characterized by a pH_{CC} varying between 3.6 and 5.6 and decreasing with soil age. The $MIA_{modified}$ values increased with soil age from 9 to 31 in the carbonate soils, and from 68 to 100 in the carbonate-depleted soils, from stages 4 to 7 (Table B-2). Magnesium had been completely leached from stage 4 onwards, Na from stage 5 and K from stage 7, while Ca was still detectable in trace concentrations (0.1-0.5%) in stage 7 (Table B-2).

The Fe_{DCB} concentrations increased from stages 1 to 4 (0.3 to 1.5/3.1 g kg^{-1}; Table B-1), then decreased to undetectable concentrations in stage 7. The concentrations increased with depth in Bw horizons of stages 4 and 5 (from 1.5 and 1.0 to 3.1 and 3.4 g kg^{-1}).

Carbonate minerals inherited from the nearshore coastal environment were detected in stages 1 to 3 (Table 3-1): calcite, calcite-Mg and aragonite. The concentrations of primary minerals (K-feldspar and plagioclase) decreased with soil age, and stages 6 and 7 consisted entirely of quartz. Kaolinite was detected in the bulk soil of the Bw2 horizon of stage 4 and BE horizon of stage 5, but not in stages 6 and 7. The clay/fine silt mineralogy of the Swan Coastal Plain is mainly composed of kaolinite and marginally of gibbsite and vermiculite (Bastian 1996).

Table 3-1 : Estimation of the mineral abundance for each XRD diffraction pattern.

Mineral abundance (%)	Quartz	Calcite	Calcite-Mg	Aragonite	K-feldpar	Plagioclase	Kaolinite
Stage 1–C	51	10	26	12	1		
Stage 2–AC	55	10	25	9	1		
Stage 3–Bw1	56	13	15	10	4	2	
Stage 4–Bw2	92				4		4
Stage 5–BE	96				2		2
Stage 6–E1	100						
Stage 7–E1	100						

3.4.2 Silicon pools in soils

The Si_{CC} concentrations were the lowest in the first three stages, then increased from stages 3 to 4, followed by a decrease towards stage 7 (Figure 3-2A). The concentrations of "adsorbed" Si (Si_{AA}) followed the same pattern (Figure 3-2B). At stage 3, Si_{AA} concentrations were higher (3.1 - 6.0 mg kg^{-1}) than Si_{CC} concentrations (1.8 - 2.6 mg kg^{-1}), while Si_{AA} concentrations decreased to undetectable levels in stages 6 and 7, contrary to those of Si_{CC} that were between 2.2 and 3.7 mg kg^{-1}. In general, the Si_{AA} concentrations were higher than Si_{CC} concentrations only for clay-rich soils across the sequence (Figure D-1). For the same soil profile, Si_{CC} and Si_{AA} concentrations were generally constant, except for the Spearwood dunes (stages 4 to 6), where concentrations increased with depth, from the eluvial E horizon to the Bw horizon (Figures 3-2A, 3-2B). These Bw horizons showed the highest Si_{CC} and Si_{AA} concentrations of the sequence.

From stage 4 to 7, Si_{CC} concentrations are positively correlated with Fe_{DCB} content, clay content and pH_{CC} and negatively correlated with $MIA_{modified}$ (Figure 3-3).

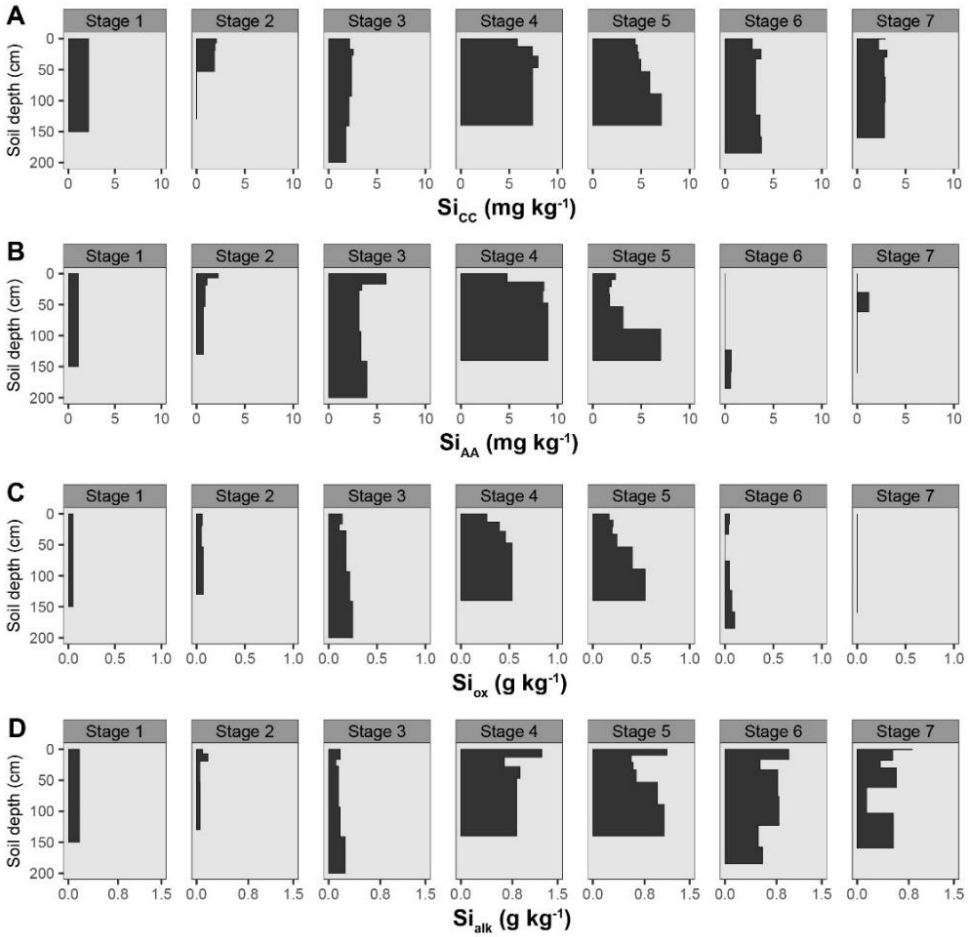

Figure 3-2 : Depth distribution of Si extracted with $CaCl_2$ in A (Si_{CC}), acetic acid in B (Si_{AA}), oxalate in C (Si_{ox}) and Na_2CO_3 in D (Si_{alk}).

The concentrations of Si_{ox} increased from stages 1 to 4 (Figure 3-2C; from 0.1 to 0.5 g kg^{-1}) followed by a decrease towards stage 7, where concentrations were below the detection limits. In stages 5 and 6, Si_{ox} concentrations increased with depth from E to Bw horizons (from 0.2 to 0.5 g kg^{-1}).

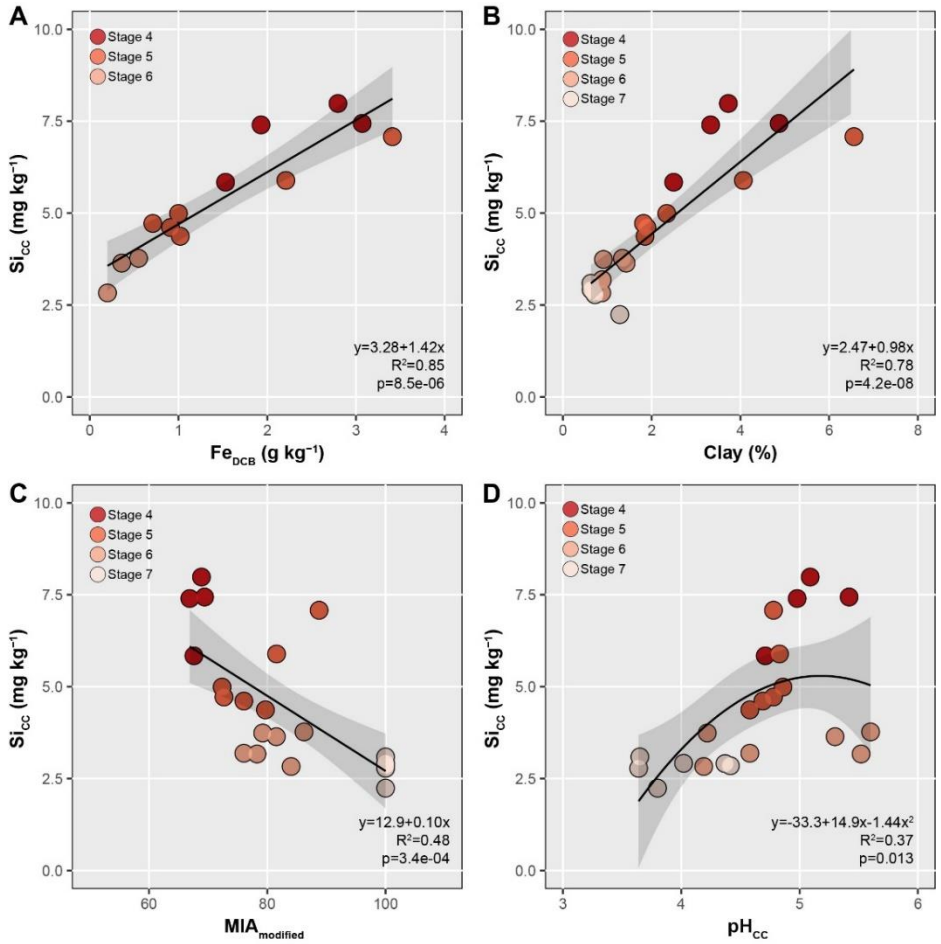

Figure 3-3 : Scatter plots of Si extracted with $CaCl_2$ (Si_{CC}) vs. Fe oxides (Fe_{DCB}) concentration in A, clay concentration in B, $MIA_{modified}$ in C and pH_{CC} in D for stages 4 to 7. Black lines indicate the regression line between both variables. Shaded areas represent 95% confidence interval of the regression. Equation regression, coefficients of determination (R^2) and p-values are shown.

The Si_{alk} concentration varied between 0.05 and 0.2 g kg^{-1} in stages 1 to 3 (Figure 3-2D). It strongly increased in stage 4 (1.2 g kg^{-1} in topsoil), before decreasing towards stages 6 and 7 (< 1 g kg^{-1}). Si_{alk} concentrations were higher in the A horizon than in subsoil. In stage 5, Si_{alk} decreased from A to E horizon (from 1.1 to 0.6 g kg^{-1}) and then increased from E to Bw horizon (1.1 g kg^{-1}).

3.5 Discussion

3.5.1 Soil development across the Guilderton chronosequence

Our results demonstrate a clear pattern of pedogenic change along the Guilderton dune chronosequence. In the early stages, carbonate loss through weathering buffers soil pH at alkaline values, and Fe oxides and clay minerals are formed. Following exhaustion of carbonate minerals, kaolinite is synthesized, the soil pH declines, and the $MIA_{modified}$ values strongly increase. In the later stages of the chronosequence, pedogenesis involves clay dissolution and Fe cheluviation, including the total loss of K-feldspars, kaolinite and plagioclase. As a result, the Guilderton chronosequence is characterized by three major soil processes: carbonate weathering and leaching, formation of clay-sized minerals followed by their loss through eluviation, resulting in quartz-enrichment.

Despite a negative water balance (-750 mm yr^{-1}) at the Guilderton chronosequence, there was substantial weathering in the soil, including carbonate depletion and loss of Fe oxides/clay minerals by eluviation. This might be explained by a wetter climate during late Holocene/Pleistocene periods and/or by the strong seasonality of current rainfall, which occurs primarily in the winter. Paleoclimatic studies indicate increased aridity in inland areas of southwestern Australia during glacial maxima (Wyrwoll *et al.* 2014), which is inconsistent with a more humid climate and more active weathering during paleoclimate events. Moreover, the climate of the coastal sandplains appears to have been well buffered from the drier conditions inland, with little variation from modern time to the late Miocene/Pleistocene, both in terms of geomorphology and climate (Wyrwoll *et al.* 2014). Soils along the Guilderton chronosequence are very well-drained due to their sandy texture, particularly so for our sampling locations on dune crests far above the water table (Turner *et al.* 2018). Therefore, rainwater moves vertically through the soil at all times during the wet season. We therefore conclude that the seasonality of rainfall (around 70% of annual rainfall occurs during a 4-month-period) drives weathering along the sequence, as supported by the presence of a petrocalcic horizon (calcrete) at 285 cm depth at stage 4 (Turner *et al.* 2018).

3.5.2 Soil process controls on Si changes over long-term pedogenesis

Si_{CC} concentrations measured in Guilderton soil chronosequence were generally low compared to values reported in the literature (<10 mg kg^{-1}; Table D-1 for a compilation of literature data), presumably due to the high proportion of sand-sized quartz minerals. Quartz is one of the most stable minerals in the Goldich dissolution series (Goldich 1938), which implies low solubility, and therefore a low rate of dissolution (Fraysse *et al.* 2009). This slow dissolution rate is reinforced by the small specific surface area of sand-sized minerals. For instance, Quigley *et al.* (2016) reported Si_{CC} values from 50 to 150 mg kg^{-1} in a wide variety of soil types in the

Serengeti grassland ecosystem in northern Tanzania/southern Kenya, dominated by higher proportion of fine-sized and reactive minerals (e.g., smectite). On the other hand, studies reported Si_{CC} concentrations closer to the present ones, ranging from 1 to 10 mg kg^{-1} in strongly weathered tropical soils in central Panama (Schaller *et al.* 2018) and 7.2 mg kg^{-1} in a weathered sandy soil located in the Chase National Park near Sydney, Australia (Cooke & Leishman 2012).

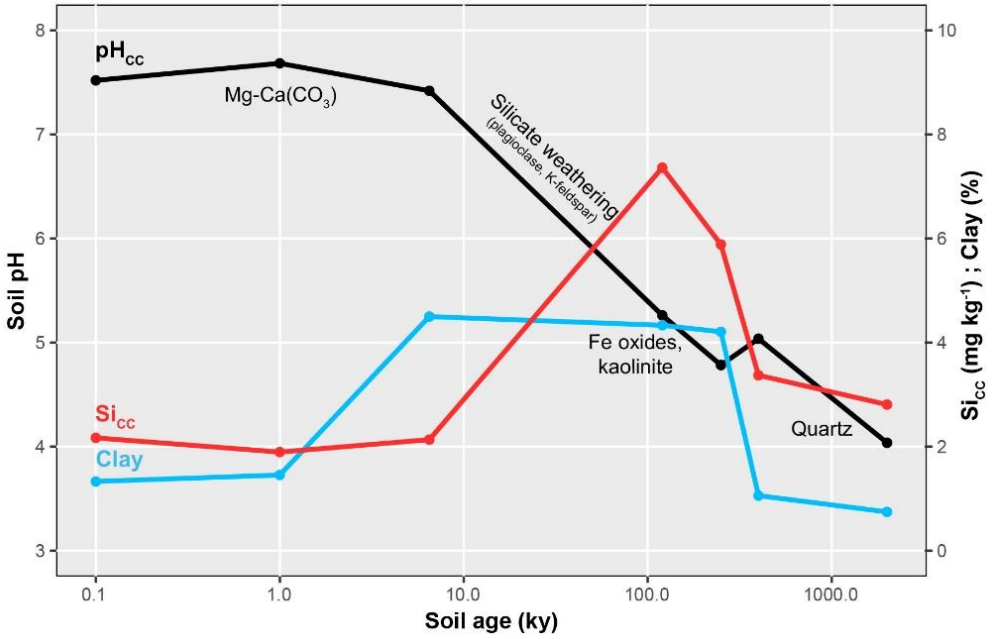

Figure 3-4 : Evolution of soil mineralogy, pH, clay and Si_{CC} concentrations across the Guilderton chronosequence. Data for each chronosequence stage are the depth-weighted mean value of all horizons of the respective soil profile. The soil age scale is logarithmic.

Long-term soil formation induced marked changes on the pool of Si_{CC} (Figure 3-4). In particular, we observed a non-linear response of plant-available Si to pedogenesis, associated with the change of soil process domain after carbonates loss.

The high values of pH (alkaline soil) in the early stages of pedogenesis might increase Si availability by increasing the dissolution of Si-bearing minerals in soils (Drever 1994; Kelly *et al.* 1998; Fraysse *et al.* 2009). However, Si_{CC} and Si_{AA} concentrations were low in these stages of soil development, those of Si_{CC} being among the lowest reported in the literature (< 2.5 mg kg^{-1}, Table D-1 for literature references). Three hypotheses may account for this low Si_{cc} concentrations: (1) the H^+ flux through the soil preferentially consumes carbonate minerals as they have a higher solubility than Si-bearing minerals (Goldich 1938); (2) a relatively low concentration of Si-bearing minerals, due to a "dilution effect" caused by the carbonate minerals; (3) an increasing sorption of Si onto Fe oxide surfaces in alkaline soils (McKeague &

Cline 1963b; Savant *et al.* 1999) could lower Si concentrations extracted in $CaCl_2$ (McKeague & Cline 1963a; Haynes & Zhou 2018; Meunier *et al.* 2018). Given the low concentrations of Fe oxides, sorbed Si (Si_{AA}) and Si associated with poorly crystalline constituents (Si_{ox}) in the first two stages of soil development, the low Si_{CC} concentrations were unlikely to be due to sorption processes (Haynes & Zhou 2018). The proportion of plant-available Si in total Si (Si_{CC}/Si_{tot} ratio) ranged from 6×10^{-6} to 10×10^{-6} in stages 1, 2, 3, then increased from 10×10^{-6} to 20×10^{-6} in stages 4 and 5, and finally decreased below 10×10^{-6} in stages 6 and 7. This demonstrates that the ability of the soil to release Si for plants decreased in the carbonate domain. We suggest that the buffering of Si release by the preferential H^+ consumption by carbonate minerals is the main process maintaining low Si availability in the early stages of soil development.

At stage 3, Si_{ox}, Fe_{DCB} and clay concentrations increased as well as the proportion of Si-bearing primary minerals. Yet, this stage was characterized by a low plant-available Si concentration, likely caused by the higher soil ability to adsorb Si, given the significant increase of Fe oxide content. This hypothesis is supported by the increase at this stage of Si extracted with acetic acid (Si_{AA}) – commonly used to estimate sorbed Si in soils (Haynes and Zhou 2018). Across the sequence, the Si_{AA} concentrations were higher than Si_{CC} concentrations only for clay-rich soils, supporting the impact of clay-sized minerals (Fe oxides, kaolinite) on monosilicic acid adsorption onto surfaces of Fe oxides and to the edge sites of kaolinite (Nguyen *et al.* 2017). We suggest that the low Si_{CC} concentration in this stage of soil development is explained by the combination of two processes: low Si release rates given H^+ consumption by carbonate minerals combined with strong Si sorption.

In the intermediate stages (stages 4 and 5), the formation of kaolinite and Fe oxides associated with the loss of carbonates and the decrease of soil pH (i.e. decrease in Si adsorption potential) explain the marked increase in Si_{CC}, Si_{AA} and Si_{ox} concentrations. These stages are characterized by the highest Si_{CC}/Si_{tot} ratio of the sequence (between 10×10^{-6} and 20×10^{-6}). From these stages and until the last one, the desorption of Si from Fe oxides and the dissolution of kaolinite appear to be the main drivers of plant-available Si concentration over soil formation.

The decrease of Si_{AA} and Si_{ox} concentrations is driven by desilication through clay mineral dissolution and Si desorption from Fe oxides. This explains that Si_{CC} concentrations decrease with increasing soil weathering and acidification. In these strongly-weathered soils, the Si_{CC}:Si_{tot} ratio was among the lowest, but still similar to the first stages of soil development (between 5×10^{-6} and 10×10^{-6}). In this soil, plant-available Si can originate from the dissolution of either quartz (Cornu *et al.* 1998; Do Nascimento *et al.* 2008) or amorphous biogenic silica (phytoliths) (Sommer *et al.* 2013; Li *et al.* 2020b). Although quartz is more abundant than phytoliths (Alexandre *et al.* 1997, 2011; Blecker *et al.* 2006; Sommer *et al.* 2013), the order-of-magnitude greater solubility of amorphous silica compared with quartz (Dove 1995; Fraysse *et al.* 2009) cannot allow us to rule out a contribution of phytoliths in the replenishment

of plant-available Si (Sommer *et al.* 2013; Li *et al.* 2020b) in the oldest soils of the chronosequence.

3.5.3 Biogenic silica accumulation in soils during long-term ecosystem development

Hot Na_2CO_3 extraction dissolves easily-soluble Si pools: phytoliths, Si adsorbed on Fe oxides and short-range ordered aluminosilicates. The fact that alkali-extractions were not specific to phytoliths is shown by the results from stage 5, where the Si_{alk} concentration decreased from A to E horizons and then increased in Bw horizons, where Si adsorbed/occluded onto clay minerals/ Fe oxides made a contribution (Barão *et al.* 2014). We discuss the concentration of Si_{alk} in the upper A and AE horizons to focus on the contribution of phytoliths, while avoiding the contribution of clay-sized minerals present in deeper Bw horizons.

The strong increase of Si_{alk} concentrations from stage 4 is related to the accumulation of biogenic silica in soils. Although soil alkalinity could increase the dissolution of phytoliths (Fraysse *et al.* 2009), we assume that this cannot entirely explain the 7 times higher Si_{alk} concentration in the topsoil of stage 4 compared to stage 3 and we relate this increase to a higher annual return of phytoliths on topsoil. This could be explained by variation in the ANPP and, therefore, litter production, or by the increase in the plant-available Si concentrations enhancing the mobility of Si in the soil-plant system. This increase could result in higher plant Si concentrations (Henriet *et al.* 2008a) and/or the selection of Si-accumulator species.

3.5.4 Soil process domains and plant-available Si concentrations

Our compilation of literature data comparing Si_{CC} concentration and soil pH values (Figure 3-5, Table D-1 for data) indicate strong variations within a pH class. This is explained by contrasting mineralogy and climate among studies. Methodological differences, including variation in shaking time and soil:solution ratio used during the 0.01 M $CaCl_2$ extraction, might also be a factor (Sauer *et al.* 2006). Nevertheless, SiCC concentrations tend to increase with increasing soil pH up to pH 7, roughly corresponding to the transition between the silicate and carbonate weathering domains. This relation is explained by the fact that soil pH is strongly related to soil weathering (Chadwick & Chorover 2001), which is the process responsible for soil desilication as demonstrated here and elsewhere (Meunier *et al.* 2018). The increase of Si_{CC} concentrations with pH does not last in the carbonate weathering domain, where Si_{CC} concentrations values tended to decrease. The assumed role of H+ consumption by carbonate minerals and increased Si sorption as mechanisms buffering plant-available Si concentrations in the carbonate weathering domain is therefore observable on a global scale. This demonstrates the non-linear response of Si_{CC} to long-term soil formation with the occurrence of a shift between the carbonate and silicate weathering domains.

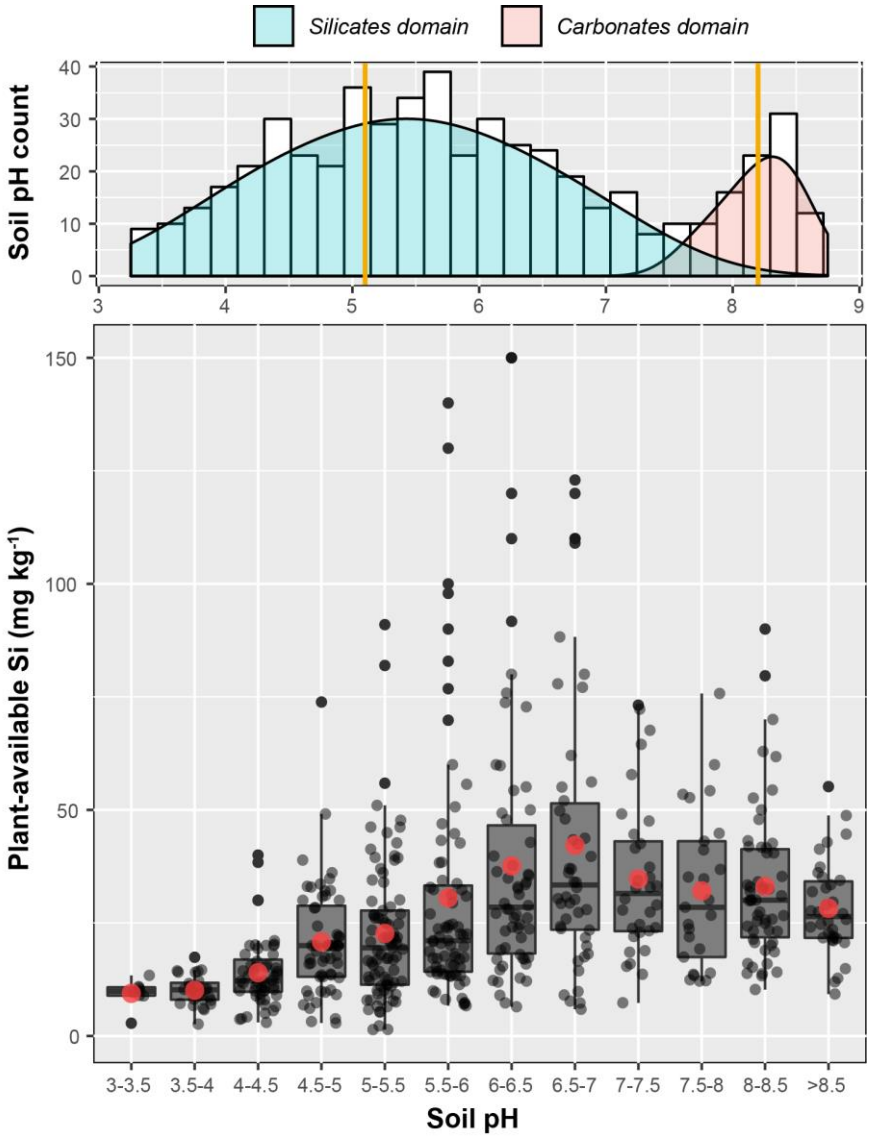

Figure 3-5 : Data of soil pH and Si_{CC} concentrations from 14 studies (n=553; Table D-1 for details). To extract data published as figures, we used WebPlotDigitizer (Rohatgi 2012). The upper histogram represents the soil pH counting, from 3 to 9. The pH value to separate the silicates domain from the carbonates domain has been arbitrarily chosen as being 7.5, to facilitate the reading. Yellow lines show the predicted pH values for $CaCO_3$-buffered soils (8.2) and $Al(OH)_3$-buffered soils (5.1; Slessarev *et al.* 2016). The bottom boxplot represents the Si_{CC} concentrations for each pH class, from 3-3.5 to >8.5. The red points indicate the mean value for each pH class. The x-axes of the upper histogram and the bottom boxplot are adjusted in terms of pH value.

3.5.5 Understanding long-term Si dynamics in soils: potential implications for ecosystem processes

The plant responses to Si availability and their potential role in ecological functions have been studied primarily in laboratory experiments under controlled conditions, with little information on Si dynamics under natural conditions (Cooke & Leishman 2011a). Lab- and model-based results may differ from field conditions, as fully isolated environmental factors in manipulation experiments aim to improve mechanistic understanding of processes that can be implemented in models. In our long-term soil chronosequence approach, the study of natural soil gradients allows us to detect and quantify non-linear responses of plant-availability of Si. Here, we show that soil processes drive marked changes in Si availability for plants during long-term ecosystem development. In particular, our results demonstrate that carbonate dissolution, clay formation and element cheluviation drive the availability of Si. A number of terrestrial ecosystem processes can be affected by Si plant-availability (Figure 3-6). This is of particular interest to elucidate how environmental factors and the resulting soil processes affect Si-related ecological functions.

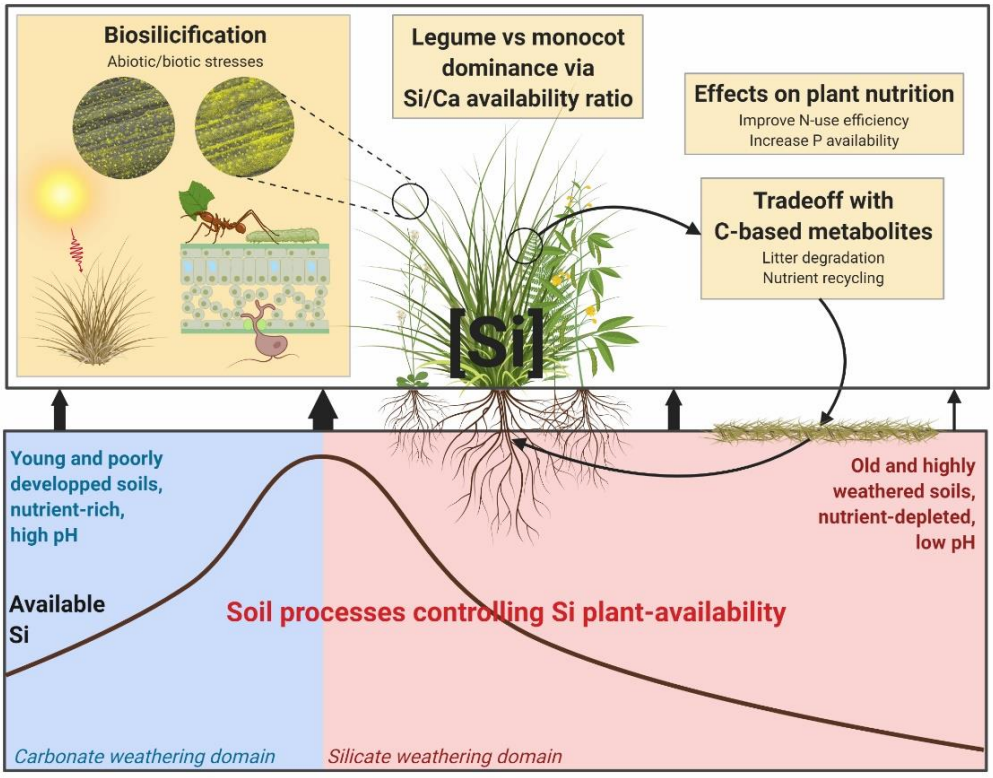

Figure 3-6 : Schematic representation of soil processes controlling Si availability across long-term ecosystem development and potential implications.

Plant biosilicification is now recognized as an important regulatory mechanism for several biotic and abiotic stresses (Coskun *et al.* 2019; Exley & Guerriero 2019) such as herbivore/fungal attack, water and UV stress. Biosilicification reinforces leaf structure, which mitigates the effect of water stress (Meunier *et al.* 2017) and increases leaf abrasiveness, which enhances tooth or mouthpart wear (Massey *et al.* 2006). Also, the digestibility of plant material by herbivores is reduced by silica deposits (Massey & Hartley 2006), and this results in a reduced feeding on plants with a high Si concentration (Massey *et al.* 2006, 2007a). The controls of Si availability on plant biosilicification during long-term soil development may have cascading effects on stress sensitivity and/or herbivore attacks.

A tradeoff between Si and carbon-based metabolites has been reported (Schoelynck *et al.* 2010; Klotzbücher *et al.* 2018c; Schaller *et al.* 2019). Silicon availability can also impact nutrient stoichiometry and organic matter decomposition rates (Schaller *et al.* 2012b, 2014; Marxen *et al.* 2016). This may have a significant impact on nutrient cycling and organic matter dynamics in terrestrial ecosystems.

Increasing Si availability can enhance the concentration of available P for plants in P-impoverished soils, and improve N-use efficiency (Ma & Takahashi 1990b; Datnoff *et al.* 2001b; Neu *et al.* 2017). This highlights the potential role of Si in interacting with macronutrients, particularly P which often limits terrestrial plant productivity, especially during ecosystem retrogression (Vitousek & Farrington 1997; Elser *et al.* 2007; Laliberté *et al.* 2012).

Schaller *et al.* (2017) recently showed that relative Si/Ca availability may have a significant effect on legume/grass dominance/competition, as grasses are Si-accumulators and legumes are Ca-accumulators. Like grasses, sedges accumulate Si (Hodson *et al.* 2005; Cooke & Leishman 2012) and are abundant along the nearby Jurien Bay chronosequence (Zemunik *et al.* 2016). Silicon availability is limited in the first stages of soil development at Guilderton, while that of Ca was likely very high in carbonate-rich soils. After carbonate exhaustion, Si availability increased, while that of Ca decreased (Turner *et al.* 2018). These contrasting responses of Si and Ca to soil development suggests that the degree of soil weathering could be a driver of legume/sedge relative distribution, which can imply likely cascading effects on grazing, organic matter decomposition and nutrient cycling in this terrestrial ecosystems (Schaller *et al.* 2017).

3.6 Conclusion

The pattern of soil Si dynamics during long-term pedogenesis with extreme mineralogical end-members has been highlighted. Our original hypothesis that plant-available Si would respond differently to the carbonate and silicate weathering domains was supported. The decrease in plant-availability of Si in the silicate-weathering domain, as predicted by desilication, was confirmed by the data and literature analysis. However, we demonstrate the existence of a buffer to Si availability exerted by carbonate minerals in the early stages of soil formation, which

is also evident on a global scale. This has not been proposed previously, and could significantly impact Si fluxes, both towards the hydrosphere and terrestrial vegetation. This is important as Si transfer to oceans affects the growth of diatoms (Olsen & Paasche 1986; Nelson & Dortch 1996), and therefore drives temporary CO_2 consumption in oceans (Harrison 2000). In terrestrial vegetation, this non-linear response of plant-availability of Si to long-term soil development may have significant effects on different processes including plant performance and distribution because Si may mitigate numerous biotic and abiotic stresses and affect legume/monocot dominance in grass- and shrubland ecosystems.

4

Plants sustain the terrestrial silicon cycle during ecosystem retrogression*

*This Chapter is adapted from

de Tombeur, F., Turner, B.L., Laliberté, E., Lambers, H., Mahy, G., Faucon, M-P., Zemunik, G., Cornélis, J-T. (2020). Plants sustain the terrestrial silicon cycle during ecosystem retrogression. *Science*

4.1 Foreword

In the previous chapter, we studied soil Si pools along the 2-million-year Guilderton chronosequence to understand the influence of long-term mineralogical evolution on Si dynamics. We emphasized the major influence of carbonates dissolution, clay formation and quartz enrichment on soil Si dynamics, and highlighted a shift in processes controlling Si availability between the carbonate and silicate weathering domains. We also evidenced an increased accumulation of biogenic silica in the older soils, suggesting stronger soil–plant Si cycling as ecosystem development proceeds. However, how phytoliths formation in plants followed by their dissolution in soils influence soil-plant Si dynamics has not been considered. The older soils are highly-desilicated and dominated by poorly-soluble quartz minerals, and phytoliths dissolution could play a key role to replenish Si in soil solution. In this new chapter, we combined results from the previous chapter to analyses of soil Si pools along the 2-million-year Jurien Bay chronosequence, and we extracted phytoliths from the soils of both chronosequences. In addition, we quantified Si and major nutrients in the most abundant plants growing along the best-studied of the two chronosequences (Jurien Bay) to indicate the degree of elemental biocycling. This experimental design and these analyses will allow us to estimate the intensity of the Si biological feedback loop as a function of soil weathering degree.

4.2 Summary

The biogeochemical silicon cycle influences global primary productivity and carbon cycling, yet changes in silicon sources and cycling during long-term development of terrestrial ecosystems remain poorly understood. Here, we show that terrestrial silicon cycling shifts from pedological to biological control during long-term ecosystem development along 2-million-year soil chronosequences in Western Australia. Silicon availability is determined by pedogenic silicon in young soils and recycling of plant-derived silicon in old soils as pedogenic pools become depleted. Unlike concentrations of major nutrients, which decline markedly in strongly weathered soils, foliar silicon concentrations increase continuously as soils age. Our findings show that the retention of silicon by plants during ecosystem retrogression sustains its terrestrial cycling, suggesting important plant benefits associated with this element in nutrient-poor environments.

4.3 Introduction

Silicon (Si) is widely recognized as an important regulator of the global carbon cycle via its effect on diatom productivity in oceans (Tréguer & Pondaven 2000) and the weathering of silicate minerals on continents (Conley & Carey 2015). It is also a beneficial plant nutrient (Epstein 2009; Debona *et al.* 2017), improving resistance to herbivory and pathogens (Hartley & DeGabriel 2016) and mitigating the negative effects of several abiotic stresses (Cooke & Leishman 2016), including nutrient limitation (Kostic *et al.* 2017; Quigley *et al.* 2020). As a result, Si significantly

improves plant performance and can contribute to the functioning of terrestrial ecosystems (McNaughton *et al.* 1985; Cooke & Leishman 2011a; Hartley & DeGabriel 2016). Detailed information on long-term controls on Si cycling therefore underpins our understanding of Si-related functions in plants, fluxes to aquatic ecosystems, and ultimately the fixation of atmospheric C in terrestrial and oceanic ecosystems.

The release of Si into the soil solution regulates its availability to plants and its transfer from land to oceans. While the concentration of dissolved Si in the soil solution has long been understood to be driven primarily by geochemical processes (i.e. mineral dissolution), it is now recognized that Si mobility is influenced strongly by plant biocycling (Alexandre *et al.* 1997; Derry *et al.* 2005; Cornelis & Delvaux 2016). The polymerization of amorphous silica in leaf tissues (i.e. the formation of phytoliths) and its return to topsoil after leaf shedding builds a pool of reactive silicate in soil (Fraysse *et al.* 2009). However, the magnitude of geochemical versus biological processes in controlling the release of Si to the soil solution remains debated. While soil scientists often assume that geochemical processes control dissolved Si concentrations (Meunier *et al.* 2018), mass-balance calculations suggest a strong imprint of biological processes (i.e. phytolith formation in plants and dissolution in soils) on the Si cycle (Bartoli 1983; Alexandre *et al.* 1997; Sommer *et al.* 2013), driven by the order-of-magnitude greater dissolution rate of phytoliths compared to clay minerals (Fraysse *et al.* 2009). As soil Si is derived ultimately from the parent rock, plant-available Si concentrations are expected to decrease with soil age through desilication (i.e. Si leaching during pedogenesis) (de Tombeur *et al.* 2020b), increasing the importance of biological processes as soils and ecosystems develop (Derry *et al.* 2005; Cornelis & Delvaux 2016). However, the emergence of biological control of terrestrial Si cycling as soils age is still poorly understood, in part because of the limited number of study systems spanning sufficiently long timescales.

To quantify changes in pedological and biological controls of Si cycling during long-term ecosystem development, we studied Si in soils and plants along a pair of 2-Ma coastal dune chronosequences in southwestern Australia (Turner *et al.* 2018). Such long-term chronosequences that have not been directly affected by Pleistocene glaciations are rare worldwide (Peltzer *et al.* 2010). The Jurien Bay and Guilderton chronosequences include the end-members of soil formation (Turner & Laliberté 2015; de Tombeur *et al.* 2020b), providing a rare opportunity to study long-term shifts in biogeochemical cycles. Soil development along these chronosequences includes carbonate leaching from Holocene soils (<6.5 ka; stage 1 to 3), formation of secondary Si-bearing minerals in young Mid-Pleistocene soils (~120 ka; stage 4) followed by their loss via dissolution in medium-aged and old Mid-Pleistocene soils (~250-500 ka; stage 5), to yield quartz-rich soils of Early-Pleistocene age (~2,000 ka; stage 6) (Turner & Laliberté 2015; de Tombeur *et al.* 2020b). Along each chronosequence we quantified the pools of reactive Si-bearing phases and plant-available Si in the soils, and physically extracted phytoliths. In addition, we quantified major nutrients in the most abundant plants growing along the best-studied of the two chronosequences

(Jurien Bay) (Hayes *et al.* 2014; Laliberté *et al.* 2014; Turner & Laliberté 2015). We used the concentrations of Si and nutrients in mature leaves to indicate the degree of elemental biocycling. We hypothesized that the pool of reactive Si in soils would be increasingly dominated by plant-derived Si (i.e. phytoliths), rather than soil-derived Si as soils aged. Consequently, plant-available Si concentrations would be driven increasingly by recycling from phytoliths. We also hypothesized that plant foliar Si concentrations would decrease with soil age due to the loss of Si-bearing minerals and quartz-enrichment, as it does for the major rock-derived nutrients such as phosphorus during long-term pedogenesis (Hayes *et al.* 2014).

4.4 Materials and methods

4.4.1 Experimental design

This chapter is based on the 2-million-years Jurien Bay and Guilderton dune chronosequences and both sampling designs (see Chapter 2 for details).

According to the first sampling design, we selected six and seven stages of soil development along the Jurien Bay and Guilderton chronosequences, respectively, for soil sampling (Figure 2-2 in Chapter 2): three Holocene stages in the Quindalup system (stages 1-3), three Middle Pleistocene stages at Guilderton (stages 4, 5A and 5B) and two at Jurien Bay (stages 4 and 5) in the Spearwood system, and one Early Pleistocene stage in the Bassendean system (stage 6).

Plants were sampled at the Jurien Bay chronosequence, according to the second sampling design. For each chronosequence stage, except for stage 5, we randomly selected five plots (10 x 10 m each) within 10 plots previously characterized (Hayes *et al.* 2014; Zemunik *et al.* 2016) (see Chapter 2 for details). The relative canopy cover of each species in each plot was estimated previously (Zemunik *et al.* 2016). In total, 25 plots were selected for plant sampling at the Jurien Bay chronosequence (Figure 2-5 in Chapter 2 for plot locations). These plots were not at the exact same location as the soil pits (Figure 2-5), but always on the same dune and pedological context, with similar age (Quindalup young, stage 1; Quindalup medium, stage 2; Quindalup old, stage 3; Spearwood stage 4 and Bassendean stage 6) (Hayes *et al.* 2014; Zemunik *et al.* 2016).

4.4.2 Soil and plant sampling

For the six and seven selected chronosequence stages, we excavated one soil profile pit (at least 1 m deep and 1 m^2 in area) at the same locations described elsewhere (Turner & Laliberté 2015; Turner *et al.* 2018), being careful not to dig at the previously disturbed location. We then sampled the same pedogenic horizons, at the same depth (Turner & Laliberté 2015; Turner *et al.* 2018). Each sample was a mixture of four subsamples, collected on each side of the soil pit. Samples were oven-dried at 40°C and sieved to 2 mm. Litter was found and sampled only at stage 6 of the Jurien Bay sequence.

In the 25 plots selected for plant sampling, we sampled the 10 most-abundant species as defined elsewhere (Zemunik *et al.* 2016), for a total of 238 individuals. In some cases, some species originally defined in the 10 most-abundant species (Zemunik *et al.* 2016) were not found on the plot, which explains that the total number of individuals sampled does not reach 250. Additional widespread species were sampled to assess species-level changes across multiple stages. All leaf material was collected over a two-week period in November 2018. Only healthy mature individuals were selected for sampling. Most of the time, leaves were sampled from one individual plant per species in each plot. When an individual did not have enough biomass for analysis (e.g., Cyperaceae spp.), samples from different individuals were bulked. In each plot, the species sampled accounted for 63% to 91% of the total canopy cover.

4.4.3 Determination of soil mineralogy and weathering indicators

We assessed soil mineralogy in one horizon of each soil profile, representative of the main soil processes occurring in the soil chronosequences, in line with the trajectory of pedogenesis: carbonate weathering, clay and Fe-oxide formation, clay dissolution and Fe cheluviation. The horizons selected for each stage were C2, CA, B1, B2, BE and E for Jurien Bay, and C, AC, Bw, B2, BE, E1 and E1 for Guilderton. The analyses were described in the section 3.3.3 (Chapter 3).

Soil total Ca, Mg, K, and Na concentrations were determined as described in the section 3.3.3 (Chapter 3). We then calculated the total reserve in bases (TRB) as the sum of total alkaline and alkaline-earth cations (Na^+, K^+, Ca^{2+}, Mg^{2+}; in $cmol_c\ kg^{-1}$) in order to estimate the degree of soil weathering.

The concentration of total free iron (Fe_{DCB}), which comprises amorphous and crystalline Fe-oxides, was determined as described in the section 3.3.3 (Chapter 3).

4.4.4 Determination of Si forms in soil

Two extraction procedures were used to estimate the pools of reactive Si that mainly contribute to the release of Si in soil solution.

First, we conducted an extraction with ammonium oxalate-oxalic acid at pH 3 (Tamm 1922), as described in the section 3.3.3 (Chapter 3).

Second, we performed Na_2CO_3 extractions (Vandevenne *et al.* 2015). This extractant easily dissolves the biogenic Si pool (mainly phytoliths here), but also Si sorbed or occluded in reactive mineral phases of pedogenic origin (Vandevenne *et al.* 2015). We performed continuous extractions with the determination of Si and Al to better discern the biogenic Si pool from the pedogenic Si pool. Briefly, 150 mg of soil was mixed with 40 mL of 0.1 M Na_2CO_3 for 5 h at 85°C. Subsamples (1 mL) of solution were taken after 15, 60, 120, 180, 240 and 300 min, and neutralized with 0.022 M HCl. The poorly-reactive Si forms (linear dissolution) were separated from the highly-reactive Si forms (nonlinear dissolution) by extrapolating the linear part of

the plot to the intercept on the y axis (De Master 1981). Then, the ratio of the highly-reactive Si forms to Al was used to trace the forms of Si extracted: a ratio >5 suggests a major contribution of phytoliths, a ratio between 1 and 5 suggests a major contribution by pedogenic clay minerals. A ratio <1 suggests the presence of a more weathered product resulting from pedogenic processes (Vandevenne *et al.* 2015). As this Na_2CO_3-reactive Si pool can have different mineral origins, it is referred as "alkali-reactive Si".

Plant-available Si concentrations were estimated through a 21-day 0.01 M $CaCl_2$ extraction with a soil:solution ratio of 1:10 (Schachtschabel & Heinemann 1967). As shaking can increase the plant-available Si concentrations due to quartz abrasion, samples were only manually shaken twice a day (Sommer *et al.* 2013). Long extractions allow an equilibration between soil and solution, thus closer to field conditions and facilitating the identification of the mineral sources controlling the plant-available Si concentration. Fifty µL of 0.1% NaN_3 was added to prevent microbial activity (Schachtschabel & Heinemann 1967). The extractant was filtered (cellulose filter, pore size <2 µm, Healthcare Whatman™), acidified with 50 µL of ultrapure 65% HNO_3 and stored in darkness at 4°C prior to analysis.

Silicon and Al were quantified in the $CaCl_2$-, oxalate- and Na_2CO_3-extractable solution by ICP-OES. All Si pools were converted into stocks over a 50 cm depth by using soil bulk density and horizon thickness.

4.4.5 Physical extraction and observation of soil phytoliths

Soil phytoliths were physically extracted by gravimetric separation (Aleman *et al.* 2013) from all soil horizons. To do so, 20 g of dry soil was sieved at 0.25 mm, transferred into a 500 mL beaker for carbonate soils or into a 50 mL centrifuge tube for non-carbonate soils. Carbonates were digested with 1 M HCl, and samples were then transferred into a 50 mL centrifuge tube. Centrifuge tubes were placed in a water bath at 80 °C where organic matter was oxidized with 15% H_2O_2. Once the reaction stopped, samples were deflocculated by shaking them with a 5% $NaPO_3$ solution for 12 h. The <2 µm fraction was then removed by three centrifugation-decanting cycles. Finally, the phytoliths were isolated with sodium polytungstate (density of 2.32 g cm^{-3}), pipetted, filtered by a 1 µm Teflon filter and weighed. Samples were rinsed three times with distilled water between each step.

In order to estimate the dissolution of soil phytoliths, we performed microscopic observations in one soil profile randomly selected for each chronosequence – stage 6 of Jurien Bay, and stage 5A of Guilderton. Soil phytoliths were mounted on glass slides using double-sided carbon tape and bridged with silver paint before being gold-coated for SEM-EDX analysis. For each horizon, we randomly selected 50 identifiable phytoliths on the micrograph and each was assigned to a class of dissolution: (1) plain phytoliths + small surface etching, (2) pronounced surface etching, and (3) strong dissolution features (Sommer *et al.* 2013).

4.4.6 Foliar mineral analyses

The 250 plant samples were washed with distilled water and dried at 70°C for 48 h. A 0.5 g sample was placed in a porcelain crucible and calcinated at 450°C for 24 h. The remaining ashes were mixed with 1.6 g of Li-metaborate and 0.4 g of Li-tetraborate in a graphite crucible and placed in an oven at 1000°C for 5 min (Nakamura *et al.* 2020a). The bead was then dissolved in 15% HNO_3 and the concentrations of Si, P, K, Ca and Mg were determined by ICP-OES.

4.4.7 Data and statistical analyses

To characterize foliar Si and nutrient concentrations in plant communities across the Jurien Bay chronosequence, we estimated the mean values of the 10 most-abundant species per plot, weighted or not by their relative cover. The cover-weighted mean (CWM) was calculated as follows (Violle *et al.* 2007):

$$CWM = \sum_{i=1}^{S} t_i \times RC_i$$

where t_i and RC_i are, respectively, the value of the trait t and its relative cover RC for a species i and S is the number of species.

The difference in the mean and CWM foliar [Si] and concentrations of other measured nutrients between the chronosequence stages were tested by one-way analysis of variance (ANOVA), followed by post-hoc multiple comparison (Fisher's Least Significant Difference [LSD] tests). Residuals were visually inspected for heteroscedasticity. When necessary, data were log-transformed to meet the model assumptions.

We ran mixed-effect models to determine how foliar [Si] and rock-derived nutrients varied with increasing soil age within the 13 species selected, treating chronosequence stage as a continuous variable. Our model for [Si] included random slopes and intercepts for individual species, whereas models for other foliar nutrients included only random intercepts since these models fit the data better than models that also included random slopes.

The relationship between phytolith concentration and plant-available Si concentration was tested for the studied soils and for the quartz-phytolith experiment using simple regression analysis. For the studied soils, we also tested mixed-effect linear regression models, using the chronosequence as the random effect; these yielded similar results and are not discussed further. All analyses were conducted in Minitab ® v18.1.

4.5 Results

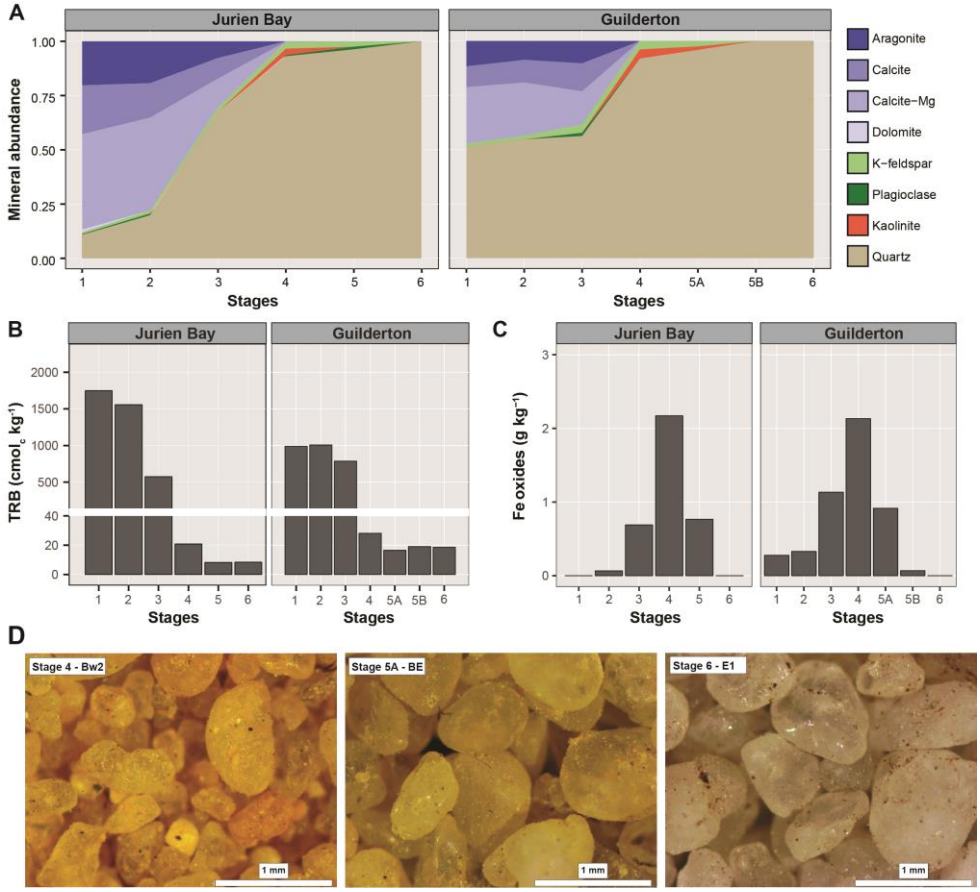

Figure 4-1 : Weathering indicators across the Jurien Bay and Guilderton chronosequences. Changes in soil mineralogy (A). Depth-weighted mean Total Reserve in Bases (TRB) (B) and Fe-oxide concentration extracted with Na-dithionite-citrate-bicarbonate (C) for the upper 50 cm of soils. Observation under a binocular microscope of the horizon Bw2 stage 4, BE stage 5A and E1 stage 6 for the Guilderton chronosequence (D). Soil age increases with increasing chronosequence stage.

Carbonate minerals dominated Holocene soils, but were completely dissolved by the youngest Pleistocene soils (~120 ka; stage 4) (Figure 4-1A). The loss of carbonate occurred in parallel with the formation of kaolinite and the relative enrichment in plagioclase and potassium feldspars, followed by the enrichment of quartz minerals by the final stage of soil development (~2,000 ka; stage 6) (Figure 4-1A). This was corroborated by an increase in the soil weathering index (Total Reserve in Bases, TRB; i.e. the sum of total Ca, Mg, K and Na), which was highest in the early stages

of soil development (≥1,000 $cmol_c$ kg^{-1}), strongly decreased after the loss of carbonates in stage 4 (21-28 $cmol_c$ kg^{-1}), and then decreased more gradually towards the final stages (8-19 $cmol_c$ kg^{-1}; Figure 4-1B). As the concentration of carbonates declined, Fe-oxide concentrations increased from stage 1 to stage 4 (from <0.3 to 2.1 g kg^{-1}), before decreasing to concentrations below the detection limits in the oldest stages (Figure 4-1C). Clay concentrations followed the same trend, increasing from ~1% in the early stages to 3-7% in stages 3 and 4, and then declining to <1% in the oldest stages. Sand bleaching from stage 4 to stage 6 supported the appearance of end-member stages of soil formation characterized by Si loss (desilication) and quartz enrichment (Figure 4-1D).

The reactive pedogenic Si pool (poorly-crystalline aluminosilicates of non-biogenic origin, estimated by oxalate extraction) increased markedly from Holocene to Pleistocene soils (stages 1-3 to stage 4), linked to the formation of clay minerals (de Tombeur *et al.* 2020b) (Figure 4-2A; from ≤ 250 kg ha^{-1} to ≥ 2,000 kg ha^{-1}). However, desilication during prolonged soil weathering resulted in the complete loss of the reactive pedogenic Si pool in the oldest stage of the chronosequences.

The Si:Al ratio of alkali-reactive Si (measured in hot 1% Na_2CO_3) indicates the origin of this pool: values >5 suggest a biogenic origin. Alkali-reactive Si stocks were lowest in the three first stages (≤ 1,200 kg ha^{-1}) and had mostly a non-biogenic origin (Si:Al 0.5–1.8; Figure 4-2B), indicating a contribution of lithogenic and/or pedogenic minerals. Alkali-reactive Si increased strongly in stage 4 (3,800–6,100 kg ha^{-1}), but the Si:Al ratio remained typical of lithogenic and pedogenic minerals (1.4–2.1). In contrast to the reactive pedogenic Si pool, however, alkali-reactive Si did not disappear during long-term pedogenesis, varying between 2,500 and 6,300 kg ha^{-1} in the most advanced stage of soil weathering and having Si:Al ratios > 5, indicating a biogenic origin (Vandevenne *et al.* 2015).

Plant-available Si quantified by extraction in 0.01 M $CaCl_2$ followed a similar pattern to the reactive pedogenic Si pool, increasing to a maximum by stage 4, and then decreasing towards the oldest stage (Figure 4-2C). The stocks of plant-available and reactive pedogenic Si were significantly correlated (R^2= 0.68; $p<0.01$; n=9) along both chronosequences.

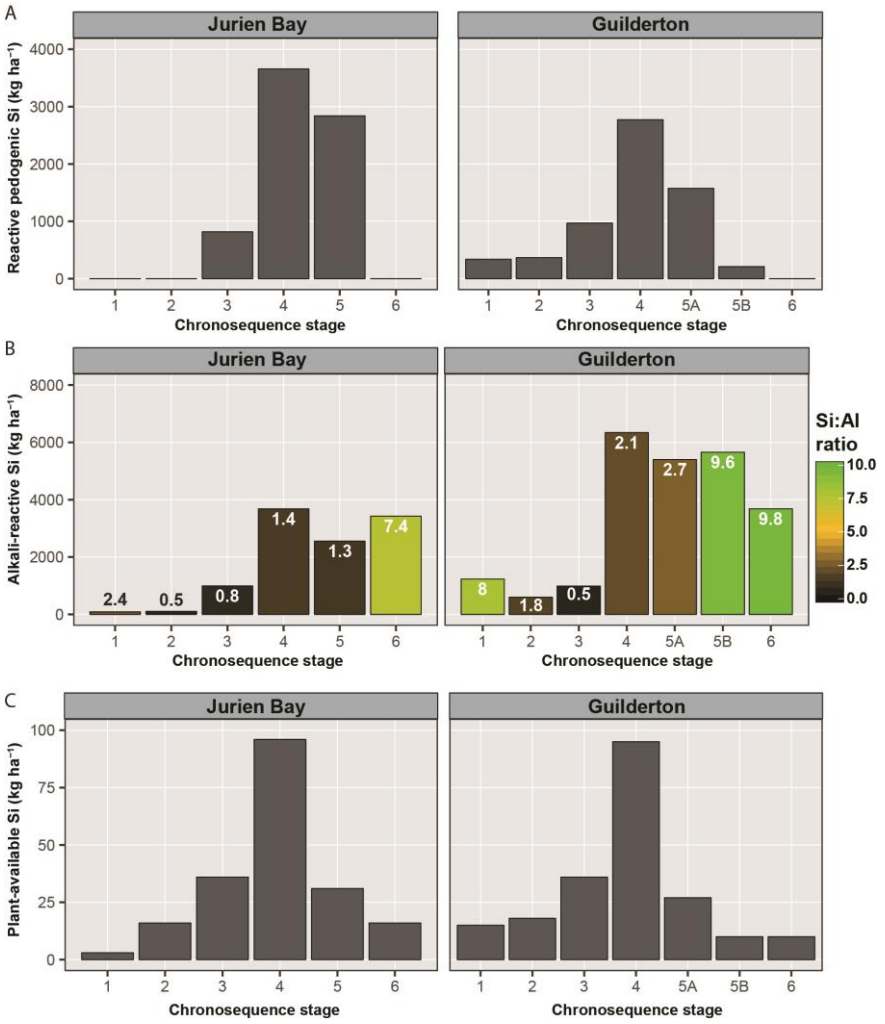

Figure 4-2 : Stocks of Si pools across the Jurien Bay and Guilderton chronosequences. Stocks of reactive pedogenic Si extracted with oxalate (A), alkali-reactive Si extracted with Na_2CO_3 (B) and plant-available Si extracted with $CaCl_2$ (C) for the upper 50 cm of soil. In (B), the bar colors and labels indicate the depth-weighted mean ratio of alkali-reactive Si to alkali-reactive Al. Soil age increases with increasing chronosequence stage.

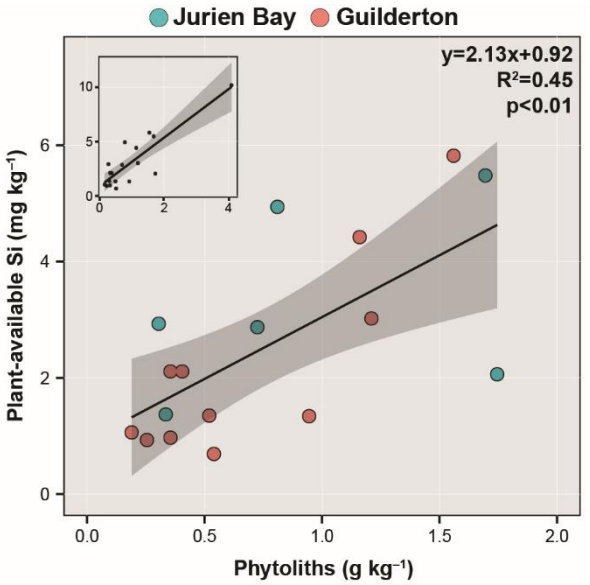

Figure 4-3 : Relationship between soil phytoliths and plant-available Si concentration from the appearance of quartz-rich horizons. The color of the dots indicates the chronosequence from which the horizon originates (Jurien Bay in blue; Guilderton in red). Black lines indicate the regression line between both variables. Shaded areas represent 95% confidence interval of the regression. Equation regression, coefficients of determination (R^2) and p-values are shown. The inset graph shows the same relationship with the addition of Jurien Bay stage 6 litter ($y = 2.25x + 0.83$; $R^2 = 0.75$; $p<0.01$).

Soil phytoliths extracted physically by gravimetric separation were concentrated in the surface soil horizon, where plant-available Si concentrations were also highest (Figure E-1). The concentration of soil phytoliths was positively correlated with that of plant-available Si in soil horizons dominated by quartz minerals (Figure 4-3). The contribution of phytoliths to plant-available Si was supported by dissolution features on phytoliths which increased with depth in the two soil profiles selected for microscopic observations (Figure 4-4; from 6-8% in topsoil to 40-42% in deeper horizons).

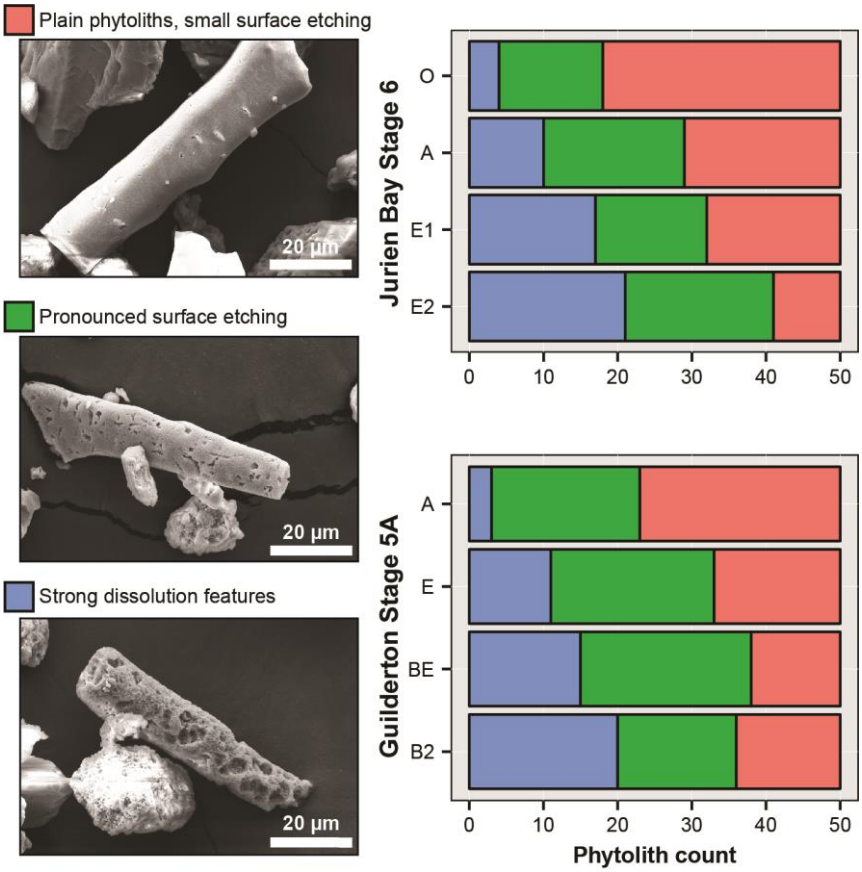

Figure 4-4 : Estimation of phytolith dissolution with depth in two soil profiles. The y-axis indicates the pedogenic horizons. Soil depth increases from the horizon OF (litter) to E2 (70-140 cm) for Jurien Bay stage 6, and from the horizon A (0-10 cm) to B2 (89-140cm) for Guilderton stage 5A.

The mean foliar Si concentration of the 10 most-abundant species per plot at Jurien Bay increased continuously with soil age, from 0.5 ± 0.2 g Si kg^{-1} in stage 1 to 4.2 ± 1.4 g Si kg^{-1} in stage 6 (Figure 4-5), where Si availability was controlled by phytolith dissolution. By contrast, foliar concentrations of the major rock-derived plant nutrients (P, Ca, K, and Mg) followed the opposite pattern, decreasing as soils aged (Figure 4-5). Similar to the species mean values, the cover-weighted mean foliar Si concentrations of the 10 most-abundant species along the Jurien Bay chronosequence increased with increasing soil age, from 0.3 ± 0.1 g Si kg^{-1} in stage 1 to 3.9 ± 1.1 g Si kg^{-1} in stage 6 (Figure E-2). By contrast, the cover-weighted mean foliar concentrations of the major rock-derived plant nutrients (P, Ca, K, and Mg) followed the opposite pattern, decreasing with soil age (Figure E-2). This trend was also found for the 13 species for which intra-specific variation was calculated (Figure E-3; Table E-1). However, only one of the 13 species occurred in the oldest stage 6, so we could

not quantify how intra-specific foliar Si concentrations would have changed in the oldest stage, where the plant-available Si concentration decreased and phytolith dissolution controlled Si availability. An analysis of the contribution by family to the community-level, cover-weighted foliar Si concentrations (Figure E-4) showed that the increase with soil age was associated with the appearance of dicot woody species (Proteaceae and Dilleniaceae) having moderate to high foliar Si concentrations (up to 6.8 g kg^{-1} for Proteaceae and up to 11.7 g kg^{-1} for Dilleniaceae). Our results provide evidence for convergence towards plants having higher foliar [Si] but low foliar concentrations of other rock-derived nutrients with increasing soil age and nutrient depletion across the Jurien Bay chronosequence. Together, these results suggest a selective advantage for plants that accumulate more Si on nutrient-depleted soils.

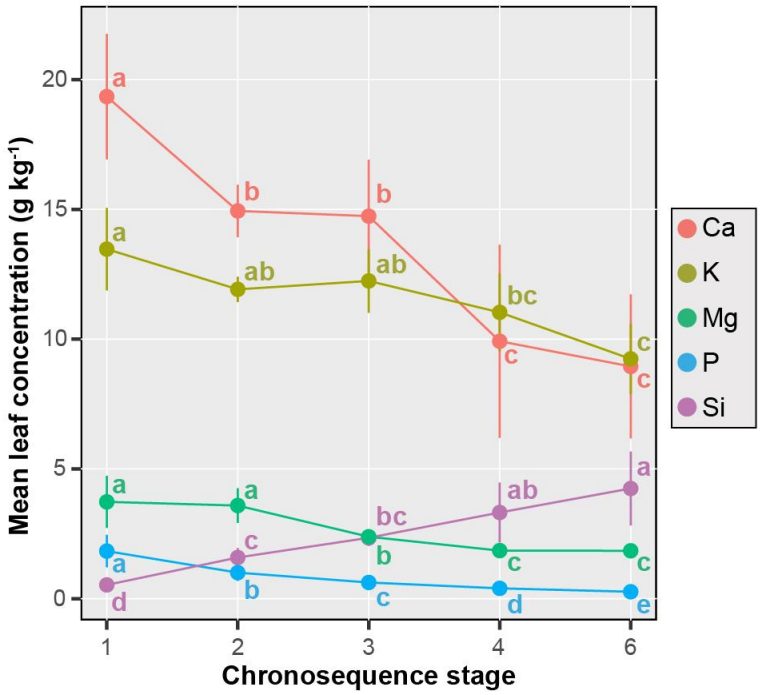

Figure 4-5 : Mean foliar concentrations of silicon, calcium, magnesium, potassium and phosphorus of mature individuals of the 10 most-abundant plant species per plot along the Jurien Bay chronosequence. Points indicate means, bars show 95% confidence intervals (n=5). Letters above each mean represent Fisher Least Significant Difference (LSD) groupings ($p<0.05$), performed on log-transformed data for silicon, magnesium and phosphorus. Soil age increases with increasing chronosequence stage.

4.6 Discussion

Our results provide clear evidence for a shift from pedological to biological control in the terrestrial Si cycle during long-term soil development. In the early and intermediate stages of soil development, the positive relationship between pedogenic-reactive and plant-available Si supports the hypothesis that geochemical processes drive Si availability (Meunier *et al.* 2018; de Tombeur *et al.* 2020b). This is consistent with the global-scale relationship between soil pH and plant-available Si (de Tombeur *et al.* 2020b), because soil pH is related to soil buffering capacity that is driven by the weathering processes. However, with increasing soil age from ~120 ka to ~2,000 ka (stage 4 to 6), the pool of pedogenic reactive Si disappeared entirely, while that of alkali-reactive Si remained large and was dominated by soil phytoliths returned to the soil via litter. Along with this shift, and despite the decrease of plant-available Si from stage 4 to 6 reaching among the lowest values worldwide (de Tombeur *et al.* 2020b), the mean foliar Si concentrations of the most abundant plant species were the highest in the last stage along the Jurien Bay chronosequence. This shows that the terrestrial Si cycling is sustained by strong plant retention of Si in highly desilicated soils. Given the abundance of quartz in these soils, its dissolution must contribute to Si availability (Sommer *et al.* 2013). However, the correlation between phytoliths and plant-available Si for the quartz-rich horizons demonstrates that the order-of-magnitude greater solubility of biogenic amorphous silica compared with quartz (Fraysse *et al.* 2009) compensates for the lower concentration of phytoliths in driving plant-available Si. We assume a negligible dust imprint on Si dynamics in topsoils along the two chronosequences (Laliberté *et al.* 2013), such that the increase in plant-available Si in the topsoil horizons of the intermediate and old soils supports the strong impact of phytolith dissolution in desilicated environments. While P, Ca, K and Mg are essential plant nutrients and associated with organic matter inside cells, Si precipitates to form prominent silica structures between cell walls and the lumen, and in extracellular and intercellular spaces of leaf epidermis (Hartley *et al.* 2015; de Tombeur *et al.* 2020a). This implies that P, Ca, K and Mg are released more readily during litter degradation (Fraysse *et al.* 2010; Dincher *et al.* 2019). Conversely, phytoliths can be preserved in the soil environment for months to millennia (Blecker *et al.* 2006; Sommer *et al.* 2013) and therefore provide a long-term source of Si to plants (Fraysse *et al.* 2010; Nakamura *et al.* 2020b). In addition, unlike most nutrients, Si is not remobilized during leaf senescence, implying that all phytoliths are returned to soil via litterfall. Our results thus show that the return of phytoliths to topsoil is a key process contributing to a slow-release source of Si that sustains the terrestrial cycle over geological time scales. We expect these results to be relevant broadly for other systems given that the chronosequences span the approximate range of soil ages worldwide, and represent three globally relevant soil domains known to occur during long-term pedogenesis: carbonate leaching, formation of secondary minerals, and their subsequent loss through eluviation (Chadwick & Chorover 2001).

The oldest soil of the Jurien Bay chronosequence are among the most strongly-weathered and nutrient-depleted worldwide (Turner & Laliberté 2015). However,

unlike the major plant nutrients for which foliar concentrations decreased markedly with increasing soil age, foliar Si concentrations showed the opposite pattern. The Jurien Bay chronosequence is characterized by strong turnover of plant species (Zemunik *et al.* 2016), reflecting the expression of selective edaphic forces acting on a species-rich regional flora over an ecological time scale (Laliberté *et al.* 2014). As a result, species adapted to older, nutrient-impoverished soils have low foliar concentrations of rock-derived nutrients (Hayes *et al.* 2014), but accumulate Si in their leaves. Increases in foliar Si concentrations could be partly due to longer leaf lifespans since Si tends to accumulate as leaves age (Motomura *et al.* 2002), and plants growing on nutrient-poor soils can increase nutrient-use efficiency producing longer-lived leaves (Aerts & Chapin 2000). The biological control of the Si cycle during ecosystem retrogression may also reflect important Si-based plant functions (Cooke & Leishman 2011a; Hartley & DeGabriel 2016; Debona *et al.* 2017). Reduced herbivory through silica deposition (McNaughton *et al.* 1985; Hartley & DeGabriel 2016) in plants growing on the older soils could have adaptive value in these nutrient-impoverished habitats by minimizing tissue loss and therefore increasing the mean residence time of nutrients and nutrient-use efficiency (Coley *et al.* 1985; Massey *et al.* 2007a). In addition, there is mounting evidence that Si allows plants to withstand P stress (Kostic *et al.* 2017), against which high leaf Si concentration could be a response trait (Quigley *et al.* 2020). Therefore, the maintenance of the terrestrial Si cycle by plants in ecosystems undergoing retrogression suggests important, but overlooked, beneficial effects in nutrient-poor environments.

5

Impact of ecosystem water balance and soil parent material on the terrestrial silicon cycle : insights from three long-term chronosequences*

* This Chapter is adapted from

de Tombeur, F., Cornélis, J-T., Laliberté, E., Lambers, H., Mahy, G., Faucon, M-P., Turner, B.L. Impact of ecosystem water balance and soil parent material on the terrestrial silicon cycle : insights from three long-term chronosequences Submitted to *Biogeochemistry*

5.1 Foreword

In the previous chapters, we highlighted the major influence of geochemical processes on long-term soil Si dynamics (*i.e.*, carbonates loss, clay formation, quartz enrichment). In the chapter 4, we also showed that soil-plant Si cycling is increasingly driven by biological processes (*i.e.*, phytolith formation in plants followed by dissolution in soils) with increasing soil weathering degree and desilication. Phytoliths dissolution seemed to control plant-available Si in the older soils of the Jurien Bay and Guilderton chronosequences, and our results suggest an increased Si biocycling as soils age along the Jurien Bay chronosequence. In this new chapter, we will consider if ecosystem water balance and soil parent material can influence the relative control of these geochemical and biological processes on soil Si dynamics by studying the 2-million-year Warren chronosequence, in addition to the Jurien Bay and Guilderton chronosequences. The Warren chronosequence is characterized by a wetter climate (water balance of +50 mm yr^{-1} against -900 and -750 mm yr^{-1} for the Jurien Bay and Guilderton chronosequence, respectively), but also by a soil parent material poorer in carbonates and weatherable minerals, because of its high quartz content (>95% compared with 51% and 11% at Guilderton and Jurien Bay, respectively).

5.2 Summary

How ecosystem water balance and soil parent material influence the long-term trajectory of silicon (Si) cycling in terrestrial ecosystems remains unclear. We addressed this by studying three 2-million-year dune chronosequences along a climatic gradient in southwest Australia, with contrasting water balance (–900 to +50 mm yr^{-1}) and carbonate content in the parent sand (5 to 80%). Along each chronosequence, we sampled soils from the progressive and retrogressive phases of ecosystem development to quantify pedogenic reactive Si (extracted in ammonium oxalate and oxalic acid), phytoliths (biogenic Si), and plant-available Si (extracted in dilute $CaCl_2$). Silicon mobilization was buffered by carbonate in the early stages of the two carbonate-rich drier chronosequences, but not in the carbonate-poor wetter chronosequence. Reactive pedogenic Si and plant-available Si peaked during clay formation after carbonate loss at the carbonate-rich drier chronosequences, but not at the carbonate-poor wetter chronosequence where almost no clay formation occurred, probably due to a combination of lower content of weatherable minerals in the soil parent material and higher weathering rates. Phytolith stocks were similar across the three chronosequences, suggesting that a climate-driven increase in biomass and associated phytolith production in wetter sites counter-balance the higher phytolith dissolution rates and translocation. Together, these results demonstrate that the initial carbonate content in the soil parent material and subsequent mineralogical evolution drive long-term soil Si dynamics, and stress the prominent influence of climate-induced increases in biomass production on the Si biological feedback loop, even in old and highly desilicated environments.

5.3 Introduction

Silicon (Si) cycling in terrestrial ecosystems is involved in key ecological and geochemical processes. Weathering of silicate minerals regulates the CO_2 concentration in the atmosphere on a geological timescale (Kump *et al.* 2000; Amiotte Suchet *et al.* 2003; Conley & Carey 2015), and the transfer of Si from continents to oceans determines the growth of diatoms (Nelson & Dortch 1996), which account for at least 10% of the photosynthesis on Earth (Raven & Waite 2004; Armbrust 2009). Moreover, Si biocycling through terrestrial vegetation influences plant performance by reducing several biotic and abiotic stresses, including herbivores and pathogens attacks, water stress, and metal toxicity (Cooke & Leishman 2016; Hartley & DeGabriel 2016; Debona *et al.* 2017).

Geochemical processes contribute to soil-plant Si cycling by controlling the dissolution of Si-bearing minerals (Cornelis *et al.* 2011a; Meunier *et al.* 2018; de Tombeur *et al.* 2020b). The magnitude of this process depends on the nature and particle-size of soil minerals and, therefore, on soil age, parent material, and subsequent weathering degree (Cornelis & Delvaux 2016; de Tombeur *et al.* 2020b). During long-term soil formation, plant-available Si concentrations may eventually increase during the dissolution of carbonate minerals and clay formation (de Tombeur *et al.* 2020b) – because carbonates are the primary soil buffer system consuming protons and alkaline pH increases Si adsorption – then decrease during advanced soil weathering stages through the weathering of silicate minerals and the subsequent loss of Si (i.e. desilication) (Savant *et al.* 1999; Chadwick & Chorover 2001; de Tombeur *et al.* 2020b). Time-dependent processes such as desilication also depend on ecosystem water balance, as increasing rainfall will accelerate the rate of chemical mineral weathering and subsequent Si loss (Chadwick *et al.* 2003).

Besides their role in enhancing soil weathering, plant-induced processes also influence the soil-plant Si cycle by taking up Si from the soil solution, leading to its precipitation as hydrated amorphous silica in plant tissue (i.e. phytoliths) (Alexandre *et al.* 1997; Derry *et al.* 2005; Carey & Fulweiler 2012; Conley & Carey 2015; Turpault *et al.* 2018; de Tombeur *et al.* 2020c). The return of phytoliths to the soil after leaf senescence builds a pool of highly reactive Si-bearing minerals (Fraysse *et al.* 2009), with a mean residence time that varies from less than one month to around 1,500 years, depending on environmental conditions (Bartoli & Souchier 1978; Alexandre *et al.* 1997, 2011; Blecker *et al.* 2006; White *et al.* 2012; Sommer *et al.* 2013; Strömberg *et al.* 2018). The dissolution of soil phytoliths has an important effect on the soil-plant Si cycle (Bartoli 1983; Alexandre *et al.* 1997; Sommer *et al.* 2013; Turpault *et al.* 2018), and their imprint intensifies with increasing soil weathering degree and desilication (de Tombeur *et al.* 2020c). Such biological processes can also be affected by climatic variables. For example, increasing temperature (Gewirtzman *et al.* 2019) or rainfall (Blecker *et al.* 2006) are expected to increase the stocks of biogenic Si in aboveground vegetation due to greater plant productivity, while increasing rainfall is expected to decrease soil biogenic Si stocks due to faster phytolith turnover rates via physical translocation and/or chemical dissolution

(Blecker *et al.* 2006; Melzer *et al.* 2012). Taken together, a rainfall-induced increase in biomass production should strengthen the importance of biological processes on the Si cycle by intensifying the Si biological feedback loop (Blecker *et al.* 2006; Cornelis & Delvaux 2016). Terrestrial Si cycling is therefore driven by geochemical and biological processes that can both be affected by climatic variables.

To better understand long-term trajectories in terrestrial Si cycling and the control of geochemical and biological processes, we explored the role of soil parent material, soil age and ecosystem water balance on Si pools along a soil age × climate gradient located in southwestern Australia (Turner *et al.* 2018). The gradient consists of four 2-million-year dune chronosequences along a climatic gradient, among which three were considered in this study: Jurien Bay, Guilderton and Warren. The Jurien Bay and Guilderton chronosequences are characterized by a negative water balance (-900 and -750 mm yr^{-1} respectively), while the Warren chronosequence has a positive water balance (+50 mm yr^{-1}). Along each chronosequence, pedogenesis involves carbonate leaching, formation of clay-sized minerals, followed by strong eluviation that induces quartz enrichment (Turner *et al.* 2018). Although the granulometry of the parent sand deposit is similar for all three chronosequences (>98% sand), carbonates and primary weatherable silicate minerals are present in smaller concentrations at the wetter Warren chronosequence compared with the Jurien Bay and Guilderton chronosequences (Turner *et al.* 2018). The Warren chronosequence is thus characterized by a parent material that is richer in quartz (>95% compared with 51% and 11% at Guilderton and Jurien Bay, respectively), leading to soils with smaller concentrations of secondary clay minerals (Turner *et al.* 2018).

The combination of geological and climatic characteristics of these three soil chronosequences provides an opportunity to understand how soil parent material, soil age, and ecosystem water balance affect long-term soil Si dynamics. For each chronosequence, we sampled soil profiles that include both the progressive and retrogressive phases of the ecosystem (Peltzer *et al.* 2010), and quantified the pools of reactive Si-bearing pedogenic and biogenic phases, and plant-available Si in the soils. We hypothesized that the contrast in the soil parent material and subsequent soil development patterns between the drier chronosequences (Jurien Bay and Guilderton) and the wetter chronosequence (Warren) would affect the long-term evolution of reactive Si and plant-available Si pools via contrasting soil mineralogy. Specifically, we predicted that the buffer exerted by carbonate minerals on silicates weathering and Si release in soil solution during the first stages of pedogenesis (de Tombeur *et al.* 2020b) would be minimal at Warren, because of the much lower initial carbonate content. We also hypothesized that the Warren chronosequence would contain less reactive Si-bearing minerals of pedogenic origin compared with the drier chronosequences, due to lower rates of formation of secondary minerals (quartz-rich parent material). Finally, we expected the soil phytolith stock to decrease with increasing ecosystem water balance from Jurien Bay/Guilderton to Warren due to faster rates of dissolution and translocation in a wetter environment (despite the relatively small parallel decrease in temperature) (Blecker *et al.* 2006). Despite this

potential decrease in phytolith stock, we expected that reactive Si-bearing minerals would be dominated by phytoliths at Warren given the slow rates of formation of pedogenic minerals, but likely greater biomass production due to a wetter climate.

5.4 Materials and methods

5.4.1 Experimental design

This Chapter is based on the 2-million-years Jurien Bay, Guilderton and Warren dune chronosequences and the first sampling design (see Chapter 2 for details).

5.4.2 Soil sampling

At each chronosequence stage, we excavated one soil profile pit (at least 1.5 m deep and 1 m^2 in area) at the same locations as described previously (Turner & Laliberté 2015; Turner *et al.* 2018) being careful not to dig in the previously disturbed area. We then sampled the same pedogenic horizons, at the same depth described in Turner and Laliberté (2015) and Turner et al. (2018). Each sample was a mix of four subsamples, collected on each side of the soil pit. Samples were air-dried and sieved to 2 mm.

5.4.3 Soil physical and chemical characterization

For each soil chronosequence, the mineralogy was assessed in horizons that are representative of the key soil processes occurring at all the soil chronosequences stages: carbonate-rich horizons, clay and Fe-oxide-rich horizons, and quartz-rich horizons. The analysis was performed as described in the section 3.3.3 (Chapter 3).

Soil total Al, Ca, Fe, Mg, K, and Na concentrations were determined as described in the section 3.3.3 (Chapter 3). We then calculated the sum of total contents in alkaline and alkaline-earth metals Na, K, Ca and Mg (in $cmol_c\ kg^{-1}$) to estimate the degree of soil weathering (Herbillon 1986). The concentration of total free iron (Fe_{DCB}), which comprises amorphous and crystalline Fe oxides, was determined as described in the section 3.3.3 (Chapter 3).

5.4.4 Determination of Si forms in soil

Two extraction procedures were used to estimate the pool of reactive Si that contributes primarily to the release of Si to soil solution. First, we conducted an extraction with ammonium oxalate-oxalic acid at pH 3 (Tamm 1922), as described in the Chapter 3 (section 3.3.3). As the oxalate extraction is specific to pedogenic Si, and given the absence of pedogenic opal in the studied soil chronosequences, we refer to it as “reactive pedogenic Si”.

Second, we used a Na_2CO_3 extraction (DeMaster 1981), which dissolves the biogenic Si pool (mainly phytoliths here), but also Si sorbed or occluded in reactive mineral phases of pedogenic origin (Barão *et al.* 2014). This extraction is described in the section 4.4.4 (Chapter 4). We term this reactive Si pool “alkali-reactive Si”.

Plant-available Si concentrations were estimated through a 21-day 0.01 M $CaCl_2$ extraction, as described in the section 4.4.4 (Chapter 4). All Si concentrations were converted into stocks to 100 cm depth by using soil bulk density and horizon thickness (Turner & Laliberté 2015; Turner *et al.* 2018).

5.4.5 Physical extraction of soil phytoliths

Soil phytoliths were physically extracted by gravimetric separation (Kelly 1990; Aleman *et al.* 2013), as described in the section 4.4.5 (Chapter 4). Phytolith concentrations were converted into stocks over 100 cm depth using soil bulk density and horizon thickness. To estimate the dissolution of soil phytoliths, we made microscopic observations in one soil profile randomly selected for each chronosequence, as described in the section 4.4.5 (Chapter 4): stage 6 of Jurien Bay, stage 5A of Guilderton and stage 5B of Warren.

5.5 Results

5.5.1 Evolution of soil properties

The three chronosequences occupied similar soil process domains and exhibited consistent pedogenic changes: pedogenesis involved carbonate loss in Holocene dunes (stages 1 to 3) followed by quartz enrichment in the old Middle Pleistocene and Early Pleistocene stage (stages 5 and 6) (Tables 2-1 and 5-1). However, the evolution of soil mineralogy and texture differed between the drier northern chronosequences (Jurien Bay and Guilderton) and the wetter southern chronosequence (Warren) (Tables 2-1 and 5-1). At Jurien Bay and Guilderton, the content of clay- and silt-sized minerals increased from stage 1 to 4 during the loss of carbonate minerals and the formation of fine-sized minerals, then decreased towards the oldest stage. This pattern was not observed at Warren, however, where texture was dominated by poorly soluble sand-sized quartz minerals without any formation of fine-sized minerals (Tables 2-1 and 5-1). The concentration of carbonate minerals in the earliest chronosequence stage was much greater at Jurien Bay and Guilderton (88% and 47% for stage 1, respectively) compared with Warren (4%). Feldspars accounted for up to 5% of soil mass at Jurien Bay and Guilderton, but only 2% at Warren, while secondary clay minerals were identified only at Jurien Bay and Guilderton (kaolinite in stage 4; 2-4%). These contrasts in soil properties between the northern chronosequences and Warren were also reflected in concentrations of total elements and Fe oxides (Figure F-1). Except for the oldest stages, the sum of total Ca, Mg, K and Na, total Al and Fe stocks, and Fe-oxide stocks were greater at Jurien Bay/Guilderton than at Warren (Figure F-1). These parent material-related differences in soil properties imply the appearance of quartz-rich soils from stage 2 onwards at Warren, but only at stages 5-6 for the Jurien Bay and Guilderton chronosequences.

5.5.2 Evolution of Si pools

Stocks of reactive pedogenic Si were greater at Jurien Bay and Guilderton than at Warren, except in the initial and final stages (Figure 5-1a). At Jurien Bay and Guilderton, the stocks of reactive pedogenic Si increased strongly from stage 1 to 4 during carbonate losses (from ≤600 kg ha^{-1} to ≥6700 kg ha^{-1}), then decreased to undetectable concentrations during quartz enrichment in the oldest stage. At Warren, reactive pedogenic Si stocks were low and constant from stage 1 to 5A (~ 900–1300 kg ha^{-1}), and then decreased in the two oldest stages (~ 600–800 kg ha^{-1}). Stocks of oxalate-extractable Al and Fe followed the same trend as reactive pedogenic Si at Jurien Bay and Guilderton, but were almost always below the detection limits at Warren (Figure F-2). The Si:Al ratio in oxalate extracts ranged from 0.3 to 0.7 at Jurien Bay and Guilderton, supporting the clay origin of the reactive pedogenic Si pool at the northern chronosequences.

Table 5-1 : Estimation of the mineral abundance for each XRD diffraction pattern from this study (quartz, carbonate minerals, feldspars and kaolinite) in %. Soil age increases with increasing chronosequence stage.

Stages	**Quartz (%)**			**Carbonate minerals[a] (%)**			**Feldspars[b] (%)**			**Kaolinite (%)**		
	Jur	Gui	War	Jur	Gui	War	Jur	Gui	War	Jur	Gui	War
1	11	51	95	88	47	4	1	2	1	0	0	0
2	20	55	99	78	44	1	2	2	0	0	0	0
3	68	56	100	31	38	0	2	5	0	0	0	0
4	93	92	98	0	0	0	4	4	1	3	4	0
5	98	-	-	0	-	-	4	-	-	0	-	-
5A	-	96	98	-	0	0	-	3	2	-	2	0
5B	-	100	100	-	0	0	-	0	0	-	0	0
6	100	100	100	0	0	0	0	0	0	0	0	0

[a]Calcite, calcite-Mg and aragonite were identified at the thee chronosequences. Dolomite was identified at the Jurien Bay chronosequence.
[b]K-feldpars and plagioclase were identified at the three chronosequences.

Contrary to reactive pedogenic Si, the stocks of alkali-reactive Si were generally greater or similar at Warren than at Jurien Bay and Guilderton, except in the intermediate stages 4 and 5A of the Guilderton chronosequence where they peaked (Figure 5-1b). In the three earliest stages, alkali-reactive Si stocks were between 2 and 30 times greater at Warren (~ 4,500–6,000 kg ha^{-1}) than at Jurien Bay and Guilderton (~ 200–2,500 kg ha^{-1}) (Figure 5-1b). In stages 4 to 5, stocks were equivalent at Jurien Bay and Warren (~ 5,200–7,700 kg ha^{-1}), but greater at Guilderton (~ 12,000–13,000 kg ha^{-1}). In the oldest stage, alkali-reactive Si stocks were equivalent for the three chronosequences (~ 5,500–7,000 kg ha^{-1}). The main origin of alkali-reactive Si differed among the sequences. At Jurien Bay and Guilderton, the Si:Al ratio indicated a major pedogenic contribution in all stages (from 0.6 to 2), except in the earliest stage at Guilderton (8.0) and oldest stages for both (7.8 and 8.4 for Jurien Bay and Guilderton, respectively). The Si:Al ratio >5 throughout the Warren chronosequence

indicates the predominance of phytoliths as main contributors to the alkali-reactive Si pool (Figure 5-1b).

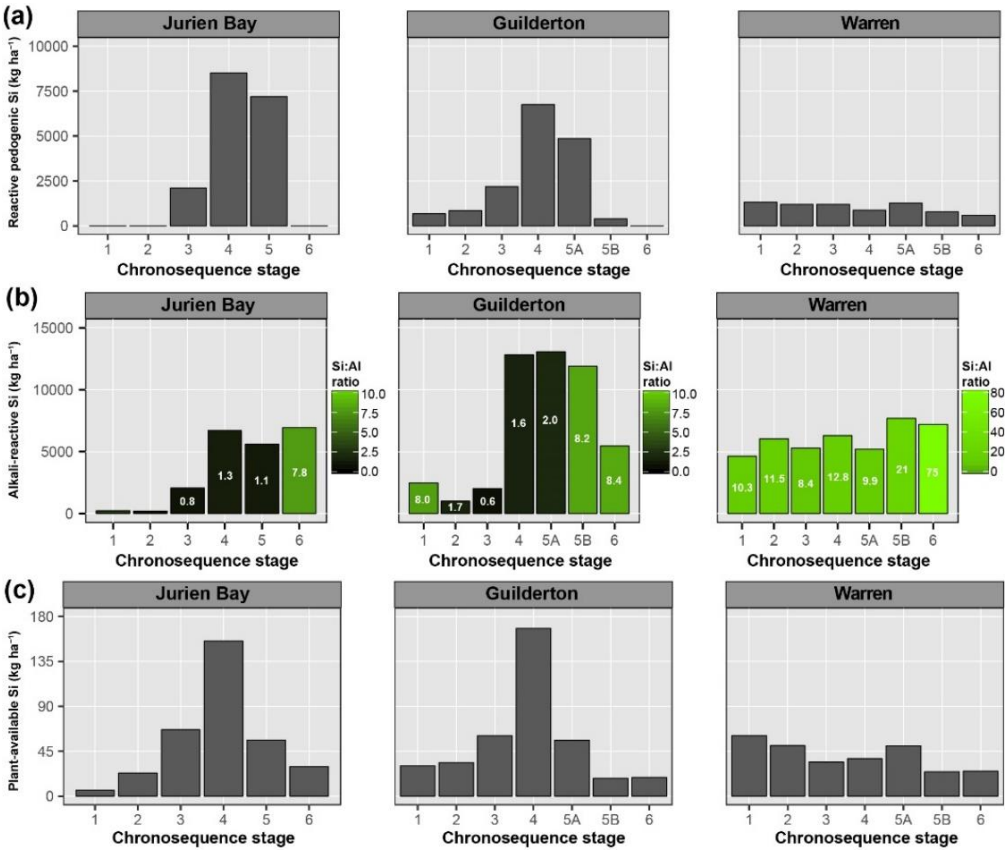

Figure 5-1 : Stocks to 1 m depth of (a) reactive pedogenic Si extracted with oxalate, (b) alkali-reactive Si extracted with Na_2CO_3, and (c) plant-available Si extracted with $CaCl_2$. In (b), the bar colors and labels indicate the depth-weighted mean Si:Al ratio in the alkali extracts. At Jurien Bay, this ratio was 3.0 and 0.6 for stages 1 and 2, respectively. The color gradient used between the values 0 to 10 is the same for the three chronosequences. Soil age increases with increasing chronosequence stage.

At Jurien Bay and Guilderton, stocks of plant-available Si followed the same trend as reactive pedogenic Si, increasing from stage 1 to 4 during carbonate loss (from ≤31 kg ha^{-1} to ≥150 kg ha^{-1}), then decreasing towards the oldest stage during quartz enrichment (~ 19–30 kg ha^{-1}) (Figure 5-1c). At Warren, plant-available Si stocks were constant from stage 1 to 5A (~ 34–61 kg ha^{-1}), before decreasing slightly in stages 5B and 6 (~ 25 kg ha^{-1}). In the two earliest stages of soil development, plant-available Si stocks were between 2 and 10 times greater at Warren than at Jurien Bay and Guilderton, but by stage 3, they were lower at Warren. Plant-available Si stocks

reached maximal values across all the chronosequences by stage 4, with values about four times greater at Jurien Bay and Guilderton than at Warren. In the oldest stages, plant-available Si stocks were similar across all sequences (~ 18-30 kg ha^{-1}). Across all soil chronosequence stages, the stocks of plant-available Si were correlated with the stocks of pedogenic reactive Si (R^2=0.66; p<0.01; n=16). The concentrations of plant-available Si generally decreased with depth over the first 30 cm, except in the early stages of pedogenesis (Figure F-3). At the intermediate stages of weathering, they increased with depth in the reddish clay-rich horizons located below the bleached horizon (e.g., Guilderton stage 5A) (Figure F-3). At Jurien Bay and Guilderton, the concentrations of plant-available Si were determined by soil phytoliths in the soil horizons dominated by quartz (from the appearance of a bleached quartz-rich horizon) (de Tombeur *et al.* 2020c).

5.5.3 Stock of soil phytoliths

Phytolith stocks to 1 m depth were generally greater or of the same order of magnitude at Warren compared with Jurien Bay and Guilderton, except in the intermediate stages 4 and 5A (Figure 5-2). At Jurien Bay and Guilderton, phytolith stocks increased from stage 1 to 4 (from ≤1,200 kg ha^{-1} to ≥3,500 kg ha^{-1}). Values were then roughly constant up to the last stage at Jurien Bay (~ 3,400–4,700 kg ha^{-1}), but decreased at Guilderton (from ~6,400 kg ha^{-1} to ~1,800 kg ha^{-1}). At Warren, soil phytolith stocks increased from stage 1 to 5A (from ~1,200 kg ha^{-1} to ~5,700 kg ha^{-1}), before decreasing in the oldest stage (~3700 kg ha^{-1}).

Soil phytolith concentrations declined with depth, except for the younger soils with low phytolith stocks (Figure F-4). The dissolution features on phytoliths increased with depth in the three soil profiles selected, but did not differ markedly across the chronosequences (Figure 5-3).

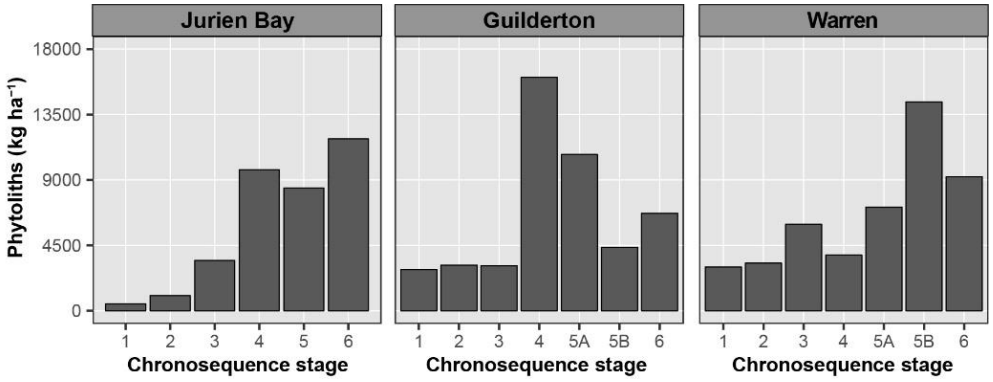

Figure 5-2 : Stocks of soil phytoliths to 1 m depth across the three chronosequences, in kg ha^{-1}. Soil age increases with increasing chronosequence stage.

5.6 Discussion

5.6.1 Control of soil parent material on long-term Si dynamics

Our results suggest that the initial properties of the soil parent material and its pedogenic consequences strongly determine long-term soil Si dynamics. At Jurien Bay and Guilderton, the reactive pedogenic Si and plant-available Si pools were low at the early stages of pedogenesis due to the high carbonate content, which impedes the formation of Fe oxides and clay minerals, and limit the weathering of primary silicate minerals (de Tombeur *et al.* 2020b). At Warren, by contrast, the low carbonate content in the earliest stages of pedogenesis does not buffer the dissolution of silicate minerals. The pools of reactive pedogenic Si and plant-available Si in the youngest soil at Warren were greater than those at Jurien Bay and Guilderton, probably due to the weathering of feldspars (even if present in small amounts) at the onset of pedogenesis. In young soils, the stocks of alkali-reactive Si of biogenic origin were also higher at Warren than at Jurien Bay and Guilderton which suggests a higher degree of Si biocycling, even though this was not reflected in the soil phytolith stocks. The carbonate content of the soil parent material is therefore a key property for Si mobilization, because it reduces the dissolution of silicate minerals during the youngest stages of pedogenesis (de Tombeur *et al.* 2020b).

Plant-available Si stocks were greatest in stage 4 of the Jurien Bay and Guilderton chronosequences after carbonate loss, during the formation of kaolinite, and when reactive pedogenic Si stocks, alkali-reactive Si stocks with a clay mineral origin, and the silt + clay content were maximal (de Tombeur *et al.* 2020b, c). This peak of plant-available Si was not observed at Warren, most likely because of the scarcity of secondary clay minerals throughout this chronosequence. Instead, reactive pedogenic Si and plant-available Si stocks decrease continuously over time, due to continuous desilication (Savant *et al.* 1999; Chadwick & Chorover 2001; de Tombeur *et al.* 2020b). Since soil parent materials differ across the climatic gradient, it is hard to determine from our results whether the absence of clay mineral formation at Warren is caused by the initial composition of the soil parent material, or by an increased desilication under a wetter climate (Chadwick *et al.* 2003). However, the higher concentration of poorly-soluble quartz minerals (Goldich 1938; Fraysse *et al.* 2009) and lower concentration of primary silicates (mainly feldpars) in the parent material at Warren likely was a major factor in the absence of clay mineral formation. Taken together, our results demonstrate that the initial properties of the soil parent material and subsequent mineralogical evolution exert a major control on long-term soil Si dynamics, and probably on Si fluxes towards vegetation and hydrosphere.

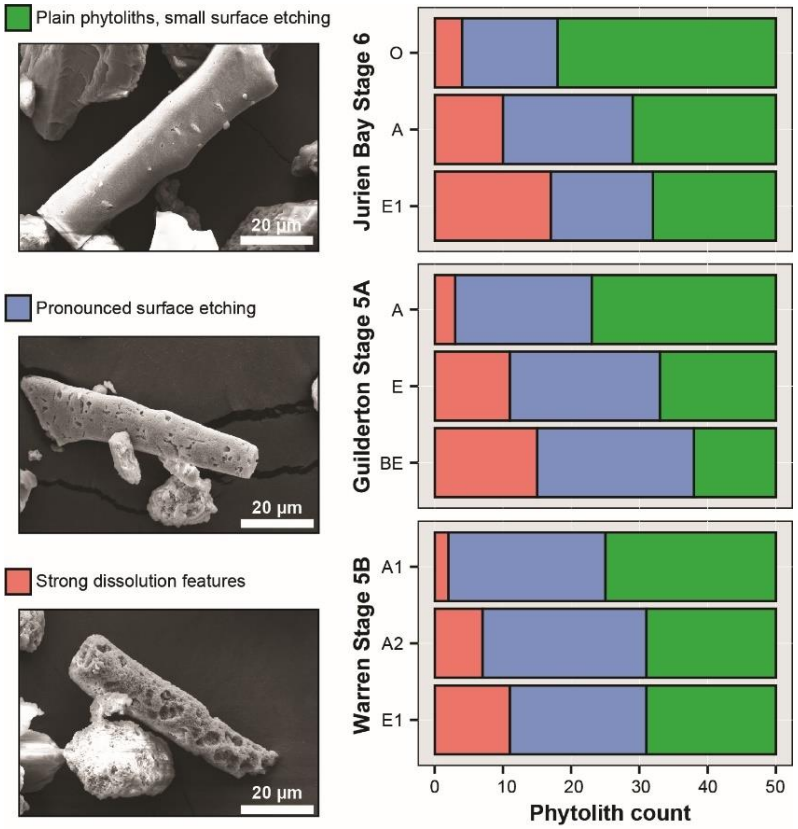

Figure 5-3 : Estimation of phytolith dissolution with depth in one soil profile of each soil chronosequence. The y-axis indicates the pedogenic horizons. Soil depth increases from the horizon O (litter) to E1 (30-70 cm) for Jurien Bay stage 6, from the horizon A (0-10 cm) to BE (33-53 cm) for Guilderton stage 5A, and from the horizon A1 (0-13 cm) to E1 (41-61cm) for Warren stage 5B.

5.6.2 Impact of ecosystem water balance on Si biocycling

In contrast to the pedogenic reactive Si pool, stocks of soil phytoliths and alkali-reactive Si of biogenic origin were generally similar or greater at Warren compared with those at the drier northern chronosequences (except at stage 4). This result does not support our hypothesis of lower belowground stocks of biogenic Si with increasing ecosystem water balance, due to faster rates of phytolith dissolution and translocation (Blecker *et al.* 2006; Melzer *et al.* 2012). Indeed, annual rainfall at Warren is between 1.8 and 2.2 times greater than that at the northern chronosequences and root-induced weathering processes (Lucas 2001; Finlay *et al.* 2020) are probably more important at Warren, since root biomass is larger there (Turner *et al.* 2018). In addition, the physical translocation of phytoliths in soil is not negligible (Alexandre *et al.* 1997; Blecker *et al.* 2006; Strömberg *et al.* 2018), especially in sandy soils

(Fishkis *et al.* 2009), and this is probably more important at Warren given the larger volume of water percolating throughout the soil profile, which could reduce phytolith stocks in the upper meter of soil. Other parameters that may impact phytolith dissolution, such as soil aggregation (Li *et al.* 2020b) and pH (Fraysse *et al.* 2009), probably play a minor role, since soil aggregation is virtually nonexistent in these sandy soils, and soil pH is similar among soils of a same stage across the three sequences. Given that the combination of higher rainfall and root-induced weathering processes did not reduce soil phytolith stocks at Warren, the presumed greater plant productivity (higher LAI) and consequently faster rate of phytolith formation in the vegetation must therefore balance the faster rates of phytolith dissolution or losses through translocation. In the same way that the proportion of organic P forms is significantly greater at Warren that at Jurien Bay and Guilderton (Turner *et al.* 2018), our results suggest that greater plant productivity maintains Si in a biogenic pool that is actively cycled, which might eventually act as a buffer against element loss by leaching from the soil profile (Porder & Chadwick 2009).

At the Jurien Bay and Guilderton chronosequences, soil phytoliths are the main source of plant-available Si on old soils where pedogenic Si reserves are depleted (de Tombeur *et al.* 2020c). Although the abundance of quartz means that its dissolution must contribute to plant-available Si (Sommer *et al.* 2006), the order-of-magnitude greater solubility of biogenic silica compared with quartz (Fraysse *et al.* 2009) compensates for the lower concentration of phytoliths in determining plant-available Si (Sommer *et al.* 2013; de Tombeur *et al.* 2020c). Throughout the Warren chronosequence, the main reactive Si pool is alkali-reactive Si with Si:Al ratios >5, suggesting that soil phytoliths are the main readily-soluble Si pool. The important role of phytolith dissolution in these quartz-rich soils is reinforced by the greater plant-available Si concentration in surface horizons, and the dissolution features observed on phytoliths that increased with soil depth (Sommer *et al.* 2013; de Tombeur *et al.* 2020c). Taken together, our results suggest that, even in extremely quartz-rich soils, a more positive water balance enhances Si biocycling through greater biomass production (Blecker *et al.* 2006), which is promoted by the relatively high chemical reactivity of phytoliths in the soil environment (Bartoli 1983; Alexandre *et al.* 1997; Blecker *et al.* 2006; Sommer *et al.* 2013).

More broadly, our results suggest that vegetation (annual net primary productivity and/or ecosystems type) is a major factor of the annual Si pump in natural ecosystems, which is not reflected in plant-available Si concentrations that are driven more by long-term geochemical processes (Gaillardet *et al.* 1999; Alexandre *et al.* 2011; de Tombeur *et al.* 2020c, b). This is supported by evidence that the greatest annual Si uptake rates occur in high-productivity rainforests on highly-weathered soils (but with low plant-available Si), or in grasslands, where plant species are Si-accumulators (Alexandre *et al.* 1997, 2011; Blecker *et al.* 2006; Melzer *et al.* 2010; Cornelis & Delvaux 2016; Vander Linden & Delvaux 2019). Moreover, although mass balance calculations indicate that soil phytolith dissolution plays a major role in the annual soil-plant Si cycle (Bartoli 1983; Alexandre *et al.* 1997; Sommer *et al.* 2013), plant-

available Si concentrations seem to be determined primarily by soil phytoliths only in soils deprived of weatherable minerals, where poorly-soluble quartz dominates soil mineralogy (Sommer *et al.* 2013; de Tombeur *et al.* 2020c). This agrees with the positive relationships between soil pH and plant-available Si when multiple soils are considered, highlighting the major role of soil weathering degree and mineralogy on plant-available Si (Miles *et al.* 2014; Meunier *et al.* 2018; de Tombeur *et al.* 2020b).

Our long-term soil chronosequences demonstrate the important influence of soil parent material, soil age and water balance on long-term Si cycling. Further insight into long-term Si cycling will be provided by complete mass-balance calculations at the ecosystem level, to estimate phytolith formation and turnover rates as a function of ecosystem water balance and reveal the extent to which climate and biological processes determine terrestrial Si cycling and fluxes towards vegetation and water courses.

6

A shift from phenol to silica-based leaf defenses during long-term soil and ecosystem development*

*This Chapter is adapted from

de Tombeur, F., Laliberté, E., Lambers, H., Faucon, M-P., Zemunik, G., Turner, B.L., Cornélis, J-T., Mahy, G. A shift from phenol to silica-based leaf defences during long-term soil and ecosystem development. *Ecology Letters*

6.1 Foreword

The previous chapters highlighted the major influence of soil age and weathering degree and soil Si dynamics. We considered the influence of both geochemical and biological processes on long-term soil Si dynamics, and we studied how ecosystems water balance and soil parent material could influence the relative contribution of these processes. A key result of the previous chapter is the increase of plant Si concentrations as soils age along the Jurien Bay chronosequence (chapter 4). Apart from suggesting that Si biocycling further increase in old and highly-desilicated soils, where phytoliths dissolution controlled plant-available Si, this result could also reflect prominent ecological theories on plant defense strategies. Indeed, the continuous increase in community-level leaf Si concentrations as soils age and in contrast with major nutrients could reflect the importance of silica-based in nutrient-poor environments, in accordance with the resource availability hypothesis. A higher expression of silica-based defenses in old soils could also be associated with a lower expression of phenol-based defenses, because trade-offs between these two strategies have been reported in the literature. In this chapter, we combined data on leaf concentrations of Si and major nutrients along the Jurien Bay chronosequence (chapter 4) to additional data at the family level, and we quantified total phenols content in the same leaves. As such, we will be able to test if soil nutrient limitation driven by long-term pedogenesis might influence the expression of two important plant defense strategies and trade-offs between them. This is particularly important to consider Si through an ecological perspective because the increase in community-level leaf Si along the chronosequence is mainly driven by species replacement and might in part explain the increased control of biological processes on Si cycling as soils age (chapter 4). Here, an ecological approach might therefore help us to better understand terrestrial Si biogeochemistry.

6.2 Summary

The resource availability hypothesis predicts that plants adapted to infertile soils have high levels of anti-herbivore leaf defenses. This hypothesis has been mostly explored for secondary metabolites such as phenolics, while it remains underexplored for silica-based defenses. We determined leaf concentrations of total phenols and silicon (Si) in plants growing along the 2-million-year Jurien Bay chronosequence, exhibiting an extreme gradient of soil fertility. We found that nitrogen (N) limitation on young soils led to a greater expression of phenol-based defenses, whereas old, phosphorus (P)-impoverished soils favored silica-based defenses. Both defense types were negatively correlated at the community and individual species level. Our results suggest a tradeoff among these two leaf defense strategies based on the strength and type of nutrient limitation, thereby opening up new perspectives for the resource availability hypothesis and plant defense research. This study also highlights the importance of silica-based defenses under low P supply.

6.3 Introduction

The resource availability hypothesis (RAH) (Coley *et al.* 1985) predicts that plant species adapted to resource-rich environments will have rapid growth rates and leaf turnover, high leaf nutrient concentrations, but low levels of anti-herbivore defenses. By contrast, the benefits of allocating resources to anti-herbivore defenses become advantageous for species adapted to nutrient-poor environments, because biomass loss by herbivory represents a significant loss of scarce nutrients (Coley *et al.* 1985; Endara & Coley 2011). This theory has been primarily explored with regard to secondary metabolites (e.g. phenolics), plant mechanical properties and nitrogen (N)-based defenses, while silica-based defenses have received far less attention (Endara & Coley 2011). For instance, in a meta-analysis testing the global consistency of the RAH (Endara & Coley 2011), the deposits of silica bodies in plants as defense mechanism (McNaughton *et al.* 1985; Hartley & DeGabriel 2016) represented only 1% of statistical tests considered in the literature (Massey *et al.* 2007a). This highlights the fact that Si-based defenses have been understudied by plant ecologists, despite representing one of the earliest anti-herbivore plant adaptations (Trembath-Reichert *et al.* 2015; Deshmukh *et al.* 2020).

Vascular plants can accumulate silicon (Si) in concentrations exceeding those of the major nutrients (0.1 to 10% of dry weight; Epstein 1994). Taken up as monosilicic acid (H4SiO4) from the soil solution, Si is translocated to sites of rapid transpiration, where it polymerizes as amorphous hydrated silica (SiO2.nH2O) between cell walls and the lumen, and in extracellular and intercellular spaces of the leaf epidermis (Kumar *et al.* 2017b; de Tombeur *et al.* 2020a). This mechanism of biosilicification has occurred in land plants for over 400 million years (Trembath-Reichert *et al.* 2015) and provides numerous benefits to plants, including resistance to abiotic stresses such as metal toxicity, salinity, nutrient deficiency or water stress (Cooke & Leishman 2016; Debona *et al.* 2017; Frew *et al.* 2018). Biosilicification also reduces herbivory by increasing leaf abrasiveness, which reduces penetration and chewing, and by decreasing the digestibility and palatability of leaves (Massey & Hartley 2006, 2009; Massey *et al.* 2006, 2007a; Johnson *et al.* 2020). Besides physical defenses, biosilicification has been linked to anti-herbivore phytohormonal signaling through the modulation of jasmonic acid, salicylic acid and ethylene, resulting in modified emissions of volatile organic compounds (Coskun *et al.* 2019; Leroy *et al.* 2019). Although the impact of silica-based defenses on herbivory has mainly been studied in Poales (e.g., grasses), it is now well-established that the positive role of Si in biotic stresses is not restricted to Si-accumulating families (Fauteux *et al.* 2006; Deshmukh *et al.* 2013; Katz 2014; Johnson *et al.* 2019a; Putra *et al.* 2020). Other taxa can have [Si] as high as in grasses (Hodson *et al.* 2005; Katz 2014), Si transporters have been identified in some legume species (Deshmukh *et al.* 2013), and it has recently been demonstrated that Si is an effective defense against herbivory in soybean (Fabaceae), even at moderate leaf [Si] (Johnson *et al.* 2019a). Despite these evidences, the expression of Si-based defenses along soil fertility gradients remains underexplored,

although we might expect them to increase with declining soil fertility as predicted by the RAH.

Besides silica-based defenses, one of the most important classes of plant defenses are phenolics compounds, which have been shown to co-vary with silica-based defenses (Cooke & Leishman 2012). In accordance with the RAH, high levels of phenolic compounds have long been considered as having adaptive value for plants growing on infertile soils (Bryant *et al.* 1983; Coley *et al.* 1985; Northup *et al.* 1995; Hättenschwiller *et al.* 2003; Kraus *et al.* 2004). It has been proposed that N limitation leads to a greater expression of phenol-based defenses than phosphorus (P) limitation, because N limitation impacts the phenylpropanoid pathway more strongly, which is involved in the synthesis of both aromatic amino acids and phenol compounds (Haukioja *et al.* 1998; Jones & Hartley 1999; Wright *et al.* 2010). While this hypothesis received support in some studies (Wright *et al.* 2010; de Long *et al.* 2016), others have instead found that P limitation significantly increases plant phenol synthesis (Hättenschwiller *et al.* 2003; Sampedro *et al.* 2011; Zhang *et al.* 2012). However, these studies generally considered one single species and/or performed fertilization to simulate nutrient limitations, while community-level studies in natural environments have not been conducted. Strong natural shifts from N to P limitation of plant productivity that occur during long-term soil and ecosystem development (Vitousek *et al.* 1993; Laliberté *et al.* 2012) might therefore impact plant phenol synthesis differently in species-rich plant communities, but this has not been explored. Furthermore, the potential covariation of phenolic foliar defenses with silica-based ones (Cooke & Leishman 2012) has never been studied along soil fertility gradients.

We determined leaf Si and total phenol concentrations in plants growing along the 2 million-year Jurien Bay soil chronosequence in south-western Australia (Turner & Laliberté 2015). This long-term soil chronosequence comprises a series of coastal dunes within a global biodiversity hotspot, supporting species-rich shrubland under a Mediterranean climate (Zemunik *et al.* 2016). It exhibits an extreme gradient of soil fertility in terms of rock-derived nutrients (P, calcium, magnesium, potassium), and shifts from N to P limitation of plant productivity as soils age (Laliberté *et al.* 2012; Hayes *et al.* 2014). Leaf concentrations of major plant nutrients decrease sharply with ecosystem age (Hayes *et al.* 2014; de Tombeur *et al.* 2020c), and plants converge towards highly efficient nutrient-use strategies on the oldest, most nutrient-impoverished soils (Hayes *et al.* 2014; Guilherme Pereira *et al.* 2019). The youngest soils can also be considered infertile from an N standpoint since their N capital has not yet built up and plant growth on these soils is limited by low N availability (Laliberté *et al.* 2012; Hayes i 2014). Long-term soil chronosequences that cover both the progressive and retrogressive phases of ecosystem development provide exceptionally strong natural soil fertility and productivity gradients (Vitousek 2004; Peltzer *et al.* 2010) along which predictions of the RAH can be tested. Furthermore, the stoichiometric shifts from N to P limitation of plant growth that occur along such retrogressive soil chronosequences (Peltzer *et al.* 2010; Laliberté *et al.* 2012; Hayes *et al.* 2014) allow us to explore extensions of the RAH about the type of foliar defenses

that are expressed depending on the type of nutrient limitation (e.g. N vs P on plant phenols: Wright *et al.* 2010; de Long *et al.* 2016), which have never been explored.

In accordance with the RAH, we hypothesized a greater expression of anti-herbivore defenses in plants growing on the oldest (P-limiting) and the very youngest (N-limiting) soils, compared with the intermediate-aged and most fertile soils where plant productivity, N and P availability peak (Laliberté *et al.* 2012, 2014), but further hypothesized that the type of defense most strongly expressed would depend on the type of nutrient limitation. Specifically, we hypothesized higher leaf phenol concentrations on the younger soils given the expected impact of N limitation on the phenylpropanoid pathway, whereas we expected silica-based defenses to be most strongly expressed in the oldest, P-impoverished soils. We expect the community-level patterns to be mostly driven by changes in plant species composition since the Jurien Bay chronosequence is characterized by a strong species turnover *(Zemunik et al.* 2016). This species turnover reflects the expression of selective edaphic forces acting on a species-rich regional flora over an ecological time scale (Laliberté *et al.* 2014).

6.4 Materials and methods

6.4.1 Experimental design

This chapter is based on the > 2-million-year Jurien Bay dune chronosequence and the second sampling design (see Chapter 2 for details).

For each of the six chronosequence stage, except for stage 5, we randomly selected five plots (10 x 10 m each) within 10 plots previously characterized (Hayes *et al.* 2014; Zemunik *et al.* 2016) according to the second sampling design (see Chapter 2 for details and Figure 2-5 for the 25 plot locations). These include both the early and retrogressive phases of long-term ecosystem development. The plots were originally selected using a random stratified sampling design (Zemunik *et al.* 2016). To characterize vegetation, seven 2 m × 2 m subplots were randomly positioned in each plot in which all individuals of all vascular plant species were counted (Zemunik *et al.* 2016). The percent canopy cover of each species was estimated, and the relative cover of each species was calculated as a fraction of the total canopy cover over the seven subplots (Zemunik *et al.* 2016). For this Chapter, the original stage 6 (see Chapter 2) will be referred as stage 5 since stage 5 was not sampled.

The main soil properties of these five stages can be found in Table 6-1. Soil total P and carbonate concentrations, cation exchange capacity and pH-$CaCl_2$ continually decrease with increasing soil age. Soil total N concentrations increase from stage 1 to stage 2 during the progressive phase of ecosystem development, then decrease towards last stages during the retrogressive phase (Laliberté *et al*. 2012; Turner & Laliberté 2015). Plant growth is most strongly limited by low N availability in the early stages, and by P availability in the advanced stages (Laliberté *et al.* 2012; Hayes *et al.* 2014). Previous studies showed that plant-available [Si] is low in the early stages

of soil development, increases in stage 4 in the Spearwood dune system, and finally decreases in the oldest stage of soil development, where it is controlled by intense biocycling (Table 6-1) (de Tombeur *et al.* 2020c, b).

Table 6-1 : Main properties of the five chronosequence stages used in this study. The chronosequence stages, dune system, geological formation and estimated soil age are based on Laliberté *et al.* (2012) and Turner & Laliberté (2015). The carbonate, total phosphorus (P) and nitrogen (N) concentrations, soil total N to total P ratio, pH-$CaCl_2$ and cation exchange capacity (CEC) are based on Hayes *et al.* (2014) and Zemunik *et al.* (2016). They result from seven soil samples (0-20 cm deep) taken in each of the five plots by chronosequence stage used in this study. The limiting nutrients are based on Laliberté *et al.* (2012) and Hayes *et al.* (2014). The expected silicon (Si) availability are from de Tombeur *et al.* (2020b).

Stage	Dune system	Geological formation	Estimated soil age (ka)	Carbonates[a] (%)	pH-$CaCl_2$[b]	CEC[b] ($cmol_c$ kg^{-1})	Total P[b] (mg kg^{-1})	Total N[b] (g kg^{-1})	Soil total N to total P ratio[b]	Limiting nutrients	Expected Si availability
1	Quindalup young	Safety Bay Sand	0.1 (Holocene)	75.2(3.5)	8.2(0.1)	30.5(4.5)	351.0(6.6)	0.5(0.0)	1.4(0.1)	N	Very low
2	Quindalup medium	Safety Bay Sand	1 (Holocene)	75.5(2.8)	7.8(0.0)	12.2(1.1)	424.4(8.3)	1.2(0.0)	2.7(0.4)	N, P and/or other nutrients	Very low
3	Quindalup old	Safety Bay Sand	6.7 (Holocene)	25.6(3.7)	7.8(0.0)	10.9(0.5)	205.7(7.0)	0.7(0.0)	3.6(0.5)	N, P and/or other nutrients	Low
4	Spearwood	Tamala Limestone	125 (Middle Pleistocene)	BDL	5.8(0.1)	3.6(0.2)	18.5(1.0)	0.2(0.0)	10.7(1.9)	P	Medium
5	Bassendean	Bassendean sand	>2000 (Early Pleistocene or Late Pliocene)	BDL	4.8(0.1)	2.5(0.2)	6.6(0.5)	0.2(0.0)	30.8(8.5)	P	Low

[a]SE is indicated in brackets. The seven soil samples were bulked before analysis (n=5).
[b]SE is indicated in brackets (n=35).
BDL, below detections limits

6.4.2 Sampling procedure

In the 25 plots selected, we sampled leaves according to two procedures. First, we sampled leaves from one individual plant for each of the 10 most-abundant species of each plot as defined in Zemunik *et al.* (2016). The number of leaves sampled per individual was adapted according to their mass, but was never less than 10. Occasionally, a species originally included in the 10 most-abundant species was not found on the plot, which resulted in less than 10 species for some plots. The 234 species sampled with this first procedure still accounted for 57% to 88% of the total cover of each plot. The community-level analyses were performed only on these species. Second, we systematically sampled the species belonging to nine families, even if they were not included in the 10 most-abundant species, in order to study family-level variation in leaf [Si] and [phenols], following the same sampling procedure: Asparagaceae, Cyperaceae, Ericaceae, Fabaceae, Haemodoraceae, Myrtaceae, Poaceae, Restionaceae and Rhamnaceae. These families were selected because they were well represented and found at all stages of the chronosequence (Zemunik *et al.* 2016), and likely had contrasting [Si] based on known phylogenetic patterns (Hodson *et al.* 2005). In total, 298 leaf samples belonging to 24 families were collected.

All leaf material was collected over two weeks in November 2018. Leaves were sampled from one healthy mature individual plant per species in each plot; when an individual did not provide sufficient biomass for analysis (e.g., Poaceae spp.), leaf samples from several individuals within the plot were combined.

6.4.3 Leaf analyses

Leaves were washed with distilled water, dried at 70 °C for 48 h and finely ground. Leaf material (0.5 g) was placed in a porcelain crucible and calcinated at 450°C for 24 h. The weight after calcination was used to calculate the ash content. The ash was mixed with 1.6 g lithium-metaborate and 0.4 g of lithium-tetraborate in a graphite crucible and heated at 1000 °C for 5 min (Chao & Sanzolone 1992). The bead was then dissolved in 15% HNO_3 and the concentrations of Si, P, calcium (Ca), magnesium (Mg) and potassium (K) were determined by inductively coupled plasma-optical emission spectrometry (Agilent Technologies, 700 series ICP-OES). Phenolic compounds were extracted from a 0.25 g ground sample stirred with 10 mL of 70% acetone for 30 min (Salminen & Karonen 2011; Schaller *et al.* 2012a; Bettaieb Rebey *et al.* 2020). Total phenols were determined in triplicate as described in Salminen & Karonen (2011) using a Folin-Ciocalteu assay with gallic acid monohydrate as standard (Merckx, Darmstadt, Germany). Total phenol concentrations were expressed as g of gallic acid equivalents (GAE) per kilogram of dry weight.

6.4.4 Soil sampling and analyses

In order to determine how Si availability in soils affected species-level variations in leaf [Si], three soil samples (top 20 cm) were taken in each of the 25 plots, for a total

of 75 soil samples. Samples were air-dried and sieved (< 2 mm). The pool of 'plant-available Si' was determined by extraction in 0.01 M $CaCl_2$ (Haymsom & Chapman 1975; Sauer *et al.* 2006). Soil was shaken for 5 h in a 1:10 soil-to-solution ratio, filtered (cellulose filter, pore size < 2 µm, Healthcare Whatman™), acidified with 50 µL of ultrapure 65% HNO_3, and stored in darkness at 4°C prior to Si determination by ICP-OES.

6.4.5 Data analyses

To characterize leaf total phenols, Si, Ca, Mg, K and P concentrations in plant communities across the chronosequence, we calculated the mean values of the 10 most-abundant species per plot, weighted or not by their relative canopy cover. The cover-weighted mean (CWM) was calculated as follows (Garnier *et al.* 2004; Violle *et al.* 2007):

$$CWM = \sum_{i=1}^{S} t_i \times RC_i$$

where t_i and RC_i are, respectively, the value of the trait t and its relative cover RC for a species i and S is the number of species.

The differences in plant-available [Si], leaf [phenols], [Si], [P], [Ca], [Mg] and [K] across the chronosequence stages were tested by one-way analysis of variance (ANOVA), followed by *post-hoc* multiple comparison (Fisher's Least Significant Difference [LSD] tests). When these analyses considered all individuals together (i.e., not the mean and CWM of the plant communities), we treated species and plots as a random factor (mixed-effect models).

We tested the relationships between leaf [Si], [phenols] and major soil properties (total P, total N, ratio soil N:P) with linear mixed-effect models, treating plot and species as random factors when all individuals were considered together, and treating chronosequence stage as a random factor when the means and CWM of the 25 plots were considered.

We also explored relationships between leaf [Si], [phenols] and foliar nutrient concentrations through Pearson tests of correlation. For the nine plant families selected, we tested the differences in leaf [phenols] and [Si] across the chronosequence stages using mixed-effect models with species and plot as random factors, followed by Fisher's LSD tests, and we tested the relationships between leaf [Si] and [phenols] with linear mixed-effect models (with plot and species as random factors).

In order to study intraspecific variation, we selected the species for which we had at least nine individuals, and distributed over at least three of the five stages of the chronosequence. These conditions were met for seven taxa: *Lepidosperma calcicola*, *Conostylis candicans* subsp. *calcicola*, *Desmocladus asper*, *Stenanthemum notiale* subsp. *notiale*, *Acanthocarpus preissii*, *Acacia lasiocarpa* var. *lasiocarpa* and *Melaleuca systena*. For each of these species, we tested the influence of plant-

available [Si] (i.e., means of the three soil samples taken in each plot) on their leaf [Si] through linear mixed-effect models, treating chronosequence stage as a random factor. We also ran mixed-effect models to determine how leaf [Si] and [phenols] varied with increasing soil age within the seven species selected, treating chronosequence stage as a continuous variable. The model for [Si] included random slopes and intercepts for individual species, whereas the model for [phenols] included only random intercepts since this model fitted the data better than the one that also included random slopes. Appropriate variance structures were specified if they significantly improved the models (Zuur *et al.* 2009).

Finally, a t-test was performed to examine the differences in leaf [Si] between dicots and monocots. All residuals were visually inspected for heteroscedasticity and appropriate transformations were performed to meet the model assumptions. All analyses were conducted in R using the 'nlme' (Pinheiro *et al.* 2020) and 'multcomp' (Hothorn *et al.* 2008) packages.

6.5 Results

6.5.1 Community-level leaf [Si] and [phenols] across the chronosequence

Leaf [Si] increased with increasing soil age, whether all individuals were considered together or the means and CWM of the 25 communities (Figure 6-1a). The mean leaf [Si] within the 25 communities increased from stage 1 (0.5 ± 0.2 g kg^{-1}) to stages 2 and 3 (1.6 ± 0.4 and 2.4 ± 0.4 g kg^{-1}), and then to stages 4 and 5 (3.3 ± 1.2 and 4.2 ± 1.3 g kg^{-1}). The CWM followed the same pattern (Figure 6-1a). The CWM leaf [Si] was negatively correlated to soil total P and positively correlated to soil N to P ratio (Figure 6-2a), as for the means (Figure G-1).

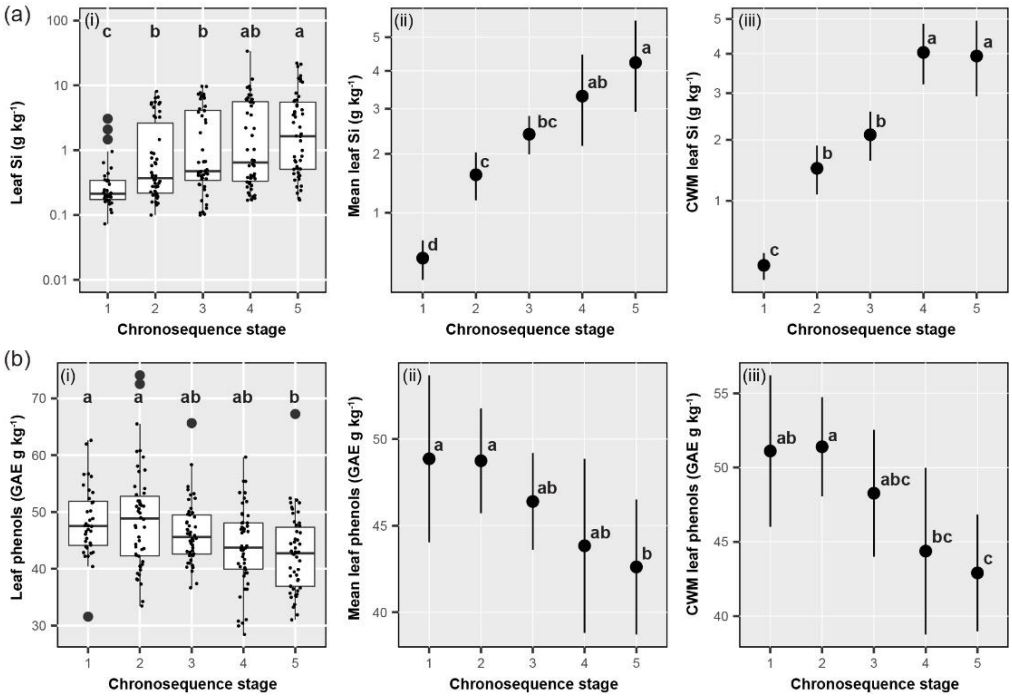

Figure 6-1 : Leaf silicon (Si) concentrations across the chronosequence stages considering all individuals (i) and the means (ii) and cover-weighted means (CWM) (iii) of the five plots per stage (a). Leaf total phenol concentrations for the same chronosequence stages and plots (b). In the box-plots, small black dots represent each individual and large black dots represent outliers (outside 1.5*inter-quartile range). In the second and third panels, black dots indicate means and bars show 95% confidence intervals (n=5). In (a), Fisher LSD groupings ($p<0.05$) were performed on log-transformed data for the first plot and on root-square-transformed data for the two others, as the scales of the axes.

By contrast, leaf [phenols] decreased with increasing chronosequence stage, whether all individuals were considered together or the means and CWM of the 25 communities (Figure 6-1b). However, only stages 1-2 and 5 were significantly different from each other when all individuals were considered together. The mean leaf [phenols] decreased from stage 1 (48.9 ± 5.5 GAE g kg^{-1}) to stage 5 (42.6 ± 3.9 GAE g kg^{-1}), as did the CWM (from 51.1 ± 5.1 to 42.9 ± 3.9 GAE g kg^{-1}). The CWM leaf [phenols] was positively correlated to soil total P and negatively correlated to soil N to P ratio (Figure 6-2b), as for the means (Figure G-1).

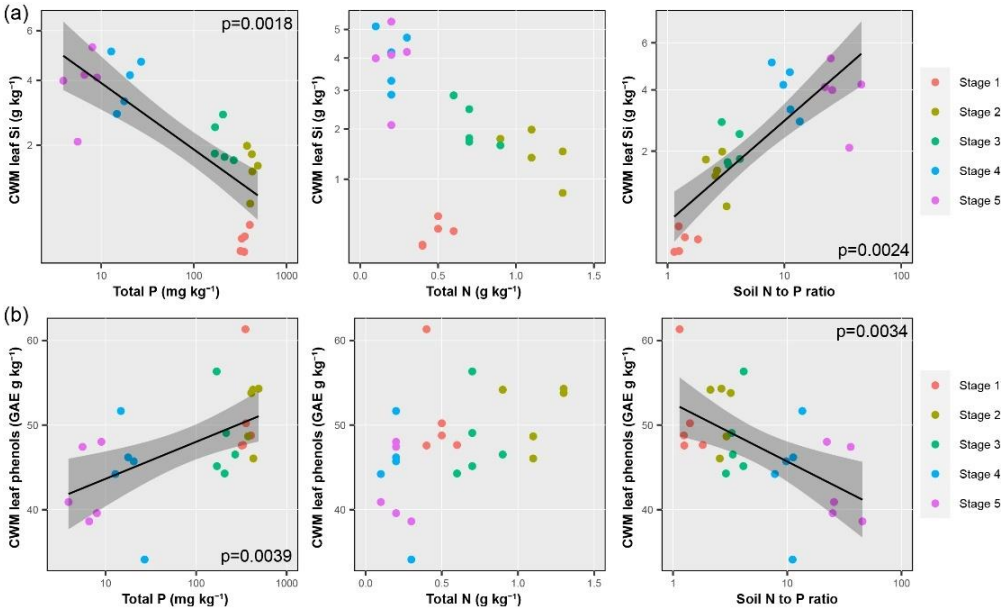

Figure 6-2 : Soil total phosphorus (P) concentrations, total nitrogen (N) concentrations and soil N to P ratio versus cover-weighted mean (CWM) leaf silicon (Si) concentrations (a) and CWM leaf total phenol concentrations (b) (n = 25 plots). Black lines indicate the regression lines between both variables, shaded areas represent 95% confidence interval of the regression and colors of the circles indicate the chronosequence stages. Axes were log-transformed for soil total P concentration and N to P ratio and root-square-transformed for CWM leaf Si concentration. The p-values of the corresponding linear mixed-effect models are indicated if < 0.05. Regression lines were removed if the model p-values were > 0.05.

Leaf [phenols] and [Si] were correlated negatively with each other when all individuals were considered (Figure 6-3a), with the means and CWM of each community (Figure 6-3b, c), and when species means were considered (Figure G-2). Leaf [ash], [Ca], [Mg], [K] and [P] decreased with increasing soil age (Figure G-3). Major leaf nutrient concentrations, including P, were therefore negatively correlated with leaf [Si], whether all samples were considered individually or as means and CWM of the 25 communities (Figure 6-3d).

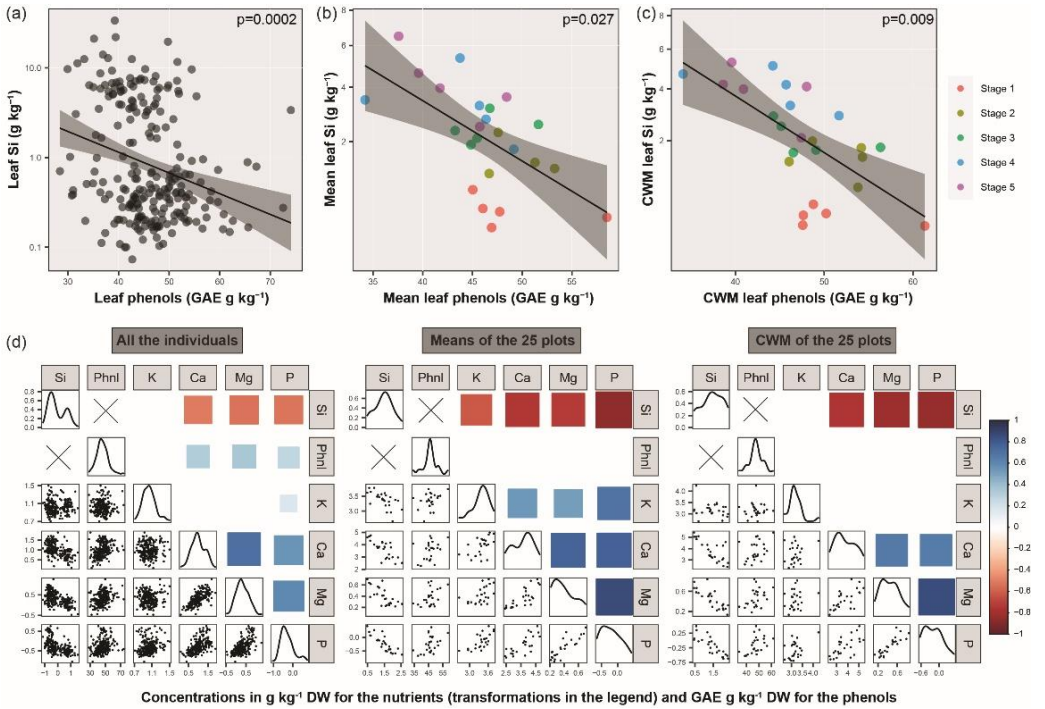

Figure 6-3 : Leaf total phenol concentrations versus leaf silicon (Si) concentrations considering all individuals (a) and the means (b) and cover-weighted means (CWM) (c) of the five plots per stage. Scatterplot correlation matrix of leaf concentrations of Si, total phenols (Phnl), potassium (K), calcium (Ca), magnesium (Mg) and phosphorus (P) considering all individuals, the means, and CWM of the five plots per stage (d). In (a), (b) and (c), black lines indicate the regression lines between both variables, shaded areas represent 95% confidence interval of the regression and colors of the circles indicate the chronosequence stages. Y-axes were log-transformed in (a) and root-square-transformed in (b) and (c). The p-values of the corresponding linear mixed-effect models are indicated if < 0.05. In (d), the size and color of the squares represent Pearson's correlation coefficient. All correlations having a p-value > 0.01 are represented by a blank space. Plots on the diagonal represent the distributions of each variable. Concentrations are in gram per kg dry weight for the nutrients and gallic acid equivalent (GAE) gram per kg dry weight for total phenols. In (d), axes were log-transformed for all variables, except for leaf [phenols] in the first plot, while root-square-transformed for leaf [Si], [Ca] and [K] and log-transformed for leaf [P] and [Mg] in the second and third plots.

6.5.2 Family and species-level leaf [Si] and [phenols] across the chronosequence

Within the Cyperaceae, leaf [Si] significantly increased with increasing soil age while leaf [phenols] decreased, and both defense types were negatively correlated through species replacement across the chronosequence (Figure 6-4). In other plant

families, leaf [Si] increased or was constant with increasing soil age, while the opposite was found for [phenols], but a significant negative relationship between both defense types was identified only for the Restionaceae (Figure G-4). For the seven species for which intra-specific variation was assessed, the mixed-effect models showed that leaf [Si] significantly increased with increasing chronosequence stage while the opposite was found for [phenols] (Table G-1).

6.5.3 Impact of species replacement on community-level leaf [Si] and [phenols]

Soil plant-available [Si] was lowest in stages 1 and 2 (1.5 ± 0.4 mg kg^{-1}), increased in stage 3 (4.0 ± 0.3 mg kg^{-1}), then in stage 4 (9.4 ± 1.0 mg kg^{-1}), before it decreased at the oldest stage (4.3 ± 0.2 mg kg^{-1}) (Table G-2). Leaf [Si] was positively related to plant-available [Si] for three species of the seven (*Lepidosperma calcicola*, *Desmocladus asper* and *Acacia lasiocarpa* var. *lasiocarpa*) for which intra-specific variations were considered (Table G-3). These species tended to accumulate more Si than those that did not show a correlation with plant-available [Si]. Despite this relationship between plant-available [Si] and leaf [Si] at the species-level (more pronounced for Si-accumulating species, with the exception of *Conostylis candicans* subsp. *calcicola*), the increase of the CWM leaf [Si] with increasing soil age was primarily driven by changes in the dominant plant families across the chronosequence (Figure G-5). The increase of the mean and CWM leaf [Si] with increasing soil age was not only driven by changes in the dominant families, but also within families and genera. For instance, *Hibbertia racemosa* had a leaf [Si] of 0.2 g kg^{-1} DW in the young stages, while *Hibbertia hypericoides* subsp. *hypericoides* reached concentrations of 11.7 g kg^{-1} DW in the oldest stage. We observed the same pattern for *Acacia* (*Acacia rostellifera* on stages 1, 2 and 3: 0.2–0.8 g kg^{-1} DW; *Acacia pulchella* var. *glaberrima* on stage 6: 2.7–4.3 g kg^{-1} DW). When considering Cyperaceae, *Ficina nodosa* (leaf [Si] from 0.2 to 0.3 g kg^{-1} DW; n=3) was found only at stage 1, while *Mesomelaena pseudostygia* (leaf [Si] from 8.8 to 43.0 g kg^{-1} DW; n=7) and *Schoenus* spp. (leaf [Si] from 4.1 to 21.2 g kg^{-1} DW; n=8) were found only at stages 4 and 5.

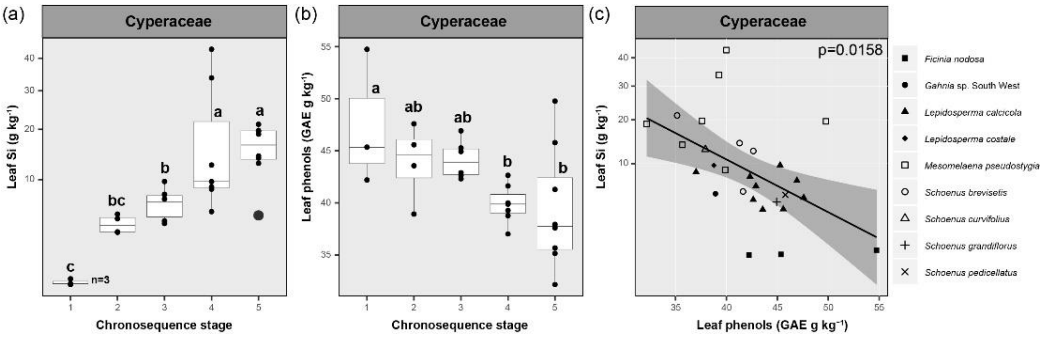

Figure 6-4 : Leaf silicon (Si) (a) and total phenol concentrations (b) across the chronosequence stages for Cyperaceae, and relationship between both for the same individuals (c). In (a) and (b), the small black dots represent each species and large black dots represent outliers (outside 1.5*inter-quartile range). In (a), Fisher LSD groupings ($p<0.05$) were performed on root-square-transformed data, as the scale of the axes. In (c), the y-axis was root-square-transformed; each symbol represents a different species, the black line indicates the regression line between both variables, the shaded area represents 95% confidence interval of the regression, and the p-value of the corresponding linear mixed-effect model is indicated.

The plant families with the strongest contribution to the CWM leaf [phenols] strongly differed across the chronosequence (Figure G-5), highlighting the importance of species replacement on the patterns observed at the community level. In contrast to leaf [Si], the contribution of each family to the CWM [phenols] was proportional to its relative cover, highlighting less variation in [phenols] among families.

6.6 Discussion

Overall, our results do not support the main prediction of the RAH, since investments in the two anti-herbivore defenses considered were not the lowest at the most fertile soils, where both N and P availability and plant productivity peak (stages 2 and 3) (Laliberté *et al.* 2012). Instead, community-level leaf [Si] was highest on old, nutrient-impoverished soils, where P limits plant productivity, while leaf [phenols] were the highest on young soils, where plant productivity is limited by N, and both defenses were negatively correlated with each other (Figure 6-5). Nevertheless, only two types of chemical defense were considered in this study and the hypothesis of an overall greater investment in defenses in the least fertile soils as predicted by the RAH should consider the full array of anti-herbivore defenses, including structural, physical and qualitative chemical defenses (Aplin & Cannon 1971; Moles *et al.* 2013; Lambers & Oliveira 2019).

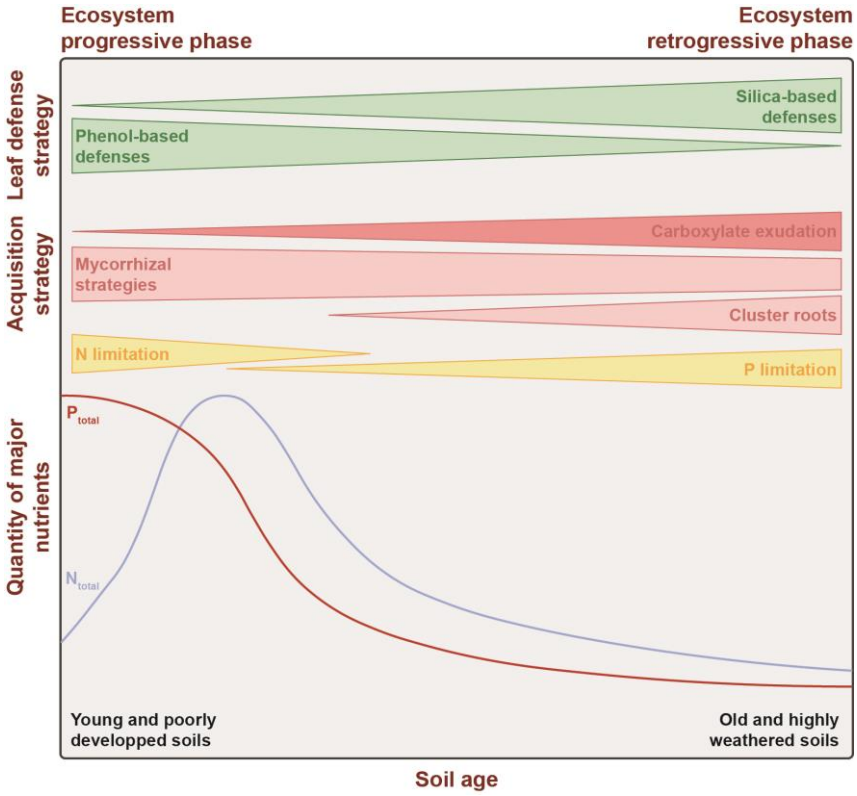

Figure 6-5 : Schematic representation (adapted from Lambers *et al.* 2008) changes in soil total phosphorus (P) and nitrogen (N), P-acquisition strategies, and leaf defense strategies during long-term ecosystem development. Changes in soil P and N are based on Hayes *et al.* (2014). At the Jurien Bay chronosequence, soil total P concentration continually declines with increasing soil age, from about 430 to 6 mg kg^{-1}, while total N concentration increases from 0.5 to 1.2 g kg^{-1} in the young soils where total [P] is relatively high, then declines to 0.2 g kg^{-1} in the oldest soil, resulting in a shift from N to P limitation of plant growth. The changes in nutrient-acquisition strategies were originally suggested by Lambers *et al.* (2008), but subsequently confirmed in Zemunik *et al.* (2015). Along the Jurien Bay chronosequence, the relative cover declines for arbuscular mycorrhizal and ectomycorrhizal species, but increases for carboxylate-releasing cluster-rooted species and others with functionally equivalent strategies. The changes in silica and phenol-based defenses are based on the present study.

The use of soil chronosequences allows us to minimize effects of other ecosystem properties (e.g., climate, topography, parent material, salt content) beyond soil age and associated changes in major nutrients (e.g. N, P) that might influence leaf [Si] and [phenols], yet we cannot completely rule out other covarying factors. In particular, soil pH declines along the chronosequence which could indirectly impact plant-available [Si] (de Tombeur *et al.* 2020b). However, our previous work has shown that community-level changes in foliar [Si] with soil age across this chronosequence

primarily arise from plant species turnover toward those that accumulate foliar [Si] as soil P availability declines, and not directly because of pH-induced changes in Si availability (de Tombeur *et al.* 2020c). Similarly, since soil nutrient availability has a greater impact on plant phenol concentrations than soil pH (Kraus *et al.* 2004), we interpret the changes in foliar [Si]| and [phenols] mainly in terms of changes in soil N and P availability that are the major drivers of plant community assembly along the Jurien Bay chronosequence (Laliberté *et al.* 2014).

6.6.1 Convergence towards silica-based defenses during ecosystem retrogression

Our results show a convergence towards plants having higher leaf [Si] on P-impoverished soils, during ecosystem retrogression. Indeed, despite the decrease of plant-available [Si] in the last stage induced by soil desilication (de Tombeur *et al.* 2020b), the intense cycling of highly-soluble plant-derived Si in the oldest soils allows maintenance of high leaf [Si] (de Tombeur *et al.* 2020c). The convergence towards plants having higher leaf [Si] with increasing nutrient depletion was accompanied by a strong decrease in leaf macronutrient concentrations, including N (Hayes *et al.* 2014; Guilherme Pereira *et al.* 2019), and an increase in leaf mass per area (LMA) and leaf dry matter content (LMDC) along the Jurien Bay chronosequence (Guilherme Pereira *et al.* 2019). These traits highlight the convergence towards slow-growing plants adapted to P-impoverished soils and nutrient-poor environments with increasing soil age (Lambers & Poorter 1992; Wright *et al.* 2004; Garnier & Navas 2013; Reich 2014). Their higher leaf [Si] suggests that these species have evolved towards higher levels of silica deposits to minimize biomass and nutrient loss by herbivores in these nutrient-poor environments, in line with the RAH (Coley *et al.* 1985). Following this hypothesis, the likely longer leaf lifespan of these species could partly explain their higher expression of silica-based defenses, since Si accumulates as a leaf ages (Motomura *et al.* 2002).

Among the dominant families growing on the last stage, the positive role of silica-based defenses on herbivore attacks has been demonstrated for Poaceae, Cyperaceae and Fabaceae to our knowledge (Massey & Hartley 2006; Wieczorek *et al.* 2015; Johnson *et al.* 2019a). However, we can reasonably extend the same mechanisms to the high monocot Si families Restionaceae, Dasypogonaceae and Haemodoraceae. These six families represent a relative cover of 41%. It has been shown that positive effect of silica-based defenses on herbivores could be identified in the low range of 2-6 g Si kg^{-1} for a Fabaceae species (Johnson *et al.* 2019a). This range is lower than that of the Dilleniaceae species (relative cover of 5%) growing at stage 5 (foliar [Si] from 6.0 to 11.7 g Si kg^{-1}). Proteaceae (relative cover of 29%) have strongly contrasted foliar [Si], from 0.2 to 6.8 g Si kg^{-1}. However, species having foliar [Si] < 2 g Si kg^{-1} represented a total relative cover of only 20% and an abundant presence of phytoliths in epidermal cells of Banksia spp. has recently been identified (Gao et al. 2020). Overall, we can assume that about two thirds of the species growing on the last stage could potentially use silica as an efficient defense against herbivores although it would

still deserve investigations as the patterns of silica deposits and defense mechanisms may differ between families. For Myrtaceae (relative cover of 16%) and others minor families (relative cover of 9%), a role of silica-based defenses against herbivores is unlikely, but would deserve investigations.

An alternative but not necessarily mutually exclusive hypothesis could be mitigation of P stress. The first evidence for a positive effect of Si for plants growing under P stress came from the Rothamsted Experimental Station (Hall & Morison 1906). Since then, other studies have made similar observations (Ma & Takahashi 1990b; Neu *et al.* 2017) and Quigley *et al.* (2020) recently proposed that high levels of biosilicification might be an adaptation to resource-poor environments. Although the mechanisms proposed are numerous and diverse, the positive role of Si under P stress is becoming clearer (Kostic *et al.* 2017), and could explain the convergence towards species having higher leaf [Si] with increasing P depletion. Overall, our results suggest that leaf Si is associated with the 'slow' end of the leaf economics spectrum (Wright *et al.* 2004; Reich 2014), with species having long-lived leaves with low macronutrient concentrations and high LMA and LDMC, but this hypothesis requires further investigation.

The increase of the CWM leaf [Si] from the P-limited ecosystem in stage 4 is partly explained by Proteaceae having high relative cover and relatively high [Si] for dicot species (up to 6.8 g kg^{-1} DW; Hodson *et al.* 2005). We have no information on Si transporters (Ma *et al.* 2006) in Proteaceae, but it is possible that the exudation of carboxylates in the rhizosphere by their cluster roots (Lambers *et al.* 2008) mobilizes Si from poorly-soluble minerals, thus favoring its uptake. These cluster roots release carboxylates into the rhizosphere and release P from strongly sorbed inorganic forms (Lambers *et al.* 2008), but also mobilize micronutrients such as manganese (Mn) (Lambers *et al.* 2015; Pang *et al.* 2018). Some carboxylate-releasing roots mobilize P from rocks that are highly resistant to weathering, such as quartzite (Teodoro *et al.* 2019). The relatively high leaf [Si] in some dicot species exhibiting such specialized P-acquisition strategies might therefore be explained by their mobilization of Si through carboxylate exudation into the rhizosphere. More generally, this mechanism might explain the convergence towards leaves with higher [Si] with increasing nutrient-depletion, because the relative cover of cluster-rooted species increases markedly along the Jurien Bay chronosequence (Figure 6-5) (Zemunik *et al.* 2015), and other species might benefit from the carboxylate exudation of their neighbors (Lambers *et al.* 2018). This mechanism may also explain why we observed species with some of the highest leaf [Si] found in literature (up to 43 g kg^{-1} DW for *Mesomelaena pseudostygia* at stage 4) (Schoelynck *et al.* 2010; Carey *et al.* 2017, 2019; Schaller *et al.* 2018; Ishizawa *et al.* 2019; Nakamura *et al.* 2019) although the Jurien Bay soils are among the most desilicated worldwide, with one of the lowest Si availability for plants (de Tombeur *et al.* 2020b).

6.6.2 Nitrogen limitation and phenol synthesis on young soils

The CWM leaf [phenols] slightly, but significantly, decreased with increasing soil age, which we interpreted as resulting from the N-limiting conditions on the youngest soils. Indeed, although some studies suggest that P limitation increases phenol synthesis (Sampedro *et al.* 2011; Zhang *et al.* 2012) including along a long-term Hawaiian soil chronosequence (Hättenschwiller *et al.* 2003), our results are in line with others showing that N limitation has a greater effect on quantitative plant secondary metabolites (Koricheva *et al.* 1998; Wright *et al.* 2010; de Long *et al.* 2016).

The apparent stronger effect of N- compared with P limitation might be explained by their different role in plant metabolism (Jones & Hartley 1999; Wright *et al.* 2010). Under N-limiting conditions, there could be a surplus of photo-assimilates because leaf growth decreases sharply, while photosynthesis continues, albeit at a somewhat slower rate (Prescott *et al.* 2020). The ammonium-N in phenylalanine, which is a precursor of both aromatic amino acids and phenolic compounds, would then be released and re-used in other N-containing molecules (Kováčik *et al.* 2007). The rest of the phenylalanine molecule then becomes available for secondary metabolic pathways, in which it is converted into C-based secondary metabolites such as phenylpropanoid derivatives (Haukioja *et al.* 1998; Koricheva *et al.* 1998; Jones & Hartley 1999). This might explain why plants growing on the young N limited environments had higher [phenols], eliminating a surplus of photo-assimilates while conserving N. Under P-limiting conditions, however, any surplus of photo-assimilates would be exported from the chloroplasts as P-containing compounds, and converted into sucrose via reactions that release P, which is retained and reused (Stitt & Quick 1989). Therefore, P-limiting conditions might not affect the pathway of secondary metabolite synthesis in a way that N limitation does (Koricheva *et al.* 1998; Wright *et al.* 2010). Although the primary function of plant phenolic compounds may be the release of N, rather than defense against herbivores, it does make leaves less palatable for mammalian herbivores such as kangaroos (Rafferty *et al.* 2005, 2010) on the youngest N-limited stages of the Jurien Bay chronosequence (Figure 6-5).

6.6.3 Conclusions and Perspectives

Leaf [phenols] and [Si] were negatively correlated when considering the means and CWM of each community, all the individuals together, and within the Cyperaceae and Restionaceae family, which suggest a tradeoff between both leaf defense strategies. This pattern was observed previously (Cooke & Leishman 2012; Moles *et al.* 2013; Frew *et al.* 2016; Simpson *et al.* 2017; Waterman *et al.* 2021), but never along a soil resource gradient. Here, the species growing on older soils and adapted to nutrient-poor environments tend to favor silica accumulation over the synthesis of phenols compared with species growing on younger soils.

Raven (1983) calculated that, on a weight basis, the energetic cost of incorporating 1 g of lignin is about 27 times higher that of incorporating 1 g of SiO_2. Given the lower

metabolic costs of incorporating Si compared with others C-based compounds having similar functions (cellulose, lignin, phenols) (Schoelynck *et al.* 2010; Cooke & Leishman 2012; Klotzbücher *et al.* 2018c; de Tombeur *et al.* 2020a), investing in silica as a defense mechanism (and eventually as leaf support for Cyperaceae) would make sense from an energetic standpoint on the oldest and most nutrient-depleted soils, where plants converge towards the 'slow' end of the leaf economics spectrum (Reich 2014; Guilherme Pereira *et al.* 2019). This energetic gain would save resources for other key aspects of the plant life cycle like growth and reproduction during ecosystem retrogression, which is key in these highly-infertile environments (Lambers 2014). Further studies should now investigate other types of anti-herbivore defenses to better evaluate the overall investment in defenses as a function ofs soil fertility along the Jurien Bay chronosequence. This is important given that plants display a wide range of defense traits, without clear evidence of tradeoffs between them globally (Moles *et al.* 2013). Overall, our study suggests that the type of nutrient limitation (i.e., N vs P) may induce tradeoffs in plant defense strategies, opening up new perspectives about the role of soil nutrient stoichiometry in the expression of plant defenses.

7

Silicon mobilization by root-released carboxylates*

*This Chapter is adapted from

de Tombeur, F., Cornélis, J-T., Lambers, H. Silicon mobilization by root-released carboxylates. *Under review in Trends in Plant Science*

7.1 Foreword

In the chapter 4, we demonstrated that soil phytoliths controlled plant-available Si in old and highly-desilicated soils of the Jurien Bay and Guilderton chronosequences. We also showed that community-level leaf Si concentrations continually increased as soils age, in contrast to the major nutrients that decreased. In the previous chapter, we demonstrated that such increase in the expression of silica-based defenses was associated with increased P limitation, and a decrease in phenol-based defenses. Moreover, we wondered if root-released carboxylates might mobilize Si for plant uptake, which has received almost no attention in the literature. The Jurien Bay chronosequence is indeed characterized by an increase in species exhibiting carboxylate-releasing P-mobilizing strategies with increasing soil age, which might explain the increase in leaf Si observed at the community and species-level. In this new chapter, presented in the form of an opinion paper, we considered if root-released carboxylates increase soil Si mobilization from different minerals by reanalyzing data from chapter 6, and by performing simple extractions with carboxylates added to soils and reference materials. We specifically considered the influence of carboxylates on phytoliths dissolution because they control plant-available Si in older soils (chapter 4), but quartz dissolution was also considered since it is the dominant mineral in advanced weathering stages. Si mobilization from phytoliths by root-released carboxylates could explain why silica-based defenses increase in old, P-poor soils (chapter 6), and could reinforce the key role of plants in maintaining Si in a biogenic pool that is actively cycled during ecosystem retrogression (chapter 4).

7.2 Summary

Plants have evolved numerous strategies to acquire poorly-available nutrients from soil, including the release of carboxylates from their roots. Silicon (Si) release from mineral dissolution increases in the presence of chelating substances, and recent evidence shows that leaf [Si] increase markedly in old phosphorus (P)-depleted soils, where many species exhibit carboxylate-releasing strategies, compared with younger P-richer soils. Here, we propose that root-released carboxylates, and more generally rhizosphere processes, play an overlooked role in plant Si accumulation by increasing soil Si mobilization from minerals. We suggest that soil Si mobilization is costly in terms of carbon, but free if those costs are met for P acquisition. Uptake of the mobilized Si by roots will then depend on whether they express Si transporters.

7.3 Manganese as a proxy for rhizosphere carboxylates

In 2015, Lambers *et al.* published an opinion paper in this journal, proposing that leaf manganese concentrations ([Mn]) can be used as a proxy for rhizosphere carboxylate (see Glossary) concentrations. This tool has now been used to screen native plant species growing in natural habitats (Hayes *et al.* 2014; Lambers *et al.*

2021; Zhong *et al.* 2021) as well as genotypes of chickpea (*Cicer arietinum*) under glasshouse conditions (Pang *et al.* 2018; Wen *et al.* 2020). The tool is also valuable to investigate to what extent neighbors depend on facilitation of their phosphorus (P) uptake by carboxylate-releasing species (Yu *et al.* 2020a, b). Results on leaf [Mn], therefore, offer tremendous potential to obtain information on rhizosphere processes that is very hard to get, especially under field conditions. Not only does it allow us to find out if a particular species uses a P-mobilizing carboxylate-releasing strategy, but it can also provide evidence for facilitation of P acquisition of neighbors of species that release carboxylates (Abrahão *et al.* 2018; Zhong *et al.* 2021). Carboxylate-releasing strategies are particularly important on severely P-impoverished ancient soils (Lambers *et al.* 2008) and on young volcanic soils with low P availability due to strong P sorption onto amorphous Fe oxides (Lambers *et al.* 2012; Ávila-Valdés *et al.* 2019).

Recently, de Tombeur *et al.* (2020c, 2021b) showed that on ancient soils along the Jurien Bay chronosequence (south-western Australia) where many species exhibit carboxylate-releasing P-mobilizing strategies, community and species-level leaf silicon concentrations ([Si]) are markedly higher than on younger P-richer soils, despite very low plant-available [Si] in soil. Conversely, all leaf macronutrient concentrations decrease with increasing soil age (Hayes *et al.* 2014; de Tombeur *et al.* 2020c, 2021b). In addition to a contribution of recycled soil phytoliths (*i.e.* phytogenic silica) as a source of plant-available Si in these old soils (de Tombeur *et al.* 2020c), this observation led us to explore if there is a causal relationship, with carboxylates not only mobilizing P and Mn, but also Si, which is abundant in soil, but not invariably readily available for plants. We propose a conceptual model (Figure 7-1) that explains why leaf [Si] increases in some species on ancient soils. We also propose ways to test our model and suggest future research directions.

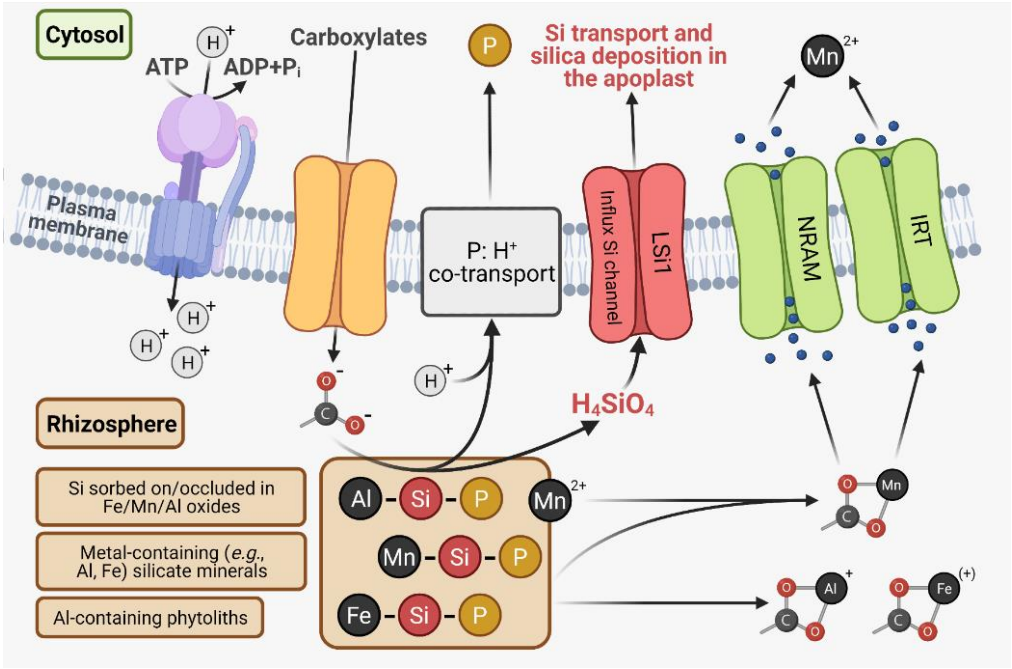

Figure 7-1 : Effects of phosphorus (P)-mobilizing carboxylates on ligand-promoted dissolution of minerals, thus releasing iron (Fe), aluminum (Al) and manganese (Mn), and co-solubilizing silicon (Si). Carboxylates (organic anions) are released via a carboxylate channel. Inorganic P (Pi) is taken up by P transporters against an electrochemical potential gradient, driven by a proton gradient resulting from active H+ transport by a H+-pumping ATPase (Nussaume et al. 2011). Carboxylates chelate metal cations (e.g., Fe, Al and Mn) of pedogenic oxides (e.g., Fe, Al and Mn oxides) and metal-containing silicates, among which probably biogenic silica (i.e. Al-containing phytoliths). In Strategy 1 species, chelated Fe moves to the root surface, where it is reduced, followed by uptake via a Fe2+ transporter [iron-regulated transporter (IRT)]; in Strategy 2 species, ligand exchange converts Fe to Fe3+-phytosiderophore (PS) complexes for root uptake via the Fe3+-PS transporter [yellow stripe 1 (YS1) and yellow stripe-like (YSL) transporter] (Kim & Guerinot 2007; Baxter et al. 2008). This transporter is not specific and transports other micronutrients, including Mn2+. Silicon occluded in metal-containing silicates as well as Si sorbed onto or co-precipitated in pedogenic oxides is subsequently released into the soil solution in the form of monosilicic acid (i.e. H4SiO4) by this ligand-promoted dissolution process (Su et al. 1995; Blake & Walter 1999). Monosilicic acid can then be taken up actively by Si transporters, e.g., LSi1, which is highly expressed in some species, e.g., rice (Oryza sativa) (Ma et al. 2006), but not in other species. On soils with low plant-available [Si], we expect accumulation of Si in plants with high rhizosphere carboxylate concentrations that highly express Si transporters. High concentrations of carboxylates in the rhizosphere may be the result of release of the Si-accumulating plants themselves, as shown here, or by their neighbors (Yu et al. 2020a). Modified from (Lambers et al. 2015).

7.4 Silicon uptake in plants

Silicon uptake in plants is predominantly an active process, and Si enters the plant from the soil solution in the form of H_4SiO_4 through specific influx channels (Si transporters) encoded by a specific gene, *OsLSi1* in rice (*Oryza sativa*) where it is constitutively expressed in the roots (Ma *et al.* 2006). The gene *Lsi1* is expressed in a range of other plant species including maize (*Zea mays*), barley (*Hordeum vulgare*), wheat (*Triticum aestivum*), soybean (*Glycine max*), and tomato (*Solanum lycopersicum*) (Chiba *et al.* 2009; Mitani *et al.* 2009; Montpetit *et al.* 2012; Deshmukh *et al.* 2013; Sun *et al.* 2020a). Plant species differ greatly in Si accumulation, ranging from 1 to 100 g kg^{-1} shoot dry weight (Hodson *et al.* 2005). The difference depends on whether a species expresses transport proteins allowing Si permeability (Coskun *et al.* 2019). In addition to actively taking up Si, plants acquire it passively (Liang *et al.* 2006). Active transport is the major mechanism in rice and maize (*Zea mays*), whereas passive uptake prevails in sunflower (*Helianthus annuus*) and wax gourd (*Benincase hispida*) at higher external Si concentrations (Liang *et al.* 2006). Even in these species active transport contributes to the total Si uptake, especially at lower external Si concentrations. Silicon occurs as hydrated amorphous silica (phytoliths) in specific cells of roots, stems and leaves.

7.5 Silicon in plants: phytoliths

Phytoliths in plants are thought to function as structural support (de Tombeur *et al.* 2021a) and in herbivore defense, by abrading herbivore mouthparts (Strömberg *et al.* 2016). Plant silicification also increases plant resistance to water stress (Meunier *et al.* 2017), reduces the soil-to-plant translocation of toxicants (Coskun *et al.* 2019), and probably interferes with the recognition process upon pathogen infection (Coskun *et al.* 2019; Leroy *et al.* 2019). Phytoliths vary widely in chemical composition. In addition to Si, carbon (C) and oxygen (O) (Alexandre *et al.* 2015), some contain aluminum (Al), and this is considered a mechanism to detoxify Al (Hodson & Evans 2020; Liu *et al.* 2021). Phosphorus may also become trapped in phytoliths (Trinh *et al.* 2017) as do a wide range of other elements, both nutrients and toxic elements (Kameník *et al.* 2013; Liu *et al.* 2021).

Silica-based defenses are considered as cheap alternatives for carbon-based quantitative defense compounds, because the formation of silica requires less metabolic energy than that of lignin (Raven 1983). There also appears to be a trade-off between investments in silica- and C-based defense/structural compounds (Simpson *et al.* 2017; de Tombeur *et al.* 2020a; Waterman *et al.* 2021). In support of this, de Tombeur *et al.* (2021b) found a trade-off between phenol- and silica-based defenses along the Jurien Bay chronosequence that exhibits a strong gradient of nutrient availability (Turner & Laliberté 2015; de Tombeur *et al.* 2021b), with a stronger expression of silica-based defenses in old P-depleted soils. Investing in silica-based defenses rather than phenol-based defenses in severely nutrient-depleted habitats, when resources are severely limiting, would make sense from an energetic

perspective (Raven 1983). However, if silica-based defense is effective and less costly, why do not all plants invest greatly in this putatively cheap defense strategy, rather than one based on more costly carbon-based quantitative defense compounds? As we explore below, this is likely because Si-based defense involves few metabolic costs only if there is plenty of plant-available Si in the rhizosphere, but may involve substantial costs if Si needs to be mobilized to become available for plant uptake.

7.6 Silicon mobilization by root-released carboxylates

7.6.1 Carboxylate effects on soil Si mobilization

Carboxylate-releasing strategies are crucial for plants growing in severely P-impoverished soils (Lambers *et al.* 2008, 2018). However, their role for plant Si uptake in mobilizing soil Si from soil minerals has never been seriously considered. Yet, root-released carboxylates do not only increase soil P and Mn mobilization, but also that of Al, iron (Fe), calcium (Ca), potassium (K) and several other metals (Gerke *et al.* 1994; Ström *et al.* 2005; Wang *et al.* 2011; Kabas *et al.* 2017). Carboxylates mobilize P from sorbed forms by complexing metal cations constituting the minerals that bind phosphate (*e.g.*, Fe and Al oxides), and displace P from the soil matrix by ligand exchange (Figure 7-1) (Reichard *et al.* 2007). This accounts for the strong increase in dissolved [Al] and [Fe] in the rhizosphere of root clusters compared with bulk soil (Gerke *et al.* 1994). Since Fe and Al oxides show a strong potential to sorb Si (Jones & Handreck 1963; Hingston & Raupach 1967; Nguyen *et al.* 2017), and because Si can be occluded in those pedogenic oxides, a release of monosilicic acid after Al/Fe oxides ligand-promoted dissolution is very likely (Figure 7-1). In support of this, the Si and Fe co-released from a quartz-rich soil containing Fe oxides is significantly increased by three carboxylates abundantly exuded by specialized roots, and the releases of both elements are positively correlated (Figure 7-2A, 7-2B). Similarly, the dissolution of primary minerals like feldpars, 2:1 clay minerals like chlorite and 1:1 clay minerals like kaolinite are also ligand-promoted, and release monosilicic acid in solution (Figure 7-2C) (Blake & Walter 1999; Cama & Ganor 2006).

Mobilizing Si from crystalline silicates via root-released carboxylates involves complexation of a metal cation. In old highly-weathered soils, Si-bearing minerals are eventually dominated by quartz and phytoliths, since most primary minerals and Al/Fe-containing secondary minerals have been lost by dissolution. Here, carboxylates may also play a role in mobilizing Si, because low-molecular-weight organic acids increase Si release from quartz (Bennett *et al.* 1988), and we may expect organic acid-induced dissolution of phytoliths through Al complexation. In support of this, the release of Si from pure quartz is slightly increased by oxalate (Figure 7-2C), yet not by two others carboxylates (malate, citrate). However, adding carboxylates in a phytoliths and pure quartz mixture with phytolith concentration commonly

encountered in soils (4 g kg^{-1}; *e.g.*, (Alexandre *et al.* 2011; de Tombeur *et al.* 2020c)) significantly increases the effect of carboxylates on Si release (Figure 7-2C). This demonstrates the prominent influence of carboxylates on phytoliths dissolution relatively to quartz dissolution. This process combined with the relatively high reactivity of phytoliths compared with soil-derived minerals might explain why Si biocycling remains intense in old soils having extremely low plant-available [Si] (de Tombeur *et al.* 2020c).

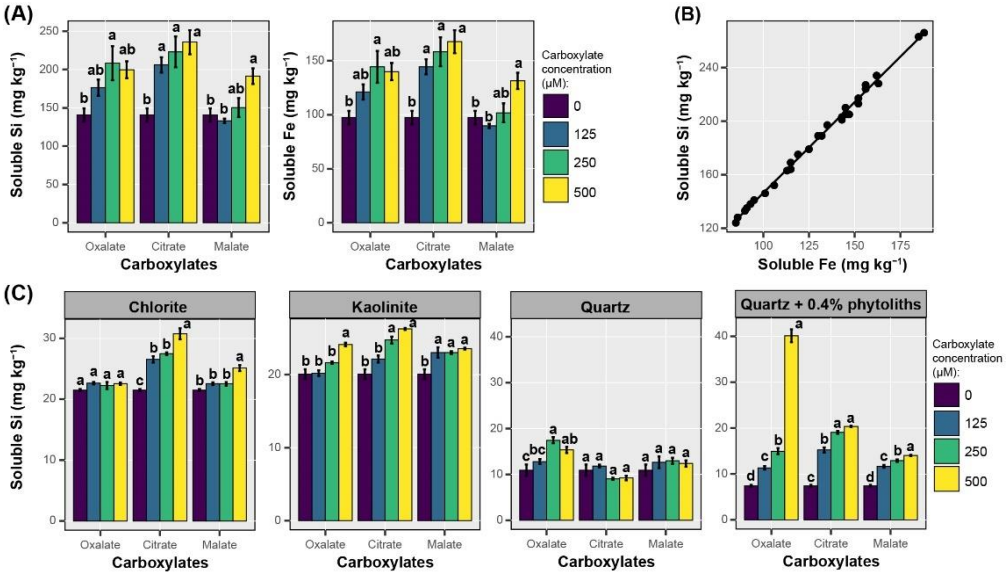

Figure 7-2 : Effects of a range of oxalate, citrate and malate concentrations on silicon (Si) and iron (Fe) release from a quartz-rich soil containing Fe oxides (stage 4 of the Jurien Bay chronosequence; (de Tombeur et al. 2020c)) (means ± SE; n = 3) (A), and relation between the release of both elements for the same soil and same carboxylates at similar concentrations (B). Effects of same carboxylates at same concentrations on Si release from pure chlorite (purchased from the Source Clays Repository, Purdue University), pure kaolinite (same manufacturer), pure quartz (Supelco®), and pure quartz mixed with sugarcane phytoliths from (de Tombeur et al. 2020a) at a 0.4% concentration (means ± SE; n = 3) (C). Three grams of soil/reference material was shaken for 16 h with 30 mL of a 0.01 M KCl solution with different carboxylate concentrations (0, 125, 250 and 500 µM) (Wouterlood et al. 2004), and Si and Fe were analyzed by ICP-OES after filtration. In (A) and (C), bar colors indicate carboxylate concentrations, and different letters indicate significant differences ($p \leq 0.05$) among carboxylate concentrations (ANOVA followed by Tukey HSD tests). In (B), the black line indicates the regression line between both variables.

7.6.2 Evidence based on relationships between leaf [Si] and [Mn]

Since leaf [Mn] can be used as a proxy for carboxylate-releasing strategies (Lambers *et al.* 2015, 2021; Pang *et al.* 2018), similar patterns for the two elements are expected if Si is also mobilized during the process (Figure 7-1). Interestingly, foliar [Si] and [Mn] increase along the Jurien Bay chronosequence, as opposed to a decrease in concentrations of all macronutrients (Hayes *et al.* 2014; de Tombeur *et al.* 2021b). For leaf [Si], such increase is not only observed at the community-level, but also within some species (de Tombeur *et al.* 2020c, 2021b). This pattern is associated with a strong decline in soil P concentration (de Tombeur *et al.* 2021b), and a subsequent increase in the relative cover of species with cluster roots or their functional equivalent (Zemunik *et al.* 2015) that release carboxylates to acquire poorly-available P (Lambers *et al.* 2008).

Interestingly, both leaf [Si] and leaf [Mn] are significantly greater in non-mycorrhizal species than in mycorrhizal species across the Jurien Bay chronosequence, with most non-mycorrhizal species known to release carboxylates (Figure 7-3A) (Hayes *et al.* 2014; Lambers *et al.* 2015). This pattern occurs across all soils of the chronosequence (expect for leaf [Si] at stage 1), despite wide variation in pH-values (~5-8) (Figure 7-4) (Hayes *et al.* 2014). In addition, high leaf [Si] in the mycorrhizal group (> 5g kg^{-1}) only occur in Poaceae, which have Si transporters (Ma *et al.* 2006), and in *Hibbertia hypericoides* individuals (Dilleniaceae) that do not release carboxylates but are typically facilitated by cluster roots of neighboring banksias (Proteaceae) (de Britto Costa *et al.* 2021; Zhong *et al.* 2021). In contrast, non-mycorrhizal species with relatively low leaf [Si] (< 5g kg^{-1}) are dominated by Proteaceae, for which the presence of Si transporters is unknown. Such similarity between leaf [Si] and [Mn] along this chronosequence is supported by a positive relationship between the concentrations of both elements when species from different families are considered (Figure 7-3B). This occurs across all soils of the chronosequence, whatever the variations in soil pH (Figure 7-5).

Since leaf [Si] vary greatly among terrestrial plant species (Hodson *et al.* 2005) due to the presence/absence of Si transporters (Deshmukh *et al.* 2020), lower leaf [Si] among mycorrhizal species likely reflects lower expression of Si transporters in this group (*e.g.*, Asparagaceae, Fabaceae, Myrtaceae, Rhamnaceae) compared with non-mycorrhizal species (*e.g.*, Cyperaceae, Haemodoraceae, Proteaceae, Restionaceae). Therefore, we also reanalyzed data from de Tombeur *et al.* (2021b) for family- and species-level variation. Interestingly, both nutrients are positively correlated for both mycorrhizal (Fabaceae, Poaceae) and non-mycorrhizal (Proteaceae, Cyperaceae) families (Figure 7-3C). The relationships are clearer for families known to strongly express Si transporters (Poaceae and Cyperaceae) than for the two others (Fabaceae, Proteaceae). Leaf [Si] and [Mn] are also correlated for *Desmocladus asper* (Restionaceae) (Figure 7-3C), a non-mycorrhizal species that forms sand-binding roots (Abrahão *et al.* 2014) and possibly capillaroid roots (Lamont 1982). Similarly,

Kothari et *al.* (Kothari *et al.* 1990) found a highly significant positive correlation between leaf [Si] and [Mn] in maize shoots. We suggest that these relations between leaf [Si] and [Mn] can be partly explained because both elements are mobilized by carboxylates in the rhizosphere (Figure 7-1).

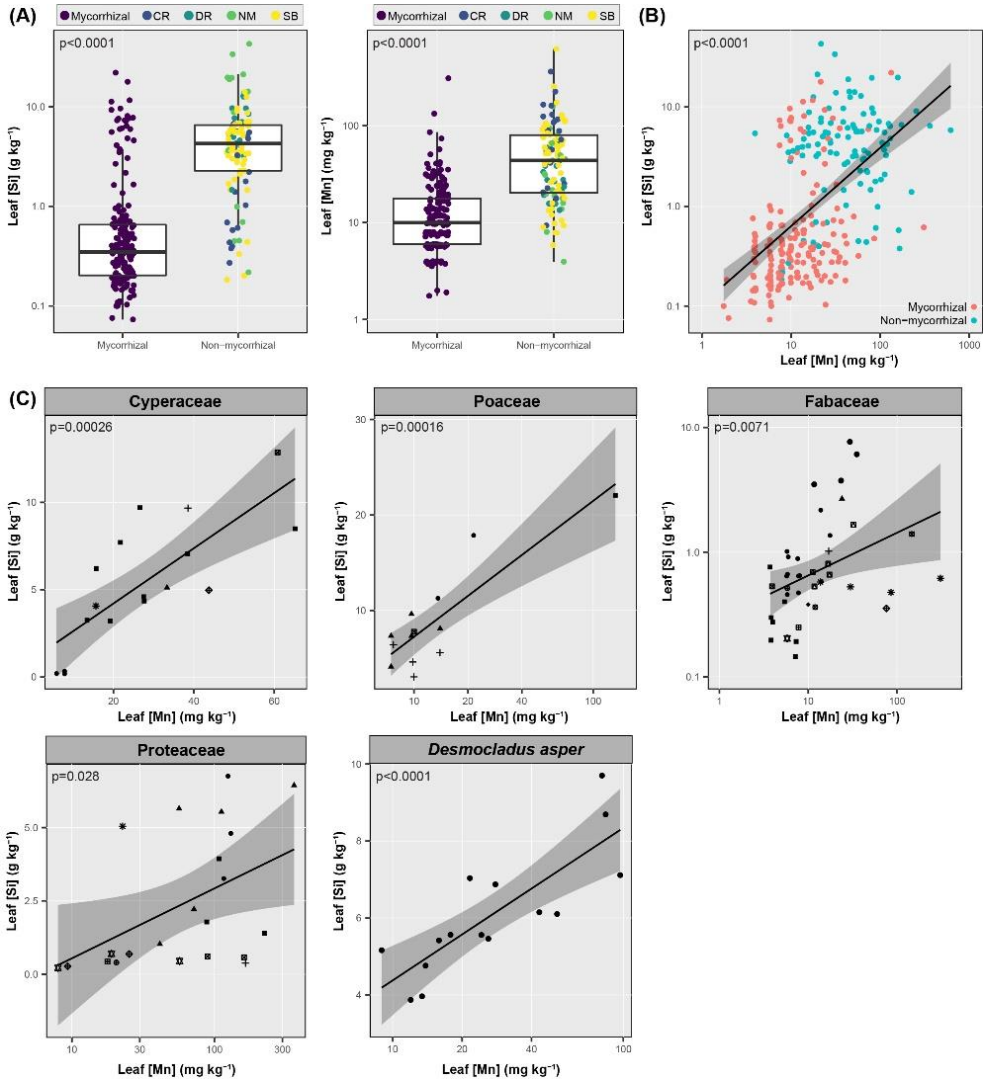

Figure 7-3 : Leaf silicon (Si) and manganese (Mn) concentrations along the Jurien Bay chronosequence as dependent on putative nutrient-acquisition strategy (A). Relationship between leaf Si and Mn concentrations for the same individuals (B), and for Cyperaceae, Poaceae, Fabaceae, Proteaceae and Desmocladus asper (Restionaceae) (C). All data (281 individuals belonging to 86 species) are from (de Tombeur et al. 2021b). Plots in (A) show boxplots with medians, 25th and 75th percentiles and whiskers extended to 1.5 times the interquartile range. Data presented beyond whiskers represent outliers. Both axes were log-

transformed, and the p-values derived from linear mixed-effects models testing the effect of nutrient-acquisition strategy on leaf nutrient concentration (with species and plot as random factors). Legend details: NM, non-mycorrhizal; CR, cluster roots; DR, dauciform roots; SB, sand-binding roots. In (B) and (C), black lines indicate the regression lines between both variables, shaded areas represent 95% confidence interval of the regression and circle colors (B) or symbols (C) indicate nutrient-acquisition strategy or different species, respectively. In (B), both axes were log-transformed. In (C), x-axes were log-transformed expect for Cyperaceae, while y-axes were log-transformed for Fabaceae. In (B), the p-value were derived from linear mixed-effects models (with species and plot as random factors). In (C), p-values were derived from Pearson tests of correlation.

In environments where soil Mn availability is far greater than the very low concentration in Jurien Bay, for example New Caledonia (Pillon *et al.* 2020), Si mobilization might be important to ameliorate Mn toxicity in carboxylate-releasing species. In 1978, Horst & Marschner (Horst & Marschner 1978) showed that *Phaseolus vulgaris* plants treated with Si showed much greater tolerance to Mn toxicity than untreated plants. In particular, 1.8 mM of Mn was toxic for leaves in the absence of Si, but this critical level was 18 mM with Si addition (Horst & Marschner 1978). The authors explained the beneficial effect of Si on Mn toxicity by the prevention of local Mn accumulation within leaf tissues and a more homogeneous distribution. This conclusion is supported by more recent studies on a range of species (Maksimović *et al.* 2012; Blamey *et al.* 2018; van der Ent *et al.* 2020).

The situation for Poaceae differs from that outlined above, because grasses tend not to enhance the release of carboxylates in response to P starvation yet do accumulate both Si and Mn (Figure 7-3C). Poaceae typically enhance the release of phytosiderophores, which are strong chelators of Fe, in response to Fe deficiency (Marschner *et al.* 1986; Ma 2005; Zanin *et al.* 2017). Phytosiderophores also mobilise zinc (Cakmak *et al.* 1996), Mn (Zhang 1993), and Si (Gattullo *et al.* 2016). Gattullo *et al.* (2016) showed that Fe-deficient barley (*Hordeum vulgare*) mobilizes Si, in addition to Fe, from smectite through the exudation of organic ligands. Interestingly, Fe-deficient maize (*Zea mays*) plants not only enhance expression of transporters for Fe^{2+}, but also those involved in transport of P (ZmPHT1;7 and ZmPHO1) (Zanin *et al.* 2017). Being strong chelators, phytosiderophores are expected to mobilize P sorbed onto Fe oxides. We are not aware of enhanced phytosiderophore release in response to P-starvation, but that is what we might expect to account for increases in leaf [Mn] in Poaceae with decreasing P availability along the Jurien Bay chronosequence (de Tombeur *et al.* 2021b).

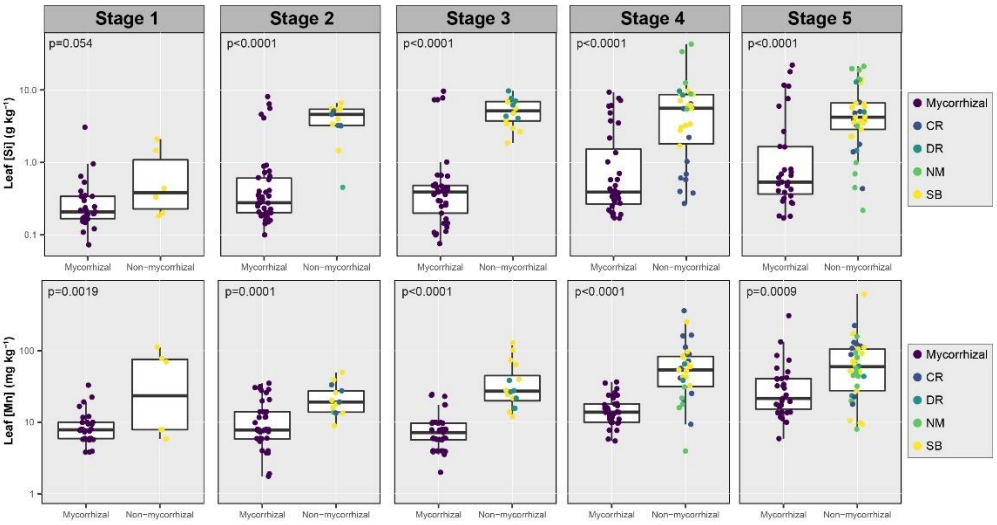

Figure 7-4 : Leaf silicon (Si) and manganese (Mn) concentrations in each stage of the Jurien Bay chronosequence as dependent on putative nutrient-acquisition strategy. Boxplots with medians, 25th and 75th percentiles and whiskers extended to 1.5 times the interquartile range. Data presented beyond whiskers represent outliers. Axes were log-transformed, and the p-values derived from linear mixed-effects models testing the effect of nutrient-acquisition strategy on leaf nutrients concentration (with species and plot as random factors). Legend details: NM, non-mycorrhizal; CR, cluster roots; DR, dauciform roots; SB, sand-binding roots.

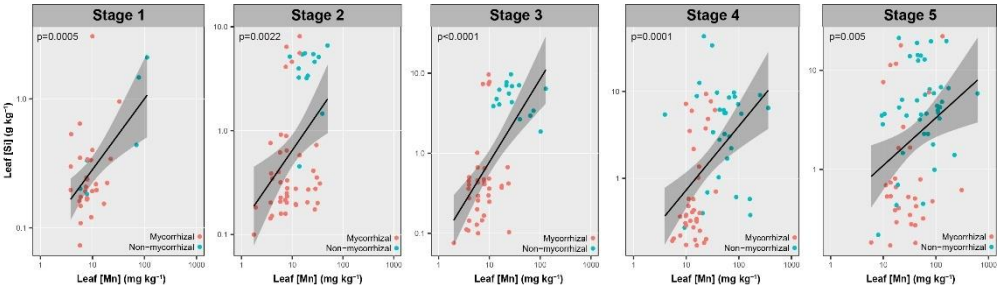

Figure 7-5 : Relationships between leaf silicon (Si) and manganese (Mn) concentrations for each stage of the Jurien Bay chronosequence. Each circle represents an individual, black lines indicate the regression lines between both variables, shaded areas represent 95% confidence interval of the regression and circle colors indicate nutrient-acquisition strategy. Both axes were log-transformed. The p-values were derived from linear mixed-effects models (with species and plot as random factors).

7.6.3 Decrease of leaf [Si] with fertilization

In wheat (*Triticum aestivum*), an elevated P supply reduces foliar [Si] (Jones & Handreck 1967), suggesting a role for chelating compounds in mobilizing both P and Si in this species. These might be phytosiderophores, as these do mobilize Si when chelating Fe (Gattullo *et al.* 2016), whereas grasses tend not to release large amounts of carboxylates. There are exceptions, however, for example oats (*Avena sativa*) (Wang *et al.* 2016) and sorghum (*Sorghum bicolor*) (Magalhaes *et al.* 2018). Carboxylate release would be suppressed under high P supply, thus reducing Si mobilization and uptake. Similarly, leaf [Si] of *Holcus lanatus* (Poaceae) increases under P deficiency (Minden *et al.* 2020), and Johnson *et al.* (Johnson *et al.* 2018) showed that leaf [Si] decreased markedly in three grass species (*Cynodon dactylon*, *Eragrostis curvula* and *Microlaena stipoides*), following fertilization (nitrogen, K, P). More generally, recent studies suggest that grasses may not have evolved silica-based defenses in response to extensive herbivory, but more in response to dry hot (Brightly *et al.* 2020) and infertile environments (Quigley *et al.* 2020). In summary, fertilization, and especially P fertilization, tends to decrease leaf [Si] in a range of Poaceae which we suggest is caused by a decrease in soil Si mobilization through the suppression of exudation of chelating substances.

7.7 Concluding remarks and perspectives

We propose that plants growing in P-impoverished environments that express Si transporters exhibit relatively higher leaf [Si] because of the mobilization of Si by root-released carboxylates or other chelators into the rhizosphere. Such a process will be expected mainly at the family or species-level, since plants exhibit great variation in their leaf [Si] due to presence/absence of Si transporters (Deshmukh *et al.* 2020). At this level, correlations between leaf [Si] and [Mn] are expected if species/individuals are sampled across a gradient of P availability, and therefore of soil carboxylate concentrations, particularly if they exhibit Si transporters. However, an overall correlation between leaf [Si] and [Mn] when species from different families are considered reveals a possible greater role of carboxylates on plant Si uptake (Figure 7-3B). Since carboxylate-releasing P-mobilizing strategies incur significant C costs (Raven *et al.* 2018), those of silica-based defenses might be more expensive than commonly realized (Raven 1983) if carboxylates or other root exudates are needed to mobilize Si from the rhizosphere, especially when plant-available [Si] is low.

While many questions remain, this paper paves the way towards the exploration of a role for root exudates in soil-plant-herbivore Si dynamics, thus providing promising perspectives for ecosystem Si research in both natural systems and agroecosystems. Indeed, the role of root exudates has been considered for mobilization of many essential nutrients, but ignored for Si, a beneficial element (Coskun *et al.* 2019). It is, however, time to consider these aspects since the significant role of Si in plant biology (Coskun *et al.* 2019) and ecology (Cooke & Leishman 2011a) is increasingly

acknowledged. A detailed understanding of the factors influencing its dynamics in soil-plant systems is therefore urgently required.

8

Silicon dynamics through the lens of soil-plant feedback interactions: perspectives for agricultural practices*

*This Chapter is adapted from

de Tombeur, F., Roux, P., Cornélis, J-T. Silicon dynamics through the lens of soil-plant feedback interactions: perspectives for agricultural practices. *'Marschner review' under review in Plant and Soil.*

Many ecologists glibly designate soil as the abiotic environment of plants, a phrase that gives me the creeps

Hans Jenny, soil scientist

8.1 Foreword

In the five previous chapters, we identified different factors influencing Si dynamics in terrestrial ecosystems. We stressed the influence of soil age and its subsequent control on soil mineralogy, the major role of soil phytoliths in providing plant-available Si, especially in old and highly-desilicated soils, a possible effect of soil fertility in enhancing Si plant biocycling by increasing the expression of silica-based defenses, and this possibly due to changes in the dominant nutrient-acquisition strategies in plant communities. In particular, root-released carboxylates seem to increase soil Si mobilization for subsequent plant uptake. Understanding the drivers of soil-plant cycles in natural ecosystems is key for global cycles and plant nutrition/growth, but also for the development of sustainable agroecosystems. Knowledge about processes influencing soil-plant elemental cycling in complex natural systems can indeed be used to ameliorate the resource-use efficiency and productivity of modern agroecosystems. In this new chapter, we will try to bridge the gap between the processes controlling soil-plant Si dynamics in natural ecosystems and the potential of different agriculture practices to stimulate Si mobility in soil-plant systems. This is important because Si is involved in a wide range of functions that contribute to plant performance and stress regulation, which can ultimately lead to increase plant productivity and crop yields, especially in desilicated environments with low plant-available Si. We particularly insist on biotic factors, because their role in soil-plant Si mobility has been neglected. The chapter is presented in the form of a literature review, and heavily relies on the processes highlighted in the first five chapters: effect of mineralogy on soil Si dynamics, high reactivity of phytoliths in the soil environments, influence of root exudates on soil Si mobilization.

8.2 Summary

Silicon (Si) is increasingly recognized as a pivotal beneficial element for plants in ecology and agricultural sciences, but soil-plant Si cycling has been considered mostly through the prism of abiotic mineral weathering, whilst numerous biological processes have been overlooked. Leveraging ecological processes that impact soil-plant Si cycling in cropping systems might ameliorate crop Si status, but this remains hypothetical to date. We aim to comprehensively compile information about biotic and abiotic processes driving soil-plant Si cycling, and translate their potential beneficial effects in agricultural practices. We emphasize the fundamental need to consider the effects of agricultural practices on Si mobility in soil-plant systems when striving towards sustainable agroecosystems. Regarding soil abiotic factors, degree of soil weathering, mineralogy, texture and pH are key predictors of soil Si dynamics, while soil aggregation processes deserve further investigation. The biological processes associated with mycorrhizal associations, silicate-solubilizing bacteria, and soil macrofauna enhance Si mobility in soil-plant systems, while the effect of root exudates is likely, but deserves further studies. Large herbivores strongly affect soil-plant Si mobility by increasing plant-derived Si turnover rates and redistribution,

thereby making integrated crop-livestock systems a promising prospect for crop Si status. Recycling crop residues and implementing suitable cover crops promotes Si mobility in soil-plant systems by leveraging the relatively high solubility of plant-derived Si-bearing minerals. The soil-root-microorganism interactions facilitated by cereal-legume intercropping systems also contributes to the mobility of Si in the soil-plant continuum. The capacity of certain agricultural practices to increase Si mobility in soil-plant systems stresses the need to understand complex soil-plant-animal interactions when aiming to enhance Si-based plant stress resistance in agroecosystems.

8.3 Introduction

Silicon (Si) is taken up by all vascular plants and contributes to a wide range of functions (Epstein 1994). Once deposited as hydrated amorphous silica in plant tissues ($SiO_2.nH_2O$; phytoliths), it helps mitigate several plant biotic and abiotic stresses (Ma 2004; Liang *et al.* 2007; Zhu & Gong 2014; Cooke & Leishman 2016; Hartley & DeGabriel 2016; Debona *et al.* 2017; Coskun *et al.* 2019), can be used as a cheap plant structural component (Raven 1983), and, eventually, increase plant primary productivity and crop yield (Savant *et al.* 1999; Liang *et al.* 2015b; Tubana *et al.* 2016; Xu *et al.* 2020). Despite overwhelming evidence for the importance of Si for plant functioning, it is still considered a non-essential nutrient by plant nutritionists (Coskun *et al.* 2019), but it is increasingly considered a key element in plant ecology (Cooke & Leishman 2011a) and agriculture, especially considering the importance of Si-accumulating species in global food production (e.g., wheat, rice, sugarcane) (Meyer & Keeping 2000; Datnoff *et al.* 2001a; Haynes 2014; Liang *et al.* 2015b; Tubana *et al.* 2016).

Over the last 30 years, soil scientists and biogeochemists studied Si in a wide range of environments to explore the role of soil properties and vegetation on soil-plant Si cycling (Bartoli 1983; Alexandre *et al.* 1997; Lucas 2001; Derry *et al.* 2005; Sommer *et al.* 2006; Henriet *et al.* 2008b, a; Cornelis *et al.* 2010; Haynes 2014; Cornelis & Delvaux 2016; Meunier *et al.* 2018; Vander Linden & Delvaux 2019; de Tombeur *et al.* 2020a, b, c; Schaller *et al.* 2021). The processes and factors governing Si release rates from minerals are well documented (Sommer *et al.* 2006; Churchman & Lowe 2012; Haynes 2014; Cornelis & Delvaux 2016; Schaller *et al.* 2021), as are the influence of plant-induced mechanisms (bioweathering and Si uptake) on terrestrial Si cycling (Lucas *et al.* 1993; Alexandre *et al.* 1997; Street-Perrott & Barker 2008; Haynes 2017; de Tombeur *et al.* 2020c). However, how certain aspects of the soil-plant-animal continuum influence Si mobility in both natural systems and agroecosystems have been overlooked, especially the contribution of biotic factors. Yet, a detailed understanding of soil-plant-animal interactions influencing Si dynamics is paramount if we seek to benefit from Si-related plant functioning in agriculture (Acevedo *et al.* 2021).

Despite its ubiquity in soils (2nd element of the Earth's crust ; Wedepohl 1995), long-term mineral weathering and subsequent desilication (i.e. Si loss by leaching) result

in soils with low plant-available Si concentrations in many areas of the world (approximately 3500 million hectares, as estimated by the land area supporting desilicated soils: Ferralsol, Podzol, Arenosol, Lixisol, Plinthosol, Acrisol and Alisol; WRB 2015). particularly in tropical and subtropical regions. In addition, agriculture further enhances desilication by harvesting and exporting large amount of Si (Desplanques *et al.* 2006; Struyf *et al.* 2010a; Clymans *et al.* 2011; Guntzer *et al.* 2012b; Keller *et al.* 2012; Vandevenne *et al.* 2015; Carey & Fulweiler 2016; Tubana *et al.* 2016; Vander Linden & Delvaux 2019). These days, rock-derived Si fertilizers are routinely applied in some agroecosystems to counterbalance these detrimental effects (Savant *et al.* 1999; Datnoff *et al.* 2001a; Haynes 2014; Liang *et al.* 2015b), and intensifying this practice might even be beneficial in less-weathered and desilicated environments (Tubana *et al.* 2016). However, such a practice relies on non-renewable resources, and low accessibility to common, rock-derived Si fertilizers in some tropical regions can jeopardize the Si benefits in these sensitive agroecosystems. Harnessing ecological processes that increase soil-plant Si mobility by promoting specific agricultural practices may ameliorate the Si status of crops worldwide, while decreasing the need for non-renewable mineral fertilizers (Lambers *et al.* 2011; Richardson *et al.* 2011; Mariotte *et al.* 2018). Indeed, recent evidence demonstrates the positive impact of certain agricultural practices such as intercropping, cover crops or integrated crop-livestock systems, on nutrient management, especially for phosphorus (P) (Hallama *et al.* 2019; Carlos *et al.* 2020; Tang *et al.* 2020).

In this review, we aim to compile knowledge about biotic and abiotic factors that govern Si mobility in soil-plant systems and translate their potential benefits in agricultural practices. We specifically emphasize how overlooked ecological/biological processes are pivotal when favoring Si biocycling in agroecosystems, and advocate the permanent need to nurture our understanding of complex interactions between physico-chemical and biological soil processes to develop sustainable agroecosystems.

8.4 Biotic and abiotic factors affecting soil-plant Si cycling

8.4.1 Physico-chemical processes controlling soil Si dynamics

Soil weathering and sorption/desorption mechanisms

Over the past decade, many studies reported a positive relationship between soil pH and plant-available Si when multiple soils were considered together (Miles *et al.* 2014; Phonde *et al.* 2014; Puppe *et al.* 2015; Klotzbücher *et al.* 2018b; Meunier *et al.* 2018; Schaller *et al.* 2018; Haynes 2019; Caubet *et al.* 2020; de Tombeur *et al.* 2020b; Schaller *et al.* 2021). Prolonged soil acidification during pedogenesis is associated with the loss of reactive Si-bearing minerals and increased desilication (Savant *et al.* 1999; Chadwick & Chorover 2001; Sommer *et al.* 2006; Henriet *et al.* 2008a; Liang

et al. 2015a; de Tombeur *et al.* 2020b). Consequently, plant-available Si concentrations inevitably decrease with the relative enrichment of poorly weatherable minerals and the decrease in soil pH during pedogenesis (Savant *et al.* 1999; Liang *et al.* 2015a; Haynes 2019; de Tombeur *et al.* 2020b). This explains why plant-available Si is directly related to soil weathering indicators in long-term soil chronosequences (de Tombeur *et al.* 2020b). This is also supported by positive relationships between plant-available Si and clay content (Miles et al. 2014; Liang et al. 2015a and references therein). However, the relation with soil pH is different when a single soil or mineralogical assemblage is considered. Increasing pH consistently decreases plant-available Si concentrations, because Si adsorption onto the surface of oxides and silicates increases gradually to about pH 9.5, reflecting the $H_4SiO_4/H_3SiO_4^-$ pKa of 9.47 (Figure 8-1 and references in the legend). This adsorption process is also time dependent as Si is hardly remobilized when sorbed over a period of several months (Haynes & Zhou 2020). On the other hand, a high pH could also increase plant-available Si concentrations via increasing dissolution rates of aluminosilicates from soil pH 7.5/8 (Drever 1994; Kelly *et al.* 1998), together with increased phytolith dissolution rates with increasing soil pH from 3 to 10 (Fraysse *et al.* 2006b, 2009).

In a compilation of literature data, de Tombeur et al. (2020b) showed that plant-available Si concentrations increase with increasing soil pH for pH<7.5, in the silicate weathering domain, but not for pH>7.5, where they were about constant, with a slight decreasing tendency (Figure 3-5). Even though aluminosilicate and phytolith dissolution rates increase for these pH values, plant-available Si concentrations do not further increase in the carbonate weathering domain (Figure 3-5). This result suggests that the fate of plant-available Si in carbonate-rich soils is increasingly controlled by adsorption processes and the preferential consumption of H^+ by carbonate minerals, with both processes involved in decreasing the Si concentration in the soil solution (Figure 8-1) (Meunier *et al.* 2018; Vander Linden & Delvaux 2019; de Tombeur *et al.* 2020b). Overall, although the controls of soil weathering, mineralogy and texture on plant-available Si are now well understood, especially for the silicate weathering domain (Cornelis & Delvaux 2016), how high pH and carbonate minerals influence Si plant-availability remains unclear, because they are driven by antagonistic processes (Haynes 2019). Moreover, Schaller et al. (2021) recently emphasized the relatively slow Si reaction rates in soils (e.g., mineral crystallization), making our understanding of Si plant-availability as a function of soil processes more complex than commonly acknowledged.

Silicon can compete with other ions via sorption/desorption mechanisms on soil exchangeable sites (Matychenkov & Ammosova 1996; Klotzbücher *et al.* 2020). In particular, research has long suggested competition between Si and phosphate ions (Smyth & Sanchez 1980; Kundu *et al.* 1988; Matychenkov & Ammosova 1996; Owino-Gerroh & Gascho 2004; Konhauser *et al.* 2007; Reithmaier *et al.* 2017; Hilbrandt *et al.* 2019; Hömberg *et al.* 2020; Klotzbücher *et al.* 2020; Schaller *et al.* 2020). Such mechanism could explain the benefits of Si addition on plant P nutrition (Hall & Morison 1906; Fisher 1929; Singh & Sarkar 1992; Owino-Gerroh & Gascho

2004; Eneji *et al.* 2008; Neu *et al.* 2017), even though other mechanisms were postulated (Ma & Takahashi 1990a, b, 1991b; Kostic *et al.* 2017). In addition to P, Si may also compete with dissolved organic matter (Reithmaier *et al.* 2017; Klotzbücher *et al.* 2020), selenium (Jordan *et al.* 2009), arsenic (Christl *et al.* 2012) and iron (Hömberg *et al.* 2020). Such sorption/desorption competitive mechanisms are pH-dependent given the low chemical reactivity of dissolved Si at low pH (Owino-Gerroh & Gascho 2004; Konhauser *et al.* 2007; Jordan *et al.* 2009; Christl *et al.* 2012). It is therefore key to adjust the pH of the sorption/desorption isotherms to values representative of soil pH changes induced by the alkaline composition of Si fertilizer used (e.g., calcium silicates).

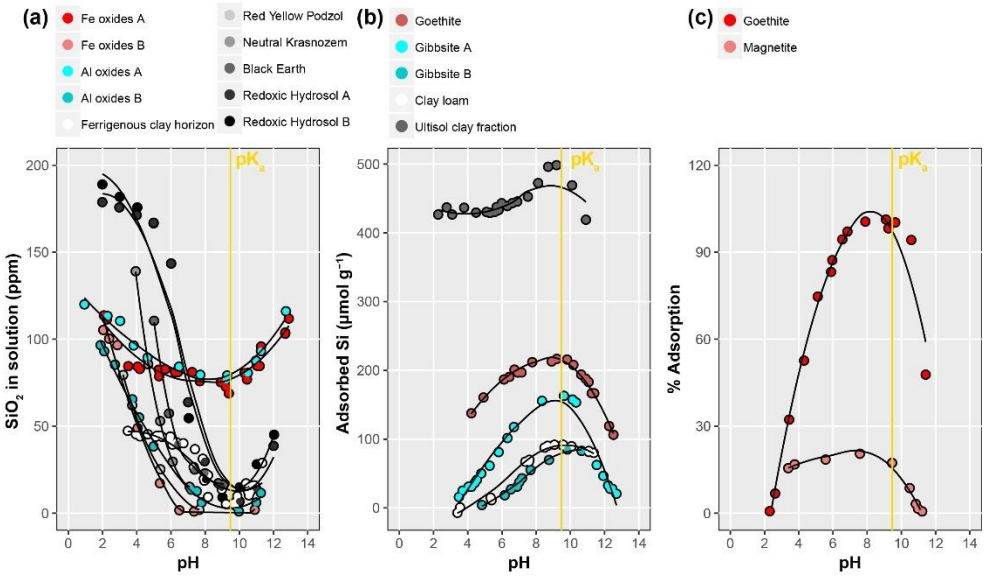

Figure 8-1 : Relationships between pH and Si concentrations in solution (a), pH and adsorbed Si (b) pH and % of Si adsorbed (c) from the literature. In (a), 'Fe oxides A' and 'Al oxides A' are from Jones and Handreck (1963); 'Fe oxides B', 'Al oxides B', 'Red Yellow Podzol', 'Neutral Krasnozem' and 'Black Earth' are from Beckwith and Reeve (1964); 'Ferrigenous clay horizon' is from McKeague and Cline (1963); 'Redoxic Hydrosol A and B' are from Haynes and Zhou (2018). In (b), 'Goethite' and 'Gibbsite A' are from Hingston et al. (1972); 'Gibbsite B' is from Hingston and Raupach (1967); 'Clay Loam' is from Obihara and Russell (1972); 'Ultisol clay fraction' is from Nguyen et al. (2017). In (c), 'Goethite and Magnetite' are from Philippini et al. (2006). Yellow lines indicate the $H_4SiO_4/H_3SiO_4^-$ pK_a (9.472), and black lines indicate the trends of the relationships.

Processes related to aggregation of particles

The mineral nature (e.g., primary silicates, secondary 2:1 or 1:1 clay minerals, amorphous silica), degree of crystallinity, magnitude of isomorphic substitution and specific surface area control its solubility (Churchman & Lowe 2012), and thus its

ability to release Si into the soil solution (Sommer *et al.* 2006; Cornelis & Delvaux 2016). However, how the interactions between soil mineral and organic constituents (Six *et al.* 2004) impact the extent to which minerals can be dissolved in aggregates is still not understood. Recently, Li et al. (2020b) showed that soil microaggregates contribute over 60% of the total phytolith stock in a Retisol. The authors proposed that entrapment of phytoliths in aggregates might slow down their dissolution, and increase their persistence in soils and sediments. This study emphasizes how the complex arrangement of soil particles influences soil Si dynamics, as is well known for C, P and N (Mikha & Rice 2004; Wright & Hons 2005; Fonte *et al.* 2014; Schubert *et al.* 2020). In addition, soil aggregates host *microbial hotspots* in pores or at mineral surfaces creating specific soil micro-environments enriched in biogeochemical processes when compared with the average bulk soil conditions, i.e. the *hot moments* (Kuzyakov & Blagodatskaya 2015). The bio-induced weathering processes in these hotspots most likely also impacts soil Si release rates into the soil solution (Uroz *et al.* 2009), but how the soil aggregate fractions and their respective hotspot affect soil Si dynamics deserve further investigation. This is of special interest since anthropogenic land transformations substantially impact soil aggregation processes, affecting soil structure (Mikha & Rice 2004; Wright & Hons 2005; Fonte *et al.* 2014; Or *et al.* 2021).

8.4.2 Biological processes controlling soil Si dynamics

Silicon biocycling: the high reactivity of phytoliths

In addition to the weathering of rock-derived minerals, the dissolution of soil phytogenic silicates (phytoliths) also strongly impact Si dynamics (Bartoli 1983; Alexandre *et al.* 1997; Meunier *et al.* 1999; Derry *et al.* 2005; Farmer *et al.* 2005; Sommer *et al.* 2013; de Tombeur *et al.* 2020c). Biogeochemical mass-balance calculations have long reported that a significant fraction of Si in the soil solution is derived from the dissolution of the phytogenic Si pool (Bartoli 1983; Alexandre *et al.* 1997, 2011; Gérard *et al.* 2008), because of its high solubility compared with that of crystalline Si-bearing minerals (Fraysse *et al.* 2006b, 2009; Cornelis & Delvaux 2016). This challenged the common view that plant-available Si concentrations were mainly driven by soil parent material, weathering degree, and subsequent soil mineralogy/texture (Savant *et al.* 1999; Chadwick & Chorover 2001; Henriet *et al.* 2008a, b; de Tombeur *et al.* 2020b). To reconcile the control of geochemical and biological processes on Si release in the soil solution, Cornelis and Delvaux (2016) suggested that the biological Si feedback loop (phytolith formation in plants and dissolution in soils) takes over soil litho/pedogenic pools in advanced soil weathering stages. This contention was recently supported by the use of long-term soil chronosequences where plant-available Si concentrations are mainly governed by soil-derived Si-bearing minerals (clay minerals) in early and intermediate stages of weathering (de Tombeur *et al.* 2020b), but increasingly by the recycling of phytoliths in old and highly-weathered soils dominated by poorly-soluble quartz minerals (de Tombeur *et al.* 2020c). The significant effect of vegetation on the soil-plant Si cycle

explains why land-use changes and management affect the global Si cycle (Struyf *et al.* 2010a; Clymans *et al.* 2011; Vandevenne *et al.* 2015; Carey & Fulweiler 2016).

Some soil organisms also accumulate Si to form various siliceous structures (Ehrlich *et al.* 2010; Puppe 2020). They are classified as zoogenic Si pool (e.g., sponge spicules), bacterial Si (e.g., *Proteus mirabilis*, Lauwers and Heinen 1974), fungal Si, protozoic Si (e.g., testate amoeba shells) or protophytic Si (e.g., diatom frustules) (Sommer *et al.* 2006; Ehrlich *et al.* 2010; Puppe *et al.* 2015; Puppe 2020). Recent evidence suggest that these pools are of a similar magnitude as the phytogenic pool, and in turn influence the terrestrial Si cycle (Sommer *et al.* 2013; Puppe *et al.* 2014, 2015, 2016). In particular, annual biosilicification from testate amoebae ranges from 17 to 80 kg ha^{-1} yr^{-1} depending on soil and ecosystem properties which is similar to or even exceeds annual Si uptake by terrestrial vegetation (Sommer *et al.* 2013; Puppe *et al.* 2015; Vander Linden & Delvaux 2019). This pioneering work opened new perspectives on the role of Si-based life forms on soil-plant Si cycling (Puppe 2020).

Biological weathering of Si-bearing minerals

In addition to the production of an easily weatherable Si pool, plants are extremely active when it comes to enhancing weathering ability of different soil constituents, either directly or indirectly. Nevertheless, plants are not stand-alone entities in their ability to affect Si cycling, but should be considered as "holobionts", which includes the microbiome associated with their development (Vandenkoornhuyse *et al.* 2015). There are numerous well-known mechanisms by which the actors of the soil-plant continuum contribute to the dissolution of Si-bearing minerals and extensive reviews can be found elsewhere (Dontsova *et al.* 2020; Finlay *et al.* 2020). Briefly, these mechanisms can be divided into two categories: biochemical and biophysical weathering. These processes are not mutually independent; rather, they often play cumulative or synergistic roles.

The main biochemical effect on Si dissolution is the alteration of the rhizosphere pH. This occurs through the release of organic acids, either as a by-product of cellular metabolism or as root exudates, plant excretion of H^+ in exchange for cationic nutrients, formation of carbonic acid (Golubev *et al.* 2005; Brantley 2008) through the release of CO_2 via root respiration or organic matter mineralization, and the release of inorganic acids from redox reactions. Proton-promoted dissolution is supplemented by ligand-promoted dissolution where organic acids, in addition to their pH altering ability, can act synergistically with strong chelators such as phytosiderophores or carboxylates to further enhance weathering of Si-bearing minerals by destabilizing mineral lattices through the binding of metal cations (Bennett *et al.* 2001; Buss *et al.* 2007). Biophysical mechanisms include hyphal tunneling, or boring and other mechanisms of penetration by plant roots or fungi along mineral weakness points (Smits *et al.* 2005; van Schöll *et al.* 2008; Teodoro *et al.* 2019). This, in turn, increases substrate porosity and, therefore, increases the mineral surface exposed to chemical weathering agents (Pawlik *et al.* 2016; Gadd 2017). Finally, plants and associated

microorganisms can also affect water movement and retention capacity through uptake and biofilms and therefore strongly influence water residence time and weathering patterns (Lucas 2001; Flemming & Wingender 2010).

While the biological impact on weathering is recognized, its contribution to the mobility of nutrients in natural and agricultural systems, including Si, remains poorly understood. In the following, we therefore aim to assess the effects of each biological agent on Si plant-availability.

Root exudates Plant roots secrete a wide range of exudates to mobilize poorly-available nutrients in the rhizosphere (Dakora & Phillips 2002; Lambers *et al.* 2006; Finlay *et al.* 2020). A long history of experimental studies has shown the increase of silicate dissolution by root exudates, through organic acids (Stillings *et al.* 1996; Drever & Stillings 1997; Cama & Ganor 2006; Bray *et al.* 2015) or forest floor extracts (van Hees *et al.* 2002). Increasing dissolution of silicates or pedogenic oxides in the presence of siderophores was also demonstrated, whether they are microbial (Liermann *et al.* 2000; Buss *et al.* 2007) or root-derived (Reichard *et al.* 2005). However, despite their importance for plant nutrient acquisition, the role of root exudates in mobilizing Si for plant uptake has been overlooked. Yet root-released carboxylates do increase the mobility of P, K, Fe, Al, Ca, P and numerous micronutrients (Gerke *et al.* 1994; Ström *et al.* 2005; Wang *et al.* 2011; Houben & Sonnet 2012; Abrahão *et al.* 2014; Colombo *et al.* 2014; Kabas *et al.* 2017; Teodoro *et al.* 2019), which justifies to suppose similar effects on soil-plant Si mobility.

Early work by Hinsinger et al. (2001) has shown the impact of banana (*Musa paradisiaca*), maize (*Zea mays*), canola (*Brassica napus*), and white lupin (*Lupinus albus*) on the weathering of a basaltic rock. After 36 days of growth, the amount of Si released from basalt in the presence of hydroponically grown plants was increased two-fold compared with the abiotic control. More recently, Burghelea et al. (2015) and Zaharescu et al. (2019) showed that buffalo grass (*Bouteloua dactyloides*) grown on schist and rhyolite for 124 to 603 days, respectively, increased the mobility of Si compared with that of an abiotic control. Furthermore, Gattullo et al. (2016) showed that Fe-deprived barley (*Hordeum vulgare*) plants rapidly released more exudates into the rhizosphere to mobilize Fe from amorphous Fe oxides. Then, when the soil-plant contact was extended to 12 days, plants overcame Fe nutritional stress and the exudation of organic ligands mobilized Si from smectite (Gattullo *et al.* 2016). These results demonstrate that root exudates are primarily influenced by macro- or micronutrients limitation, but that co-solubilization of Si is very likely. In support of this claim, recent studies showed an increase in leaf Si concentrations with decreasing soil P concentrations and Si plant-availability along a long-term soil chronosequence (de Tombeur *et al.* 2020c, 2021b), particularly in old and highly-weathered environments where carboxylate-releasing strategies are common (Lambers *et al.* 2008; Zemunik *et al.* 2015), suggesting a role for carboxylates in mobilizing soil Si from poorly-soluble forms for plant uptake. Future research is required to elucidate to which extent Si is co-mobilized by different nutrient-acquisition strategies. In addition, even though Si is not considered an essential nutrient (Coskun *et al.* 2019),

future studies should test if root exudation patterns are directly influenced by low Si availability.

Mycorrhizal associations With nearly 90% of plants harbouring either arbuscular mycorrhizal (AM) or ectomycorrhizal fungi (EM) symbionts (Brundrett 2002; Smith & Read 2008), mycorrhizas exhibit strong control over major ecosystem processes including plant nutrient acquisition (Marschner & Dell 1994; Clark & Zeto 2000; Richardson *et al.* 2009), biogeochemical cycles (Högberg *et al.* 2001; van Hees *et al.* 2006), plant diversity and productivity (Van Der Heijden *et al.* 1998, 2008) and weathering potential (Leake & Read 2017; Smits & Wallander 2017). Plants enable mycorrhizal fungal growth and activity by translocating various organic compounds (sugars, lipids) into the roots (Jiang *et al.* 2017; Rich *et al.* 2017). In exchange of plant photosynthates, fungi develop hyphal networks into the soil and enhance weathering processes for lithogenic nutrient acquisition (Van Breemen *et al.* 2000; van Schöll *et al.* 2006, 2008). In 1990, Kothari et al. provided the first evidence of Si mobilization by mycorrhizal fungi by showing an increase in maize (*Zea mays*) root Si concentrations after inoculation with an arbuscular mycorrhizal fungi (Kothari *et al.* 1990). Since then, other studies have shown that the presence of mycorrhizal fungi may significantly increase the Si concentrations of different species (maize, sugarcane, banana, chickpea, pigeon pea, soybean), and in different plant organs (roots, leaves, stems) (Table 8-1) (Yost & Fox 1982; Clark & Zeto 1996; Garg & Bhandari 2016; Oye Anda *et al.* 2016; Frew *et al.* 2017b, a, 2020; Garg & Singh 2018; Gbongue *et al.* 2019). Root Si concentrations are positively correlated with the degree of arbuscular mycorrhizal colonization, which reduces root herbivory (Frew *et al.* 2017a). Moreover, the root Si concentrations with increased mycorrhizal colonization increases only in plants that grow on a Si-deficient soil, and not in those on a high-Si soil (Frew *et al.* 2017a). This pattern was confirmed by other studies where the effects of mycorrhizal fungi on plant Si concentrations were less important, or even absent, when Si was supplied to plants (Oye Anda *et al.* 2016; Frew *et al.* 2017b).

Even if the effects of mycorrhizas on plant Si concentration depend on initial Si availability in soil, these results reveal that root mycorrhizal colonization can be a significant driver of plant Si uptake and concentrations in plants, with a direct impact on herbivory. In some cases, plant Si concentrations have indeed more than doubled after inoculation with mycorrhizal fungi (Oye Anda *et al.* 2016). More broadly, although phylogenetic variation and the presence or absence of Si transporters remain the main explanations for variation in plant Si accumulation (Hodson *et al.* 2005; Ma *et al.* 2006, 2007; Deshmukh & Bélanger 2016; Deshmukh *et al.* 2020), nutrient-acquisition strategies like mycorrhizal associations and root-released carboxylates could play a significant, but so far overlooked role. This is of special interest since both strategies increase with decreasing P availability (Abbott *et al.* 1984; Tang *et al.* 2001; Covacevich *et al.* 2007; He *et al.* 2020), in particular the carboxylate-releasing strategies that are common in highly-weathered and low P soils because of their lower C costs compared to mycorrhizal fungi strategies (Raven *et al.* 2018), and P-depleted soils are often also Si-depleted, due to high weathering degree.

Table 8-1 : Effect of arbuscular mycorrhizal fungi on plant Si concentrations from the literature. We used WebPlotDigitizer to extract data published as figures (Rohatgi 2012).

Plant	Organ	AM fungi	Increase in plant [Si] (%)	Reference
Maize	Shoot	*Glomus* sp.	+3% to +66% for acid soils -28% to -6% for alkaline soils +78% to +252% of Si content (weight by plant) for acid soils -9% to +25% of Si content (weight by plant) for alkaline soils	Clark and Zeto (1996)
Chickpea	Shoot	*Funneliformis mosseae*	+17-20%	Garg and Bhandari (2016)
Banana	Pseudostem	*Rhizophagus irregularis*	+149% without Si +88% with Si	Oye Anda et al. (2016)
Banana	Leaves	*Rhizophagus irregularis*	+84% without Si +70% with Si	Oye Anda et al. (2016)
Banana	Roots	*Rhizophagus irregularis*	+109% without Si +30% with Si	Oye Anda et al. (2016)
Sugarcane	Roots	*Glomus* sp.	+50% to +102% without Si -4% to +22% with Si	Frew et al. (2017b)
Sugarcane	Roots	*Glomus* sp.	+42% to +71% for the low Si soil +0% to +18% for the high Si soil (ns)	Frew et al. (2017a)
Sugarcane	Leaves	*Glomus* sp.	-29% to -21% for the low Si soil (ns) -20% to -4% for the low Si soil (ns)	Frew et al. (2017a)
Pigeon pea	Leaves	*Rhizophagus irregularis*	+10%	Garg and Singh (2018)
Banana	Roots	*Rhizophagus irregularis*	+30% (Si content; weight by plant)	Gbongue et al. (2019)
Banana	Leaves	*Rhizophagus irregularis*	+14% (Si content; weight by plant)	Gbongue et al. (2019)
Soybean	Leaves	/	+28% to +208% (depending on P supply)	Yost and Fox (1982)

'ns' stands for "not significant"

Bacteria Bacteria may colonize mineral surfaces, initiate or accelerate weathering, and stimulate plant growth (Jackson 1971; Bosecker 1997; Banfield *et al.* 1999; Bennett *et al.* 2001; Vessey 2003; Calvaruso *et al.* 2006; Uroz *et al.* 2009; Burghelea *et al.* 2015; Zaharescu *et al.* 2019; Finlay *et al.* 2020). Bacteria often associate with fungi in soil to form biofilms on substrate surfaces via excretion of extracellular polymeric substances (EPS) which causes very localized weathering "hotspots" (Flemming & Wingender 2010; Deveau *et al.* 2018; Guennoc *et al.* 2018; Finlay *et al.* 2020). The subsequent dissolution of lithogenic nutrients can therefore be used by all organisms of these hotspots including plants, making the soil-plant continuum a very effective biogeochemical engineer and enhancing overall plant nutrition. Increased rates of weathering and Si release in the presence of certain bacteria have been demonstrated for different mineralogical contents such as feldspar (Barker *et al.* 1998; Welch & Ullman 1999; Wang *et al.* 2015), hornblende (Liermann *et al.* 2000), mica (Barker *et al.* 1998; Liu *et al.* 2006; Wang *et al.* 2015), smectite (Dong *et al.* 2003; Kim *et al.* 2004), amorphous silica (diatoms and sponge) (Bidle & Azam 1999;

Schröer *et al.* 2003), granite (Song *et al.* 2007; Wu *et al.* 2008) and saprolite (Brucker *et al.* 2020). These days, a large number of silicate-solubilizing bacteria (SSB) have been identified, belonging to different genera: *Aeromonas*, *Aminobacter*, *Azotobacter*, *Bacillus*, *Burkholderia*, *Cellvibrio*, *Collimonas*, *Dyella*, *Ensifer*, *Enterobacter*, *Flavobacterium*, *Frateuria*, *Janthinobacterium*, *Kosakonia*, *Labrys*, *Microbacterium*, *Paracoccus*, *Proteus*, *Pseudomonas*, *Rhizobium* and *Sphingomonas* (Uroz *et al.* 2009; Meena *et al.* 2014; Hu *et al.* 2018).

In a pioneering work, Zahra et al. (1984) showed that soil inoculation with *Bacillus circulans* significantly increases Si release from different minerals and subsequent Si uptake by different crop species (barley, maize and clover), demonstrating a key role of bacteria in increasing plant-available Si. More recently, an increasing number of studies demonstrated the impact of SSB on plant Si uptake, and a potential positive effect on plant growth (Table 8-2 and references therein). In these studies, soluble Si concentrations increased by up to 60%, while plant Si content increased by up to 78% (Table 8-2). Future research is needed to identify the abundance, diversity and functions of SSB in different geopedoclimatic contexts, as well as their ability to stimulate soil-plant Si mobility.

Table 8-2 : Effect of silicate-solubilizing bacteria on soluble/plant-available Si and leaf Si concentrations from the literature. We used WebPlotDigitizer to extract data published as figures (Rohatgi 2012).

Plant	Organ	Bacteria	Increase in soluble [Si] (%)	Increase in plant [Si] (%)	Reference
Rice	Leaf	*Enterobacter ludwigii* GAK2	/	+24%	Lee et al. (2019)
Rice	Leaf	*Rhizobium* sp. (IIRR-1)	from +12.4 to +60.2%, depending on silicates	from +9.0% to +78.5% of Si content (weight by plant), depending on silicates	Chandrakala et al. (2019)
Maize	Leaf and root	*Kosakonia* sp.	+10%	+23% for both leaf and root	Hu et al. (2019)
Rice	Leaf	*Bacillus mucilaginosus* and *Aspergillus niger*	from ns to +12%, depending on bacteria application ratio	from ns to +32%, depending on bacteria application ratio	Sun et al. (2020)
Rice	Leaf	*Bacillus amyloliquefaciens*	/	+29%	Bist et al. (2020)
Rice	Whole plant	*Burkholderia eburnea* CS4-2	/	+24%	Kang et al. (2017)
Maize	Leaf and root	*Flavobacterium* sp.	+16%	ns for leaves; +20% for roots	Hu et al. (2018)

'ns' stands for "not significant"

Soil macrofauna

Soil macrofauna like earthworms, beetles and termites contribute to nutrient cycling, soil formation or primary production (Jouquet *et al.* 2011; Blouin *et al.* 2013), but little is known about their effect on soil Si dynamics. Yet, soil macrofauna might affect Si release in soil solution by enhancing the mineralization of organic matter (Ingham *et al.* 1985; Schulmann & Tiunov, Alexei 1999), which may accelerate Si release from phytoliths (Vandevenne *et al.* 2013). Macrofauna also increase the chemical (Jouquet *et al.* 2002; Carpenter *et al.* 2007) and physical (Suzuki *et al.* 2003) weathering of silicate minerals. Recently, Bityutskii et al. (2016) showed that earthworm casts in a sandy and sandy loam soils had a significantly higher soluble Si concentration than the non-bioturbed soil (up to 12 times for *Lumbricus terrestris* casts in the sandy soil). Moreover, the concentrations and translocation rates of Si in the xylem sap of maize and cucumber plants significantly increased when plants grew on a soil previously bioturbed by earthworms. Following this research, Hu et al. (2018) isolated SSB from the gut of *Pheretima guillelmi*, and showed that they markedly increased the release of Si from feldspar and quartz powder, enhanced the uptake and accumulation of Si by maize, and promoted seedling growth. In addition, significantly more SSB were found in the earthworm gut than in the surrounding soil. The authors thus demonstrated that the increased soil-to-plant translocation of Si following earthworm activity was at least in part explained by the presence of SSB in earthworm guts (Hu *et al.* 2018). In accordance with this, Georgiadis et al. (2019) showed that the release of dissolved Si from quartz, which is highly resistant to weathering (Goldich 1938), was much more important after passage through the gut of *Eisenia andrei*. They interpreted this as resulting from a combination of mechanical alteration (Suzuki *et al.* 2003), and the presence of SSB in the earthworm gut (Hu *et al.* 2018). In addition, soil macrofauna strongly impact the redistribution of material in the soil profile (Jouquet *et al.* 2011; Blouin *et al.* 2013). For instance, Jouquet et al. (2020) showed that termite activity impacted the distribution of phytoliths and clay minerals type (1:1 versus 2:1) in south Indian forest soils which could, in turn, impact the concentration of plant-available Si in soil profiles. Overall, soil macrofauna have a significant but overlooked effect on soil Si dynamics, whose magnitude still needs to be determined.

Large herbivores

Large herbivores can cause important changes in ecosystem-scale nutrient cycling (Bardgett & Wardle 2003; Veldhuis *et al.* 2018; Forbes *et al.* 2019; Hwang & Metcalfe 2021). They can either accelerate nutrient cycling through the conversion of aboveground biomass into labile waste products, or decrease it through selective foraging and subsequent shifts towards species that decompose more slowly (Bardgett & Wardle 2003; Forbes *et al.* 2019). Compared with N, P and C (e.g., Veldhuis et al. 2018; le Roux et al. 2020; Sitters et al. 2020), the impact of large herbivores on Si dynamics is poorly quantified. Yet faeces of large herbivores exhibit high silica

concentrations (from 17 to 163 g silica kg^{-1} for large African herbivores ; Hummel et al. 2011), as does sheep urine (up to 259 mg silica L^{-1} ; Nottle and Armstrong 1966). As a consequence, large herbivores strongly impact the land-to-ocean Si transfer by foraging grasses and transporting phytoliths from land ecosystems directly to rivers (Schoelynck *et al.* 2019). Given the abundance of Si-accumulating species in grassland ecosystems, the impact of large herbivores on phytolith redistribution within the same ecosystem (not land-to-river transfer; Schoelynck et al. 2019) is probably also significant. We estimate that large herbivores in a savanna ecosystem ingest and displace from 0.005 ± 0.002 kg Si ha^{-1} yr^{-1} (grey duiker) to 23.2 ± 3.8 kg Si ha^{-1} yr^{-1} (buffalo) (Table 8-3). The higher value corresponds to yearly litterfall of a short grass ecosystem of the Central Great Plains, USA (Blecker *et al.* 2006). This redistribution of phytoliths could, in turn, modify the spatial variability of plant-available Si given their high reactivity in soil environments (Alexandre *et al.* 1997; Blecker *et al.* 2006; Sommer *et al.* 2013; de Tombeur *et al.* 2020c).

Table 8-3 : Estimation of yearly Si inputs to soils by different large herbivores in a savanna ecosystem, and potential effect on Si cycling.

Species	**Scientific name**	**Dung produced**[a]	**Dung [BSi]**[b]	**Dung Si input**[c]	**$MRT_{particle}$**[d]	**Effect on Si cycling**[e]
		g ha^{-1} day^{-1}	g kg^{-1}	kg Si ha^{-1} yr^{-1}	hours	
Buffalo (ruminant)	*Syncerus caffer*	1017.5	133.5 ± 22	23.2 ± 3.8	49	+++
Elephant	*Loxodonta Africana*	432.7	53 ± 10.5	3.9 ± 0.8	30	++
Grey duiker (ruminant)	*Giraffa camelopardalis*	1.3	22 ± 8.5	0.0 ± 0.0	45	+/-
Impala (ruminant)	*Aepyceros melampus*	199.9	123 ± 49	4.2 ± 1.7	-	++
Nyala (ruminant)	*Tragelaphus angasii*	8.6	38 ± 13	0.1 ± 0.0	-	+/-
White rhino	*Ceratotherium simum*	124.2	75 ± 13	1.6 ± 0.3	44	+
Wildebeest (ruminant)	*Connochaetes taurinus*	52.5	135 ± 14.5	1.2 ± 0.1	-	+
Zebra	*Equus burchellii*	76.6	126 ± 17.5	1.6 ± 0.2	28	+

[a]Data from Veldhuis et al. (2018)
[b]Data from Hummel et al. (2011). Means of wet and dry season data were considered.
[c]BSi was converted to Si by dividing by 2.1394.
[d]Food particles' mean retention time (MRT) comes from Steuer et al. (2011) for buffalo, elephant, and zebra, and from Müller et al. (2011) for grey duiker and white rhino
[e]estimated through the combination of yearly dung Si input and $MRT_{particle}$ control on phytolith turnover rates (Vandevenne *et al.* 2013).

Although silica ingestion can reduce the apparent digestibility of herbage (Shewmaker *et al.* 1989; Hartley & DeGabriel 2016; Johnson *et al.* 2021), how phytoliths are processed during digestion remains poorly known. Some herbivores have a neutral to slightly alkaline stomach (e.g., pH 7.3 for *Lama guanicoe* ; Beasley

et al. 2015) and phytolith dissolution rates increase significantly from pH 5 to pH 8 (Fraysse *et al.* 2009). In 1971, Blackman & Bailey showed that up to 39% of silica was dissolved after 24 h of ingestion in a cow rumen (Blackman & Bailey 1971). More recently, Vandevenne et al. (2013) showed that phytolith concentrations in cow, sheep, horse and donkey faeces were two to four times higher than those in the corresponding grazed plants, and that readily-soluble Si concentrations increased in faeces compared with pasture forage (except for horse faeces). Moreover, relative to the initial phytolith content in dungs, 60%, 16% and 8% of Si was mobilized in rain water after 24 h for cow, horse and sheep faeces, respectively, but only 4% for the corresponding pasture forage. These results demonstrate that herbivores have a strong potential to increase Si mobility in soil-plant systems by releasing dissolved Si in urine and increasing phytolith turnover rates, probably through the degradation of organic matrices and an onset of phytolith dissolution in the digestive tract (Vandevenne *et al.* 2013).

Vandevenne et al. (2013) suggested that ruminants (sheep and cows), which achieve greater particle size reduction through higher food particles' mean retention time (MRT) (Johnson *et al.* 2021), have a greater potential to quickly mobilize the highly-soluble fraction of phytoliths, partly via urine, compared to non-ruminants (horse and donkey). Following this idea, ruminants (that have longer food particles' MRT), such as buffalo or duiker, would increase the phytoliths turnover more strongly than non-ruminants such as elephant or zebra do (Table 8-3). Therefore, ruminants that produce large amounts of dung will have a greater impact on soil-plant Si dynamics, and eventually on land-to-ocean Si transfer (Vandevenne *et al.* 2013), compared with non-ruminants that produce moderate amounts of dung (Table 8-3). Overall, large herbivores play a significant but overlooked role in Si biogeochemistry (but see Hwang and Metcalfe 2021) by affecting phytolith turnover rates and distribution in terrestrial ecosystems.

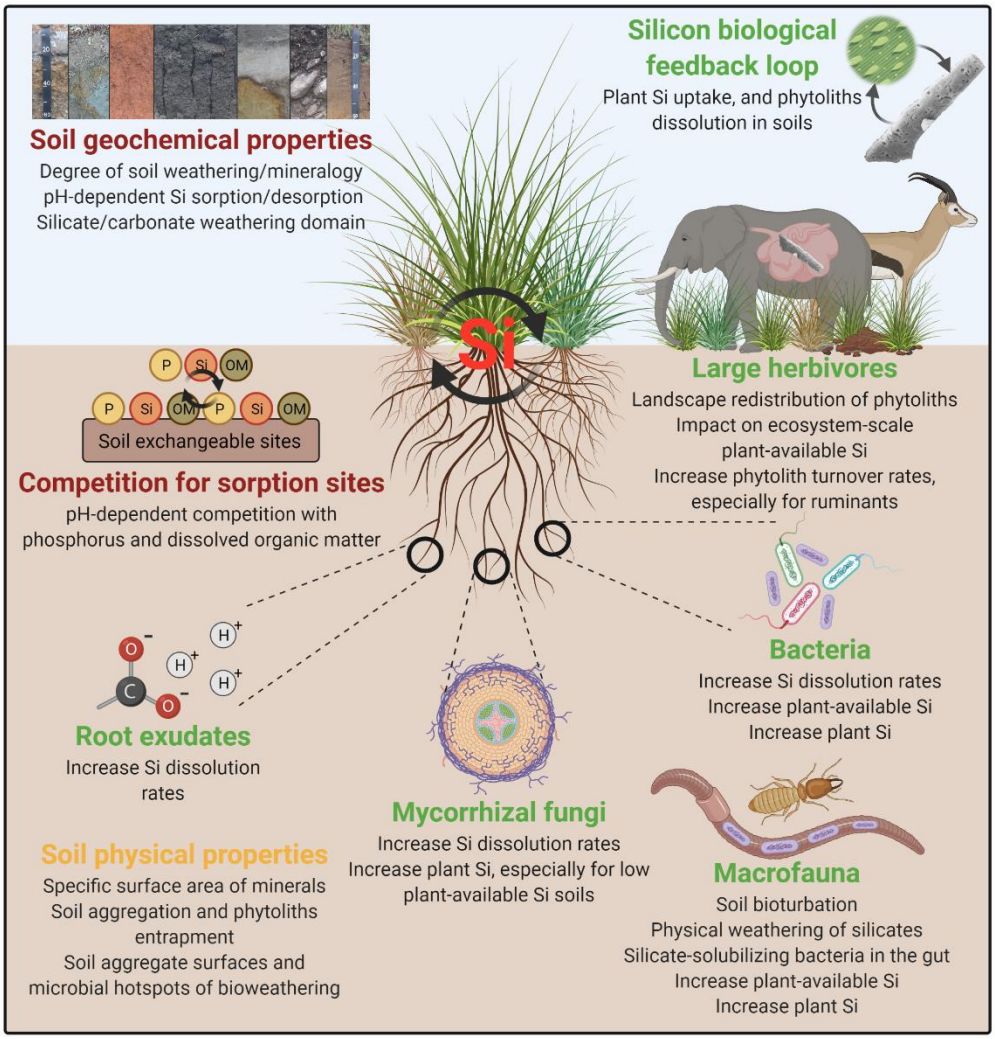

Figure 8-2 : Biotic and abiotic factors influencing soil-plant Si dynamics.

8.5 Silicon and agriculture practices

Knowledge acquired from complex natural systems can be used to increase the resource-use efficiency and productivity of modern agroecosystems (Lambers *et al.* 2011; Mariotte *et al.* 2018). After highlighting biotic and abiotic factors influencing soil-plant Si mobility (Figure 8-2), next we discuss the potential of certain agricultural practices to impact soil Si dynamics and stimulate soil-plant Si cycling.

8.5.1 Leveraging the high reactivity of phytoliths: recycling crop residues

Recycling agricultural residues is key to ameliorate the crop Si status and limit long-term desilication (Guntzer *et al.* 2012b; Meharg & Meharg 2015; Haynes 2017). Annual Si uptake by crop species may be an order of magnitude greater than that in natural ecosystems (Vander Linden & Delvaux 2019) and removing crop residues at harvest is common in some parts of the world (Klotzbücher *et al.* 2015) which lowers the soil phytolith pool (Desplanques *et al.* 2006; Guntzer *et al.* 2012b; Keller *et al.* 2012).

The application of different crop residues to soil increases Na_2CO_3-extractable Si (up to 37% in Yang et al. 2020), water-soluble Si concentrations (up to 15% in Ma and Takahashi 1991b; up to 50% in Watanabe et al. 2017; up to 44% in Yang et al. 2020), plant Si concentration (up to 17% in Ma and Takahashi 1991b; up to 136% in Sistani et al. 1997; up to 168% in Hossain et al. 2001; up to 57% in Yang et al. 2020), and plant Si uptake (up to 25% in Ma and Takahashi 1991b; up to 212% in Marxen et al. 2016). The same pattern occurs for manure, which increases acetic acid-extractable Si and NaOH-extractable Si concentrations by 101% and 32%, respectively, after 10 years of application to a Gleysol (Song *et al.* 2014). Klotzbücher et al. (2018b) also found that manure application tends to increase acetate-extractable Si concentrations, especially together with liming. These results highlight the benefit of returning phytoliths to topsoil because of their fast dissolution rates to replenish the soil solution in dissolved Si (Wickramasinghe & Rowell 2006; Seyfferth *et al.* 2013; Marxen *et al.* 2016; Klotzbücher *et al.* 2018a), with subsequent positive impacts on plant Si uptake. Recently, the use of pyrolyzed Si-rich crop residues (i.e. Si-rich biochar) as a potential alternative to common Si fertilizers has attracted a lot of attention (Xiao et al. 2014; Li and Delvaux 2019; Wang et al. 2019b for reviews). According to Li and Delvaux (2019), the pyrolysis has the advantage of (1) concentrating Si in biochar compared with unpyrolyzed crop residues; (2) providing a liming effect and (3) enhancing the reactive surface area; both (2) and (3)contribute to increasing phytolith dissolution. Numerous recent studies show that the application of different biochars increases soil soluble Si and/or plant Si concentrations (Houben *et al.* 2014; Liu *et al.* 2014; Ibrahim *et al.* 2016; Qian *et al.* 2016; Abbas *et al.* 2017; Koyama & Hayashi 2017; Alvarez-Campos *et al.* 2018; Li *et al.* 2018; Limmer *et al.* 2018; Leksungnoen *et al.* 2019; Li *et al.* 2019b; Seleiman *et al.* 2019; Wang *et al.* 2019a; Huang *et al.* 2020; Wang *et al.* 2020; de Tombeur *et al.* 2021a), confirming its potential as a suitable Si fertilizer (Li & Delvaux 2019). The types of biochar used, application rates (on a Si basis), and increase in percentages of soil soluble Si and/or plant Si concentrations are reported in Table 8-4.

Recycling crop residues via direct incorporation, burning or biochar/manure/compost production and subsequent application has therefore a strong potential to increase crop Si uptake. However, the application rates used in most studies largely exceed coherent annual crop yields. For instance, considering biochar, the application of pyrolyzed material to concentrations of 1% (w/w) or more (bulk density of 1.3 g cm^{-3}; depth incorporation of 10 cm), which corresponds to yearly crop yields of approximately 43 t ha^{-1} (taking into account a pyrolysis yield of 30%) is common. This generally exceeds mean cereal yields worldwide (up to about 13 t ha^{-1}; Ritchie and Roser 2013), except for sugarcane (up to about 120 t ha^{-1}; Ritchie and Roser 2013), and the fraction not available for pyrolysis has to be considered. Li and Delvaux (2019) calculated that a realistic application rate of biochar in the tropics would be around 1.7 t ha^{-1} yr^{-1}, which is about an order of magnitude lower than what was applied in some studies. We, therefore, stress the importance of performing long-term studies in agroecosystems with minimal inputs from external sources and outputs of crop residues (Hughes *et al.* 2020), to better assess the long-term sustainability of such recycling practices. In these systems, detailed analyses of soil and plant Si pools must be conducted, as well as mass-balance calculations, to study the magnitude of desilication as a function of crop residue management. For example, Hughes et al. (2020) recently showed that enhanced Si accumulation in rice grain in highly-weathered soil environments could further contribute to long-term desilication. Furthermore, the effect of crop residue quality on organic matter decomposition rates in contrasting soil, climatic and agricultural contexts should be considered because of its key role in dissolved Si release rates (Fraysse *et al.* 2006a, 2010; Marxen *et al.* 2016; Nakamura *et al.* 2020b).

Table 8-4 : Effect of biochar application on soluble/plant-available Si and leaf Si concentrations from the literature. Si application rates were calculated with biochar application rates and Si concentrations in biochars, when available. The longest time step was considered when soluble Si was assessed through kinetic extractions or measured multiple times during the experiment. We used WebPlotDigitizer to extract data published as figures (Rohatgi 2012).

Plant	Biochar	Application rate (g Si kg^{-1} substrate)	Increase in soluble Si (%)	Increase in leaf [Si] (%)	Reference
Sugarcane	Rice hulls biochar	1.1 and 2.1	/	+457% and +921%	Alvarez-Campos et al. (2018)
Sugarcane	Hardwood yard biochar	0.07 and 0.14	/	+7% and +43%	Alvarez-Campos et al. (2018)
Sugarcane	Horse manure/barn shavings biochar	0.6 and 1.2	/	+57% and +214%	Alvarez-Campos et al. (2018)
Rice	Rice husk biochar	0.1, 0.7 and 7.2	/	+13%, +23% and +70%	Koyama and Hayashi (2017)[a]
Rice	Rice husk biochar	0.3, 0.6 and 1.2	+44%	-31%, +17% and -21% (ns)	Leksungnoen et al. (2019)
Rice	Wheat straw biochar	/	from ns to +320% (depending on experimental sites)	from ns to +58% (depending on experimental sites)	Liu et al. (2014)
Rice	Rice husk biochar	/	/	+31%	Limmer et al. (2018)
Rice	Rice husk biochar	1.1 and 1.7	/	+13% and +7%	Wang et al. (2020)
Rice	Wood sawdust biochar	0.0006 and 0.0012	/	-3% and -8% (ns)	Wang et al. (2020)
Cotton	*Mischantus* straw biochar	1.0	up to +29% for a Cambisol up to +59% for a Nitisol	+20% (Cambisol) +28% (Nitisol)	Li et al. (2018)
Cotton	Softwood biochar	0.02	up to -9% for a Cambisol ns for a Nitisol	-15% (Cambisol) (ns) -7% (Nitisol) (ns)	Li et al. (2018)
Wheat	Rice straw biochar	0.0045 and 0.7695	ns and +77% for a Cambisol ns and +475% for a Nitisol	+69% and +200% (Cambisol) +111% and +667% (Nitisol)	Li et al. (2019)
Wheat	Rice straw biochar	/	+22% to +136%	+19% to +58%	Abbas et al. (2017)
Sunflower	Rice straw biochar	0.77	/	+111%	Seleiman et al. (2019)[b]
Alfalfa	Rice husk biochar	/	+27% to +55%	+65% to 115%	Ibrahim et al. (2016)
Ryegrass	Rice straw biochar	0.5 and 2.2	/	+21% and +35%	Wang et al. (2019)
Rice	Rice husk biochar	0.4 and 2.3	+47% and +141%	+156% and +271%	de Tombeur et al. (2021)

Rice	Cotton stalk biochar	0.01 and 0.05	+7% and +30%	ns and +60%	de Tombeur et al. (2021)
/	*Miscanthus* biochar	0.4 and 1.1	+6% and +37%	/	(Houben *et al.* 2014)
/	Coffee husks biochar	0.3 and 0.9	-9% to +8%	/	(Houben *et al.* 2014)
/	Woody material biochar	1.3 and 3.8	-13% to +10%	/	(Houben *et al.* 2014)
/	Rice-husk biochar	/	from ns to +25% for the 500°C biochar (depending on biochar application rate)	/	Huang et al. (2020)
/	/	/	from ns to +159% for the 400°C biochar (depending on biochar application rate)	/	Qian et al. (2016)

[a]Application rates were calculated with soil bulk density and biochar incorporation depth.
[b]Application rate was calculated considering a soil bulk density of 1.3 g cm^{-3}
'ns' stands for "not significant"

8.5.2 Harnessing Si biocycling and recycling using cover crops

Cover crops are grown specifically for covering the soil during the off-season to reduce soil erosion, increase soil organic matter content and microbial diversity, and improve nutrient cycling (Reeves 1994; Adetunji *et al.* 2020). The positive impact of cover crops on N, P and C cycles has been extensively demonstrated (Abdalla *et al.* 2019; Hallama *et al.* 2019), while their effects on soil Si dynamics are unknown. In the short term, cover crops could have detrimental effects by consuming the pool of soil readily-soluble Si during the winter, lowering Si plant availability for main crops in summer. However, in the long term, the yearly transfer of Si stored in the cover crop via plant residues will significantly increase the soil phytogenic Si pool, and the cover crop will reduce phytolith losses through erosion (Figure 8-3a). This conversion of litho/pedogenic Si-bearing minerals to phytoliths could significantly stimulate Si mobility in agroecosystems since the dissolution rates of phytoliths are an order of magnitude greater than those of typical soil clay minerals (Fraysse *et al.* 2009). Such positive effect would be particularly significant in highly-desilicated soils, where phytolith dissolution has a major effect on the soil-plant Si cycle (Alexandre *et al.* 1997; Sommer *et al.* 2013; de Tombeur *et al.* 2020c).

Table 8-5 : Estimation of shoot Si stocks in common cover crop species.

	Family	Shoot biomass[a] (t ha^{-1})	Shoot Si concentration[b] (g kg^{-1})	Shoot Si stocks (kg ha^{-1})
Legume cover crops				
Lupinus sp.	Fabaceae	0.7-12.4 (*n*=6)	2.8-4.5	2-56
Pisum sativum	Fabaceae	3.7-3.9 (*n*=3)	2.8-5.6	10-22
Vicia sp.	Fabaceae	4.3-8.0 (*n*=7)	2.4-4.8	10-38
Non-legume cover crops				
Avena sp.	Poaceae	7.9-13.2 (*n*=6)	11.5-15.1	91-200
Lolium sp.	Poaceae	1.4-10.0 (*n*=3)	9.7-36.4	14-364
Secale cereale	Poaceae	1.5-12.7 (*n*=11)	12.6	19-160
Brassica sp.	Brassicaceae	2.2-4.1(*n*=4)	2.3-11.2	5-46

[a]Data from Hallama et al. (2019)
[b]Data from Hodson et al. (2005) for all species. Additional data from Xiao et al. (2016) for *Pisum sativum*, Hasan et al. (2020) for *Vicia* sp., Soratto et al. (2012) for *Avena* sp. and Song et al. (2009) for *Brassica* sp.

Based on shoot biomass data of common cover crop species (Hallama *et al.* 2019), we estimated Si stocks in aboveground biomass of cover crops (Table 8-5). For legumes and *Brassica* sp. cover crops, from 2 to 56 kg Si ha^{-1} could annually be brought to soil via crop residues. This range, despite being very large, approximately corresponds with the annual Si uptake in major forest ecosystems worldwide, expect bamboo forests (Vander Linden & Delvaux 2019). The use of Poaceae sp. as cover crops would allow an extreme degree of annual Si inputs, up to 360 kg Si ha^{-1} for *Lolium* sp., which approximately corresponds to Si uptake in sugarcane agroecosystems (Vander Linden & Delvaux 2019). In addition, cover crops may also impact Si dynamics by providing a legacy of increased mycorrhizal abundance, modifying rhizosphere physico-chemical properties (e.g., pH, soil aggregation, root exudates) or changing soil microbial communities and earthworms abundance (Roarty *et al.* 2017; Hallama *et al.* 2019; Adetunji *et al.* 2020; Euteneuer *et al.* 2020). Finally, Si-rich cover crops could diminish herbivore populations, with beneficial legacy effects on the main crop (Vernavá *et al.* 2004).

8.5.3 Facilitative interactions: cereal-legume intercropping systems

Intercropping (Smith & McSorley 2000) has the potential to globally increase yields, reduce fertilizer inputs and save land (Martin-Guay *et al.* 2018; Li *et al.* 2020a), while increasing soil C and N content, ameliorating mineral nutrition and reducing effects of pests (Hinsinger *et al.* 2011; Brooker *et al.* 2015; Cong *et al.* 2015; Xue *et al.* 2016; Tang *et al.* 2020). To our knowledge, the impact of intercropping systems on Si dynamics has been considered only once, through the study of rice (*Oryza sativa*) intercropped with water spinach (*Ipomoea aquatic*) (Ning *et al.* 2017). Plant-available Si concentrations in soil were not markedly impacted by the intercropped system compared with rice monoculture, yet they significantly increased when water spinach was cultivated alone, likely because spinach accumulates less Si than rice

(Ning *et al.* 2017). However, leaf Si concentrations and mineralomass (i.e. Si concentration × leaf dry weight) of rice plants significantly increased in the intercropping system compared with the rice monoculture (up to ~25% for Si concentrations and ~75% for Si mineralomass) (Ning *et al.* 2017). Moreover, the disease index of rice sheath and the incidence of leaf folders significantly decreased in the intercropped system, possibly due to higher Si concentrations (Ning *et al.* 2017).

The pioneering work of Ning et al. has opened up new compelling directions in intercropping-Si research. Here, we propose different processes that could affect soil-plant Si dynamics in cereal-legume intercropping agroecosystems (Figure 8-3b). First, more Si would be available for cereal crop uptake since grasses accumulate more Si than legumes. In the long term, cereal-legume intercropping might even slow down soil desilication, even though mass-balance calculations should be performed to estimate Si stocks in biomass and export from harvests. However, the opposite effect might occur for legume crops, for which less Si would be available than in a monoculture system (Ning *et al.* 2017). This is important to consider since Si has beneficial effects also for legumes, and may promote the symbiotic relationship with nitrogen-fixing bacteria in root nodules (Putra *et al.* 2020). Second, cereal-legume intercropping might induce a wide range of facilitative interactions (Li *et al.* 2014). Under conditions of Fe and Zn deficiencies, cereals secrete phytosiderophores in the soil solution to mobilize Fe and Zn (Ahmed & Holmström 2014), which can then be transferred to both crops (Zuo *et al.* 2000; Xue *et al.* 2016). The same mechanism applies to legumes that may secrete carboxylates to mobilize P, especially under P deficiency (Lambers *et al.* 2006, 2015; Pang *et al.* 2018), which could in turn benefit both crops (Xue *et al.* 2016; Lambers *et al.* 2018). As discussed above, Si co-solubilization or desorption by root exudates such as phytosiderophores and carboxylates is likely, but this needs to be further assessed to determine if such facilitative interactions also occur for this element. Similarly, facilitation via common mycorrhizal networks and nutrient transfer can occur for N and P (Walder *et al.* 2012), but has not been addressed for Si. Third, earthworm abundance and biomass can greatly increase in cereal-legume intercropping systems compared with monocultures (Schmidt et al. 2001, 2003) which could increase plant-available Si concentrations and Si soil-plant mobility (Figure 8-2). Finally, intercropping might also impact Si dynamics by changing soil microbial diversity and modifying the physico-chemical properties of the rhizosphere (Brooker *et al.* 2015), but the direction of these processes needs to be elucidated.

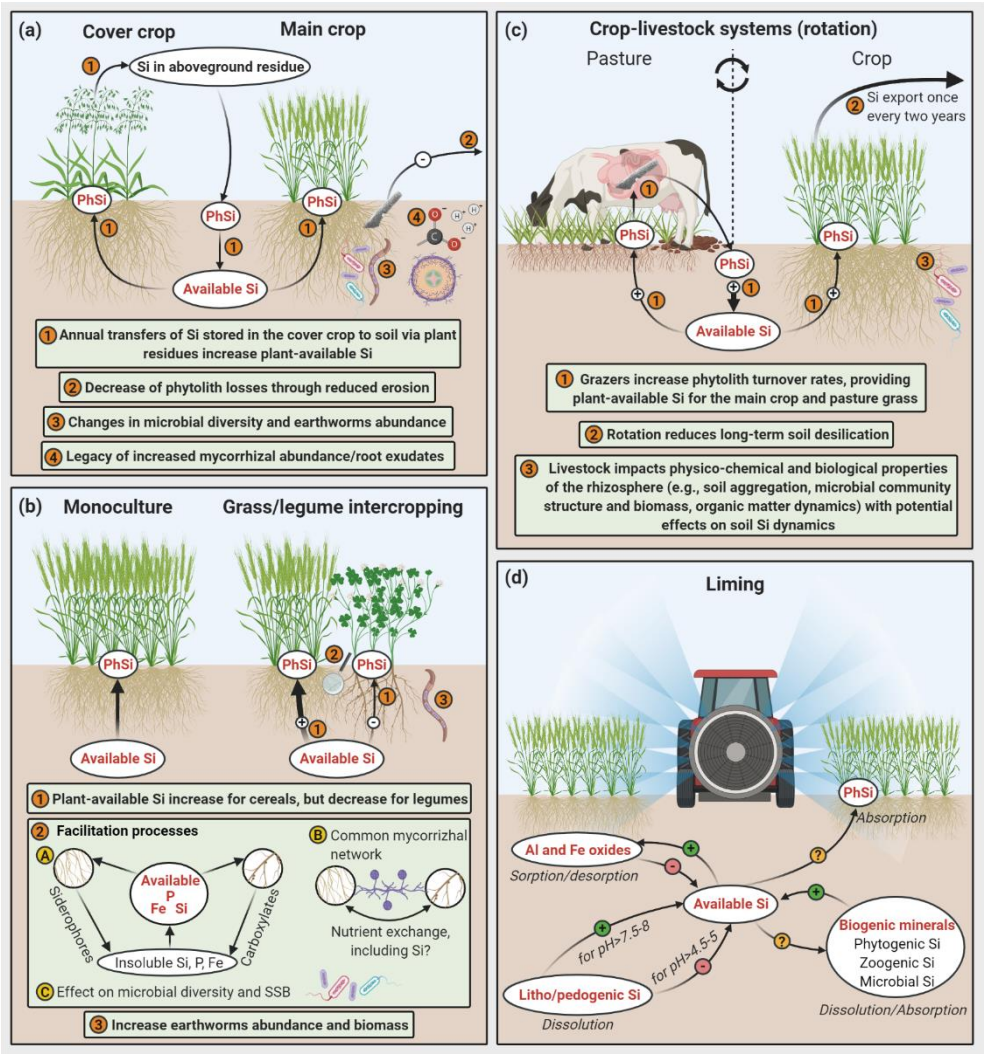

Figure 8-3 : Effects of agricultural practices on soil-plant silicon (Si) dynamics. (a) The transfer of Si stored in the cover crop to soil via plant residues may substantially increase the soil phytogenic Si pool (PhSi), thus contributing to increase plant-available Si concentrations (available Si) (# 1). Cover crops could also lower phytolith losses though reduced erosion (Adetunji et al. 2020) (# 2), modify microbial diversity and earthworm abundance (Roarty et al. 2017; Euteneuer et al. 2020) (# 3), and provide a legacy of increased mycorrhizal abundance/root exudates (Hallama et al. 2019) (# 4), thereby impacting soil-plant Si dynamics. (b) Cereal-legume intercropping may increase plant-available Si concentrations for the cereal crops, but decrease it for the legume crops (Ning et al. 2017) (# 1). Numerous facilitation processes with beneficial effects on soil-plant Si mobility may also occur (# 2): taking advantage of different nutrient-acquisition strategies (Li et al. 2014; Xue et al. 2016), sharing nutrients via common mycorrhizal network (Walder et al. 2012), or modifying microbial diversity (Brooker et al. 2015), including silicate-solubilizing bacteria (SSB).

Cereal-legume intercropping may also increase plant-available Si concentrations and plant Si uptake through enhanced earthworm abundance and biomass (Schmidt et al. 2001, 2003) (# 3). (c) Integrating crops and livestock will increase Si release from phytoliths in animal dung (Vandevenne et al. 2013), which will provide Si for the main crop and pasture grass (# 1). Pasture/crop rotation could also reduce long-term soil desilication by reducing Si export from harvest (once every two year) (# 2). Crop-livestock systems modify physical, chemical and biological properties of the rhizosphere (Brewer & Gaudin 2020), that could, in turn, influence soil-plant Si dynamics (# 3). (d) Increase in soil pH after liming increases Si adsorption on soil colloids, which, in turn, reduces Si concentrations in the soil solution (Figure 8-1). Raising pH above 4.5-5.0 decreases aluminosilicate dissolution rates, while raising pH above 7.5-8.0 increases those rates (Drever 1994; Kelly et al. 1998; Haynes 2019). Raising pH in the range 3.0-9.0 increases phytolith dissolution rates (Fraysse et al. 2009). The pH/liming effects on Si absorption by soil living organisms and plants is unknown.

8.5.4 Grazers as biocatalysts of Si cycling: crop-livestock systems

Despite recent simplification and specialization of agricultural systems worldwide, integrated crop-livestock systems have been employed for millennia and remain the main agriculture model for over two thirds of global farmers, and represent about half of the world's food (Russelle *et al.* 2007; Herrero *et al.* 2010; Lemaire *et al.* 2014). Integrated crop-livestock systems have the potential to improve carbon and nutrient cycling/use efficiency (Alves *et al.* 2019; Brewer & Gaudin 2020; Carlos *et al.* 2020). Based on the evidence of Si mobilization by large herbivores (Figure 8-2), we suggest several benefits of integrated crop-livestock systems on soil-plant Si dynamics, based on a simple pasture/crop rotation (Figure 8-3c). First, large ruminants strongly increase phytolith turnover rates (Blackman & Bailey 1971; Vandevenne *et al.* 2013). For instance, Vandevenne et al. (2013) estimated that a cow-based pasture mobilizes between 18 and 28 kg Si ha^{-1} yr^{-1}, against 1.3-1.8 kg Si ha^{-1} yr^{-1} in ungrazed pastures. In the long term, greater Si mobilization potentially accelerates soil desilication through Si leaching (Vandevenne *et al.* 2013). However, in the short term, it will most likely increase plant-available Si concentrations for the subsequent crop, especially if soil texture-related leaching potential is low. Second, pasture/crop rotations will reduce long-term soil desilication because Si exports through crop harvest will occur only once every two years. Finally, integrating crops and livestock impacts numerous aspects of soil-plant systems such as soil aggregation, microbial community structure/biomass and annual net primary production (Brewer & Gaudin 2020), which could ultimately also affect the soil-plant Si cycle. Crop-livestock systems are promising to enhance Si mobility in soil-plant systems, particularly through the effects of ruminants on phytolith turnover, and therefore deserve further investigations.

8.5.5 Liming and soil-plant Si dynamics: a gap between theory and practice

The effect of liming on soil pH in agroecosystems may affect Si dynamics through antagonistic processes (Figure 8-3d), as discussed above. Therefore, the liming effect is still unclear because it strongly depends on the initial pedological context in terms of soil pH, mineralogy, buffering capacity and phytolith content (Haynes 2019; Vander Linden & Delvaux 2019). Previous studies showed either an increase (Castro & Crusciol 2013; Klotzbücher *et al.* 2018b) or a decrease (Keeping *et al.* 2017; Kostic *et al.* 2017; Haynes & Zhou 2018) in soil Si availability with liming, while others found no significant effect (Mathews *et al.* 2009; Bhat *et al.* 2010). However, different extractants were used to estimate plant-available Si concentrations in these studies (e.g., $CaCl_2$, acetic acid). In fact, liming is expected to increase the pool of adsorbed Si, often associated with acetate and acetic acid extractants, while decreasing the soluble Si pool, often associated with $CaCl_2$ or water extractants (Figure 8-1) (Sauer *et al.* 2006; Georgiadis *et al.* 2013). Haynes and Zhou (2018) confirmed this pattern by showing an increase of Si-acetic acid by about 75-110% and a decrease of Si-$CaCl_2$ by about 25-35% for the pH range 5.0-6.5 in limed Podzol and Gleysol. The authors also found a decrease of alkali-extractable Si, suggesting a loss of phytoliths following increasing dissolution rates (Haynes & Zhou 2018). More recently, Caubet et al. (2020) showed that French agricultural soils had higher Si-$CaCl_2$ concentrations than non-cultivated soils. The authors interpreted this difference as resulting from the pH increase after liming that could modify clay mineralogy (Cornu *et al.* 2012) and increase phytolith dissolution for soils with clay size mineral contents ranging between 5 and 32%. In their study, soils were classified by parent material types, where soils developed on sediments were separated into two groups: carbonated soils (>1% carbonates) and non-carbonated soils (<1% carbonates). In the non-carbonated group, Si-$CaCl_2$ also correlates with the 2-µm fraction cation exchange capacity, used as a proxy of the nature of clay-size minerals. This supports a possible effect of clay assemblage on Si availability that can be superimposed on the liming effect in cultivated land compared with non-cultivated land (forests, wetlands, pastures, parks). Indeed, soils with higher weatherable mineral reserves and subsequently higher Si availability are preferred for agriculture.

As soil extractants are only proxies for plant-available Si concentrations, the liming effect on soil Si dynamics should be addressed by quantifying plant Si concentrations. Although some studies showed that liming had no significant effect on plant Si uptake (Bhat *et al.* 2010; Castro & Crusciol 2013; Keeping *et al.* 2017), others found a marked decrease (Mathews *et al.* 2009; Tavakkoli *et al.* 2011). In particular, Tavakkoli et al. (2011) showed that rice (*Oryza sativa*) leaf Si concentrations decrease markedly from pH 5.5 to pH 9.5, and that differences are most important when wollastonite is supplied (up to 91% lower), and for the most weathered soil (Ferralsol). Mathews et al. (2009) also noted a decrease in Si concentrations of *Pennisetum clandestinum* of about 30% with increasing calcium carbonate application, and in the pH range of 5.2-6.2. These studies could highlight that raising soil pH above 6.0 may

reduce plant Si uptake, possibly because of increased Si adsorption and subsequent decline of Si plant-availability (Figure 8-1). Phytolith dissolution rates strongly increase in this pH range (Fraysse *et al.* 2009) which possibly enhances plant Si uptake (Guntzer *et al.* 2012b), but the size of the phytogenic Si pool is low compared with the litho/pedogenic-Si pool (Alexandre *et al.* 1997, 2011; Sommer *et al.* 2013). Phytoliths can, therefore, not be the main factor of Si plant-availability and subsequent plant uptake in certain pedological contexts (Keller *et al.* 2021). Overall, the effect of liming on soil-plant Si dynamics is still unclear because numerous antagonistic processes occur on different time scales (Figure 8-3d) (Haynes 2019; Vander Linden & Delvaux 2019).

8.6 Conclusions and perspectives

Soil-plant Si cycling is mainly studied through the prism of abiotic mineral weathering or plant Si uptake followed by soil phytoliths dissolution (e.g., Bartoli 1983; Lucas et al. 1993; Alexandre et al. 1997; de Tombeur et al. 2020a), while biotic factors tend to be overlooked. In addition, research on Si in ecology and soil-plant interactions has taken a long time to be initiated (Cooke & Leishman 2011a), especially compared with that on plant macronutrients, probably because Si is still considered as a non-essential, yet beneficial, element. Finally, numerous studies on biological weathering have been conducted, on different scales (Barker *et al.* 1998; Banfield *et al.* 1999; Lucas 2001; Uroz *et al.* 2009; Finlay *et al.* 2020), but rarely in the framework of plant Si nutrition and subsequent positive influence on plant performance or crop yield. We have stressed the importance of biotic factors such as mycorrhizal associations, SSB, soil macrofauna, large herbivores and root exudates on soil-plant Si mobility, and suggest different mechanisms by which these processes may affect Si dynamics and stimulate soil-plant Si cycling in agroecosystems.

9

Soil and climate affect foliar silicification patterns and silica-cellulose balance in sugarcane (*Saccharum officinarum*)*

*This Chapter is adapted from
de Tombeur, F., Vander Linden, C., Cornélis, J-T., Godin, B., Compère, P., Delvaux, B. (2020). Soil and climate affect foliar silicification patterns and silica-cellulose balance in sugarcane (*Saccharum officinarum*). *Plant and Soil*

9.1 Foreword

In the previous chapter, we emphasized the need to improve our understanding of factors controlling soil-plant Si dynamics to ameliorate the sustainability of agroecosystems. The key role of Si in agriculture is indeed increasingly acknowledged, but Si-related agriculture studies remain predominantly focused on the application of Si fertilizers, and the influence of natural processes remain overlooked. In this chapter, we propose to test if one of the factors highlighted in previous chapters, namely soil weathering degree, influences foliar silicification of sugarcane leaves at the cellular level. This shift in scale study is fundamental to understand whether some of the factors highlighted earlier in the thesis can induce beneficial effects for crops. Sugarcane is an important crop worldwide, and silicification is now seen as the main mechanism explaining the Si-related functions in plants. Understanding how soil weathering degree and its subsequent control on plant-available Si concentrations (chapters 3 and 8) influence foliar silicification patterns of this important crop is therefore needed. Silica deposits are thought to act as structural components, and trade-offs with C-based compounds have been reported in this document (chapter 6) and elsewhere. Therefore, we took the opportunity of this study to also analyze C-based structural components to test the occurrence of trade-offs.

9.2 Summary

Silicon (Si) has beneficial effects in a variety of plant species and environments. Soil and climate affect silica accumulation in given plant species, but their roles on foliar silicification patterns and balance between silica and C-rich biopolymers as structural components is poorly known. We studied silica deposition *in situ* in sugarcane leaves collected in three tropical environments differing in soil and climate. Plant silica deposits were physically extracted from leaves through wet digestion. Leaves were observed and mapped for Si by ESEM-EDX. The C-rich biopolymers in leaves were determined by the Van Soest method. Silicon accumulation in the leaves was related to bioavailable Si in soil and plant transpiration. Epidermal silica deposits were either limited to silica cells as dumbbell-shaped phytoliths, or expanded to long and short cells arranged in prominent veins fully silicified, depending on whether the leaf Si concentration was lowest or highest. The size of silica deposits increased with increasing leaf Si through an increasing number of conjoined silicified cells. Leaf ash-free cellulose and Si concentrations were negatively correlated. Soil and climate impact markedly the magnitude of foliar silicification, with possibly significant impact on mechanical properties and Si-related plant functions. Environmental conditions further impact the counterbalance between silica and cellulose as leaf structural components via different levels of Si accumulation.

9.3 Introduction

Since the recognition of the anomaly of silicon (Si) in plant biology (Epstein 1994), a number of advances have contributed to elevate Si to the status of beneficial

substance. This recognition stimulates further progress towards the optimal exploitation of Si in agricultural practices. Si-induced functions in plant indeed alleviate various abiotic stresses (Adrees *et al.* 2015; Cooke & Leishman 2016; Meunier *et al.* 2017; Neu *et al.* 2017), enhance plant protection against herbivores (McNaughton *et al.* 1985; Keeping & Meyer 2006; Massey & Hartley 2006; Leroy *et al.* 2019), pests and diseases (Fauteux *et al.* 2005; Cai *et al.* 2008; Camargo *et al.* 2013) while they increase photosynthetic efficiency (Kang *et al.* 2016) and plant biomass (Tubana *et al.* 2016). Coskun *et al.* (2019) proposed a comprehensive model linking the Si-induced functions in plants through the "apoplastic obstruction hypothesis". Their model defines Si as an "extracellular prophylactic agent against stresses (as opposed to an active cellular agent)", and highlights the role of extracellular silica deposits on Si-induced functions.

Biosilicification in plant occurs in the lumen and cell walls but also in extracellular and intercellular spaces (Yoshida *et al.* 1959; Hodson *et al.* 1985; Kaufman *et al.* 1985; Sangster *et al.* 2001; Hodson 2019). In some cases, callose could be a "catalyst" for silica deposition (Law & Exley 2011; Exley 2015; Guerriero *et al.* 2018). The structural role of silica in plants (Ando *et al.* 2002; Li *et al.* 2015) is attributed to the hardness property of silica (Perry & Fraser 1991; Perry & Keeling-Tucker 2000), which strengthens plant tissues (Epstein 1999; Bauer *et al.* 2011). Silica may indeed act as a compression-resistant structural component (Raven 1983; Epstein 1994), hence contributing to the mechanical resistance of vegetal structures. The inverse relationship between the concentrations of Si and of cellulose (Schoelynck *et al.* 2010) or lignin (Bonilla 2001; Suzuki *et al.* 2012; Yamamoto *et al.* 2012; Klotzbücher *et al.* 2018c) highlights the balance between Si and C components in plants (Cooke & Leishman 2012; Schaller *et al.* 2012a, 2019; Frew *et al.* 2016; Simpson *et al.* 2017). However, evidence for the structural role of Si, and thus balance with C-rich biopolymers, is lacking (Bauer *et al.* 2011; Cooke *et al.* 2016; Schoelynck & Struyf 2016; Soukup *et al.* 2017; Katz 2019).

Monosilicic acid (H_4SiO_4) is taken up from soil solution, translocated to plant transpiration sites (Ma *et al.* 2006) where water loss promotes silica precipitation as amorphous opal-A ($SiO_2.nH_2O$) forming phytoliths. The Si uptake in vascular plants depends on phylogenetic variation (Hodson *et al.* 2005; Deshmukh & Bélanger 2016), soil processes and properties (Lucas *et al.* 1993; Meunier *et al.* 1999; Henriet *et al.* 2008a, b; Cornelis & Delvaux 2016; Quigley *et al.* 2016; de Tombeur *et al.* 2020b; Li *et al.* 2020b), including soil physico-chemical and water properties (Rosen & Weiner 1994; Quigley & Anderson 2014; Li *et al.* 2019b), and climatic conditions (Jones & Handreck 1967; Euliss *et al.* 2005), as well as on increased Si acquisition by specific mycorrhizal fungi (Oye Anda *et al.* 2016; Frew *et al.* 2017a, b; Gbongue *et al.* 2019). An important soil property is the reserve of weatherable primary minerals inherited or derived from the parent rock: this reserve represents the primary source of H_4SiO_4 in soils, and thus of Si available for plants (Henriet *et al.* 2008b, a; Klotzbücher *et al.* 2015; Cornelis & Delvaux 2016).

Given the beneficial effect of foliar silicification on plant functions and stress regulation, understanding how environmental conditions impact this process is important. In addition, since a tradeoff between Si and C-rich biopolymers has been highlighted in the literature, it deserves to be investigated under natural conditions, with a complete understanding of the factors controlling plant Si accumulation. Finally, an analysis of the biosilicification patterns could provide support for the mechanical role of silica and thus for the balance with C-rich biopolymers, which remains unclear in the literature.

Here, we study the biosilicification patterns and balance between Si and C-rich biopolymers as leaf structural components in sugarcane cultivated in contrasting soil and climate conditions. We hypothesize that the reserve of soil weatherable minerals and evapotranspiration potential will be key drivers of the magnitude of silica deposits on leaf epidermis via contrasted level of Si accumulation. We further hypothesize that leaves with low foliar Si concentration will have higher cellulose concentrations as a mechanical compensatory role (Yamamoto *et al.* 2012; Guerriero *et al.* 2016).

9.4 Materials and methods

9.4.1 Environnemental setting

Our fieldwork was carried out in sugarcane (*Saccharum officinarum* L.) plantations established in three sites in Guadeloupe (16°15'N; 61°33'W). Soils largely differed (Table 9-1; Colmet-Daage & Lagache, 1965): they key out as Nitisol, Andosol and Vertisol in the WRB system (IUSS 2014). The Nitisol is highly weathered and formed from old andesitic ash (Colmet-Daage & Lagache 1965; Komorowski *et al.* 2005). The young Andosol (30–18 ka BP; Boudon *et al.* 1987) developed on Eocene andesitic ash in perhumid conditions (Colmet-Daage & Lagache 1965). The Vertisol formed in smectitic materials derived from Pleistocene limestone (Komorowski *et al.* 2005) under drier conditions (Colmet-Daage & Lagache 1965). In the Nitisol-Andosol sites, mean annual precipitation (MAP) and mean annual temperature (MAT) (Table 9-1, Figure 9-1a) are, respectively 2910–3170 mm and 25.4–25.3°C whereas the mean relative ten-day evapotranspiration (ETP) is 34.2–34.5 mm (Table 9-1). In the Vertisol site, MAP amounts to 1275 mm, MAT is 26.7°C whilst the mean relative ten-day ETP reaches 42.0 mm, and the average monthly precipitation is invariably below 100 mm from December to July (Figure 9-1a). Monthly precipitation decreases from December to April in all sites. The wettest site is the Andosol one (Table 9-1) where the daily ETP measured during the 'dry' season prior to fieldwork (Figure 9-1b) shows very little variation in contrast to the Nitisol and Vertisol sites, in which a maximum value occurs in March. The water regime has greatly affected soil processes and mineral composition (Colmet-Daage & Lagache 1965). Abundant precipitation and intense leaching have enhanced mineral weathering and export of solutes to watersheds.

Table 9-1 : Some general characteristics of the three sites and sugarcane cultivars.

Reference Soil Group[1]	Coordinates	Altitude (masl)	Soil parent rock	MAP[2] mm
Nitisol	16°10'36''N 61°38'04''W	163	andesitic ash (Pliocene)	2910
Andosol	16°02'59''N 61°35'33''W	150	andesitic ash (Eocene)	3170
Vertisol	16°25'32''N 61°27'29''W	18	limestone (Pleistocene)	1272

Reference Soil Group[1]	MAT[3] (°C)	ETP[4] (mm/decade)	Soil moisture regime[5]	Cultivar
Nitisol	25.4	34.5	udic	R570
Andosol	25.3	34.2	perudic	R579
Vertisol	26.7	42.0	ustic	B80689

[1]WRB key (IUSS 2014)
[2]Mean Annual Precipitation
[3]Mean Annual Temperature (2016, 2017)
[4]calculated from monthly and decade (10-day) data (2016, 2017)
[5]qualified following USDA's Soil Survey Laboratory Staff (2017), based on data from Colmet-Daage & Lagache (1965)

The composition of the soils (Colmet-Daage & Lagache 1965) thus distinctly differs between the two wet sites and the Vertisol one, in agreement with the MAP threshold of 1400 mm above which humidity and intense leaching enhanced the processes of desilication and base exhaustion in similar environments, whilst below that threshold, silica and bases were retained (Chadwick *et al.* 2003). Soil processes have indeed led to the accumulation of secondary minerals such as kaolinite and Fe oxides in the Nitisol, Al-rich allophanic substances and gibbsite in the Andosol (Colmet-Daage & Lagache 1965; Ndayiragije & Delvaux 2003), denoting strong desilication (Churchman & Lowe 2012). In contrast, silica was retained in the Vertisol in which secondary Si-rich swelling clay minerals accumulate (Colmet-Daage & Lagache 1965). This mineralogical contrast originates from differences in soil age and soil moisture regime (Table 9-1), leading to decreasing water availability and increasing ETP in the sequence Andosol–Nitisol–Vertisol.

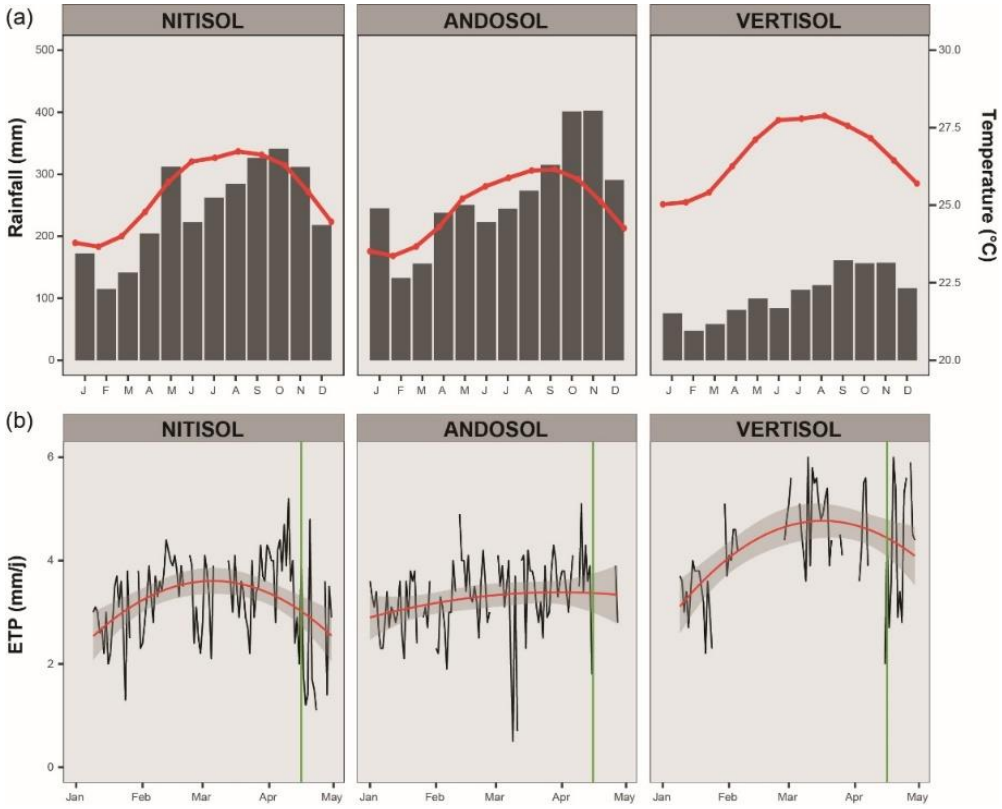

Figure 9-1 : Monthly precipitation and temperature as averaged over 25 years (from 1993 to 2018) in the three sites (a). Daily ETP as measured from January to May 2017 in the selected sugarcane fields in (b). Leaf sampling took place from 11th to 13th April 2017 (green bars in b).

In these environments, sugarcane has long been cultivated. The sugarcane cultivars differed between sites (Table 9-1). *Saccharum officinarum* is a model Si–accumulator, but leaf Si concentration varies very little between cultivars (<0.02 g kg^{-1}) (Keeping & Meyer 2006; Keeping *et al.* 2013).

9.4.2 Sample collection

The topsoils were sampled at 0–20 cm soil depth in April 2017. The TVD (top visible dewlap) sugarcane leaves were sampled from primary shoots or stalks while tillers and suckers were avoided. The midrib was removed (McCray *et al.* 2011). Topsoil and foliar samples were collected in triplicates in each site. For each replicate, three soil subsamples and twenty leaf subsamples were randomly collected to constitute a composite sample.

9.4.3 Soil analyses

Soil samples were air-dried and sieved at 2 mm. Soil pH was measured in H_2O and KCl 1 M with a solid:liquid ratio of 1g:5ml. Exchangeable cations and cation exchange capacity (CEC) were determined by 1 M ammonium acetate pH7 (Olsen *et al.* 1982). $CaCl_2$-extractable Si ($CaCl_2$-Si) is considered to assess bioavailable Si in soils (Haymsom & Chapman 1975; Sauer *et al.* 2006). Four grams of soil were shaken with 40 ml of a $CaCl_2$ 0.01 M solution for 6h. After centrifugation, the supernatant was filtered and analyzed for Si concentration by ICP-AES. Total elemental concentrations in soil were determined after calcination at 450 °C for 24 hours, followed by a fusion at 1000 °C for 5 min in a graphite crucible with Li-tetraborate and Li-metaborate (Chao & Sanzolone 1992). After dissolution of the fusion bead in 10% HNO_3, element concentrations were measured by ICP-AES. The total reserve in bases (TRB) in soils was computed as the sum of major alkaline and alkaline-earth cations (Ca, Mg, K and Na in $cmol_c\ kg^{-1}$) to estimate soil weathering stage (Herbillon 1986).

9.4.4 Plant analyses

Leaf samples were thoroughly washed with 70% ethanol in order to remove potential particles from aeolian deposits. They were dried for four days in an oven at 65 °C and grinded. Si concentration was determined after calcination at 450 °C for 24 hours. The ash concentration was determined by weight difference before and after the calcination. Then, 100 mg of ashes were calcinated at 1000°C for 5 min in a graphite crucible with Li-tetraborate and Li-metaborate (Chao & Sanzolone 1992; Nakamura *et al.* 2020a). After the dissolution of the fusion bead in 10% HNO_3, the concentrations of Si, Ca, Mg and K were measured by ICP-AES. Carbon concentration in leaves was measured by flash dry combustion and expressed as dry weight (DW; 103 °C for 4 hours) and ash-free dry weight percentages respectively (AFDW).

Leaf fiber concentration was determined on ground leaf samples according to the detergent fiber method (Van Soest & Wine 1967; Van Soest 1973; Schoelynck *et al.* 2010; Godin *et al.* 2014, 2015). Briefly, on the one hand, the content of neutral detergent fibers (NDF containing cellulose, hemicelluloses and lignin) was determined using two extractants: (1) 0.1 mmol/L phosphate buffered at pH 7 for 15 min at 90°C, (2): Van Soest neutral detergent at 100°C for 1 h with the addition of sodium sulfite. The NDF fraction was incinerated at 550 °C for 3 h, and the mass loss allowed us to calculate the percentage of NDFom by difference (NDF without residual ash). On the other hand, the contents of acid detergent fibers (ADF containing cellulose and lignin) and acid detergent lignin (ADL containing lignin) were determined using the following extractants: (1) 0.1 mmol/L phosphate buffer at pH 7 for 15 min at 90°C, (2) Van Soest neutral detergent at 100°C for 1 h without the addition of sodium sulfite, (3) Van Soest acid detergent at 100°C for 1 h to get the ADF fraction, (4): sulfuric acid 72 % for 3 h to obtain the ADL fraction. The ADL fraction was incinerated at 550 °C for 3 h, and the mass loss allowed us to calculate

the percentage of ADFom and ADLom by subtraction (ADF and ADL without residual ash). The cellulose, hemicellulose and lignin concentrations expressed as dry weight percentages (g kg^{-1} DW) were then estimated as ADFom–ADLom, NDFom–ADFom, and ADLom, respectively (Godin *et al.* 2014, 2015). More details on the method can be found in Godin *et al.* (2011). Finally, the three structural components were expressed as dry weight (g kg^{-1} DW; 103 °C for 4 hours) and ash-free dry weight percentages (g kg^{-1} AFDW).

One of the three leaf samples from each site was used for physical extraction and microscopical observation of silica deposits. The extraction was carried out by wet digestion adapted from Kelly 1990, Fraysse *et al.* 2009 and Corbineau *et al.* 2013. Ten grams of washed and ground leaf material were transferred into a glass baker with 10% HCl at 80°C to dissolve carbonates if any. Ultrapure 65% HNO_3 was gradually added in order to remove the major portion of organic tissues. Then, ultrapure the mixture 65% HNO_3/30% H_2O_2 was gradually added in the baker at 80°C as long as the reaction went on and the residue remained colored. The residue was carefully rinsed with deionized water and transferred into polypropylene tubes for centrifugation at 3700 rpm for 5 min. Rinsing was repeated 3 times. The residue was oven dried at 50°C during 48h.

9.4.5 SEM observation and X-ray microanalysis

Extracted silica deposits were spread on glass slides covered with double-sided carbon tape and directly observed in a FEI ESEM Quanta 600 at 30 kV accelerating voltage and in low-vacuum mode (1.3 mbar).

Besides, leaf samples were mounted on glass slides using double-side carbon tape and bridged with silver paint before to carbon-coated in a Balzers MED010 evaporator. They were imaged with the backscattered-electron (BSE) detector in a FEI ESEM-FEG XL-30 working at 30 kV accelerating voltage and fitted with a Bruker 129 eV X-ray detector for elemental microanalysis. The Si distribution was obtained on the abaxial side of the leaves by elemental Si mappings acquired on the Si Kα peak at 1.74 keV at 3 different magnifications (x38, x75 and x150). Stomata and dumbbell-shaped phytoliths per mm^2 of leaf surface were counted on the BSE images for the three magnifications, on five squares (200*200 pixels, i.e. 0.41 mm^2) randomly positioned on the images. In the same five squares, the area percentage of yellow pixels (Si signal) on Si elemental mappings was measured with the software GIMP v2.10.8.

9.4.6 Statistical analyses

Statistical analyses were performed using the software MiniTab®18.1. Means were compared based on least significant differences (LSD Fisher) and various letters were significantly different at the 95% level of confidence. Potential correlations were tested with Pearson's chi-square tests.

9.5 Results

9.5.1 Soil properties and mineral concentrations in plants

As shown in Table 9-2a, soil pH was 5.8 (Nitisol, Andosol) and 7.2 (Vertisol) in water, 4.8 (Nitisol and Andosol) and 5.9 (Vertisol) in KCl. CEC ($cmol_c\ kg^{-1}$) was 25.8 in the Nitisol, 47.6 in the Andosol and 59.9 in the Vertisol. Base saturation in topsoils was 12% (Andosol) and 31% (Nitisol) in the wettest sites, but reached 85% in the Vertisol. $CaCl_2$-Si (mg kg^{-1}) followed the sequence Nitisol (16.8) < Andosol (31.3) < Vertisol (55.1). TRB ($cmol_c\ kg^{-1}$) followed the same trend (Table 9-2b): Nitisol (35) < Andosol (110) < Vertisol (114). Subtracting the exchangeable content from the total one for each cation gives the respective content of non-exchangeable base (Table 9-2b).

Table 9-2 : Selected soil properties: (a) Average (n=3) values of pH, contents of exchangeable bases (Ca, Mg, K, Na), sum of exchangeable bases (SEB), cation exchange capacity (CEC), base saturation (BS), $CaCl_2$–extractable Si ($CaCl_2$-Si). For $CaCl_2$–Si, SE are given under brackets. (b) Average (n=3) values of total elemental contents (Ca, Mg, K, Na), Total Reserve in Bases (TRB), contents of non-exchangeable bases (total – exchangeable content), total reserve of non-exchangeable bases.

(a)	pH		Exchangeable bases ($cmol_c\ kg^{-1}$)				SEB[1]	CEC	BS[2]	$CaCl_2$-Si
	H_2O	KCl	Ca	Mg	K	Na	$cmol_c\ kg^{-1}$	$cmol_c\ kg^{-1}$	%	mg kg^{-1}
Nitisol	5.8	4.8	4.3	1.9	1.8	0.1	8.1	25.8	31	16.8 (0.8)b
Andosol	5.8	4.8	2.1	2.1	1.3	0.2	5.7	47.6	12	31.3 (1.6)b
Vertisol	7.2	5.9	42.1	7.9	0.4	0.8	51.2	59.9	86	55.1 (11.0)a

(b)	Total elemental concentration ($cmol_c\ kg^{-1}$)				TRB[3]	Non-exchangeable bases ($cmol_c\ kg^{-1}$)[4]				Non-exch. reserve[5]
	Ca	Mg	K	Na	$cmol_c\ kg^{-1}$	Ca	Mg	K	Na	$cmol_c\ kg^{-1}$
Nitisol	11.5	15.6	6.2	2.0	35.4	7.2	13.7	4.4	1.9	27
Andosol	15.8	83.6	5.0	5.5	110.0	13.7	81.5	3.7	5.3	104
Vertisol	56.6	49.6	4.2	3.6	113.9	14.7	41.7	3.8	2.8	63

[1]Sum of exchangeable bases
[2]BS=SEB/CEC*100
[3]TRB is the sum of the total contents of major alkaline and alkaline-earth cations (Herbillon 1986)
[4]The non-exchangeable cation content is the difference between the total and exchangeable content for each cation.
[5]Sum of the contents of non-exchangeable bases (TRB – SEB).

Their sum represents the reserve of non-exchangeable bases, occluded in soil minerals. This reserve ($cmol_c\ kg^{-1}$) increases in the sequence: Nitisol (27) < Vertisol (63) < Andosol (104). Table 9-2b further shows that the content of non-exchangeable Mg largely contributed to the total non-exchangeable reserve.

9.5.2 Mineral concentrations in plants

The leaf Si concentration ($g\ kg^{-1}$) (Table 9-3) followed the order Nitisol (7) < Andosol (14) < Vertisol (21). As far as the major cations are concerned, the sum of their contents ($cmol_c\ kg^{-1}$) followed the same sequence Nitisol (56) < Andosol (59) < Vertisol (79). The dominant cation in sugarcane leaves was K from the Andosol and Nitisol sites (>50%), but Ca from the Vertisol one (44%).

Table 9-3 : Mineral contents and balances in sugarcane leaves : average (n=3) values of foliar contents of Si, Ca, Mg, K; sum of cations Ca, Mg, K (Sc), cationic proportions in Sc, and Mg/Ca atomic ratio. SE are given under brackets for the leaf mineral contents.

	Leaf mineral content ($g\ kg^{-1}$)				**Sc**	**Cationic proportion in Sc (%)**			**Ratio Mg/Ca**
Site	Si	Ca	Mg	K	$cmol_c\ kg^{-1}$	Ca	Mg	K	
Nitisol	7.0 (0.3)c	2.6 (0.1)b	1.2 (0.0)b	13.2 (0.1)a	56	23	17	60	0.76
Andosol	14.7 (0.2)b	2.1 (0.1)b	2.2 (0.1)a	11.8 (0.4)b	59	18	31	51	1.70
Vertisol	21.0 (1.1)a	7.0 (0.3)a	1.5 (0.2)b	12.5 (0.3)ab	79	44	15	40	0.35

9.5.3 Localization of leaf silica deposits

As shown in Figure 9-2, silica deposits can be classified into three different types according to their morphology and location: (i) surface dumbbell-shaped phytoliths located in silica cells (Figure 9-2a), (ii) silicified guard cells of stomata arranged in rows (Figure 9-2a) and (iii) silicified epidermal long and short cells arranged in longitudinal veins (Figures 9-2b, 9-2c, 9-2d).

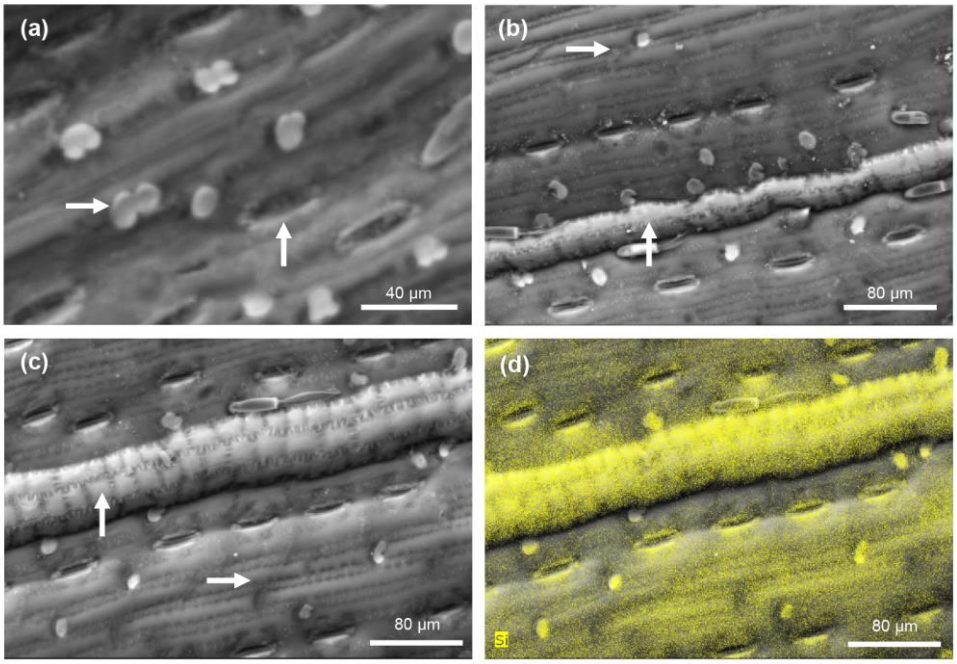

Figure 9-2 : BSE-LV-SEM images performed on a sugarcane leaf (abaxial surface) from the Vertisol site (a-c) and combined image with EDX elemental mapping of Si (d). Intense white BSE (a-c) and yellow (d) signals indicate silica deposits. The horizontal and vertical arrows in (a) indicate, respectively, dumbbell-shaped phytoliths and stomata. The horizontal and vertical arrows in (b) and (c) indicate veins made of long cells and short cells, respectively.

The size, forms and density (number per mm²) of the dumbbell-shaped phytoliths were constant whatever the site (Figures 9-3a-j). Silica deposits in stomata were less important than in silica cells as evidenced by a lower yellow signal (Figures 9-3g-i) and their density was significantly higher in leaves from the Andosol site as compared to the two other ones (Nitisol, Vertisol) (Figure 9-3k).

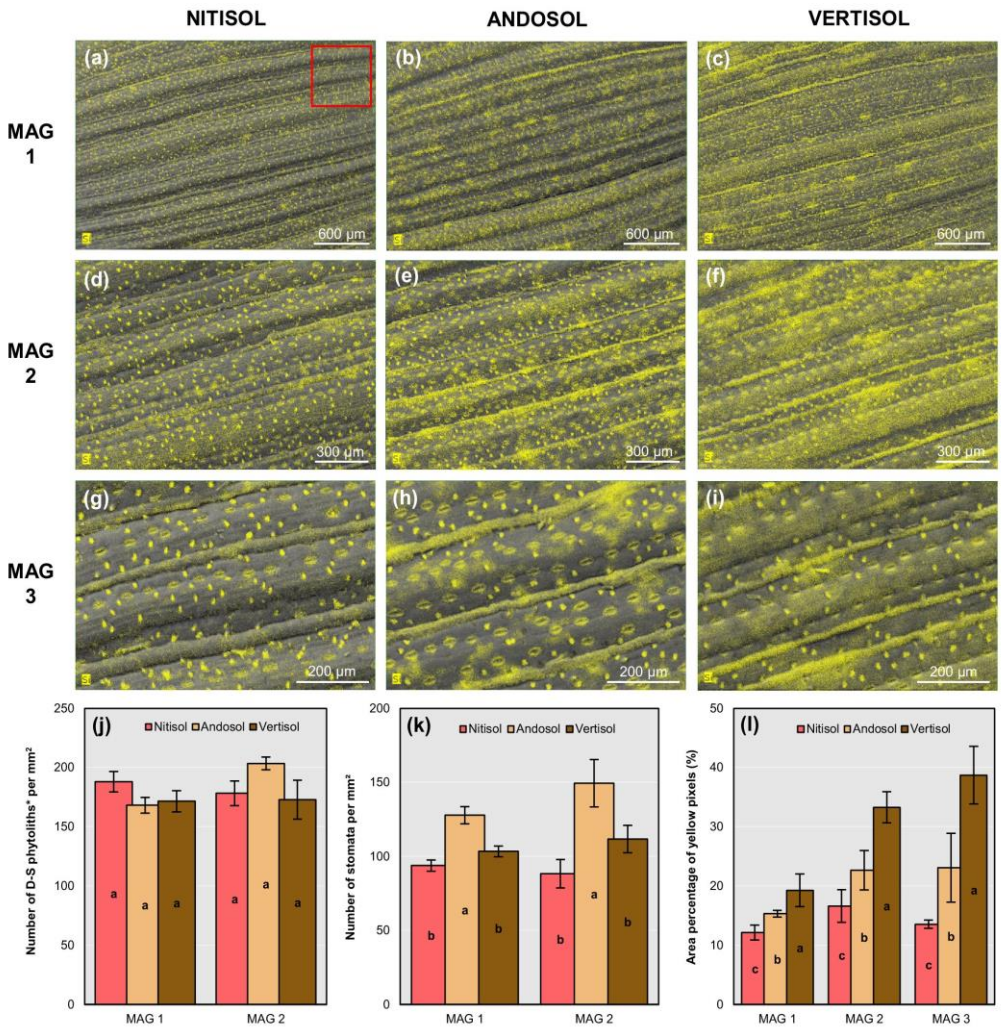

Figure 9-3 : Combined BSE-LV-SEM/EDX-Si mapping images of abaxial surfaces of sugarcane leaves from the three sites, at three direct magnifications (a-i). Number of dumbbell-shaped (DS) phytoliths per mm² (j) and stomata (k) for the three soils for MAG 1 and MAG 2. Relative area of yellow pixels (%) for the three soils and magnifications (l). The red square in (a) visualizes the area used for counting the number of phytoliths, stomata and yellow pixels.

The silicification in long and short cells greatly depended on the site as shown on Si mappings in Figure 9-3. Indeed, the silicification in veins increased in the sequence Nitisol < Andosol < Vertisol. Prominent veins of about 20-70 µm wide were formed by 2 to 3 rows of short broad epidermal cells (Figures 9-3b, c, d), the lumens of which appeared fully silicified only at the Andosol and Vertisol site (Figures 9-3e, f, h, i).

Between these prominent veins, more flattened and wider veins (up to 200 µm) were located between longitudinal stomata rows and included several rows (5-10) of thin elongated epidermal cells. In the leaves from the Vertisol site, flat veins appeared strongly silicified compared to those from the Nitisol and Andosol site (Figures 9-3). Despite a high proportion of silicified stomata in the Andosol site, the total surface area affected by silicification significantly increased in the order Nitisol < Andosol < Vertisol (Figure 9-3l).

9.5.4 Structures of extracted silica deposits

Extracted silica deposits showed different structures (Figure 9-4): (i) silicified cell walls (Figure 9-4a), (ii) silicified long cells (Figure 9-4b) and short cells (Figure 9-4c), (iii) elongated rod-shaped structures (Figure 9-4d), (iv) silicified cell lumens (Figure 9-4c, e), and (v) dumbbell-shaped phytoliths (Figure 9-4f). Most of them corresponded to silica deposits occurring exclusively in epidermal cells. This is the case for dumbbell-shaped phytoliths and long and short silicified cells from veins. Other structures may correspond to silicified cells in inner tissues or to partial silicification. This is the case of silicified cell walls, cell lumens of different shapes and long rods. Deposits from stomata guard cells were not seen probably because of their small size and non-characteristic shape. Very large deposits up to 350 µm long and 150 µm wide and with several cells in thickness were observed (Figure 9-4e).

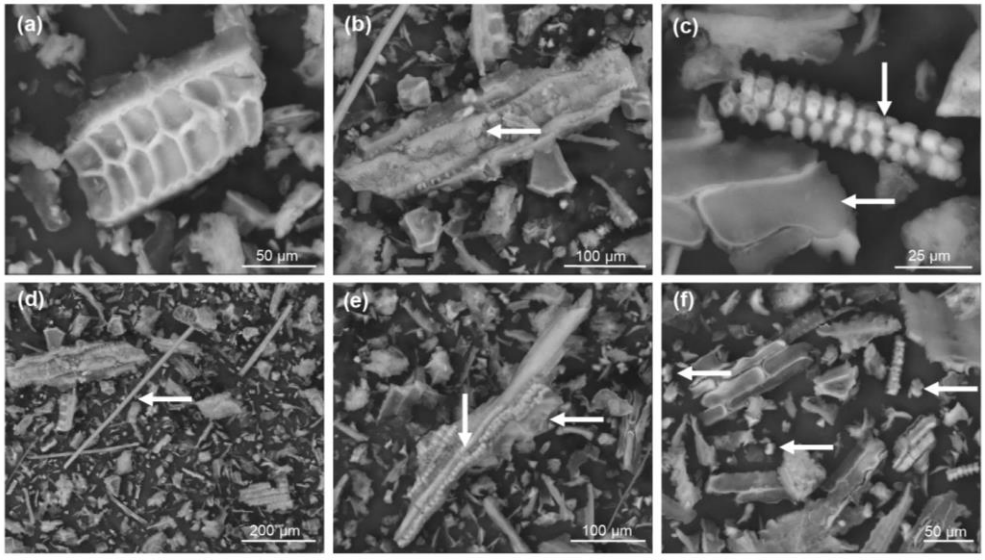

Figure 9-4 : BSE-LV-SEM images of extracted silica bodies from Vertisol sugarcane leaves. The arrow in image (b) indicates silicified long cells. The horizontal and vertical arrows in image (c) indicate respectively silicified short cells and cell lumens. The arrow in image (d) indicates a silicified rod-shaped structure. The horizontal arrow in image (e) indicate a large multicellular structure up to 350 µm long and 150 µm wide and the vertical arrow shows around 35 silicified cell lumens attached in length on this structure. The arrows in image (f) indicate dumbbell-shaped phytoliths.

The comparison of the 3 sets of 3 pictures in Figure 9-5 taken at fixed magnification gives evidence that the size of silica deposits increased in the sequence Nitisol < Andosol < Vertisol (Figure 9-5). For the Nitisol site, small-sized dumbbell-shaped deposits (<50µm) and short rod-spicules (most probably from stomata guard cells) dominated in leaves and multicellular deposits occurred only marginally (Figure 9-5g). Large multicellular deposits up to 200 µm were observed for the Andosol site (Figure 9-5h), and even larger than 200 µm for the Vertisol site (Figures 9-5f, i).

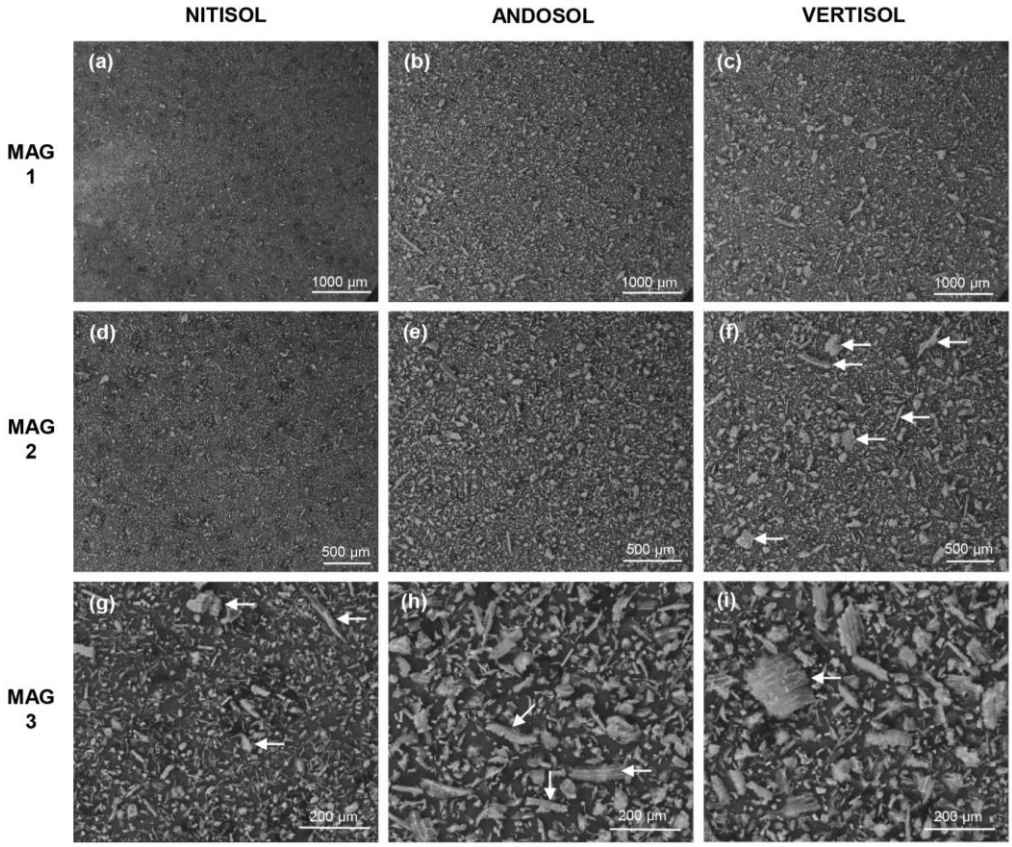

Figure 9-5 : Magnification series of BSE-LV-SEM views of silica structures extracted from leaves of sugarcane grown in the 3 different soils. Both particle size and number of large particles increase obviously from the Nitisol to the Vertisol. The arrows in images (f) and (i) indicate structures larger than 200 µm. The arrows in image (g) show multicellular structures. The vertical, horizontal and diagonal arrows in image (h) indicate respectively attached cells lumens, long cells and short cells.

9.5.5 Carbon, cellulose, hemicellulose and lignin concentration

Ash concentrations (g kg^{-1} DW) increased in the order Nitisol (54) < Andosol (66) < Vertisol (89) (Table 9-4). Carbon concentrations (g kg^{-1} DW) did not differ between leaves from the wet sites Nitisol (469) and Andosol (465), but were lower for the Vertisol site (455 g kg^{-1}). Leaf C and cellulose concentration was negatively correlated with Si concentration (Figure 9-6a, c). After ash correction, C concentrations were similar for the three different sites (Figure 9-6b), but cellulose concentrations (g kg^{-1} AFDW) differed in the order Nitisol (374) > Andosol (365) > Vertisol (356) (Table 9-4) and was negatively correlated with Si concentration (Figure 9-6d). After ash correction, the concentrations of hemicelluloses and lignin were not correlated to leaf Si concentration (Figures 9-6e, f).

Table 9-4 : Average values (n=3, SE into brackets) of ash, carbon, cellulose, hemicellulose and lignin concentrations of the sugarcane leaf samples, expressed as dry weight percentages (g kg^{-1} DW) and/or ash-free dry weight percentages (g kg^{-1} AFDW).

Site name	Ash	Carbon		Cellulose		Hemicellulose		Lignin	
	DW	DW	AF DW	DW	AF DW	DW	AF DW	DW	AF DW
Nitisol	54 (1)c	469 (1)a	496 (1)c	354 (4)a	374 (4)a	322 (5)ab	341 (5)b	53 (1)a	56 (1)a
Andosol	66 (1)b	465 (1)a	498 (1)b	341 (1)b	365 (1)b	337 (0)a	360 (0.7)a	40 (1)c	43 (1)c
Vertisol	89 (3)a	455 (2)b	500 (1)a	324 (2)c	356 (0.1)c	312 (7)b	343 (0.7)b	46 (2)b	50 (2)b

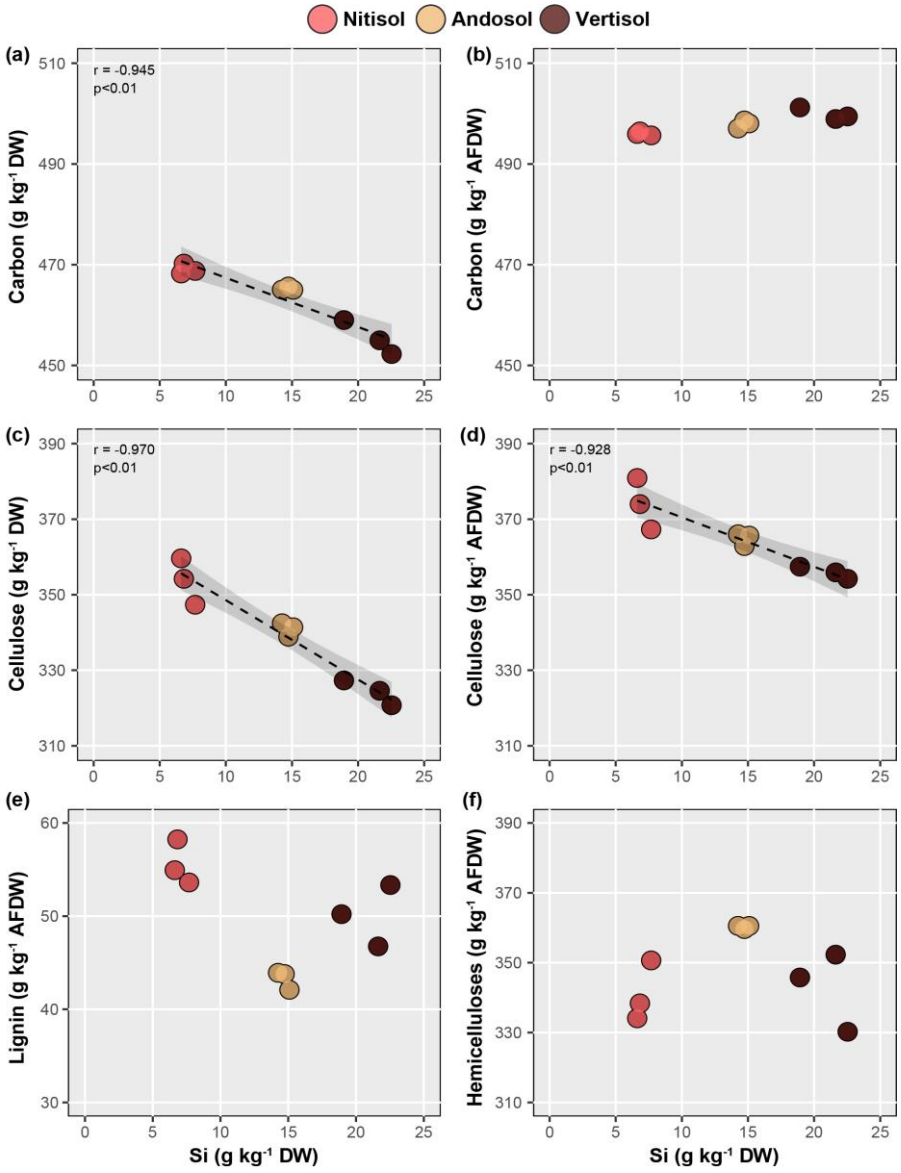

Figure 9-6 : Plots of the carbon (a, b), cellulose (c, d), lignin (e) and hemicellulose (f) in g kg-1 DW (a, c) and g kg^{-1} AFDW (b, d, e, f) against Si concentration (in g kg^{-1} DW) in leaves from sugarcanes cropped on the Nitisol (light brown), Andosol (orange-brown) and Vertisol (dark brown).

9.6 Discussion

9.6.1 Control of soil and climate on leaf Si concentration

The soil non-exchangeable reserve ($cmol_c\ kg^{-1}$) of weatherable minerals (Table 9-2) is, by far, the largest in the Andosol (104): it is 3.8 and 1.6 times higher than in the Nitisol (27) and the Vertisol (63), respectively. In the Vertisol, total Ca massively includes exchangeable Ca, which accounts for 74% of total Ca, whereas exchangeable Mg represents only 16% of total Mg. In this soil, calcium carbonate provides exchangeable Ca, which contributes to saturate the exchange complex while non-exchangeable Mg is occluded in the octahedral sheet of smectite (Colmet-Daage & Lagache 1965). In this line, the Vertisol is very poor in primary silicate weatherable minerals, as confirmed by the near disappearance of feldspars (K) and Na-plagioclases (Table 9-2). Consequently, non-exchangeable Mg content is here the most pertinent indicator to discriminate the soil weathering stages between these three soils. Despite it directly impacts the leaf Mg concentration (Figure 9-7a), non-exchangeable Mg content does not affect in the same way the leaf Si content (Figure 9-7b), which is, by far, the largest in sugarcane leaves sampled in the Vertisol site, where it is controlled by bioavailable Si in soil (Figure 9-7c). Thus, in the wet sites (Andosol, Nitisol), soil weathering stage primarily controls Si accumulation in sugarcane cropped in similar climate conditions as reported earlier for banana (Henriet *et al.* 2008a, b) and rice (Klotzbücher *et al.* 2015). In contrast, in the Vertisol site, the impact of soil weathering stage is less important: climate affects water availability and plant transpiration (ETP, Table 9-1, Figure 9-2) as well as smectite stability in soil, which is controlled by high silica activity in soil solution (Rai & Kittrick 1989) as promoted by the occurrence of a prolonged dry season (Colmet-Daage & Lagache 1965). In any case, the bioavailability of Si in soil controls leaf Si content (Figure 9-7c). Hypothesizing a negligible cultivar effect, our data thus corroborate that Si accumulation in a given plant species is affected by both the soil weathering stage (Henriet *et al.* 2008a, b; Klotzbücher *et al.* 2015) and plant transpiration fluxes (Euliss *et al.* 2005; Henriet *et al.* 2006; Issaharou-Matchi *et al.* 2016). We can expect a larger pool of soil biogenic silica (BSi) in the Vertisol, which could also release Si in soil solution, and influence Si availability (Sommer *et al.* 2013). As demonstrated earlier (Henriet *et al.* 2008b, a), weatherable primary minerals are the original source of plant available Si, hence of the stock of BSi, which in turn, contribute to control aqueous Si in soil solution (Lucas *et al.* 1993). As recently reviewed, the stock of soil BSi is related to plant available Si, and is controlled by a number of factors among which soil weathering stage and climate are preponderant for a given plant species (Cornelis & Delvaux 2016; Vander Linden & Delvaux 2019). In line with these previous statements, we hypothesize that BSi stock would decrease from Vertisol to Andosol and Nitisol, and contribute to the pool of plant available Si differently, but in a similar sequence.

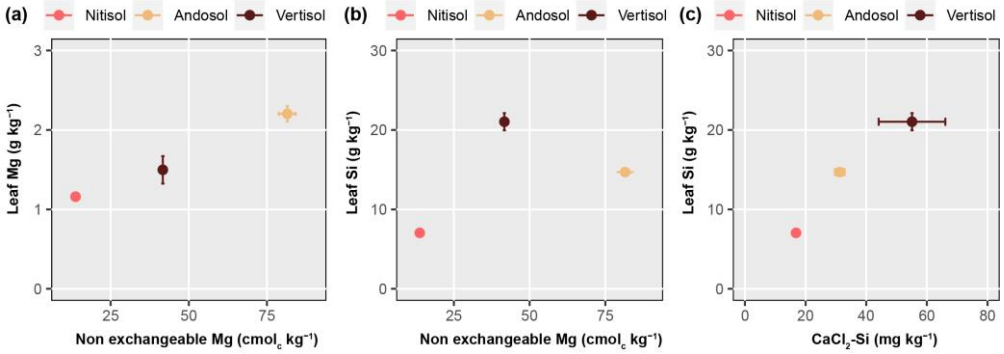

Figure 9-7 : Plots of (a) sugarcane leaf Mg concentration and (b) sugarcane leaf Si concentration against the content of non-exchangeable Mg in soil; and (c) sugarcane leaf Si concentration against soil $CaCl_2$ extractable Si content ($CaCl_2$-Si).

9.6.2 Effect of environmental conditions on silicification patterns in sugarcane leaves

Our data also highlight that soil and climate conditions affect biosilicification patterns in sugarcane leaves. As show in Figure 9-3l, the relative area affected by silica deposits largely increases with the increase in $CaCl_2$-Si in soil and resulting leaf Si contents, from 13.5 % in Nitisol to 23.1% in Andosol and 38.7% in Vertisol sites. In contrast, the number of dumbbell-shaped phytoliths are very similar between the three sites (Figure 9-3j). Although a significant higher number of stomata per mm² was observed for the Andosol site, the area affected by these silicified structures is small compared to the one of silicified veins. This is consistent with literature data showing that silica deposits in silica cells is an active and physiologically regulated process occurring during the first stage of leaf development, independently of transpiration rate (Motomura *et al.* 2002, 2006; Kumar *et al.* 2017a; Kumar & Elbaum 2018). In contrast, silica deposits in long and short cells is a passive process depending on silica saturation during cell dehydration (Kumar *et al.* 2017b; Alexandre *et al.* 2019). While the silicification of long and short cells depends on the leaf stage development (Alexandre *et al.* 2019), our results show that environmental conditions (soil, climate) also impact on this process through Si plant-availability in soil (Hartley *et al.* 2015) and plant transpiration. Therefore, we suggest that environmental conditions have a direct influence on leaf epidermal silicification that directly controls some of the major Si-related functions as defense against pathogen intrusion (Cai *et al.* 2008), herbivory (Epstein 2009; Keeping *et al.* 2009) or water and UV stress (Meunier *et al.* 2017; Coskun *et al.* 2019).

It has been demonstrated that the leaf erectness of rice leaves was improved after Si fertilization (Yamamoto *et al.* 2012; Kido *et al.* 2015), the process being still unclear (Bauer *et al.* 2011; Cooke *et al.* 2016). Our results show that the size of silica deposits extracted from the leaves increases with increasing leaf Si concentrations

(Figure 9-5). Larger Si bioavailability in soil and plant transpiration in the Vertisol site promote the formation of larger silica deposits, with more joint silicified cells, as observed under irrigation (Rosen & Weiner 1994). Here, we hypothesize that the formation of large multicellular silica deposits could be crucial to explain the increase in leaf erectness under Si fertilization. They are much larger, concern no only isolated epidermal cells but also deeper leaf tissues, and are thus probably more prone to play a mechanical role compared to deposits in silica cells and stomata of the epidermis. Indeed, they are especially concentrated in longitudinal reinforcement veins that thus could form continuous rigid silicified columns running all along leaf surfaces. Moreover, compact deposits of several cell columns not only concern epidermal cells but also involve deep plant tissues to form local rigid plates. This hypothesis should now be tested under controlled conditions, with a complete analysis of leaf mechanical properties.

9.6.3 Balance between silica and cellulose as structural components

Cellulose is majorly responsible for the biomechanical strength in plant leaves (Kitajima *et al.* 2012, 2016). Since the deposition of silica is less energy-consuming than the biosynthesis of C-rich biopolymers (Raven 1983), tradeoffs may occur between these two types of structural components (Schoelynck *et al.* 2010; Klotzbücher *et al.* 2018c; Schaller *et al.* 2019). Here, the ash-free C concentration does not differ between the 3 sites, highlighting the dilution of C by Si when no ash-corrections are made (Figure 9-8) (Cooke & Leishman 2012). However, the leaf cellulose concentration (g kg^{-1} AFDW) decreases with increasing leaf Si concentration (Figure 9-6d). This supports that cellulose is the C-rich biopolymer whose synthesis increases with decreasing silica deposits, a compensatory role for Si deprivation (Guerriero *et al.* 2016). The increase in cellulose synthesis in plants deprived in Si is located in the cell layer just beneath the abaxial epidermis and in short cells in the adaxial epidermis (Yamamoto *et al.* 2012), corresponding to the cell concerned with silica deposits in plants from Si-rich soils in this study (Figure 9-4e). Therefore, the control of both the Si bioavailability in soil and plant transpiration on leaf Si concentration may modulate the synthesis of cellulose in epidermal cells, most probably those forming reinforcement veins, supporting the balance between C-rich biopolymers and silica reported earlier (Schoelynck *et al.* 2010; Suzuki *et al.* 2012; Klotzbücher *et al.* 2018c).

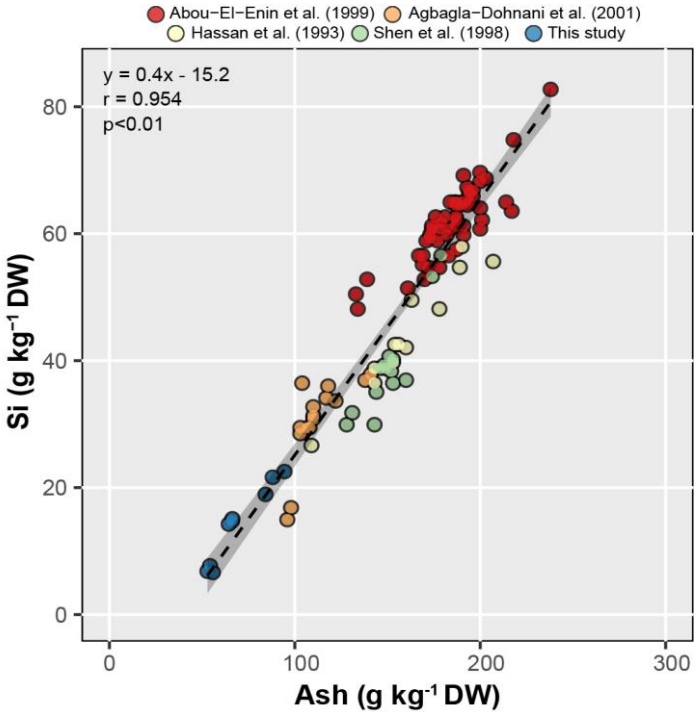

Figure 9-8 : Plot of leaf ash concentration (g kg^{-1}) against leaf Si concentration (g kg^{-1}) in the Poaceae family (n=103). Blue dots are the sugarcane leaves of this study. All the others are rice straw from Hasan *et al.* 1993 in yellow, Shen *et al.* 1998 in green, Abou-El-Enin *et al.* 1999 in red and Agbagla-Dohnani *et al.* 2001 in orange.

9.6.4 New insights on soil disease-suppressiveness?

This property is the ability of soils to reduce or inhibit the growth and activity of present soilborne pathogens (Cook & Baker 1983; Alabouvette 1999). Silicon-induced functions in plant enhance plant protection against among others fungal diseases (see e.g. (Fauteux *et al.* 2005, 2006). On the other hand, in a given climatic context, Si bioavailability in soil largely depends on soil type and processes (Cornelis & Delvaux 2016). The spread of Panama disease, caused by *Fusarium oxysporum cubense* race 4 on banana, was governed by soil type as reported by Stotzky & Martin, (1963). These authors showed that this disease weakly developed in plants cropped on soils rich in swelling clays (smectite) whereas it led to the eradication of the sensitive banana cultivar *Gros Michel* in all other soils. This novelty was followed worldwide by a number of studies on various crops highlighting the presence of smectite as a factor suppressing plant diseases induced by soilborne pathogens (Stotzky 1986), leading to the concept of soil suppressiveness (Alabouvette 1999) and using soil clay mineral composition to predict this specific property (Stotzky 1986). The casual link between the occurrence of smectite and soil suppressiveness was,

however, poorly established so far. Soil suppressiveness was proposed to be based on biotic interactions depending on abiotic characteristics of the soil, especially pH and the nature of clay minerals (Alabouvette 1999; Alabouvette *et al.* 2006). The role of the soil microbiome was strengthened recently (Schlatter *et al.* 2017). However, the impact of soil and climate conditions on Si accumulation in plant and biosilicification patterns reported here may open new routes in the appraisal of soil suppressiveness. Indeed, smectite is stable in soil at pH around or above neutrality and H_4SiO_4 concentration over 1 mM in soil solution. Because of the plant protective Si-induced functions, the high bioavailability of Si in soil might thus contribute to the suppressiveness of high base saturated swelling clayey soils, in addition to the effects of smectite properties on microbial ecology (Stotzky 1986; Alabouvette 1999). This challenging hypothesis requires, however, further investigation.

9.7 Conclusion

Our data corroborate that soil weathering stage and plant transpiration strongly impact Si accumulation in plant. We further show that soil and climate affect the localization and size of silica deposits in leaves of sugarcane, a high-Si accumulator. These environmental factors thus play a crucial role on leaf silicification patterns, and likely on their resulting effects on the mechanical reinforcement of plant leaves and Si-related functions (Coskun *et al.* 2019). In addition, the strong impact of environmental conditions on the size and shapes of silica deposits could impact markedly their dissolution rate in soils (Nakamura *et al.* 2020b), which could in turn influence the mobility of Si in soil-plant systems (Cornelis & Delvaux 2016). We further highlight that the increase in leaf Si concentration correlates with a lower synthesis of cellulose in sugarcane leaves. Yet, we cannot conclude on any casual mechanistic link between the increase in leaf silicification magnitude and the decrease in cellulose concentration. This should be further investigated since lignocellulosic and siliceous constituents do not play identical physiological roles in plants (Soukup *et al.* 2017).

10

Biochar affects silicification patterns and physical traits of rice leaves cultivated in a desilicated soil (Ferric Lixisol)*

*This Chapter is adapted from

de Tombeur, F., Cooke, J., Collard, L., Cisse, D., Saba, F., Lefebvre, D., Burgeon, V., Hassan Bismarck, N., Cornélis, J-T. Biochar affects silicification patterns and physical traits of rice leaves cultivated in a desilicated soil (Ferric Lixisol). *Plant and Soil*.

10.1 Foreword

In the chapters 4 and 5, we highlighted the important role of phytoliths dissolution to provide plant-available Si in natural ecosystems, especially in highly-desilicated soils. In the chapter 8, we stressed the importance of recycling crop residues to ameliorate crop Si status and limit long-term desilication, based on evidence from the literature. This can be achieved through direct residues incorporation, burning or biochar/manure/compost production and subsequent application. We particularly insisted on the use of pyrolyzed Si-rich crop residues (i.e., Si-rich biochar) as a potential alternative to common Si fertilizers because of its recent increased attention. Finally, the previous chapter demonstrated that studying silicification at the cellular level can help up to understand its positive effects on plant fitness. In this chapter, we propose to test if the application of Si-rich biochar to an agricultural, desilicated soil from Burkina Faso, where access to common Si fertilizers is low, could increase the foliar silicification of upland rice. Since leaf silicification has structural and defensive functions, we also quantified some leaf physical traits to test the occurrence of trade-offs. Assessing if sustainable agriculture practices might increase crop Si status in developing countries through the relatively high reactivity of biogenic silica in soils is timely in the face of global changes and resource depletion.

10.2 Summary

Increasing the leaf silicification of cereal crops to ameliorate defenses against stresses and improve yield constitutes a major challenge in (sub-)tropical regions with highly desilicated soils. We tested the efficacy of different biochars – as readily available alternatives to commercial fertilizers – to increase leaf silicification and understand subsequent impacts of leaf traits that might benefit crops. We compared the application of two biochars (rice-derived biochar with 198 g kg^{-1} of Si and cotton-derived biochar with 4 g kg^{-1} of Si) and wollastonite (240 g kg^{-1} of Si) at two application rates on the leaf silicification patterns and leaf traits of rice growing in pots containing highly desilicated soil (Ferric Lixisol) from Burkina Faso. Leaf Si increased from 19.0 to 70.4 g kg^{-1} with Si addition (control < cotton biochar < wollastonite < rice biochar), resulting in larger epidermal silica deposits. Leaf carbon (C), leaf mass per area (LMA) and leaf arc decreased and were negatively correlated with leaf Si, however, surprisingly, the leaf force to punch and the plant biomass decreased. We demonstrate the effective use of rice biochar in desilicated environments to improve the Si status of cereal crops and their associated leaf traits. In particular, the decrease in LMA with rice biochar application shows a promising capacity of rice biochar to reduce rice leaf C costs. *In situ* trials are now needed to investigate whether or not these beneficial effects may result in increased crop yields through resilience against environmental stresses.

10.3 Introduction

Vascular plants accumulate silicon (Si) in their tissue, often in concentrations exceeding those of the major macronutrients (Epstein 1994). Silicon is taken up from the soil solution as monosilicic acid (H_4SiO_4), transported in the xylem, and deposited in extra- and intercellular spaces as hydrated amorphous silica (SiO_2, nH_2O) (Ma *et al.* 2006; Yamaji & Ma 2011; Exley 2015; Hodson 2019). Biosilicification has occurred in land plants for over 400 million years (Trembath-Reichert *et al.* 2015), and numerous plant functions have been associated with this mechanism (Epstein 1994, 2009; Cooke & Leishman 2016; Hartley & DeGabriel 2016; Debona *et al.* 2017; Coskun *et al.* 2019). In particular, silicification in plants increases their resistance to water stress (Meunier *et al.* 2017), pathogens and herbivore attack (Massey & Hartley 2006; Massey *et al.* 2007a; Frew *et al.* 2016), reduces the soil-to-plant translocation of toxicants (Gong *et al.* 2006; Coskun *et al.* 2019), and probably interferes with the recognition process occurring upon pathogen infection (Frew *et al.* 2018; Coskun *et al.* 2019; Hall *et al.* 2019; Leroy *et al.* 2019). The beneficial effects of Si in graminoid crops (e.g. wheat, rice, maize, sugarcane) can enhance agricultural productivity and food security, particularly in marginal areas (Savant *et al.* 1999; Datnoff *et al.* 2001a; Tubana *et al.* 2016).

Through the weathering of Si-bearing minerals, a part of Si is dissolved in the soil solution or is reversibly adsorbed onto mineral surfaces, and therefore made available for plant uptake. The concentration of available Si depends on the nature and particle-size of minerals (Cornelis *et al.* 2011b, 2014; Meunier *et al.* 2018; de Tombeur *et al.* 2020b), and on the degree of Si biocycling (Bartoli 1983; Alexandre *et al.* 1997; Lucas 2001; Cornelis & Delvaux 2016; Vander Linden & Delvaux 2019; de Tombeur *et al.* 2020c). Available Si concentrations decrease with increasing degree of soil weathering and relative content of poorly-soluble 1:1 clay minerals and quartz (Savant *et al.* 1999; de Tombeur *et al.* 2020a). As a consequence, highly-weathered tropical soils are characterized by low available Si concentrations (Meunier *et al.* 2018; de Tombeur *et al.* 2020a). On these highly desilicated soils, Si-accumulating crops are often supplied with Si fertilizers to counterbalance Si exports from harvest (Guntzer *et al.* 2012b; Keller *et al.* 2012), to reduce disease and increase yield (Datnoff *et al.* 2001a; Liang *et al.* 2015b; Klotzbücher *et al.* 2018a). However, access to common Si fertilizers (e.g. wollastonite) in remote areas is low. In these locations, the simplest and most accessible way to increase Si availability for plant uptake is to use amendments derived from organic products, such as rice crop residues or Si-rich biochar (Li & Delvaux 2019; Li *et al.* 2019b).

Silicon-accumulating species have very variable [Si] (e.g. from 1.6% to 10.7% of dry weight for leaves of different rice cultivars in Klotzbücher *et al.* 2018). Such variations in the degree of leaf silicification may impact their properties, although it remains poorly studied. For instance, silica has long been attributed to have a structural role in leaves (Raven 1983), though the underlying mechanisms remain elusive (Bauer *et al.* 2011; Cooke *et al.* 2016). The silicification of the leaf epidermis is thought to improve the erectness of leaves under Si fertilization (Ando *et al.* 2002;

Zanão Júnior *et al.* 2010; Yamamoto *et al.* 2012), but there is no clear evidence of a relationship between the two parameters. This however needs to be understood as changes in leaf erectness can impact light interception (Ando *et al.* 2002), and in turn the photosynthetic and growth rates. In addition, several studies showed that Si addition increases leaf toughness (Yamamoto *et al.* 2012; Kido *et al.* 2015; Simpson *et al.* 2017; Johnson *et al.* 2019b). However, these studies performed tearing and shearing tests, while the impact of epidermal silicification on the force required to punch through leaves remains unknown. Finally, because silica deposits are energetically less demanding than the synthesis of C-based compounds (Raven 1983), they represent a cheaper alternative to other plant traits performing structural and defensive functions. Indeed, tradeoffs with phenolic compounds (Cooke & Leishman 2012; Frew *et al.* 2016; Johnson & Hartley 2018; Waterman *et al.* 2021) and with C-based structural components (Schoelynck *et al.* 2010; Klotzbücher *et al.* 2018c; Schaller *et al.* 2019; de Tombeur *et al.* 2020a) have been reported. On this basis, silicification could impact the leaf mass per area unit (LMA), which also exerts a major control on leaf toughness and deterring herbivory (Peeters 2002; Onoda *et al.* 2011; Kitajima *et al.* 2012, 2016), but this remain unexplored. This is important since the construction of thinner/less dense leaves at the expense of a high degree of epidermal silicification would reduce the leaf C costs of cultivated grasses, and could ultimately explain the yield increase observed after Si fertilization (e.g. Tubana et al. 2016).

Burkina Faso relies heavily on Si-accumulating crop species such as rice and maize (Traoré *et al.* 2015; MAAH 2020), grown predominantly on highly desilicated soils, but with poor access to common Si fertilizers. Through a pot experiment in controlled conditions, we sought to determine if the application of biochar on a highly-desilicated soil from Burkina Faso (1) can be a Si source for local rice varieties, (2) can impact the patterns of leaf silicification, and (3) can impact other leaf traits with structural and defensive functions. We hypothesized that biochar from high-Si accumulating rice would result in higher plant Si accumulation of the rice crop compared to low-Si accumulating cotton-based biochar. Secondly, we hypothesized that a higher degree of Si accumulation will result in an increase of leaf silicification, resulting in straighter leaves. Thirdly, we hypothesized that a higher degree of leaf silicification could affect the LMA and the force required to punch leaves, but without conjecture on the direction of the response.

10.4 Materials and methods

10.4.1 Soil selection and sampling

The soil selected for the experiment was a Ferric Lixisol developing on a granitic parent material and showing a ferruginous crust between 20 and 40 cm depth. The soil has a sandy loam texture (73% sand, 15% silt and <12% clay), a low CEC (2.9 $cmol_c$ kg^{-1}), a soil pH-H_2O of 6.1 and significantly lower soil pH-KCl (4.8). The mineralogy is dominated by quartz and kaolinite (Table 10-1), which is typical for highly

desilicated soils. This is corroborated by the low Si concentrations extracted with $CaCl_2$ (11.2 mg kg^{-1}) compared to literature (de Tombeur *et al.* 2020b for a review).

Table 10-1 : Physico-chemical characteristics of the Lixisol used for the experiment. Standard-errors are indicated in brackets (n=3). The term 'CEC' stands for 'cation exchange capacity' and 'Si_{CC}' is the Si concentration extracted with CaCl2 0.01M after 32 days.

Particle-size distribution[a] (%)			**pH-KCl[b]**	**pH-H2O[b]**	**CEC[c]**	**Si_{CC}**
Sand	Silt	Clay			$cmol_c\ kg^{-1}$	$mg\ kg^{-1}$
73.3 (1.6)	14.5 (0.9)	12.2 (0.6)	4.8 (0.0)	6.1 (0.3)	2.9 (0.0)	11.2 (0.4)

[a]Gravimetric sedimentation after OM removal with hydrogen peroxide.
[b]1:5 soil to solution ratio. 1M KCl for pH-KCl
[c]Metson method (1956)

Mineralogy[d]				
Quartz	Kaolinite	K-feldspars	Anatase	Mica/Illite
72%	23%	2%	2%	1%

[d]XRD analysis on bulk soil and clay-sized fraction. Carried out by a Bruker D8- Advance Eco diffractometer generating CuK radiation. Minerals identified with EVA 3.2 software and then quantified by TOPAS software.

Soil samples were collected in January 2019 near Koumbia, a village located in province of Tuy, in southwest Burkina Faso (11°13'N, 3°43'W). The weather is characterized as a Sudanian climate, with a rainy season between May and September. The mean annual rainfall varies between 1000 and 1200 mm and the mean monthly temperature between 22°C and 35°C. Four subplots under typical cotton-maize rotation were randomly selected to collect the soil required for the pot experiment. The soil was collected above the ferruginous crust.

10.4.2 Silicon amendments

We studied two potential biochar-based Si amendments that can easily be produced by local farmers, making them more accessible than conventional Si fertilizers. Biochar was produced from two crop residues, rice husks (rice biochar) and cotton stalks (cotton biochar), at the University of Nazi Boni, Bobo-Dioulasso, Burkina Faso. The biochar was produced through pyrolysis at approximately 450°C during 80 minutes using a conventional Top-Lit UpDraft (TLUD) oven. Characteristics of both biochars were determined according to the European Biochar Certificate (EBC) by Eurofins Umwelt. Both biochars were compared to wollastonite, a conventional Si fertilizer (Datnoff *et al.* 2001a), provided by Vanderbilt Chemicals, LLC (W10).

10.4.3 Pot experiment

The experiment was conducted in a greenhouse at Gembloux Agro-Bio Tech, ULiège (Belgium). Three Si-based amendments were applied (rice biochar referred as R, cotton biochar referred as C and wollastonite referred as W), with two input rates of 5 and 30 t ha^{-1}: R5, R30, C5, C30, W5 and W30. The control (no Si fertilization) is referred as 'T'. The lower application rate of 5 t ha^{-1} corresponds to what can be commonly found in biochar experiments in tropical agro-ecosystems (Nair *et al.* 2017). However, given typical rice husk yields are approximately ~600 kg ha^{-1} which produce about ~100-300 kg ha^{-1} of biochar (pyrolysis yield about 30%), amending 5 t ha^{-1} of rice husk biochar at once is unrealistic for farmers. A distribution of the amendment over the years should therefore be considered. The higher rate was included to examine the potential impacts of higher Si inputs to soil and accumulation in leaf tissues. Rice cultivar FKR 45 N was selected as it is commonly cultivated in Burkina Faso (Traoré *et al.* 2015). It has a growth cycle of 95 days. The experiment was carried out in pots (10.5*10.5*22 cm), in a randomized complete block design. The seeding rate was 70 to 90 kilograms per hectare, which represents one plant per pot. Dibbling seeding was performed, followed by a thinning after 10 days to select the healthiest plant. 150 kg ha^{-1} of NPK (14-23-14) and 100 kg ha^{-1} of urea (46% N) were applied after respectively 20 and 35 days of experiment, which is a typical fertilization pattern in Burkina Faso. Pots were watered daily with 150 mL of tap water.

10.4.4 Soil analyses

Soil pH-KCl was determined using 1M KCl (mass ratio soil:solution 1:5). The amount of bioavailable nutrients (P, Ca, Mg, K) in soil were assessed using ammonium acetate-EDTA 1M extractable solution (Lakanen & Erviö 1971), in which elements were measured by atomic absorption spectroscopy (Ca, Mg, and K) or by spectrophotometry (P). Total C and N contents were determined with a CN analyzer.

The pool of available Si, referred as Si_{CC}, was estimated through a kinetic 0.01M $CaCl_2$ extraction (Haymsom & Chapman 1975; Sauer *et al.* 2006; Georgiadis *et al.* 2013; Li *et al.* 2019b), in triplicates, with a solid:liquid ratio of 5g:50 mL. The solution was hand-shaken twice a day (Sommer *et al.* 2013) to avoid quartz abrasion (McKeague & Cline 1963a). At each time step (6h, 24h, 8 days and 32 days), the solution was centrifuged at 4750g for 5 minutes and the supernatant was filtered. The pH of the 32-day extracts was measured. Each extract was then acidified by addition of 50 µl of ultrapure 65% HNO_3, and stored in darkness at 4 °C prior to analysis. Silicon was measured by ICP-OES.

We normalized the Si_{CC} concentrations by the total Si content of each soil amendment, according to the following equation (Li *et al.* 2019b):

$$RE_{Si} = \frac{(Si_{cc}treatment - Si_{cc}control)}{Total\ Si\ treatment} * 100$$

where RE_{Si} is the Si_{CC} release efficiency, $Si_{cc}treatment$ and $Si_{cc}control$ are the contents of Si released from each treated soil and control soil, respectively, after 32 days of $CaCl_2$ extraction and $Total\ Si\ treatment$ is the total content of Si of each treated soil. All terms are expressed in mg.

10.4.5 Plant analyses

All leaves from each plant were harvested, rinsed with distilled water, dried at 50°C for 48h, and ground to powder. Leaf Si, Ca, Mg, P and K concentrations were determined by ICP-OES after calcination at 450 °C for 24 hours (ash content), followed by a fusion in a graphite crucible at 1000 °C with 0.4 g of Li-tetraborate and 1.6 g Li-metaborate (Chao & Sanzolone 1992; Kowalenko & Babuin 2014; Nakamura *et al.* 2020a), and the dissolution of fusion beads in 10% HNO_3. Leaf carbon and nitrogen concentrations were quantified with a CN analyzer.

Phytoliths were extracted through wet digestion (adapted from Kelly 1990; Fraysse *et al.* 2009; Corbineau *et al.* 2013). For each amendment, 0.1g of dried leaf material was taken from each five replicates and mixed to obtain a sample of 0.5g. The sample was transferred to a glass beaker with 10% HCl at 80°C to remove carbonates. After three rinsing cycles with distilled water, 65% HNO_3 was gradually added in order to remove the majority of organic tissue. After rinsing, 65% HNO_3/30% H_2O_2 mixture (2:1) was gradually added to the beaker, maintained at 80°C, until the reaction was no longer active and the residue no longer colorful. The residue in the beaker was carefully rinsed with deionized water and transferred into polypropylene tubes for centrifugation at 3700 rpm for five minutes. This washing was repeated three times. The residue was oven-dried at 50°C during 48h.

For each treatment, one leaf sample was randomly selected from one of the five plant replicates and mounted on a glass slide using double-sided carbon tape and bridged with silver paint, before being carbon-coated in a Balzers MED010 evaporator (de Tombeur *et al.* 2020a). Images were obtained through a backscattered-electron detector in a FEI ESEM-FEG XL-30 working at 30 kV accelerating voltage and fitted with a Bruker 129 eV X-ray detector for elemental microanalysis. The Si distribution on leaf surfaces was obtained on both the abaxial and adaxial sides of the leaves by elemental Si mapping acquired on the Si Kα,β peak at 1.74 keV. To compare the Si concentrations on the leaf surfaces between treatments, we randomly positioned 7 squares on each image (200*200 pixels) in which we counted the percentage area of yellow pixels (representing the Si signal on the elemental mappings) (de Tombeur *et al.* 2020a). The phytolith samples extracted from plant material were spread on glass slides covered with double-sided carbon tape, gold-coated and observed under the same conditions as the leaves.

Plant height was measured at the end of the experiment. Leaf arc was measured on the third-highest leaf as the distance between the midpoint of the line joining the apex to the point of blade insertion and the midpoint on the adaxial surface of the leaf (Zanão Júnior *et al.*, 2010; Figure H-1 for a shematic representation). Leaf Mass per

Area (LMA; 1/SLA) was calculated as the ratio of leaf dry mass to leaf area ($g\ m^{-2}$), on the third-highest leaf.

The adaxial surface of the highest leaf was used to perform punching tests (Onoda *et al.* 2011). Tests were performed using an SMS® TA-XT2 texture machine. Biomechanical properties were derived from force-displacement curves using the software SMS® Exponent (version 6.1.16.0). We used a flat-ended, sharp-edged cylindrical steel punch with a 3 mm diameter (7.07 mm^2 punch area), and a die mounted onto the moving head of the test machine. The die moved downwards at a constant speed. The punch was applied halfway along the longitudinal axis of the leaf and halfway between the midrib and the leaf margin. The force was divided by the circumference of the punch to give the force to punch ($kN\ m^{-1}$) (Onoda *et al.* 2011).

10.4.6 Statistical analyses

Means were compared through one-way analyses of variance (ANOVA), followed by *post hoc* multiple comparison (Tukey's Least Significant Difference [LSD] tests), after verifying that the conditions of the model were satisfied. Letters indicate results that were significantly different at the 95% level of confidence. Potential correlations were tested with Pearson's chi-square tests. Statistical analyses were performed using the software MiniTab®18.1.

10.5 Results

10.5.1 Biochar properties

The rice husks and cotton stalks contained 69 and 2 $g\ kg^{-1}$ Si respectively which, after pyrolysis, led to biochars with Si concentrations of 198 and 4 $g\ kg^{-1}$ (Table 10-2). The Si concentration of wollastonite was 240 $g\ kg^{-1}$. The concentrations of other nutrients were far more similar between both biochars, with the exception of Ca which was higher in cotton biochar (14 $g\ kg^{-1}$ for cotton biochar and 2 $g\ kg^{-1}$ for rice biochar) and Fe which was higher in rice biochar (13 $g\ kg^{-1}$ for rice biochar and 1 $g\ kg^{-1}$ for cotton biochar).

Table 10-2 : Characteristics of the biochars used as Si amendments.

	Crop residue[a]	Biochar[b]						
	Si	OC	Si	P	Mg	Ca	K	Fe
	g kg^{-1}	g kg^{-1}						
Rice husks/biochar	69	409	198	2	2	2	7	13
Cotton stalks/biochar	2	709	4	1	2	14	9	1

[a]Alkaline fusion with Li-tetra/metaborate at 1000°C, after calcination. Quantified by ICP-AES.
[b]Determined by European Biochar Certificate (EBC), Eurofins Umwelt. Both biochars fullfill EBC's premium quality requirement for heavy metal content.

10.5.2 Effect of amendments on soil properties

Compared to the control, only W30 significantly increased pH-KCl (Table 10-3). Biochar amendment significantly increased the OC and N contents in soils. All the amendments (except R5 and W30) increased bioavailable Mg concentrations, while only biochar-treated soils increased the concentration of bioavailable P (except R5). The only amendment that impacted bioavailable K concentration was C30. All the amendments increased bioavailable Ca concentration, except for R5.

Table 10-3 : Soil pH-KCl and concentrations of OC, total N and bioavailable P, K, Mg and Ca for the different amendments. The standard-errors are indicated under brackets (n=3). The letters represent Fisher HSD groupings ($p \leq 0.05$).

Amendment	**Input rate**	**pH-KCl**	**OC**	**Total N**	**Bioavailable nutrients (mg 100g^{-1})**			
	t ha^{-1}		g kg^{-1}	%	P	K	Mg	Ca
Control (T)	-	4.84 (0.03)bc	3.46 (0.10)e	0.30 (0.01)de	0.13 (0.03)c	3.91 (0.35)b	3.68 (0.23)d	19.76 (1.63)e
Rice biochar	5	4.86 (0.13)bc	5.82 (0.41)c	0.35 (0.04)cde	0.18 (0.00)bc	3.96 (0.15)b	5.37 (0.59)bcd	23.22 (1.41)de
Rice biochar	30	4.70 (0.06)c	11.03 (0.40)a	0.45 (0.05)abc	0.22 (0.02)ab	4.94 (0.19)b	6.32 (0.82)abc	25.68 (1.94)cd
Cotton biochar	5	4.71 (0.05)c	7.77 (0.57)b	0.50 (0.05)ab	0.27 (0.03)a	4.31 (0.57)b	7.55 (1.06)a	33.00 (2.49)b
Cotton biochar	30	5.07 (0.12)b	12.68 (1.08)a	0.53 (0.02)a	0.24 (0.02)ab	8.83 (1.01)a	7.05 (0.56)ab	33.00 (0.60)b
Wollastonite	5	5.04 (0.12)b	5.58 (0.84)cd	0.40 (0.06)bcd	0.19 (0.01)bc	3.65 (0.17)b	6.17 (0.92)abc	29.48 (2.43)bc
Wollastonite	30	6.54 (0.03)a	3.97 (0.01)de	0.28 (0.00)e	0.18 (0.00)bc	3.93 (0.08)b	4.55 (0.07)cd	42.84 (0.80)a

After 32 days of extraction, the Si_{CC} concentrations of the treated soils were significantly higher compared to the control (11.2 mg kg^{-1}) (Figure 10-1). Concentrations were the lowest in the cotton biochar amendments (12.0 and 14.5 mg kg^{-1} for C5 and C30), intermediate in the rice biochar amendments (16.4 and 26.9 mg kg^{-1} for R5 and R30), and the highest in the wollastonite amendments (143.7 and 189.2 mg kg^{-1} for W5 and W30). Although the pH-KCl measured in soils increased only for W30 (Table 10-3), pH measured in the 32-day $CaCl_2$ extractions increased significantly: T < R5 < C5 < C30 < R30 < W5 < W30 (Table H-1), and were positively correlated with Si_{CC} concentrations (Figure H-2).

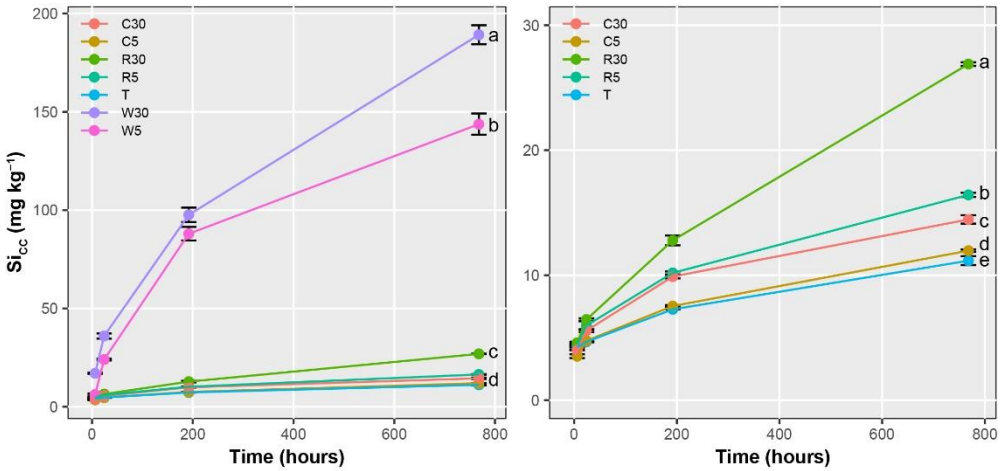

Figure 10-1 : Kinetic extraction of Si with $CaCl_2$ 0.01M for the different amendments. The second plot is a zoom of the first plot without the wollastonite treatments. The colors indicate the different treatments. The error bars represent the standard errors (n = 3) and the letters represent Fisher HSD groupings ($p \leq 0.05$) after 32 days of extraction.

10.5.3 Leaf Si and nutrients concentration

Leaf [Si] varied strongly among the Si-based amendments (Figure 10-2). The concentration in the control plants was the lowest at 19.0 ± 3.0 g kg^{-1}. Concentrations of plants grown with both cotton biochar amendments and W5 were similar to the control, and ranged between 20 and 30 g kg^{-1}. Leaf [Si] more than doubled in R5 and W30 with 48.7 ± 2.0 and 52.5 ± 3.2 g kg^{-1} respectively. R30 resulted in the highest leaf [Si] at about three times the control: 70.4 ± 2.3 g kg^{-1}. Considering only the biochar amendments and the control, leaf [Si] was positively correlated with Si extracted with $CaCl_2$ for 32 days (Figure 10-3). The leaf concentrations of macronutrients showed large variations within the same treatment (Figure H-3). Only W30 increased leaf [N] compared to the control, while R30, C30, W5 and W30 increased leaf [P] (Figure H-3). No amendments increased leaf [K], leaf [Ca] (but it

decreased for W5) or leaf [Mg] (but it decreased for R30, W5 and W30) (Figure H-3).

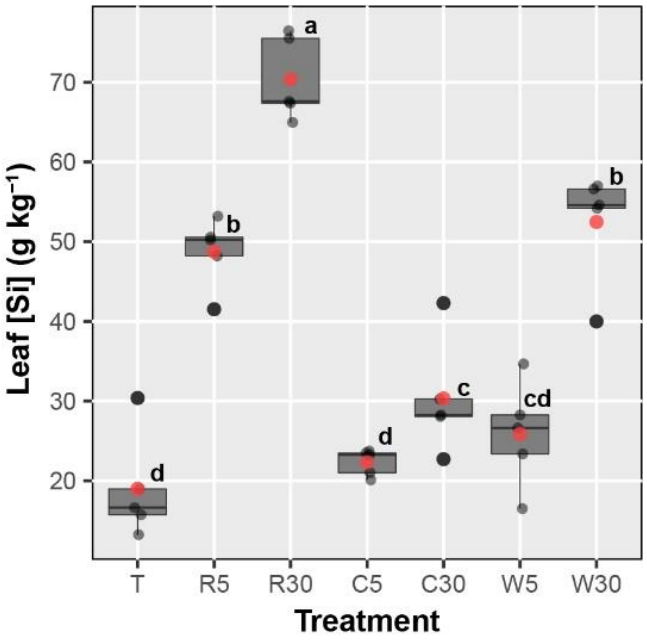

Figure 10-2 : Boxplot of rice leaf silicon concentration for the different amendments. The central horizontal bar in each box shows the median, the box represents the interquartile range (IQR), the whiskers show the location of the most extreme data points that are still within a factor of 1.5 of the upper or lower quartiles, and the large black points are values that fall outside the whiskers. The small opaque black points represent the data (n = 5), and red points indicate the overall mean. The letters represent Fisher HSD groupings ($p \leq 0.05$).

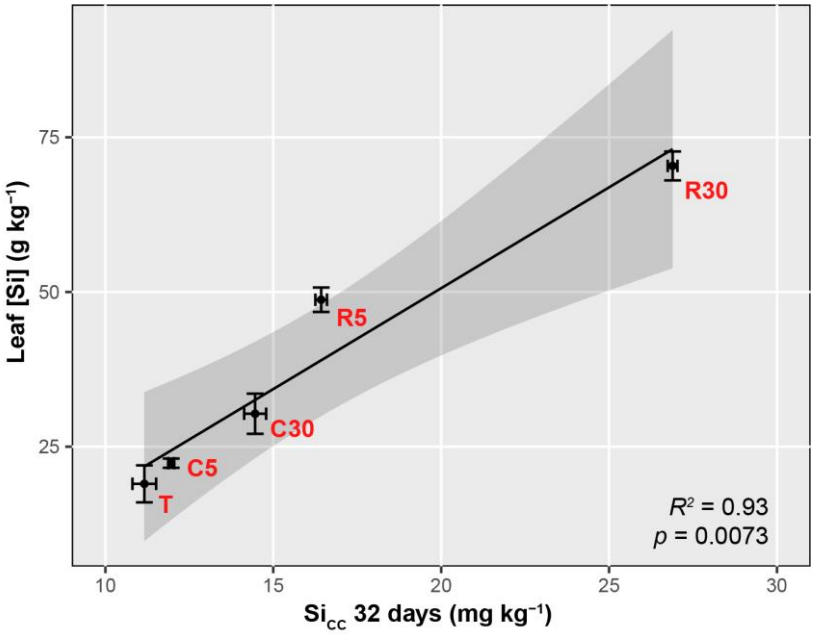

Figure 10-3 : Relationship between soil Si extracted with $CaCl_2$ 0.01M for 32 days and rice leaf Si concentration for the control and the biochar amendments. The error bars represent the standard errors (n= 3 for Si_{CC}; n=5 for leaf [Si]). The coefficient of determination (R^2) and p-value of the regression line are shown. The shaded area represents the 95% confidence intervals.

10.5.4 Leaf surface silicification and leaf phytoliths structure

The degree of silica deposition on the adaxial leaf epidermis was larger for both rice biochar and wollastonite amendments compared to the control and the cotton biochar amendments (Figure 10-4a, b). While rows of dumbbell-shaped cells were entirely silicified in all amendments (silica cells; Kumar and Elbaum 2018), silica was deposited more heavily in the areas between those rows, for both wollastonite and rice biochar amendments (Figure 10-4a). The same trend was observed for the abaxial surface (Figure 10-4b; Figures H-4 and H-5 for images).

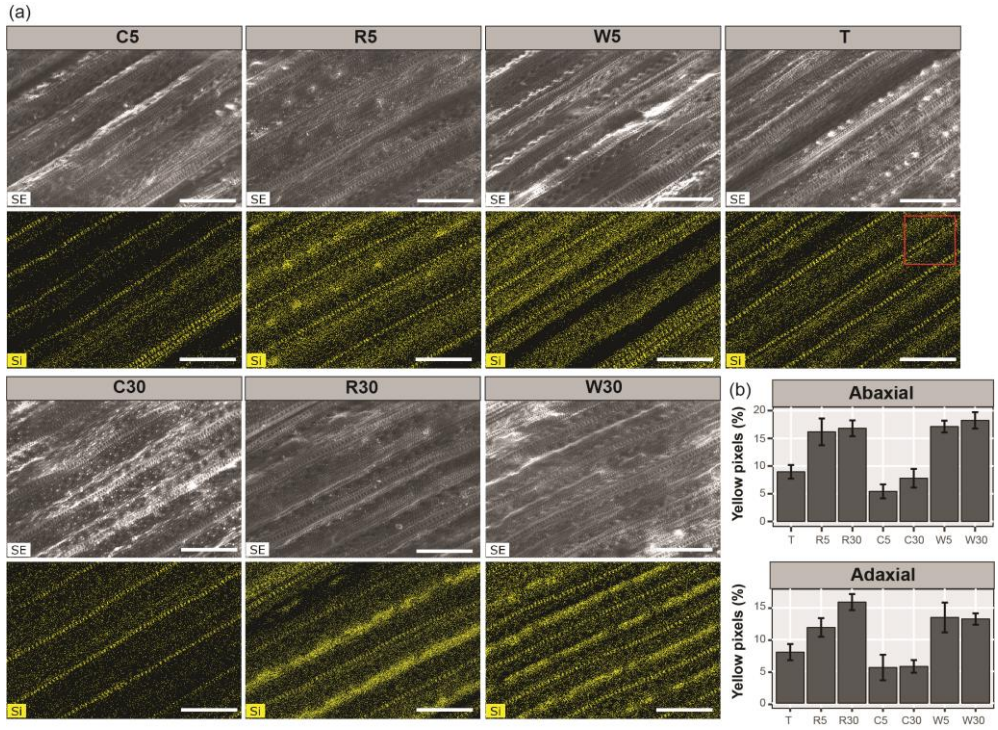

Figure 10-4 : SEM-derived images and Si mapping (EDX) of the leaf adaxial surfaces for the different amendments in (a). Area percentage of yellow pixels (%) on the leaf abaxial and adaxial surfaces for the different amendments in (b). In (a), the red square on T mapping exemplifies the area used to count the yellow corresponding to Si (see materials and methods). The scale bars have the same size and are equivalent to 200 µm for all the images. In (b), the error bars represent the standard-deviations (n=7 randomly selected squares by images).

The average size of phytoliths was significantly higher for all rice biochar and wollastonite amendments compared to the control (Figure 10-5). Phytoliths of at least 500 µm in length, and with many conjoined silicified cells, were commonly found in these 4 amendments, but they were absent from the control and cotton biochar amendments.

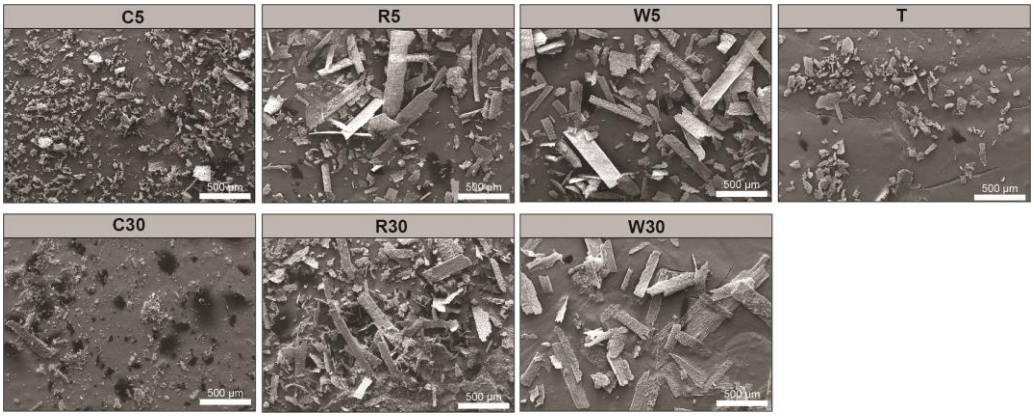

Figure 10-5 : Images of phytoliths physically extracted from rice leaves for the different amendments. The scale bars have the same size and are equivalent to 500 µm for all the amendments.

10.5.5 Impact of Si accumulation in rice leaf traits

Leaf [ash] was positively correlated with leaf [Si], which is negatively correlated to leaf [C] (Figure 10-6a, b). Plant height was greater than the control for R5, W5 and C30, lower for W30, not significantly different for R30 and C5, and was unrelated to leaf [Si] (Figure 10-6c). Plant biomass was significantly lower for R30 and W30 (Table 10-4) and was negatively correlated with leaf [Si] (Figure 10-6d). The LMA was lowest in the Si-rich leaves R5, R30 and W30 (Table 10-4) and was negatively correlated to leaf [Si] (Figure 10-6e). The leaf arc and the force to punch were negatively correlated with leaf [Si] (Figure 10-6f, g). Compared to leaf Si, the other nutrients were poorly correlated with the traits discussed above (Figure H-6). Plant biomass was negatively correlated to leaf [N] and positively correlated to leaf [Mg], the force to punch was negatively correlated to leaf [P], and leaf arc was positively correlated with leaf [Mg] (Figure H-6).

Table 10-4 : Leaf ash and C content, plant height and biomass, leaf mass per area (LMA), leaf arc and force to punch for the different amendments. The standard-errors are indicated in brackets (n=5). The letters represent Fisher HSD groupings ($p \leq 0.05$).

Amendment	Input rate	Leaf ash	Leaf C	Height	Biomass	LMA	Leaf arc	Force to punch
	t ha^{-1}	%	g kg^{-1}	cm	g	g m^{-2}	cm	kN m^{-1}
Control (T)	-	10.7(1.4)c	394(3)b	61.4(2.3)b	1.8(0.1)a	55.3(3.6)a	10.5(0.6)a	0.30(0.02)b
Rice biochar	5	18.8(1.1)ab	364(4)cd	76.4(1.8)a	1.5(0.1)ab	37.1(2.1)c	7.8(0.6)b	0.30(0.01)b
Rice biochar	30	19.1(1.3)ab	353(7)d	65.8(1.4)b	1.2(0.1)b	35.2(2.0)c	4.0(0.2)c	0.22(0.01)c
Cotton biochar	5	10.7(1.0)c	408(4)a	65.9(2.4)b	1.8(0.1)a	43.7(4.3)bc	9.6(0.3)a	0.39(0.03)a
Cotton biochar	30	11.9(1.3)c	407(3)ab	77.1(2.4)a	1.6(0.1)a	41.6(4.2)bc	9.8(0.3)a	0.30(0.02)b
Wollastonite	5	16.2(1.6)b	369(6)c	72.2(2.3)a	1.6(0.1)a	49.2(2.8)ab	7.3(0.6)b	0.30(0.02)b
Wollastonite	30	20.2(1.2)a	376(4)c	48.3(2.0)c	0.7(0.0)c	34.6(2.0)c	5.4(0.6)c	0.22(0.01)c

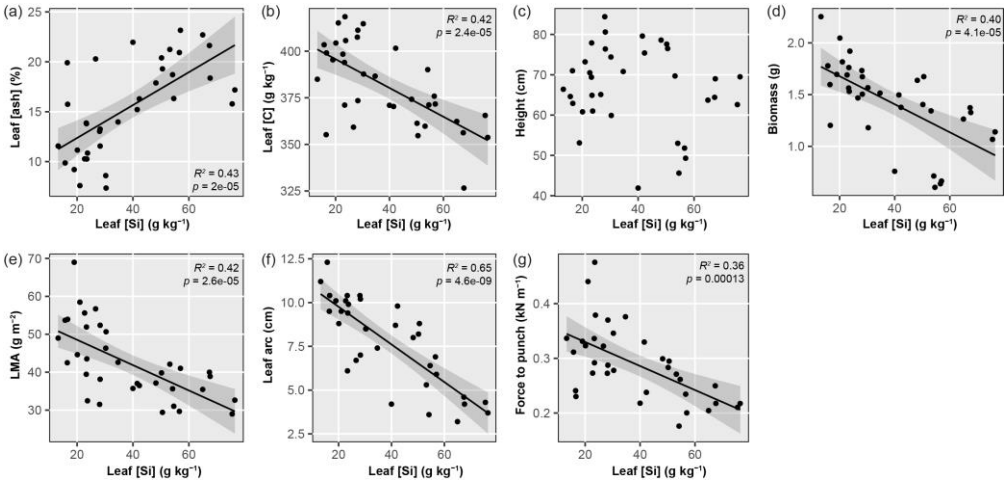

Figure 10-6 : Plots of rice leaf Si concentrations versus: ash concentration in (a), carbon concentration in (b), plant height in (c), plant biomass in (d), leaf mass per area in (e), leaf arc in (f) and force to punch in (g) (n = 35). The coefficient of determination (R^2) and p-value of the regressions are shown. Shaded areas represent 95% confidence intervals.

10.6 Discussion

10.6.1 Rice biochar as a potential Si amendment in highly desilicated soils of Burkina Faso

Amendments significantly increased the available Si concentration in the studied desilicated soil, corroborating previous studies using biochar (Houben *et al.* 2014; Li *et al.* 2018, 2019b; Wang *et al.* 2018) and wollastonite (Tavakkoli *et al.* 2011; Haynes *et al.* 2013; Babu *et al.* 2016). The more pronounced Si_{CC} increase under the rice biochar amendments compared to the cotton biochar amendments is explained by higher Si concentrations in the pyrolyzed feedstock (Table 10-2). After normalizing

Si_{CC} concentrations by the total Si content of the amendment (RE_{Si}; Table 10-5), the ability to release Si is higher for cotton biochar than for rice biochar. This may occur because the silica is present as minute deposits, scattered throughout the organic matrix of cotton-biochar (Figure H-7), which results in higher surface area per unit Si and therefore higher solubility than the larger phytoliths present in rice. The higher Si_{CC} concentrations, by an order of magnitude, in wollastonite compared to the biochar amendments has previously been observed by Li *et al.* (2018). This cannot be entirely explained by a higher total Si content, as wollastonite RE_{Si} was significantly higher than rice biochar RE_{Si} (for both input rates) and to cotton biochar RE_{Si} for the highest input rate of 30 t ha^{-1} (Table 10-5). Besides different inherent dissolution rates between phytoliths and wollastonite, the organic matrices of biochars could contribute to slowing down the dissolution of phytoliths (Fraysse *et al.* 2006a, 2010; Nakamura *et al.* 2020b), which could explain the higher Si_{CC} concentrations in soil amended with wollastonite. Finally, the positive relationship between Si_{CC} and pH_{CC} (Figure H-2) has been observed elsewhere (Miles *et al.* 2014; Meunier *et al.* 2018; Li *et al.* 2019b; de Tombeur *et al.* 2020b), and suggests that the liming effect of biochar amendments may contribute to increased phytolith dissolution (Fraysse *et al.* 2009; Li *et al.* 2019b).

Table 10-5 : Silicon release efficiency (RE_{Si}) for the different amendments. The standard-errors are indicated in brackets (n=3). The letters represent Fisher HSD groupings ($p \leq 0.05$).

Amendment	**Input rate** t ha^{-1}	**RE_{Si}** %
Rice biochar	5	1.5(0.1)d
Rice biochar	30	0.8(0.0)d
Cotton biochar	5	10.4(1.1)b
Cotton biochar	30	7.2(0.7)c
Wollastonite	5	30.5(1.2)a
Wollastonite	30	6.8(0.2)c

The 32-day $CaCl_2$ extractions accurately estimated the plant-available Si for biochar-treated soils, supporting recent studies (e.g. Li et al. 2019, Wu et al. 2019) (Figure 10-3). Although wollastonite released Si at a much faster rate than biochars, leaf [Si] of R5 and R30 were 1.9- and 1.3-fold higher than the W5 and W30 respectively. In addition, leaf [Si] with the rice biochars amendments were the highest: 2.5 and 3.7 fold higher than the control for the application rates of 5 and 30 t ha^{-1} respectively. These results confirm that phytolith-rich biochar is an efficient slow-release Si amendment for desilicated soils (Li & Delvaux 2019; Wang *et al.* 2019b), with cascading positive effects for plant growth (Zama *et al.* 2018; Leksungnoen *et al.* 2019; Li *et al.* 2019a; Huang *et al.* 2020; Wang *et al.* 2020). Rice-husk biomass is an agriculture residue that is readily available for biochar production in Burkina Faso (FAO 2014), and this work provides strong evidence that the production of biochar from this residue is a very promising way to recycle Si-rich agricultural wastes from rice fields to increase Si plant-availability in soils of Burkina Faso. To ensure

maximum sustainability for the use of biochar, the input feedstock and pyrolyzing unit must be as close to the field as possible, owned by the local farmers.

10.6.2 Rice biochar increases the degree of leaf silicification, but does it impact physical traits?

The application of rice biochar markedly increased the degree of rice leaf silicification (up to 70 g kg^{-1} of Si for R30, or about 15% of silica by dry weight), which are extremely high levels (Hodson *et al.* 2005). The impact of this high degree of silicification on leaf and plant traits is discussed below.

Leaf [Si] and leaf arc were negatively correlated, which confirms that Si accumulation in grasses contributes to leaf straightness. The four amendments (wollastonite, rice biochars) for which leaf arc significantly decreased compared to the control were also those for which silica was more abundantly deposited on both the adaxial and abaxial sides of leaf epidermis, and the size of phytoliths was larger (more conjoined silicified cells) (de Tombeur *et al.* 2020a; Guerriero *et al.* 2020). In addition, negative correlations between the percentage area of silica deposits on leaf surface (Figure 10-4) and leaf arc were found for both abaxial (R^2=0.69; n=7; $p<0.05$) and adaxial sides (R^2=0.82; n=7; $p<0.01$). These results highlight the key role of the degree of leaf silicification, especially the number of conjoined silicified cells, in the control of leaf erectness. By contrast, rows of silica cells (specialized epidermal cells with the entire lumen filled with silica, forming dumbbell-shaped phytoliths; Kumar and Elbaum 2018) do not seem to play a role in leaf erectness, because they were entirely silicified for all amendments, irrespective of leaf [Si] and leaf arc values. As leaf arc values were not correlated with macronutrients (Figure H-6), we conclude that rice biochar is an effective soil amendment to improve leaf erectness through silicification. This can have a positive influence on plant fitness as changes in leaf erectness can impact light interception (Ando *et al.* 2002).

Under rice biochar amendments, the LMA decreased by a factor of 1.6 compared to the control, and we observed a strong negative correlation between leaf [Si] and LMA, which, to our knowledge, has not been demonstrated before. Lower LMA is explained either by thinner leaves of the same density, or by less dense leaves of the same thickness. Given silica is denser than C-based compounds and that leaf [Si] and [C] were negatively correlated, thinner leaves seem more likely. The negative correlation may indicate a tradeoff between a high degree of leaf silicification and thicker leaves that perform similar plant functions. Both leaf silica deposits and higher leaf thickness impact leaf water status (Búrquez 1987; McBurney 1992; Gong *et al.* 2003; Meunier *et al.* 2017), mechanical properties (Schoelynck *et al.* 2010; Onoda *et al.* 2011; Klotzbücher *et al.* 2018c), and potential to deter herbivores feeding (Peeters 2002; Massey *et al.* 2006). Investing in silica deposits when plant-available Si is enhanced by Si-based amendments rather than the construction of thick leaves could perform functions such as 1) minimizing leaf water loss and/or 2) improving leaf erectness and/or 3) reducing herbivory, and at a lower energetic cost (Raven 1983).

Silica deposits in the leaf epidermis can also increase leaf abrasiveness (Hartley *et al.* 2015; Hall *et al.* 2020), which can in turn reduce herbivore feeding (Massey & Hartley 2006; Massey *et al.* 2007a; Hall *et al.* 2020), and reduce the digestive efficiency of herbivores (Massey *et al.* 2006). Since the magnitude of silica deposits on leaf surface increased with leaf [Si] (Figure 10-4), it seems likely that the application of rice biochar can contribute to reducing biotic stress in rice growing on the desilicated soils of Burkina Faso. Surprisingly, the force required to punch leaves was negatively correlated with leaf [Si], which seems somewhat contradictory given the evidence of defense against herbivores for Si-rich leaves. Although some research showed that Si increases the force required to tear (Yamamoto *et al.* 2012; Kido *et al.* 2015; Simpson *et al.* 2017) and shear (Johnson *et al.* 2019b) leaves, our results suggest that it is not the case for punching, as other leaf parameters may change along with epidermal silicification. In particular, the Si-rich leaves of the present study could possibly be penetrated more easily because of their lower LMA (Onoda *et al.* 2011). However, the ability of penetrometers to estimate leaf mechanical properties and to mimic herbivores penetration remains controversial (Sanson *et al.* 2001). In addition, with the main pests of rice in Burkina Faso attacking stems (Ba *et al.* 2008), further work on the impacts of biochar/Si on stem properties would be valuable.

Finally, although the decrease in LMA and leaf [C] with increasing leaf [Si] suggests that effective Si amendments diminish the leaf C costs of rice crops, plant height was not correlated with leaf [Si] and not strongly impacted by the different treatments (with the exception of W30 for which it significantly decreased due to limited growth), and plant biomass decreased with increasing leaf [Si]. This contrasts with previous studies showing the positive effects of Si on the overall plant growth (e.g. Zanão Júnior *et al.* 2010), but is in line with others showing no clear effects of Si addition (e.g. Ando *et al.* 2002). It is possible that plant height did not increase significantly because of a limited root growth in the pots used for the experiment, or because Si has beneficial effects on plant growth mainly for stressed plants (Fauteux *et al.* 2006). Since plant height was not markedly affected by Si addition, the decrease in plant biomass with increasing leaf [Si] could be explained by the net decrease in LMA for Si-rich leaves, though the total leaf area was not measured. More generally, the lack of positive effect of both biochars on plant growth is surprising given its global positive effect (Biederman & Stanley Harpole 2013), but has nevertheless already been reported in the literature (Haefele *et al.* 2011; Güereña *et al.* 2013; Tammeorg *et al.* 2014; Reibe *et al.* 2015). This indicates a need for in-situ studies into the effect of rice biochar on rice yields, keeping in mind that the application of biochar in agroecosystems plays other roles such as C storage and improved nutrient retention though an increase in the cation exchange capacity (Gul *et al.* 2015), which could have a long-term positive impact on soils of Burkina Faso.

We conclude that the use of rice biochar as a Si amendment on desilicated soils of Burkina Faso is an efficient method to increase the degree of silicification of rice leaves, which in turn impacts leaf traits likely to contribute positively to plant fitness. This is of special interest as our study demonstrates an efficient way to transfer Si-

related fertility from rice field in lowlands to highly desilicated soils of cotton, maize and rice fields in upland positions. Given these promising results, further *in situ* work is now needed to examine if the positive effects of silicification from Si-rich biochar – as well as the overall positive effects of biochar on soil properties (Gul *et al.* 2015) – can protect plants against pest attacks while increasing plant productivity and crop yields in agroecosystems of Burkina Faso. The long-term impact (10-20 years) of biochar application on rice Si uptake should also be tested as a more realistic for the local agricultural context, with amendment rates between 200 and 400 kg of biochar per hectare per year.

11

Conclusions and perspectives

The main theme of this thesis was to explore the long-term dynamics of Si in terrestrial ecosystems, and investigates some factors driving soil-plant Si dynamics in agroecosystems. In particular, we first wondered how the soil reactive Si pools and plant-available Si evolved during 2-million-years of soil development, and what were the contributions of geochemical and biological processes on soil Si dynamics. We then investigated whether soil fertility could influence the expression of silica-based defenses in species-rich shrubland vegetation, and if P-acquisition strategies developed by plants adapted to P-depleted environments could also mobilize Si from the rhizosphere. These questions were based on the study of three long-term soil chronosequences located on a climatic gradient in southwestern Australia, which allowed us to isolate the effect of time on soil-plant Si dynamics. Following this, we tried to understand how knowledge on soil-plant Si dynamics learned from complex natural systems could help us to improve Si-use efficiency and crop Si status in agroecosystems. The reflection was based on the results obtained from the first chapters, as well as through a literature review. Finally, we investigated how soil properties and the recycling of Si-rich crop residues could enhance the foliar silicification and its subsequent beneficial effects in two common crop species (sugarcane and maize).

11.1 Long-term changes in soil Si dynamics

The results obtained from the **chapters 3, 4 and 5** highlighted a strong influence of long-term soil and ecosystem development on the soil-plant Si dynamics and its drivers (Figure 11-1). First, our results demonstrated that soil Si dynamics could be buffered by carbonate minerals at the very first stages of pedogenesis (Figure 11-1). Indeed, the reactive pedogenic Si and plant-available Si pools were relatively low in the youngest soils of the Jurien Bay and Guilderton chronosequences. This is probably because carbonate minerals are the primary proton consumers during soil formation (Chadwick & Chorover 2001), which could reduce the weathering of silicate minerals, and because Si adsorption by secondary clay minerals and Fe oxides is high in alkaline soils, which in turn lowers dissolved Si concentrations in soil solution (Haynes & Zhou 2018). A literature analysis confirmed the shift in processes controlling Si availability between the carbonate and silicate weathering domains. However, the study of the Warren chronosequence, which contained much less carbonate minerals in its soil parent material, showed that such buffer to Si mobilization occurs only for carbonate-rich soil parent material. Indeed, the pools of reactive pedogenic Si and plant-available Si in the youngest soil at Warren were greater than those at Jurien Bay and Guilderton, probably due to the weathering of feldspars at the onset of pedogenesis. The carbonate content of the soil parent material seems therefore to be a key property for Si mobilization at the onset of pedogenesis.

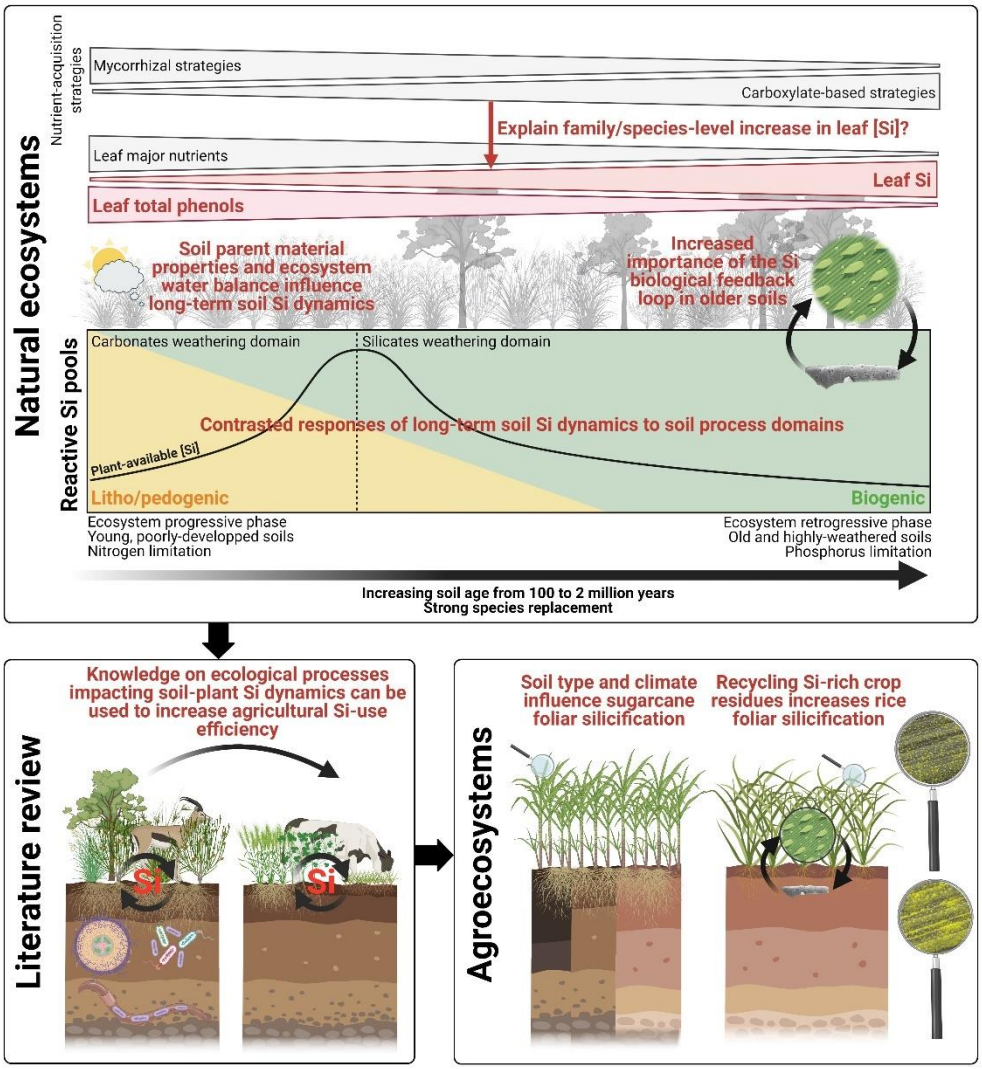

Figure 11-1 : General overview of the main highlights and findings of this PhD thesis.

Second, once carbonate minerals were exhausted, our results showed that clay and Fe oxides controlled soil Si dynamics and plant-available Si concentrations. Plant-available Si stocks were greatest in the intermediate stages of the Jurien Bay and Guilderton chronosequences after carbonate loss, during the formation of kaolinite, and when reactive pedogenic Si stocks, alkali-reactive Si stocks with a clay mineral origin, and the silt + clay content were maximal (Figure 11-1). However, this peak of plant-available Si was not observed at Warren, probably because the formation of secondary clay minerals is almost absent throughout this chronosequence, due to the

lower content of weatherable minerals in the soil parent material. Instead, reactive pedogenic Si and plant-available Si stocks continuously decrease over time, due to continuous desilication. These results therefore suggest that the initial carbonates content in the soil parent material do not only drive soil Si dynamics at the onset of pedogenesis, but also on the long-term through its subsequent impact on soil mineralogical evolution.

Third, our results indicate that the Si cycle shifts from geochemical to biological control as the soil and ecosystem develop. An extreme degree of desilication was observed with increasing soil age up to 2 million years: proxies of soil weathering degree reached their maximal values, clay minerals and Fe oxides were lost through dissolution and cheluviation, and soils were largely dominated by quartz minerals. In fact, these soils are among the most weathered, desilicated, and with some of the lowest available Si concentrations worldwide. Interestingly, while the pool of reactive pedogenic Si entirely disappeared in these old soils, which was accompanied by a strong decline in plant-available Si concentrations, the pool of alkali-reactive Si remained large and was dominated by soil phytoliths that controlled plant-available Si concentrations in these old and desilicated soils (Figure 11-1). Along with this shift in reactive Si pools, chemical analyses performed on the leaves of the most abundant plants growing along the Jurien Bay chronosequence suggested that Si biocycling did not decrease on these old, desilicated soils. In fact, unlike concentrations of major nutrients, which declined markedly in strongly weathered soils, foliar silicon concentrations increased continuously as soils age, and LAI is rather constant along the Jurien Bay chronosequence (Turner *et al.* 2018). These results suggest that Si biocycling further increases in highly desilicated environments, where plant-available Si is mainly controlled by biological processes (i.e., soil phytoliths dissolution). Overall, this suggests that the Si terrestrial cycle is increasingly controlled by an intense Si biological feedback loop on old and desilicated soils. This pattern should now be reinforced/confirmed by complete mass-balance calculations at the ecosystem level to determine precisely the contribution of litho/pedogenic versus biogenic Si-bearing minerals on dissolved Si, as I discuss below (section 11.4.1).

It is important to note that the pattern of increasing community-level leaf Si concentrations along the Jurien Bay chronosequence was accompanied with species replacement along the chronosequence, with dicot woody species in the Proteaceae and Dilleniaceae contributing most strongly to the increase in foliar Si concentrations on the oldest soils (Figure 11-2). Therefore, the primary explanation for this pattern is most likely phylogenetic, because it exerts a major control on plant Si accumulation (Hodson *et al.* 2005). Although evapotranspiration could play a role on Si accumulation, the climate is very similar along the chronosequence which allowed us to rule out this hypothesis, especially compared to the major role of phylogenetic variation. Phylogenetic corrections can be performed when analyzing interspecific data to account for the non-independence of observations due to their common history (e.g., Revell 2010, 2012). This kind of correction could have been performed in this

work, but getting a phylogeny tree was challenging, because a significant fraction of the species considered does not have sequence data in GenBank.

Although we could not take phylogeny into account in our analyses, and it most likely influenced community-level leaf [Si] (Figure 11-2), it is worth pointing out that the same pattern of increasing leaf Si and decreasing major nutrient concentrations across the chronosequence also occurred within some families (in particular Cyperaceae, see **chapter 6**), and within the few individual species that were sampled across multiple stages of the chronosequence (see **chapters 4 and 6**). Moreover, the species turnover across the Jurien Bay chronosequence reflects the expression of selective edaphic forces acting on a species-rich regional flora over an ecological time scale (Laliberté *et al.* 2014). As a result, species adapted to older, nutrient-impoverished soils have low foliar concentrations of rock-derived nutrients (Hayes *et al.* 2014) but accumulate more Si in their leaves, which could possibly be seen as an ecological signal reflecting plant Si-based functions as we discuss below, but this would deserve further investigations. Finally, it seems important to note that we do not explain the likely increased Si biocycling in older stages (most likely explained by a shift towards species accumulating more Si with increasing soil age) by the shift in Si sources over pedogenesis (from pedogenic to biogenic control). However, it still demonstrates that Si biocycling can remain intense and possibly even increase in highly-desilicated, low plant-available Si soils where phytoliths are the main contributors to Si mobility in the ecosystem, thereby suggesting an increased control of the Si biological feedback loop as soils age (**chapter 4**), as initially hypothesized.

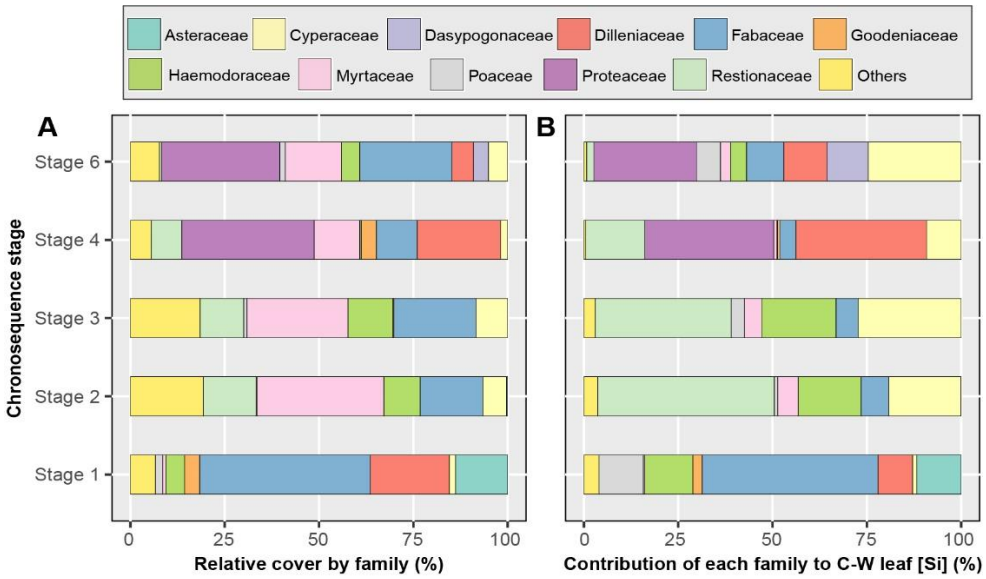

Figure 11-2 : The relative cover by family across the Jurien Bay chronosequence (%) in (A), and the contribution by family to the community-level, cover-weighted (C-W) foliar [Si] in (B). Soil age increases with increasing chronosequence stage.

Finally, the study of the wetter Warren chronosequence suggested that a climate-induced increase in biomass production could stimulate the Si biological feedback loop (Cornelis & Delvaux 2016), even in old and highly desilicated environments. Indeed, for a same chronosequence stage, the stocks of soil phytoliths were roughly similar across the three chronosequences. Yet, a wetter climate generally implies lower belowground stocks of biogenic Si, due to faster phytolith dissolution and translocation (Blecker *et al.* 2006). The fact that this was not the case when we compared the two dry chronosequences to the Warren chronosequence may indicate that the greater plant productivity and consequently faster rate of phytolith formation in the Warren vegetation balance the faster rates of phytolith dissolution or losses through translocation. This result suggests that greater plant productivity maintains Si in a biogenic pool that is actively cycled, as for P (Turner *et al.* 2018), but this challenging hypothesis would require the complete assessment of Si stocks and fluxes for the 20 visited sites as previously highlighted.

Overall, the **chapters 3, 4 and 5** highlights the responses of soil Si dynamics to long-term soil weathering. We stressed the major influence of soil mineralogy on soil Si dynamics, with a possible increased control of biological processes with increasing soil age and/or ecosystem water balance. Further insights could now be provided by a detailed determination of Si stocks and fluxes in the soil-plant systems of the 20 visited sites, as discussed below (section 11.4.1).

11.2 Silica-based defenses and soil fertility

In the **chapter 6**, we tried to leverage ecological approaches to better understand why foliar Si concentrations of the dominant plants growing along the Jurien Bay chronosequence continually increase with increase soil age, as mentioned above. We showed that such patten was associated with a strong decline in soil fertility, in particular soil P content (Figure 11-1). This might reflect higher expression of silica-based defenses in nutrient-poor soils, in accordance with the RAH postulating that plants adapted to nutrient-poor environments deploy high levels of anti-herbivore defenses (Coley *et al.* 1985). In this same chapter, we also showed that the increase in foliar Si concentrations along the Jurien Bay chronosequence was associated with a decline in leaf total phenol concentrations (Figure 11-1), also found at the community, family, and species-level (**chapter 6**). In particular, our results suggest that N limitation on young soils led to a greater expression of phenol-based defenses (because it impacts the phenylpropanoid pathway more strongly than P limitation; Haukioja *et al.* 1998; Jones & Hartley 1999; Wright *et al.* 2010), whereas old, P-impoverished soils favored silica-based defenses. This suggests that the strength and type of nutrient limitation might drive tradeoffs among leaf defense strategies, thereby opening up promising perspectives for the RAH. Moreover, given the presumably lower metabolic costs of incorporating Si compared with other C-based compounds having similar functions (Raven 1983), our results might reflect that investing in silica as a defense mechanism on the oldest and most nutrient-depleted soils could make sense from an energetic standpoint.

Nevertheless, it is important to highlight alternative interpretations and conclusions. First, as explained above, the community-level pattern was mostly associated with changes in the dominant families across the chronosequence (although also found within some families/species), and phylogeny exerts a strong control on plant Si accumulation (Hodson *et al.* 2005). The increasing community-level leaf [Si] might only result from the presence of taxa that express this trait more strongly due to their evolutionary history, without being a true ecological signal reflecting a need to reduce herbivory in the older, nutrient-depleted soils. Second, although we can safely assume that about two thirds of the species growing on the last chronosequence stage could potentially use silica as an efficient defense against herbivores (see section 6.6.1 for a discussion on the link between the degree of Si accumulation and silica-based defenses), no studies have been conducted for a significant fraction of the species growing along the chronosequence (**chapter 6**). Third, Si serves many other functions than defenses against herbivores, which may eventually explain the patterns we observed along the Jurien Bay chronosequence. More broadly, we tend to associate the expression of certain traits with the functions they play today, but silica accumulation could possibly be seen as an "exaptation" rather than adaptation (Gould & Lewontin 1979). Indeed, we still have no convincing evidence for an adaptive origin of this trait (Strömberg *et al.* 2016), which could have been selected for other functions than it plays today, or even randomly selected. If so, a selective advantage for high-Si plants in older soils to avoid herbivory could actually not make sense. Finally, if increasing leaf [Si] across the chronosequence is at least partly explained by an increased abundance of species exhibiting P-mobilizing strategies as soils age (**chapter 7**, next paragraph), this could be seen as an advantageous co-effect for plants growing in older P-depleted soils, but without reflecting a real need to increase silica-based defenses in the older, unfertile soils.

The increase in leaf Si concentrations along the Jurien Bay chronosequence led us to explore if specialized nutrient-acquisition strategies particularly prevalent in these low-P environments, namely **carboxylate**-releasing strategies, might mobilize soil Si for plant uptake. In the form of an opinion article, we suggest in the **chapter 7** that the influence of root-released carboxylates on soil Si mobilization in P-depleted soils is likely, and especially from phytoliths (Figure 11-1). This reflection was based on positive correlations between leaf Si and Mn concentrations found along the chronosequence, because leaf Mn concentrations can be used as a proxy for root-released carboxylates (Lambers *et al.* 2015; Pang *et al.* 2018), and experiments demonstrating that carboxylates increase Si release from different soils and reference materials. Additionally, literature shows that P fertilization tends to decrease leaf Si in a range of species which could be caused by a decrease in soil Si mobilization through the suppression of exudation of chelating substances, thus supporting our conclusion. The mobilization of Si from phytoliths by root-released carboxylates could explain why leaf [Si] increase in old, P-poor soils (**chapter 6**), and could reinforce the increasing role of plants and biological processes on soil-plant Si dynamics during ecosystem retrogression (**chapter 4**). Overall, our results might suggest that southwestern Australian species occupying edaphic niches characterized

by extremely low soil P reserves and having specific carboxylate-based, P-acquisition strategies and high levels of endemism (Lambers 2014; Gao *et al.* 2020; Westoby & Falster 2021) will tend to also have higher leaf Si concentrations, possibly to increase their defense against herbivory in these harsh environments.

Another key output from this chapter is to open reflections about the C costs of Si uptake/silica-based defenses. They are considered as being much lower than those of C-based compounds since Raven (1983) calculated that, on a weight basis, the energetic cost of incorporating 1 g of lignin is about 27 times higher than of incorporating 1 g of SiO_2. However, the **chapter 7** suggests that they might be more expensive than commonly realized if carboxylates or other root exudates are needed to mobilize Si from the rhizosphere, which was not considered in the initial suggestions of Raven (1983). Yet, it is well admitted that C costs to mobilize soil nutrients from poorly-available forms might be important, especially for P (Raven *et al.* 2018). In P-depleted environments, it is worth pointing out that Si mobilization could be free in terms of carbon if those costs are met for P acquisition. Overall, the **chapters 6 and 7** highlighted that ecological approaches can help to better constrain terrestrial biogeochemical cycles, and emphasized a potential role of silica-based defenses in low P environments, possibly resulting from shifts in dominant nutrient-acquisition strategies in the ecosystem. However, these two chapters also opened numerous questions and hypotheses that still need to be verified, in particular through the setup of experiments performed under controlled conditions, as I detail below.

11.3 Soil-plant Si dynamics and agriculture practices

In the **chapter 8**, we demonstrated that knowledge on ecological processes influencing soil-plant Si dynamics gained from natural systems might be exploited in agroecosystems to improve crops Si status (Figure 11-1). We also highlighted that soil-plant Si dynamics cannot be seen only through the prism of abiotic mineral weathering, and that numerous biological processes also influence soil-plant Si dynamics. In particular, we showed that mycorrhizal associations, silicate-solubilizing bacteria, soil macrofauna and large herbivores significantly stimulate Si mobility in soil-plant systems, while the effect of root exudates is likely but needs further research, as discussed in the **chapter 7**. These processes could be exploited in different cropping systems such as covers crops, cereal/legume intercropping, or integrated crop-livestock systems. To our knowledge, this chapter represents the first attempt to bridge the gap between the biotic factors influencing soil-plant Si dynamics and Si-use efficiency in agroecosystems.

Finally, we demonstrated that the degree of foliar silicification of cereal crops was highly dependent on the soil weathering degree and climate (**chapter 9**), and could be enhanced by applying pyrolyzed Si-rich crop residues to soil (**chapter 10**) (Figure 11-1). This change in scale study along the thesis was key to understand whether some of the factors highlighted earlier could induce beneficial effects for crops. This is of

special interest since silicification in plants increases their resistance to water stress, pathogens and herbivore attack, reduces the soil-to-plant translocation of toxicants, and possibly interferes with the recognition process occurring upon pathogen infection (Coskun *et al.* 2019; Leroy *et al.* 2019). Moreover, such beneficial effects of Si in graminoid crops (*e.g.*, wheat, rice, maize, sugarcane) can enhance agricultural productivity, and food security (Tubana *et al.* 2016). It is therefore timely to precisely identify the factors driving foliar silicification, and how sustainable agriculture practices could enhance this process.

Finally, these two chapters also suggested close links between foliar silicification and other chemical or physical traits associated with leaf support and/or defense. In particular, we showed that Si accumulation and increased silicification was associated with a decline in cellulose in sugarcane leaves, and in leaf mass per area in rice leaves. In rice leaves, a strong negative correlation between leaf Si concentrations and leaf arc demonstrated the impact of silicification on leaf erectness. These results highlight the mechanical properties of leaf silicification, which might eventually lead to tradeoffs with other traits having similar functions. Potential tradeoffs between a high degree of silicification and other leaf traits having comparable functions should now receive specific attention (see section 11.4.3), in particular through the implementation of experiments under controlled conditions. Overall, the **chapter 8, 9 and 10** stressed the major importance of understanding natural processes to improve agroecosystems sustainability through enhancing Si-use efficiency.

11.4 Future directions

11.4.1 Combining soil extractions to mass-balance calculations

The **chapters 3, 4 and 5** demonstrated the major impact of soil parent material, soil age and water balance on long-term Si dynamics. The main approach of these studies was the use of different extractants to estimate specific soil Si pools ($CaCl_2$, acetic acid, Na_2CO_3 and oxalate). It has the advantage to collect soil samples and perform analyses later, without setting up instrumented experimental sites (*e.g.*, Cornelis *et al.* 2010; Turpault *et al.* 2018). In fact, this was probably the only possible approach for this thesis given the high number of studied sites (20 for soil profiles and 25 for plant sampling plots) combined with challenging access (see section 1.3 in chapter 1) . However, such approaches also have disadvantages. First, even though progress was made to properly estimate soil Si pools with extractions (*e.g.*, Sauer *et al.* 2006; Georgiadis *et al.* 2013), soils are extremely complex and heterogenous systems, and associate a specific soil Si pool to an extractant remains challenging. Specifically, the use of $CaCl_2$ 0.01M to estimate the pool of 'plant-available Si' is widely used and accepted in the literature, but this should be combined with the setting up of lysimeters to collect soil solutions, when possible. Having these two proxies of 'mobile Si' would allow to go further in the working hypothesis. Moreover, Si quantification in soil solution collected with lysimeters is most likely closer to what can be leached out

from the soil profile and transferred towards hydrosphere, which could give stronger information about Si fluxes.

Second, the implementation of instrumented experimental sites would have allowed us to assess complete mass-balance calculations at the ecosystem level, as previously done elsewhere (*e.g.*, Bartoli 1983; Alexandre *et al.* 1997, 2011; Gérard *et al.* 2008; Sommer *et al.* 2013; Turpault *et al.* 2018). One of the main advantages of this approach is to determine more accurately the contribution of biological processes (phytoliths formation in plants and dissolution in soils) and geochemical processes (dissolution of soil-derived minerals) to dissolved/plant-available Si (*e.g.*, Alexandre *et al.* 1997, 2011). In particular, we showed in the **chapter 4** that phytoliths controlled plant-available Si concentrations mostly when all soil-derived minerals other than quartz were exhausted. Before, the pedogenic reactive Si pool (extracted with oxalate) was the main contributor to the plant-available Si pool. However, mass-balance calculations could have shown that, on biological time scales, phytoliths also largely contribute to the dissolved Si pool and annual soil-plant Si cycling in younger and less weathered soils, but without being the drivers of the plant-available Si concentrations, as it is the case in older soils. Overall, further insight into long-term Si cycling could be provided by complete mass-balance calculations at the ecosystem level for each site (which was complicated to assess within these ecosystems, see section 1.3 in chapter 1 on this point), to estimate phytolith formation and turnover rates, and reveal the extent to which climate and biological processes determine terrestrial Si cycling and fluxes towards vegetation and water courses. In the same vein, the use of resistant titanium (Ti) and zircon (Zr) minerals to weathering could be used to better constrain the extent to which soil formation has been accompanied by losses and gains of various components, including Si (Fitzpatrick & Chittleborough 2002). Finally, since fire significantly impacts the terrestrial Si cycle through ash exports (Alexandre *et al.* 2011) and occurs in these ecosystems, future studies should include this disturbance in mass-balance calculations.

Overall, the scientific approach adopted for the chapters **3, 4 and 5** was at the interface of soil science methods (that is, the use of extractants to trace soil Si dynamics) and ecological methods (that is, community-level weighted means of trait values to roughly estimate elemental biocycling, including that of Si) (see section 1.3 in chapter 1 on this point). Such scientific approach allowed us to answer several questions, but complete biogeochemical studies are now necessary to build up a complete picture of the Si cycling as a function of soil weathering degree.

11.4.2 Studying other soil chronosequences and soil process domains

One advantage of the Jurien Bay, Guilderton and Warren chronosequences is that they comprised very end-members of pedogenesis (from carbonate to quartz-rich soils), different pedogenic thresholds (*e.g.*, carbonates and clay loss) and soil process domains (*e.g.*, carbonates dissolution, clay formation and dissolution). This is made possible by rather specific soil parent materials with high content of sand-sized

quartz/carbonate minerals. This leads to a rapid quartz-enrichment and little formation of secondary minerals after carbonates loss, because of the low content of weatherable primary silicate minerals (*e.g.*, feldpsars) in the initial soil parent material. In this regard, they can be seen as *model systems* because they are *simpler than other systems of its type* (*i.e.*, long-term soil chronosequences), *so the property of interest is not obscured by others* (Vitousek 2004). Such model systems allowed us to enhance our understanding of long-term Si dynamics in soil-plant systems in the first five chapters of this thesis. However, despite the important surface cover of sandy soils worldwide (about 10% for Arenosols that are among the most extensive soils in the world according to the WRB; about 3.5% for Podzols), their low silt and clay content make these chronosequences not highly representative of soil types on a large scale. Therefore, it would be useful to study soil-plant Si dynamics in other soil chronosequences with different pedogenic thresholds and soil process domain and confront the results with those acquired in this thesis.

11.4.3 Silicon and the plant economics spectrum: developing trait-based approaches

Over the past three decades, plant ecologists have become increasingly interested in quantifying key plant functional traits (Violle *et al.* 2007) and correlations between them in order to better understand how terrestrial plants allocate their resources (Wright *et al.* 2004, 2005; Díaz *et al.* 2016). A major step was the proposition of the worldwide leaf economics spectrum (LES), which describes a universal spectrum of leaf economics comprising key leaf properties such as specific leaf area (SLA), leaf lifespan or photosynthetic rates. The LES has further been amended to integrate root and whole-plant traits, leading to the 'fast-slow' plant economics spectrum (PES) (Freschet *et al.* 2010). The spectrum runs from fast-growing species having traits associated with rapid resource acquisition to slow-growing species having traits involved in conservation of resources. Given that other prominent ecological theories, such as the RAH (Coley *et al.* 1985), predict trade-offs between plant growth rate and defense (Züst & Agrawal 2017), the species associated with the 'slow' end of the spectrum will invest more resources to anti-herbivore defenses (Mason & Donovan 2015; Armani *et al.* 2020) to minimize tissue loss and increase the mean residence time of nutrients (Coley *et al.* 1985). These influential works on plant functional traits have provided a solid understanding of how plants allocate their resources depending on biotic and abiotic factors worldwide, and have been pivotal in plant ecology.

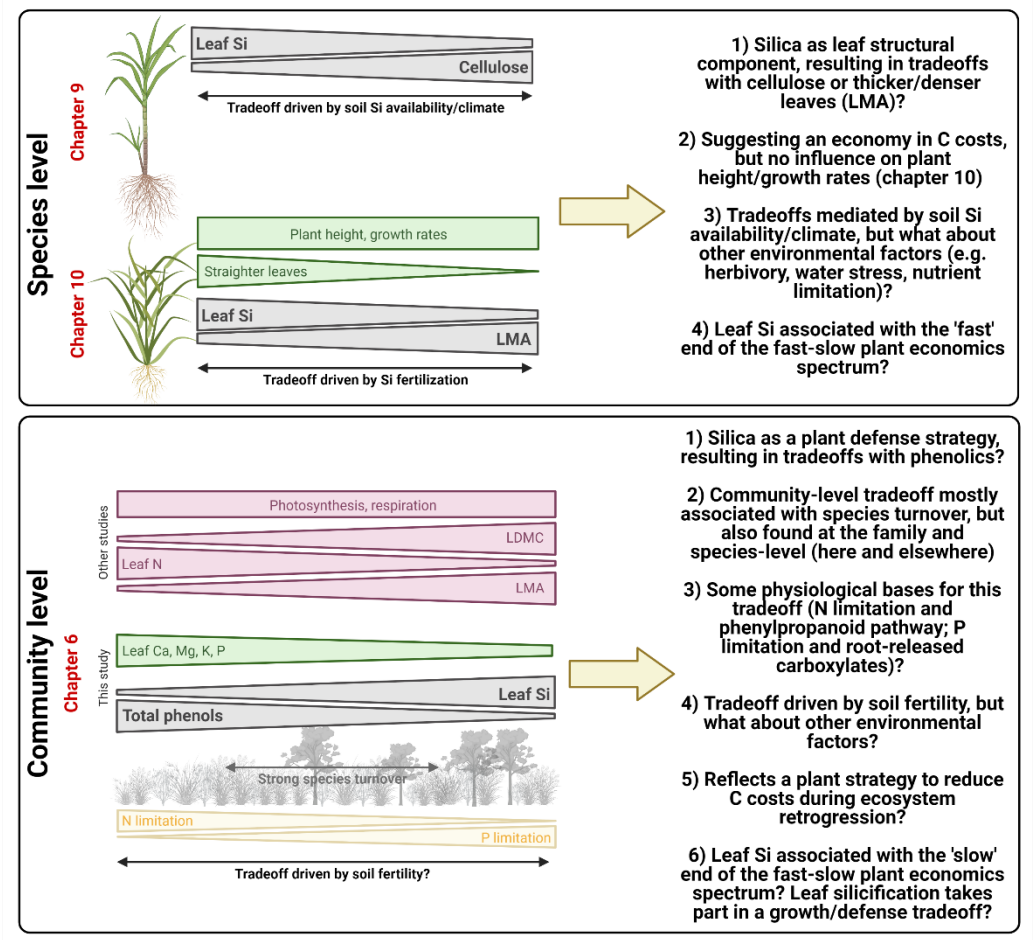

Figure 11-3 : Tradeoffs between leaf Si and other leaf functional traits found in this PhD, potential interpretations, and perspectives they open up.

In this thesis, we found negative correlations between leaf Si and cellulose in sugarcane, and between leaf Si and leaf mass per area (LMA) in rice (chapters 9 and 10, respectively) (Figure 11-3). Since C-based compounds are thought to come with much greater C costs than silicification (Raven 1983), investing in silica rather than cellulose for leaf construction could represent an energetic gain. Similarly, the negative relationship between leaf Si and LMA could reveal that investing in silica deposits rather than the construction of thick leaves could perform functions such as 1) minimizing leaf water loss and/or 2) improving leaf erectness and/or 3) reducing herbivory, and at a lower energetic cost (Raven 1983). Overall, these two studies may suggest that increased silicification, at least when enhanced by Si fertilization or mediated by soil plant-available [Si], could be associated with the ‘fast end’ of the fast-slow plant economics spectrum, at least at the species level, and for Si-

accumulating species. This would be consistent with the enhanced photosynthetic rates following Si addition observed in the literature (Lavinsky *et al.* 2016), even though we could not identify increased rice growth rates in our study (chapter 10; Figure 11-3). Further studies should now quantify Si and major plant functional traits characteristics of the plant economics spectrum at the species level and in experiments where not only Si availability is manipulated, but also other key environmental factors (herbivory, nutrients, water availability, etc.). Interestingly, Cooke & Leishman reported a negative correlation between leaf longevity and Si concentration across 155 plant species (Cooke & Leishman 2011b). They suggested that, in shorter-lived leaves, Si would be a metabolically cheap alternative to C for structural, stress alleviation and defensive functions, allowing a more favorable leaf carbon balance. This work, therefore, suggested that Si is associated with the 'fast' end of the PES and would be consistent with our findings at the species level.

However, given the growth–defense trade-off (Züst & Agrawal 2017), the role of Si as an effective defense against herbivores (Hartley & DeGabriel 2016), and the fact that it accumulates continuously with leaf aging (Motomura *et al.* 2002), we may also expect that Si is associated with the 'slow' end of the PES. In fact, one of the key outputs from this thesis is the increase in leaf [Si] with increasing soil age and decreasing soil nutrients, especially P (Figure 11-3). Leaf [Si] was therefore negatively correlated to leaf [P] (**chapter 6**), but also possibly to leaf [N] and SLA that both decreases with increasing soil age (Hayes *et al.* 2014; Guilherme Pereira *et al.* 2019). Similarly, leaf lifespan should theoretically increase with increasing soil age, because plants growing on nutrient-poor soils often increase nutrient-use efficiency by producing longer-lived leaves (Aerts & Chapin 2000). Therefore, leaf Si could also be positively correlated with leaf lifespan, which would make sense since Si tends to accumulate as leaves age (Motomura *et al.* 2002). This suggests that leaf Si could be associated with the 'slow' end of the leaf economics spectrum (Wright *et al.* 2004; Reich 2014), with species having long-lived leaves with low macronutrient concentrations and low SLA. High degree of silicification may indeed have been fostered in slow-growing plants adapted to low-nutrient habitats, for instance to reduce herbivory (growth/defense tradeoff), yet this compelling hypothesis received almost no attention in the literature and remains to be tested.

Overall, developing trait-based approaches to explore the position of Si in the PES would allow us to better understand the functional role of Si in plant ecology (Figure 11-4). To do so, modulating key environmental parameters (*e.g.*, soil nutrients) in both experimental and field studies, and at both intra- and interspecific levels, should now be realized. Detailed analyses of the literature (*e.g.*, via plant trait databases) could also help to achieve this goal. Also, the results of this PhD suggest different patterns at the intra versus interspecific levels (Figure 11-3), which would also deserve further investigations.

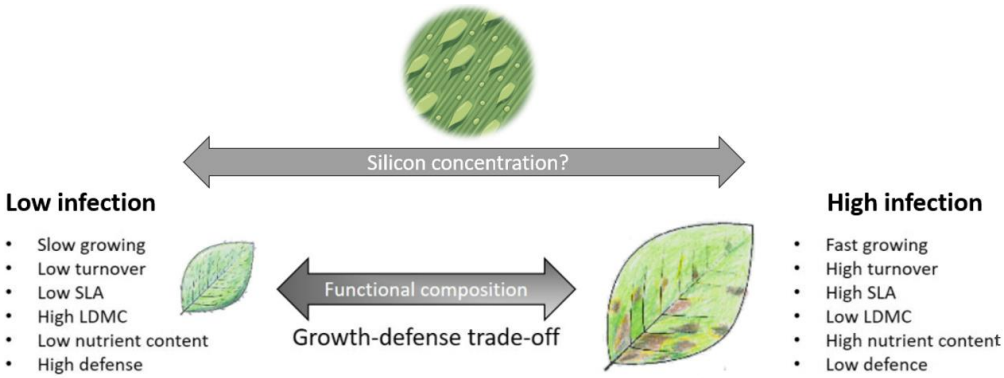

Figure 11-4 : How Si is postionned in the leaf economics spectrum and/or plant growth/defense tradeoff ? Adapted from Cappelli *et al.* (2020).

11.4.4 Silicon and nutrient-acquisition strategies

The pivotal role of Si in plant biology and ecology is increasingly appreciated, but the factors involved in plant Si accumulation have received little attention in the context of nutrient-acquisition strategies. In this thesis, we suggested that root-released carboxylates, and more generally rhizosphere processes (e.g., root-released phytosiderophores), could play an overlooked role on plant Si accumulation, by increasing soil Si mobilization from poorly-soluble forms. Although these processes have been examined in detail for many nutrients (e.g., P, Zn, Fe) (Lambers *et al.* 2006, 2015; Xue *et al.* 2016), they remain overlooked for Si, probably because it is considered as a non-essential nutrient for plant growth. Future studies should now address the following questions:

- Is the greater expression of silica-based defenses for species growing in low-P environments, in accordance with the resource availability hypothesis, accounted for by root-released carboxylates? Similarly, is the increase in leaf [Si] for Poaceae sp. growing under P deficiency accounted for root exudates, like siderophores?
- Can plant Si uptake be enhanced by facilitative interactions between species, with one increasing plant-available [Si] though carboxylate release?
- Should C costs related to plant Si accumulation consider nutrient-acquisition strategies? If so, what are the real C costs of plant Si accumulation? How does it vary among Si-accumulating and non-accumulating species, and as a function of soil P availability?
- Do carboxylate-releasing P-solubilizing strategies provide an alternative and additional explanation for the wide variation in leaf [Si] among terrestrial plants?

- Do other root traits commonly associated with nutrient-acquisition (*e.g.*, root hairs, architecture, biomass) influence plant Si uptake?
- Does the release of phytosiderophores by Poaceae increase Si mobilization in the rhizosphere and subsequent plant uptake?

Besides root exudates, mycorrhizal associations also represent major nutrient-acquisition strategies for terrestrial plants (Richardson *et al.* 2009). Contrary to root exudates, we have more evidence of their role in mobilizing Si from the rhizosphere and increasing subsequent plant Si uptake (**chapter 8** and references therein). However, the underlying mechanisms remain unresolved. Moreover, we do not know the extent to which this process is significant for plant Si uptake compared to the relative expression of Si transporters and other biotic factors (e.g., plant-available Si, evapotranspiration potential, herbivory). Finally, the influence of mycorrhizal associations on plant Si uptake has been considered only for a few crop species and under controlled conditions (**chapter 8** and references therein), and field studies are now needed.

11.4.5 Boundaries in Si research in agriculture

Despite the significant new insights into Si research in agriculture provided by the **chapter 8**, many questions remain. In particular, a better understanding of the biotic factors regulating soil-plant Si dynamics and how they could be leveraged in modern agroecosystems is needed:

- What is the abundance and diversity of silicate solubilizing bacteria (SSB) in soils? In which soil types/mineralogy are they most found? To which extent SSB contribute to the plant-available Si pool and subsequent plant Si uptake compared to abiotic mineral weathering, and by which mechanisms? How agriculture practices impact SSB abundance, diversity and functions?
- Does plant Si nutrition could be ameliorated through common mycorrhizal networks (CMN) in intercropping systems?
- If root exudates mobilize poorly-soluble soil Si forms, does it occur only in P-depleted soils and without P fertilization? Can carboxylate-releasing strategies be exploited in cereal-legume intercropping agroecosystems, with legumes releasing carboxylates (*e.g.*, *Cicer arietinum*; Pang *et al.* 2018) and mobilize soil Si, which could in turn benefit both crops?
- Is the significant earthworms-related increase in soil-plant Si mobility significant at the soil profile scales? Do cover crops, intercropping or integrated crop-livestock systems (ICL) influence this process by modifying earthworm's abundance and diversity?
- What is the impact of large herbivores on global Si biogeochemistry? To which extent do they stimulate soil-plant Si mobility in natural ecosystems and ICL? Does ICL influence Si dynamics through changes in microbial communities and biomass, soil aggregation or organic matter dynamics?

- How decomposition dynamics influence Si release from phytoliths dissolution in different geopedoclimatic contexts, and for different species? What are the long-term advantages and disadvantages of different residue management practices (i.e., direct incorporation, burning, or biochar/manure/compost production and subsequent application)?
- What are the short and long-term effects of cover crops on soil-plant Si mobility? Could legumes cover crops significantly stimulate Si mobility compared to grasses cover crops? Does the absence of cover crops significantly increase soil phytolith losses through soil erosion?
- How soil aggregation and soil structure impact soil-plant Si dynamics? Do the *microbial hotspots* on soil aggregate surfaces affect soil Si dynamics and release in soil solution? Is it significant at the soil profile scales? How modifications of soil structure and aggregation by anthropogenic activities influence these processes?

11.5 Final conclusions

Better understand element cycling in terrestrial ecosystems is fundamental to preserve Earth's climate and sustain global food production, especially since we are living in the Anthropocene age. The research presented in this thesis illustrated how model systems (Vitousek 2004) like long-term soil chronosequences can help us to better constrain soil-plant element dynamics, and how knowledge on ecological processes can be leveraged to improve agroecosystems sustainability (Mariotte *et al.* 2018). In particular, this thesis provided the following insights:

- Soil age and weathering degree exert a strong control on soil-plant Si dynamics. We stressed the major influence of soil mineralogical evolution driven by long-term pedogenesis on soil Si dynamics, with potential increased control of plant Si biocycling with increasing soil age and ecosystem water balance.
- Silica-based defenses seem to play an important role for plants growing in old highly-weathered soils where P limits plant productivity, while phenol-based defenses are more expressed in young soils where productivity is limited by N. The strength and type of nutrient limitation could drive tradeoffs in plant defense strategies, opening up promising perspectives for the resource availability hypothesis.
- Higher expression of silica-based defenses in low P soils may result from increased soil Si mobilization by root-released carboxylates, a P-acquisition strategy particularly prevalent in these environments. The C costs of silica-based defenses might be more expensive than commonly realized if carboxylates or other root exudates are needed to mobilize Si from the rhizosphere, especially when plant-available Si concentration is low.

- Mycorrhizal associations, silicate-solubilizing bacteria, root exudates, soil macrofauna and large herbivores significantly stimulate Si mobility in soil-plant systems. These ecological processes could be exploited in different cropping systems such as covers crops, cereal/legume intercropping, or integrated crop-livestock systems. Recycling crop residues will also increase Si-use efficiency in agroecosystems through the high reactivity of phytoliths in soil environments.
- The degree of epidermal silicification of graminoid crop species is highly influenced by soil weathering degree and by the recycling of Si-rich crop residues. We also highlight the mechanical properties of leaf silicification, which might eventually lead to tradeoffs with other traits having similar functions.

These findings are of special interest because the Si dynamics in soil-plant systems have a strong influence on both the C cycle and plant performance that is increasingly appreciated by soil scientists, plant ecologists, biogeochemists and in agricultural research. Besides, this thesis stresses the need to develop multidisciplinary approaches to better understand elements mobility in ecosystems. Since scientific research must answer questions but also open up new ones, this thesis ended with a series of perspectives for soil-plant Si research in both natural systems and agroecosystems.

Appendix A : The Jurien Bay chronosequence

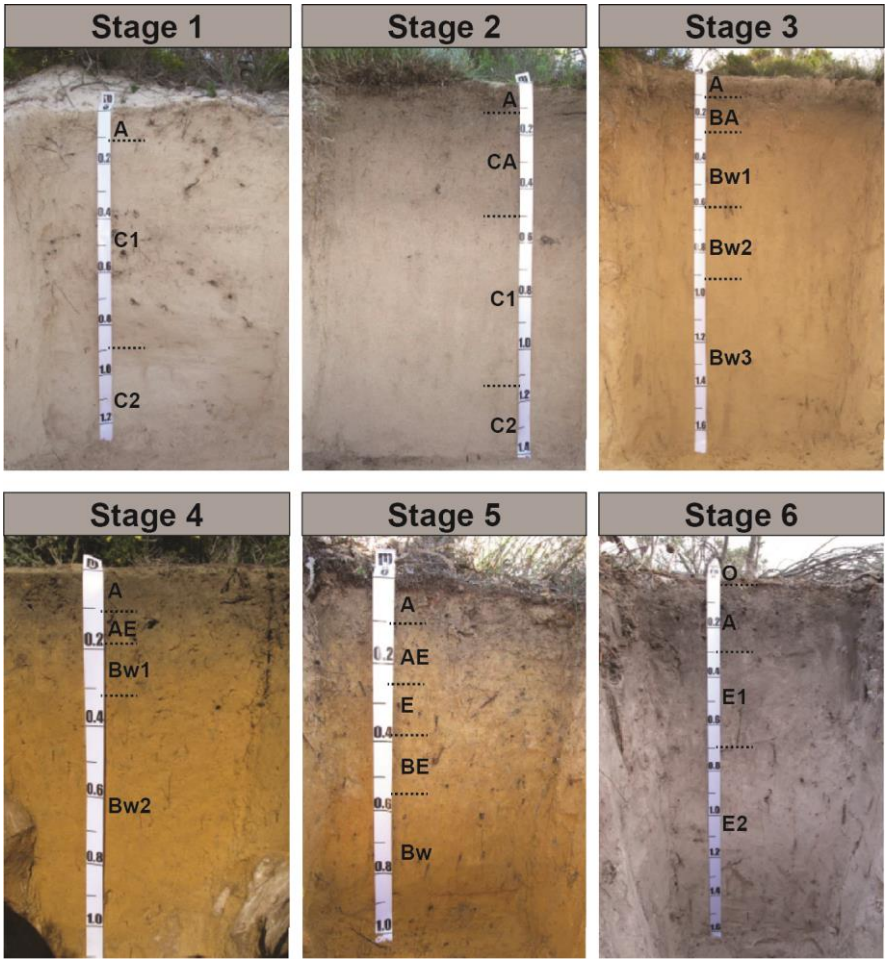

Figure A-1 : Soil profiles of the Jurien Bay chronosequence, from Turner & Laliberté (2015)

Table A-1 – Estimated age, particle-size distribution, carbonate concentration, pH-$CaCl_2$, effective cation exchange capacity and OC concentration of the Jurien Bay chronosequence soils, according to Turner & Laliberté, (2015).

Stage	Soil age	Soil depth	Horizon	Carbonates (%)	Sand (%)	Silt (%)	Clay (%)	pH-$CaCl_2$	OC (%)	ECEC ($cmol_c\ kg^{-1}$)
1	100 yr	**ENTISOL: Carbonatic, thermic, Typic Xeropsamments**								
		0-12	AC	77.4	97.6	1.6	0.9	7.6	1.4	3.4
		12-88	C1	83.2	98.3	1.0	0.7	8.3	0.6	11.0
		88+	C2	83.1	98.4	0.9	0.7	8.3	0.6	34.5
2	1000 yr	**ENTISOL: Carbonatic, thermic, Typic Xeropsamments**								
		0-13	A	76.7	92.3	4.1	3.6	8.0	2.1	8.5
		13-51	CA	73.5	95.0	2.6	2.4	8.1	1.6	5.2
		51-116	C1	81.1	97.5	1.2	1.3	8.2	0.4	5.0
		116+	C2	80.1	97.7	1.0	1.3	8.3	0.6	6.4
3	6500 yr	**ENTISOL: Siliceous, thermic, Typic Xeropsamments**								
		0-12	A	20.9	92.9	3.9	3.2	7.5	1.7	9.6
		12-26	BA	24.7	95.6	1.8	2.6	7.8	1.6	7.1
		26-60	B1	28.9	97.3	1.3	1.4	8.0	1.2	4.3
		60-93	B2	26.2	98.1	0.8	1.1	8.1	1.4	3.6
		93-165	B3	29.5	98.0	0.9	1.1	8.2	0.8	4.3
4	120 kyr									
		0-11	A	-	93.2	3.7	3.1	5.5	0.9	5.1
		11-18	AE	-	94.7	3.2	2.1	5.8	0.4	2.3
		18-33	B1	-	94.1	3.4	2.5	6.2	0.2	2.1
		33-100	B2	-	94.0	2.6	3.4	6.2	0.2	1.4
5	500 kyr	**ENTISOL: Thermic, Xeric Quartzipsamments**								
		0-11	A	-	97.0	1.8	1.3	5.0	0.6	2.0
		11-25	AE	-	97.3	1.7	1.0	5.3	0.3	0.7
		25-38	E	-	97.4	1.4	1.1	5.6	0.1	0.5
		38-55	BE	-	97.5	1.3	1.2	5.8	0.1	0.3
		55-140	B	-	97.7	1.2	1.1	5.6	0.0	0.3

6	2 Myr	**ENTISOL: Thermic, Xeric Quartzipsamments**								
		0-3	O	-	97.7	0.9	1.5	3.9	9.2	4.9
		3-30	A	-	96.1	3.4	0.	4.2	0.7	2.4
		30-70	E1	-	97.0	2.6	0.4	4.4	0.2	0.7
		70-165	E2	-	98.8	1.1	0.1	4.7	0.0	0.1

Table A-2 – Soil total elemental concentrations and Total Reserve in Bases (TRB) along the Jurien Bay chronosequence.

Stage	Horizon	Ca (%)	Mg (%)	K (%)	Na (%)	Al (%)	Fe (%)	Mn (mg kg^{-1})	P (mg kg^{-1})	TRB ($cmol_c$ kg^{-1})
1	AC	31.10	1.90	0.10	0.22	0.11	0.02	11.40	392.32	1720
	C1	31.70	1.97	0.10	0.21	0.11	0.02	11.20	384.47	1756
	C2	31.30	1.92	0.10	0.22	0.12	0.02	10.73	378.07	1732
2	A	27.70	1.42	0.12	0.18	0.16	0.04	17.20	458.22	1510
	CA	28.80	1.52	0.11	0.18	0.13	0.02	<10	371.38	1573
	C1	28.50	1.56	0.11	0.19	0.12	0.02	<10	297.62	1561
	C2	27.50	1.50	0.12	0.19	0.13	0.02	<10	288.46	1507
3	A	10.40	0.41	0.24	0.09	0.40	0.14	23.80	142.70	563
	BA	10.60	0.39	0.23	0.08	0.38	0.15	24.80	139.21	571
	B1	10.70	0.48	0.21	0.09	0.35	0.13	21.40	125.68	583
	B2	9.06	0.44	0.16	0.08	0.30	0.10	11.90	64.59	496
	B3	10.10	0.47	0.19	0.09	0.32	0.10	12.40	103.43	551
4	A	0.19	<0.02	0.40	0.05	0.30	0.29	31.70	37.97	22
	AE	0.24	<0.02	0.44	0.05	0.27	0.32	35.70	38.84	25
	B1	0.09	<0.02	0.43	0.05	0.24	0.31	30.10	26.62	18
	B2	0.10	<0.02	0.53	0.06	0.25	0.41	39.60	32.73	21
5	A	0.17	<0.02	0.08	<0.02	0.30	0.14	11.50	15.27	10
	AE	0.13	<0.02	0.09	<0.02	0.27	0.12	15.80	11.78	9
	E	0.08	<0.02	0.06	<0.02	0.24	0.11	11.50	10.47	5
	BE	0.14	<0.02	0.06	<0.02	0.25	0.12	<10	9.16	8
	B	0.13	<0.02	0.07	<0.02	0.31	0.16	13.30	9.60	8
6	O	0.45	0.04	0.06	0.04	0.12	0.06	<10	4.36	29
	A	0.15	<0.02	0.04	<0.02	0.06	0.02	<10	7.86	8
	E1	0.14	<0.02	0.04	<0.02	0.05	<0.02	<10	6.84	8
	E2	0.21	<0.02	0.05	<0.02	0.05	0.02	<10	5.24	12

Appendix B : The Guilderton chronosequence

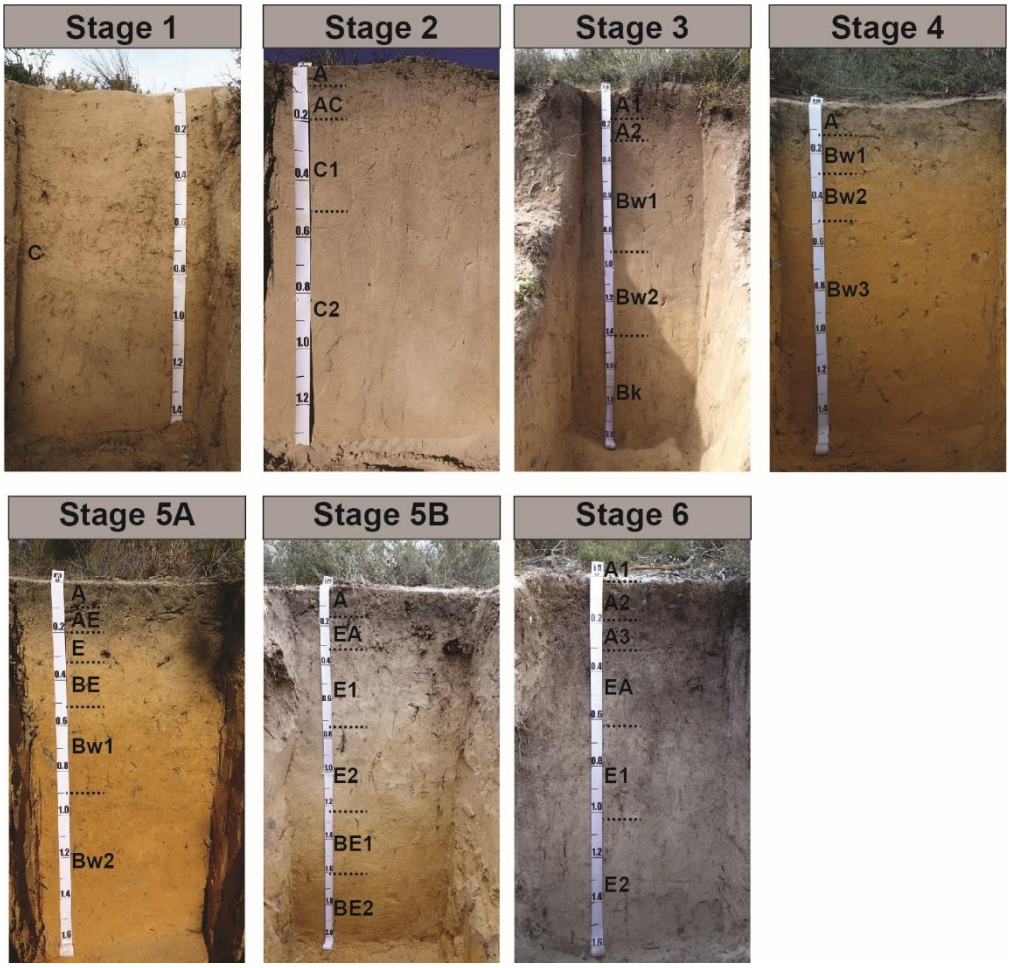

Figure B-1 : Soil profiles of the Guilderton chronosequence, from Turner *et al.* (2018)

Table B-1 – Estimated age, particle-size distribution, carbonate concentration, pH-$CaCl_2$, effective cation exchange capacity and OC concentration of the Guilderton chronosequence soils, according to Turner *et al.* (2018). Iron extracted with DCB (Fe_{DCB}; Fe oxides).

Stage	Soil age	Soil depth	Horizon	Carbonates (%)	Sand (%)	Silt (%)	Clay (%)	pH-$CaCl_2$	OC (%)	ECEC (cmolc kg^{-1})
1	100 yr	**ENTISOL: Carbonatic, thermic, Typic Xeropsamments**								
		0-150	C	45	98.6	0.1	1.3	7.5	0.2	15.1
2	1000 yr	**ENTISOL: Carbonatic, thermic, Typic Xeropsamments**								
		0-7	A	48	95.1	1.2	3.6	7.2	0.7	3.5
		7-19	AC	47	96.5	1.1	2.3	7.5	0.6	2.9
		19-53	C1	49	97.7	0.9	1.4	7.6	0.4	2.1
		53-130	C2	50	98.4	0.4	1.1	7.8	0.1	3.7
3	6500 yr	**ENTISOL: Carbonatic, thermic, Typic Xeropsamments**								
		0-17	A1	29	89.1	4.2	6.7	7.1	1.0	9.2
		17-27	A2	33	89.1	3.8	7.1	7.3	0.8	8.5
		27-93	Bw1	40	93.2	1.8	5.1	7.4	0.4	4.8
		93-141	Bw2	43	95.3	1.0	3.6	7.5	0.4	3.3
		141-200	Bk	41	95.7	0.8	3.5	7.5	0.3	3.6
4	120 kyr	**ENTISOL: Thermic, uncoated, Xeric Quartzipsamments**								
		0-13	A	-	96.2	1.3	2.5	4.7	0.3	0.6
		13-28	Bw1	-	94.7	1.9	3.3	5.0	0.2	0.4
		28-47	Bw2	-	93.8	2.4	3.7	5.1	0.1	0.4
		47-140	Bw3	-	92.6	2.6	4.9	5.4	0.0	0.4
5A	250 kyr	**ENTISOL: Thermic, uncoated, Xeric Quartzipsamments**								
		0-10	A	-	97.1	1.1	1.9	4.6	0.7	0.3
		10-21	AE	-	96.4	1.7	1.9	4.7	0.1	0.3
		21-33	E	-	96.6	1.6	1.8	4.8	0.1	0.1
		33-53	BE	-	96.3	1.4	2.3	4.9	0.0	0.1
		53-89	Bw1	-	94.4	1.6	4.1	4.8	0.1	0.2
		89-140	Bw2	-	91.6	1.8	6.6	4.8	0.1	0.3

5B	400 kyr	**ENTISOL: Thermic, uncoated, Xeric Quartzipsamments**							
		0-17	A	-	98.5	0.6	0.9	4.2	0.4	0.4
		17-33	EA	-	98.5	0.6	0.9	4.2	0.2	0.1
		33-76	E1	-	98.6	0.5	0.9	4.6	0.1	0.0
		76-123	E2	-	98.1	1.0	0.9	5.5	0.0	0.0
		123-158	BE1	-	97.2	1.3	1.4	5.3	0.0	0.1
		158-185	BE2	-	96.4	2.2	1.3	5.6	0.1	0.1
6	2 Myr	**ENTISOL: Thermic, uncoated, Xeric Quartzipsamment**							
		0-1	A1	-	99.3	0.1	0.7	4.4	0.4	0.6
		1-18	A2	-	97.2	1.5	1.3	3.8	2.9	2.7
		18-30	A3	-	98.6	0.7	0.6	3.7	0.8	1.1
		30-62	EA	-	98.9	0.4	0.7	3.6	0.3	0.2
		62-103	E1	-	98.9	0.4	0.6	4.0	0.1	0.0
		103-160	E2	-	98.9	0.4	0.7	4.4	0.0	0.0

Table B-2 – Soil total elemental concentrations, Total Reserve in Bases (TRB) and $MIA_{modified}$ along the Guilderton chronosequence.

Stage	Horizon	Si (%)	Ca (%)	Mg (%)	K (%)	Na (%)	Al (%)	Fe (%)	Mn (mg kg^{-1})	P (mg kg^{-1})	TRB ($cmol_c$ kg^{-1})	$MIA_{modified}$
1	C	22.6	17.93	1.01	0.15	0.13	0.19	0.12	46.30	135.43	988	8.9
2	A	22.4	18.20	0.98	0.16	0.13	0.23	0.12	43.60	93.83	998	10.4
	AC	22.1	18.30	1.01	0.15	0.13	0.21	0.12	41.60	30.11	1006	9.6
	C1	22.3	18.30	1.07	0.15	0.12	0.20	0.10	34.10	66.77	1011	8.7
	C2	24.5	16.60	0.99	0.14	0.11	0.19	0.06	19.80	89.03	919	8.1
3	A1	28.3	13.00	0.38	0.52	0.14	0.71	0.25	60.50	71.57	699	37.8
	A2	26.8	14.20	0.39	0.50	0.14	0.67	0.23	52.10	8.73	759	36.4
	Bw1	25.6	16.00	0.54	0.46	0.15	0.61	0.17	32.40	94.70	861	28.9
	Bw2	27.7	14.80	0.58	0.40	0.14	0.52	0.12	16.00	80.30	802	25.1
	Bk	30.8	12.00	0.50	0.37	0.12	0.48	0.10	12.60	49.31	654	26.1
4	A	42.7	0.28	<0.02	0.54	0.05	0.81	0.21	<10	<4.36	30	67.6
	Bw1	44.9	0.17	<0.02	0.68	0.06	0.98	0.25	<10	13.96	28	66.9
	Bw2	44.3	0.08	<0.02	0.80	0.08	1.26	0.36	12.93	20.37	28	68.9
	Bw3	43.9	0.15	<0.02	0.83	0.08	1.32	0.39	12.90	19.64	32	69.4
5A	A	44.2	0.10	<0.02	0.20	<0.02	0.48	0.14	<10	<4.36	10	79.7
	AE	43.6	0.24	<0.02	0.25	<0.02	0.48	0.14	11.50	<4.36	18	76.0
	E	46.2	0.29	<0.02	0.24	<0.02	0.39	0.11	12.10	<4.36	21	72.7
	BE	45.6	0.16	<0.02	0.32	<0.02	0.50	0.16	16.90	8.73	16	72.4
	Bw1	45.1	0.11	<0.02	0.32	<0.02	0.84	0.30	14.30	7.42	14	81.6
	Bw2	44.7	0.12	<0.02	0.24	<0.02	1.12	0.44	15.70	29.68	12	88.8
5B	A	45.1	0.46	<0.02	0.03	<0.02	0.07	0.05	10.10	<4.36	23	84.0
	EA	46.0	0.33	<0.02	0.03	<0.02	0.06	0.04	12.40	<4.36	17	79.2
	E1	46.0	0.31	<0.02	0.03	<0.02	0.05	0.05	16.20	<4.36	16	76.1
	E2	45.9	0.30	<0.02	0.03	<0.02	0.05	0.06	16.80	<4.36	16	78.3
	BE1	45.9	0.34	<0.02	0.04	<0.02	0.08	0.09	22.30	<4.36	18	81.5
	BE2	45.8	0.24	<0.02	0.03	<0.02	0.09	0.10	17.90	<4.36	13	86.2
6	A1	44.2	0.47	<0.02	<0.02	<0.02	0.02	<0.02	<10	<4.36	23	100.0

A2	44.1	0.28	<0.02	<0.02	<0.02	0.03	0.02	<10	<4.36	14	100.0
A3	43.0	0.42	<0.02	<0.02	<0.02	<0.02	<0.02	<10	<4.36	21	100.0
EA	48.6	0.42	<0.02	<0.02	<0.02	0.03	0.04	14.80	13.53	21	100.0
E1	45.1	0.11	<0.02	<0.02	<0.02	<0.02	0.02	<10	4.95	6	100.0
E2	46.0	0.35	<0.02	<0.02	<0.02	<0.02	0.03	<10	<4.36	18	100.0

Appendix C : The Warren chronosequence

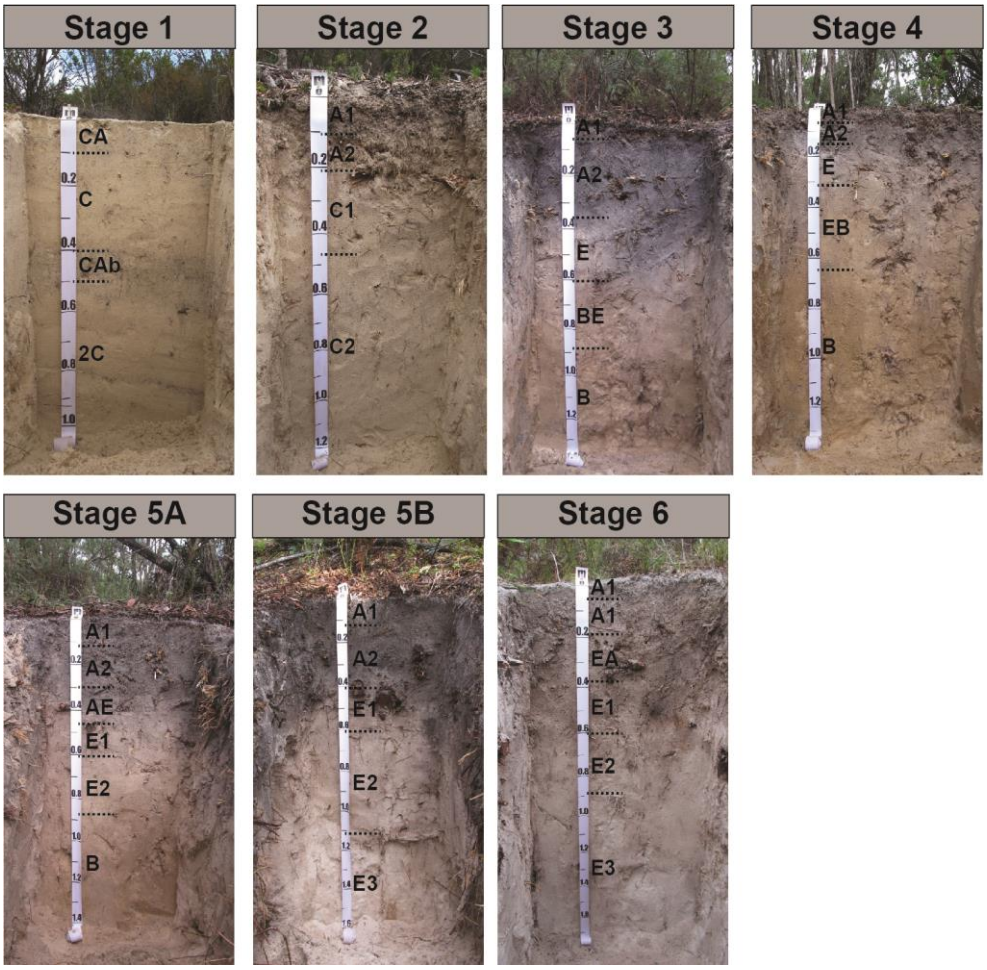

Figure C-1 : Soil profiles of the Warren chronosequence, from Turner *et al.* (2018)

Table C-1 – Estimated age, particle-size distribution, carbonate concentration, pH-$CaCl_2$, effective cation exchange capacity and OC concentration of the Guilderton chronosequence soils, according to Turner *et al.* (2018).

Stage	Soil age	Soil depth	Horizon	Carbonates (%)	Sand (%)	Silt (%)	Clay (%)	pH-$CaCl_2$	OC (%)	ECEC (cmolc kg^{-1})
1	100 yr	**ENTISOL: Thermic, uncoated, Xeric Quartzipsamments**								
		0-10	CA	3.8	98.7	0.8	0.5	8.1	0.1	2.2
		10-41	C	3.5	99.4	0.2	0.4	8.2	0.0	2.9
		41-50	Cab	3.6	98.7	0.8	0.4	8.3	0.0	4.7
		50-103	2C	4.8	99.1	0.5	0.4	8.1	0.0	4.5
2	1000 yr	**ENTISOL: Thermic, uncoated, Xeric Quartzipsamments**								
		0-11	A1	0.2	98.7	0.6	0.7	7.2	0.9	3.0
		11-21	A2	0.9	98.7	0.5	0.7	7.6	0.2	1.9
		21-46	C1	1.9	99.1	0.3	0.6	8.1	0.1	1.7
		46-120	C2	1.7	99.2	0.2	0.5	8.3	0.2	2.6
3	6500 yr	**ENTISOL: Thermic, uncoated, Typic Quartzipsamments**								
		0-5	A1	0.0	95.0	4.4	0.6	4.8	4.0	11.1
		5-37	A2	0.2	95.4	3.7	0.8	5.1	0.5	2.3
		37-60	E	0.3	99.0	0.6	0.4	5.4	0.0	0.3
		60-87	BE	0.1	98.6	1.0	0.4	5.4	0.0.	0.3
		87-130	B	0.1	99.3	0.3	0.4	5.6	0.0	0.2
4	120 kyr	**ENTISOL: Thermic, uncoated, Xeric Quartzipsamments**								
		0-6	A1	-	98.4	0.8	0.8	4.8	0.9	1.5
		6-16	A2	-	98.4	0.9	0.7	4.6	0.4	0.9
		16-32	E	-	98.4	1.0	0.6	4.7	0.1	0.3
		32-64	EB	-	98.7	0.9	0.4	4.9	0.1	0.2
		64-200	B	-	99.4	0.1	0.5	5.2	0.0	0.2
5A	250 kyr	**ENTISOL: Thermic, uncoated, Xeric Quartzipsamments**								
		0-13	A1	-	97.9	1.1	1.1	4.4	1.0	1.8
		13-30	A2	-	98.5	0.6	0.9	4.5	0.3	1.1
		30-46	AE	-	98.7	0.8	0.5	4.6	0.1	0.4
		46-61	E1	-	99.2	0.4	0.4	4.6	0.0	0.1

		61-87	E3	-	99.3	0.4	0.3	4.8	0.0	0.1
		87-200	B	-	99.0	0.5	0.5	4.7	0.0	0.1
5B	400 kyr	**ENTISOL: Thermic, uncoated, Xeric Quartzipsamments**								
		0-13	A1	-	97.7	1.4	0.9	3.9	1.0	2.2
		13-41	A2	-	98.3	1.0	0.7	3.8	0.5	1.2
		41-61	E1	-	99.4	0.3	0.4	4.2	0.1	0.2
		61-113	E2	-	99.4	0.2	0.4	4.6	0.0	0.1
		113-180	E3	-	99.6	0.2	0.2	4.6	0.0	0.0
					99.3	0.3	0.4	4.8	0.0	0.1
6	2 Myr	**ENTISOL: Thermic, uncoated, Xeric Quartzipsamment**								
		0-6	A1	-	98.5	0.6	0.9	4.9	1.3	1.8
		6-19	A2	-	98.2	1.2	0.5	3.7	0.4	0.5
		19-37	EA	-	98.0	1.3	0.7	3.6	0.3	0.4
		37-60	E1	-	99.0	0.5	0.5	3.9	0.1	0.1
		60-88	E2	-	99.3	0.4	0.3	4.2	0.0	0.0
		88-320+	E3	-	99.3	0.5	0.2	4.8	0.0	0.0

Table C-2 – Soil total elemental concentrations and Total Reserve in Bases (TRB) along the Warren chronosequence.

Stage	Horizon	Ca (%)	Mg (%)	K (%)	Na (%)	Al (%)	Fe (%)	Mn (mg kg^{-1})	P (mg kg^{-1})	TRB ($cmol_c$ kg^{-1})
1	CA	1.43	0.06	0.14	0.05	0.18	0.05	<10	5.24	81.7
	C	1.44	0.06	0.12	0.04	0.15	0.04	<10	13.96	81.7
	Cab	1.50	0.07	0.11	0.04	0.15	0.06	12.90	21.38	85.5
	2C	1.60	0.09	0.07	0.02	0.09	0.04	<10	12.66	89.9
2	A1	0.15	<0.02	0.07	<0.02	0.09	0.03	<10	12.22	9.6
	A2	0.35	<0.02	0.08	0.02	0.10	0.04	<10	14.84	20.6
	C1	0.77	0.03	0.08	<0.02	0.09	0.03	<10	13.09	43.2
	C2	0.93	0.04	0.07	<0.02	0.08	0.03	<10	16.58	51.4
3	A1	0.34	0.04	0.09	0.02	0.11	0.05	52.30	5.67	23.4
	A2	0.17	<0.02	0.08	<0.02	0.10	0.04	11.50	10.47	10.7
	E	0.14	<0.02	0.08	<0.02	0.10	0.03	<10	9.16	8.9
	BE	0.06	<0.02	0.09	0.02	0.11	0.05	<10	10.47	6.4
	B	0.10	<0.02	0.07	<0.02	0.09	0.04	<10	8.29	6.6
4	A1	0.25	<0.02	0.08	<0.02	0.10	0.04	26.90	<4.36	14.4
	A2	0.09	<0.02	0.09	<0.02	0.11	0.04	13.20	12.66	6.9
	E	0.07	<0.02	0.10	0.02	0.12	0.04	<10	10.91	7.2
	EB	0.07	<0.02	0.10	0.02	0.13	0.06	11.80	11.78	7.0
	B	0.06	<0.02	0.08	<0.02	0.10	0.04	<10	10.33	4.8
5A	A1	0.24	<0.02	0.07	<0.02	0.08	0.03	12.80	5.67	13.6
	A2	0.10	<0.02	0.06	<0.02	0.07	0.02	<10	9.16	6.3
	AE	0.16	<0.02	0.06	<0.02	0.07	0.04	<10	15.71	9.3
	E1	0.09	<0.02	0.06	<0.02	0.07	0.03	<10	11.35	6.0
	E3	0.10	<0.02	0.05	<0.02	0.07	0.03	<10	7.86	6.4
	B	0.05	<0.02	0.06	<0.02	0.08	0.03	<10	11.78	4.2
5B	A1	0.23	<0.02	0.06	<0.02	0.07	0.03	14.20	<4.36	12.9
	A2	0.10	<0.02	0.04	<0.02	0.05	<0.02	<10	8.29	6.1
	E1	0.11	<0.02	0.04	<0.02	0.05	<0.02	<10	8.29	6.5
	E2	0.07	<0.02	0.04	<0.02	0.05	<0.02	<10	8.73	4.5

	E3	0.06	<0.02	0.04	<0.02	0.05	0.02	<10	9.60	4.2
6	A1	0.18	<0.02	0.04	<0.02	0.05	<0.02	62.80	9.60	10.1
	A2	0.11	<0.02	0.04	<0.02	0.06	0.02	<10	16.58	6.8
	EA	0.09	<0.02	0.03	<0.02	0.04	<0.02	<10	8.73	5.2
	E1	0.11	<0.02	0.03	<0.02	0.04	<0.02	<10	6.84	6.1
	E2	0.15	<0.02	0.03	<0.02	0.04	<0.02	<10	6.55	8.5
	E3	0.13	<0.02	0.03	<0.02	0.04	<0.02	<10	7.86	7.2

Appendix D: Supplementary Material of Chapter 3

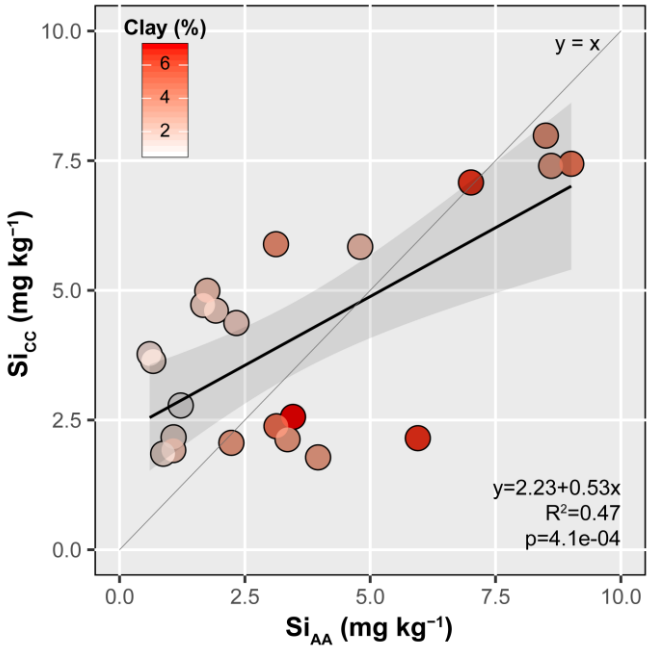

Figure D-1 : Si_{CC} concentrations versus Si_{AA} concentrations (mg kg^{-1}) along the Guilderton chronosequence. Black lines indicate the regression line between both variables. Shaded areas represent 95% confidence interval of the regression. Equation regression, coefficients of determination (R^2) and p-values are shown. The filling color of the points indicates the clay concentration of the sample.

Table D-1 – Literature data used for soil pH and Si_{CC} concentrations found in Figure 3-6. Soil types have been translated into descriptions to harmonize between the different classifications systems.

Study area	Soil types	Protocol	Number of points	Si-$CaCl_2$ range	pH-range	Reference
South India	Arid soils, Smectite-rich soils, Sandy soils, Weakly-developed soils, Clay-enriched horizon soils, Highly weathered 1:1 clay minerals/Fe oxides soils	0.01M $CaCl_2$	200	1-83	4.9-9.5	(Meunier *et al.* 2018)
Eastern South Africa	Weakly-developed soils, Clay-enriched horizon soils, Organic-rich soils, Smectite-rich soils, Highly weathered 1:1 clay minerals/Fe oxides soils, Sandy soils	0.01M $CaCl_2$, shaking 16h, 1:10 soil:solution	98	5-123	3.5-6.9	(Miles *et al.* 2014)
Central Panama	Clay-enriched horizon soils, Weakly-developed soils, Highly weathered 1:1 clay minerals/Fe oxides soils, Sandy soils	0.01M $CaCl_2$, shaking 1h, 1:10 soil:solution	76	1-40	3.3-7.4	(Schaller *et al.* 2018)
Belgium	Acidic weakly-developed soils	0.01M $CaCl_2$, shaking 5h, 1:10 soil:solution	39	7-17	3.3-4.6	Personal data
Belgium	Clay-enriched horizon soils	0.01M $CaCl_2$, shaking 16h, 1:10 soil:solution	36	6-73	3.8-8.1	(Vandevenne *et al.* 2015)
Central France	Weakly-developed soils	0.01M $CaCl_2$	21	10-40	4.1-4.7	(Cornelis *et al.* 2011b)
Serengeti National Park (Tanzania, Kenya)	Volcanic soils, Arid soils, Organic-rich soils , Smectite-rich soils	0.01M $CaCl_2$, shaking 16h	18	50-150	5.5-8.2	(Quigley *et al.* 2016)
South India	Highly weathered 1:1 clay minerals/Fe oxides soils	0.01M $CaCl_2$, shaking 1h, 1:10 soil:solution	18	22-56	4.4-5.4	(Narayanaswamy & Prakash 2009)
Guadeloupe Island	Smectite-rich soils, Highly weathered 1 :1 clay minerals/Fe oxides soils	0.01M $CaCl_2$, shaking 5h, 1:10 soil:solution	12	16-68	4.9-8.3	Personal data
Western India	Aluvial soils	0.01M $CaCl_2$, shaking 1h, 1:10 soil:solution	9	12-25	7.2-8.1	(Malav & Shaikh 2015)
Guadeloupe Island	Volcanic soils , Weakly-developed soils , Highly weathered 1:1 clay minerals/Fe oxides soils	0.01M $CaCl_2$, shaking 5h, 1:10 soil:solution	6	19-54	5.1-6.0	(Henriet *et al.* 2008a)
USA (Louisiana)	Saturated smectite-rich soils, saturated highly weathered 1:1 clay minerals/Fe oxides soils, Weakly-developed soils, Saturated clay-enriched horizon soils	0.01M $CaCl_2$, shaking 1h, 1:10 soil:solution	6	17-37	5.0-8.0	(Babu *et al.* 2016)

Guadeloupe Island	Volcanic soils, Weakly-developed soils, Highly weathered 1:1 clay minerals/Fe oxides soils	0.01M $CaCl_2$, shaking 5h, 1:10 soil:solution	5	9-48	5.5-6.7	(Henriet *et al.* 2008b)
Ethiopia	Hydromorphic soils	0.01M $CaCl_2$	4	20-98	5.2-5.9	(Cornelis *et al.* 2014)
Eastern Germany	Hydromorphic soils	0.01M $CaCl_2$, shaking 16h, 1:10 soil:solution	4	6-10	6.3-6.6	(Höhn *et al.* 2008)
Eastern Australia	Sandy soils	0.01M $CaCl_2$, shaking 12h	2	7-21	5.6-5.7	(Cooke & Leishman 2012)

Appendix E : Supplementary Material of Chapter 4

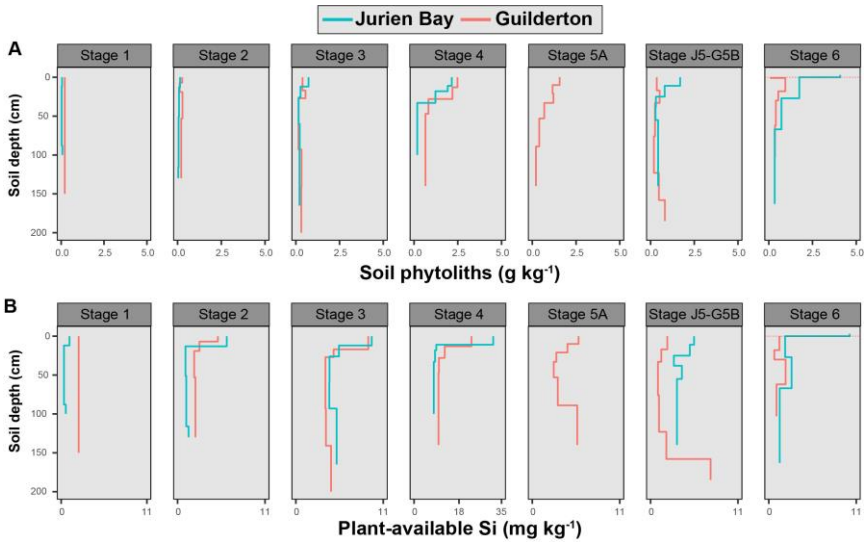

Figure E-1 : Depth distribution of soil phytoliths (A) and plant-available Si (B) concentrations across the Jurien Bay and Guilderton chronosequences. At Jurien Bay stage 6, the red dotted lines indicate the transition between litter and soil. In the sixth panels, 'J5' stands for Jurien Bay stage 5 and 'G5B' stands for Guilderton stage 5B. Soil age increases with increasing chronosequence stage.

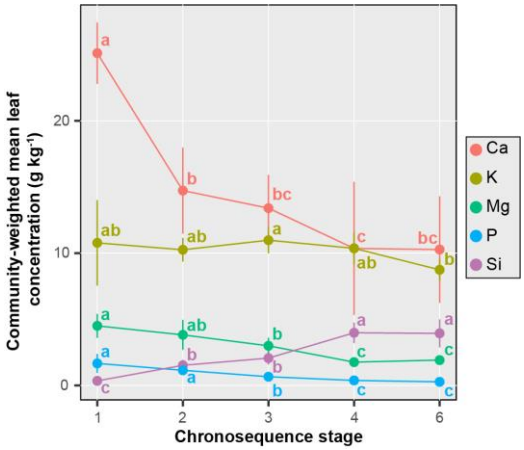

Figure E-2 : Cover-weighted mean foliar concentrations of silicon, calcium, magnesium, potassium and phosphorus of mature individuals of the 10 most-abundant plant species per plot along the Jurien Bay chronosequence. Points indicate means, bars show 95% confidence intervals (n=5). Letters above each mean represent Fisher Least Significant Difference (LSD) groupings ($p<0.05$), performed on log-transformed data. Soil age increases with increasing chronosequence stage.

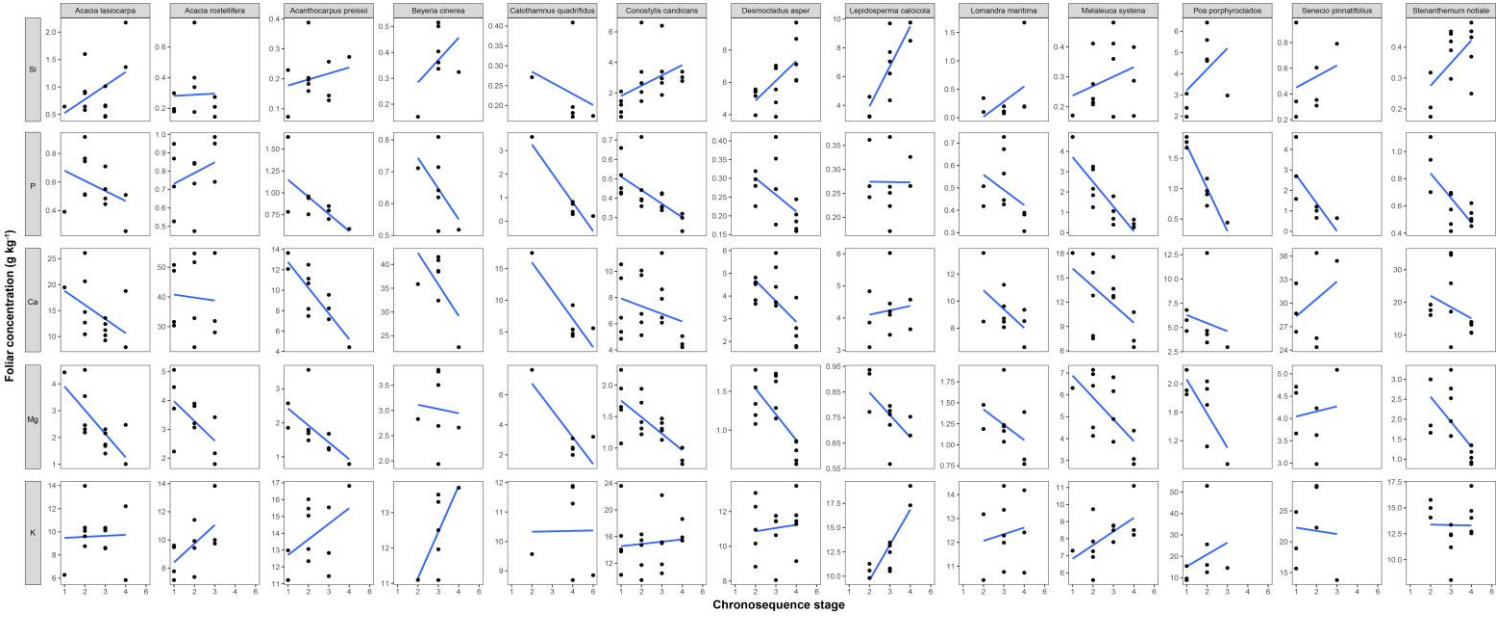

Figure E-3 : Intraspecific variation in foliar silicon, phosphorus, calcium, magnesium and potassium concentrations for the 13 species sampled from at least three chronosequence stages. Soil age increases with increasing chronosequence stage. Blue lines represent linear regression fits for each species and element for visualization. Overall model results are presented in Table E-1.

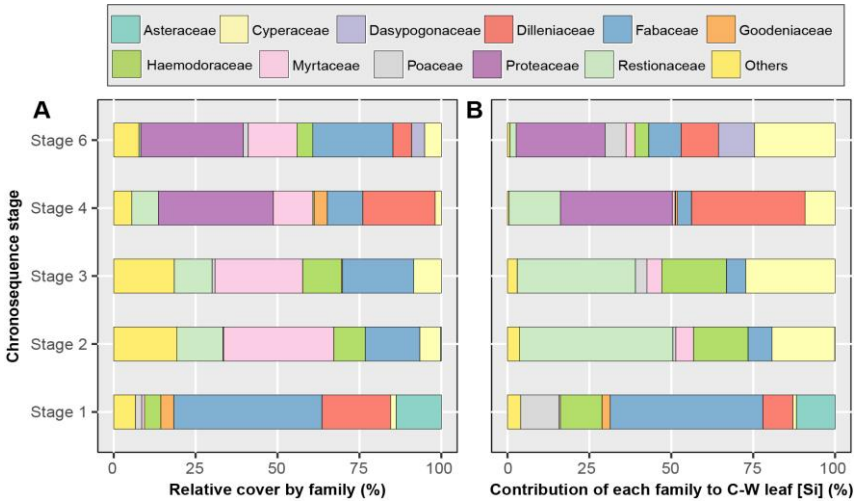

Figure E-4 : The relative cover by family across the Jurien Bay chronosequence (%) in (A), and the contribution by family to the community-level, cover-weighted (C-W) foliar [Si] in (B). Soil age increases with increasing chronosequence stage.

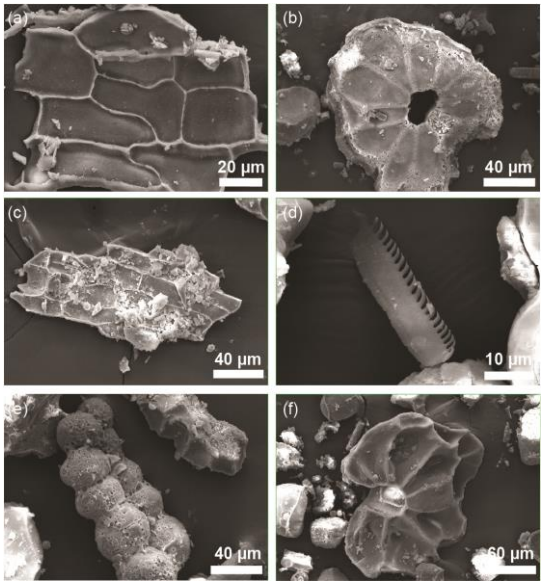

Figure E-5 : Examples of phytoliths found in the Jurien Bay and Guilderton soils. Phytoliths from image (a), (b), (c) and (e) were found in the topsoil of Guilderton stage 4 and those from image (d) and (f) were found in the topsoil of Jurien Bay stage 4.

Table E-1 – Results of the mixed-effect models considering the 13 species for which intraspecific variation in foliar concentrations of rock-derived elements (including Si) with respect to soil age were estimated.

Foliar concentration	Slope (Chronosequence stage)	p-value
Si	0.50	<0.05
P	-0.24	<0.01
Ca	-1.27	<0.01
Mg	-0.36	<0.01
K	0.49	0.18

Table E-2 – Total number of plant species sampled for foliar chemical analyses per chronosequence stage (with five plots per stage) at Jurien Bay. Soil age increases with increasing chronosequence stage.

Chronosequence stage	Number of species sampled
1	18
2	22
3	16
4	25
6	31

Appendix F : Supplementary Material of Chapter 5

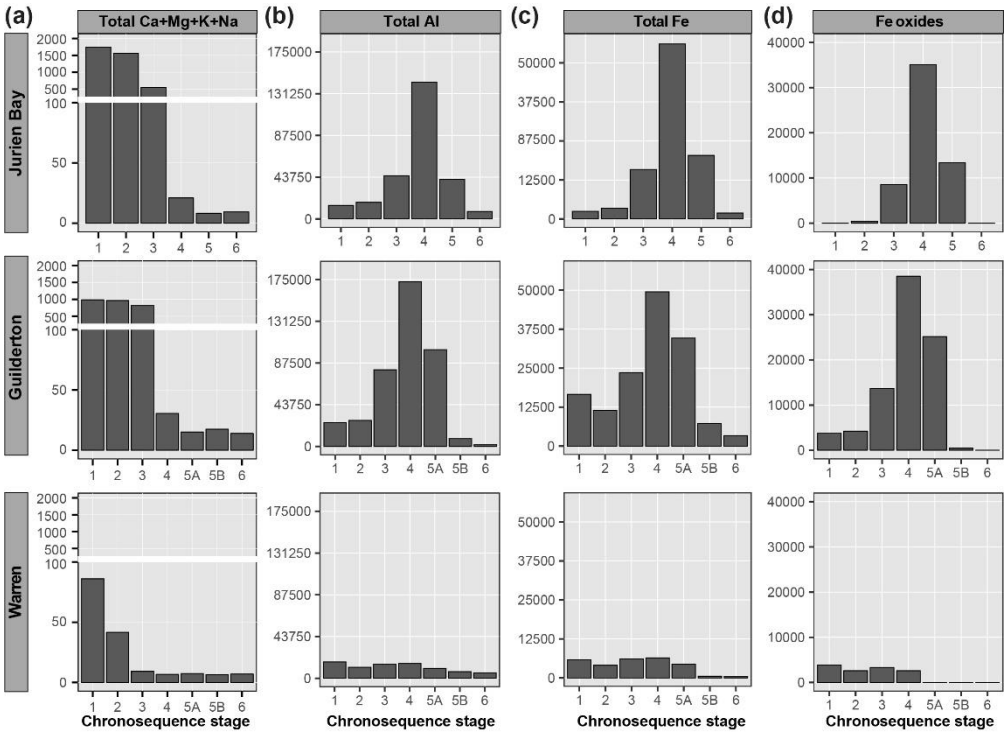

Figure F-1 : One-meter, depth-weighted mean, sum of total Ca, Mg, K and Na in $cmol_c\ kg^{-1}$ across the chronosequences (a). One-meter depth stocks of total Al (b), total Fe (c) and Fe oxides (Fe extracted with DCB) (d) in $kg\ ha^{-1}$. Soil age increases with increasing chronosequence stage.

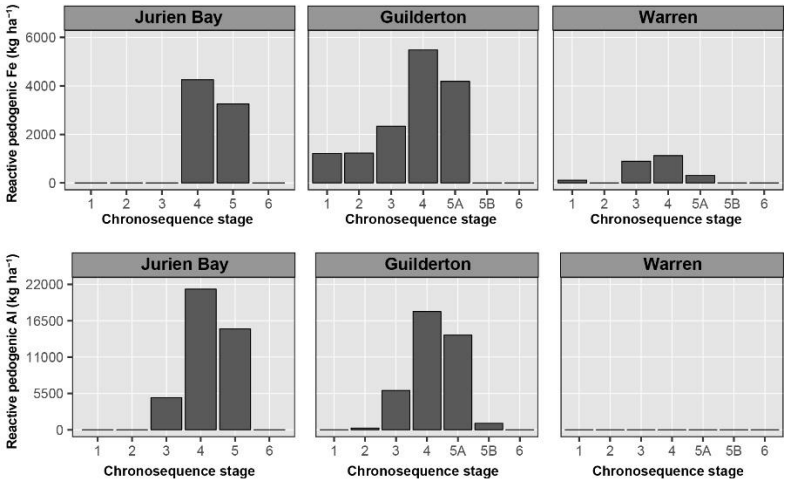

Figure F-2 : One-meter depth stocks of Fe and Al extracted with oxalate (pedogenic reactive Fe and Al), in kg ha^{-1}. Soil age increases with increasing chronosequence stage.

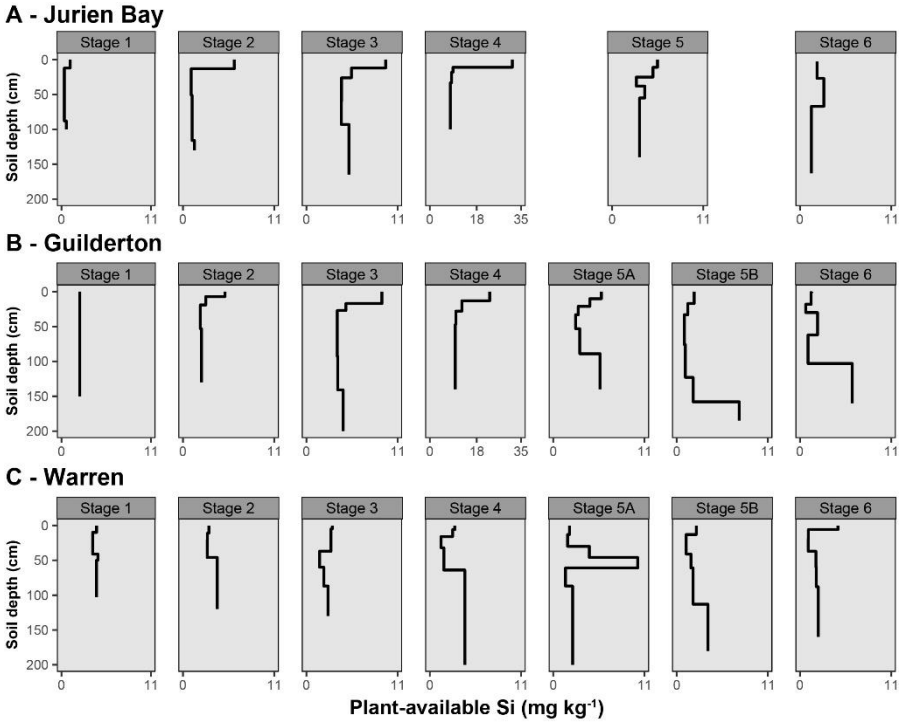

Figure F-3 : Depth distribution of plant-available Si concentrations (mg kg^{-1}) across the chronosequence stages. Soil age increases with increasing chronosequence stage.

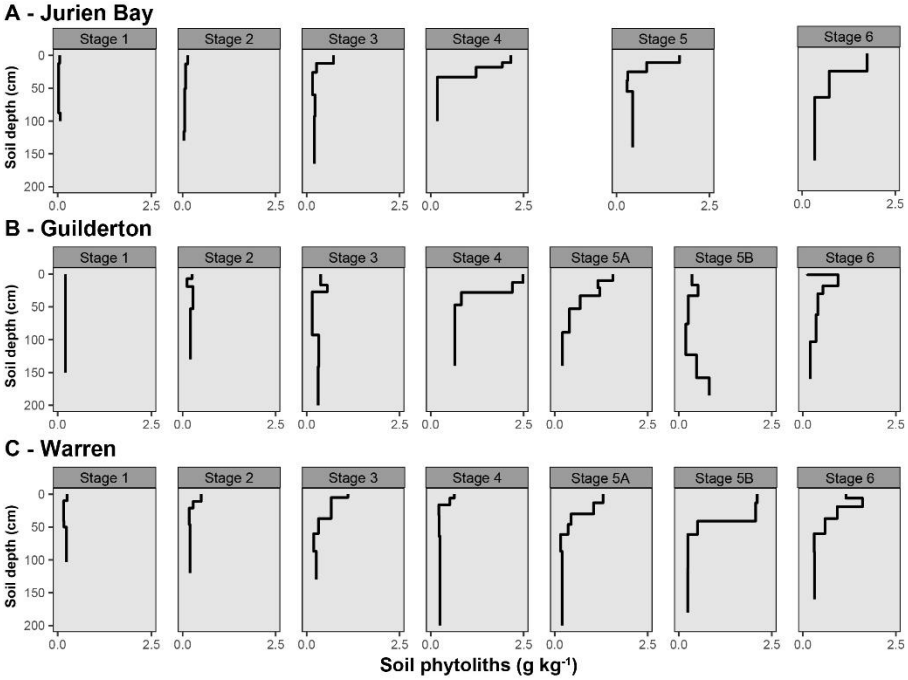

Figure F-4 : Depth distribution of soil phytoliths concentrations (g kg^{-1}) across the chronosequence stages. Soil age increases with increasing chronosequence stage.

Appendix G : Supplementary Material of Chapter 6

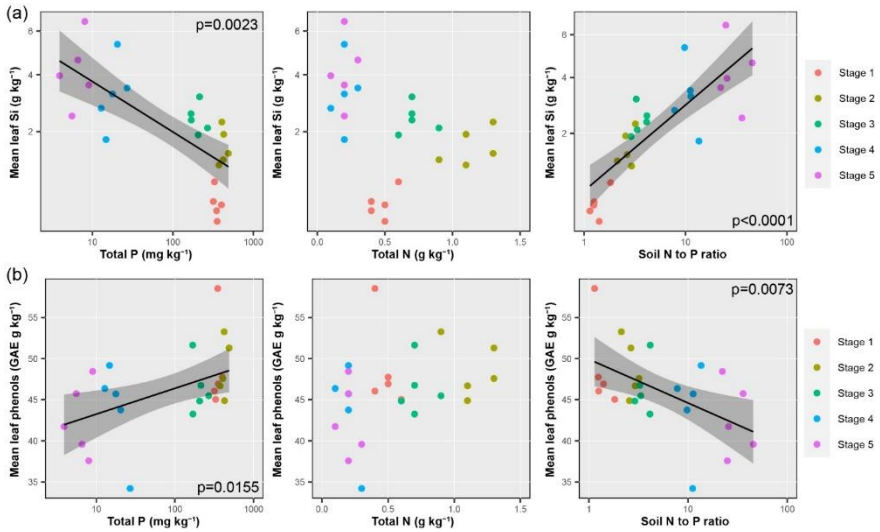

Figure G-1 : Soil total phosphorus (P) concentrations, total nitrogen (N) concentrations and soil N to P ratio versus mean leaf silicon (Si) concentrations (a) and mean leaf total phenol concentrations (b) (n = 25 plots). Black lines indicate the regression lines between both variables, shaded areas represent 95% confidence interval of the regression and colors of the circles indicate the chronosequence stages. Axes were log-transformed for soil total P concentration and N to P ratio and root-square-transformed for mean leaf Si concentrations. The p-values of the corresponding linear mixed-effect models are indicated if < 0.05. Regression lines were removed if the model p-values were > 0.05.

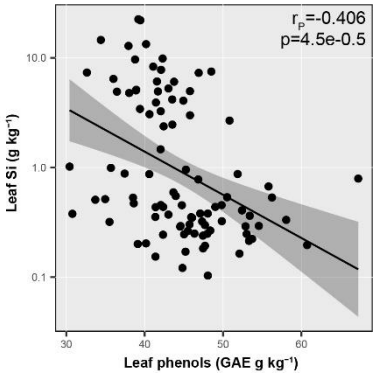

Figure G-2 : Relationship between concentrations of leaf total phenols and leaf silicon (Si) considering species means of all individuals considered in this study. The Pearson correlation coefficient (r_P) is shown, with the associated p-value. The y-axis is log-transformed.

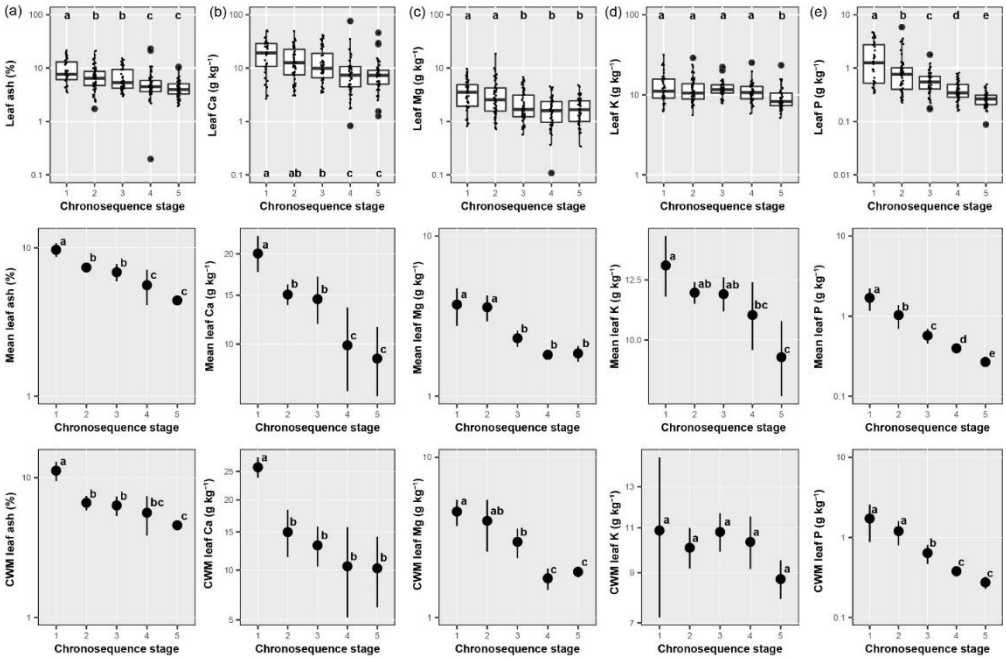

Figure G-3 : Concentrations of leaf ash (a), calcium (Ca) (b), magnesium (Mg) (c), potassium (K) (d) and phosphorus (P) (e) across the chronosequence stages considering all individuals and the means and cover-weighted means (CWM) of the 25 communities (n=5). For the box-plots, the small black dots indicate the species, large black dots represent outliers (outside 1.5*inter-quartile range), and Fisher LSD groupings ($p<0.05$) were performed on log-transformed data, as the scales of the axes. For the plots considering means and CWM, black dots indicate means and bars show 95% confidence intervals (n=5). Fisher LSD groupings ($p<0.05$) were performed on log-transformed data for ash, Mg and P and square-root-transformed data for Ca and K, as the scales of the axes.

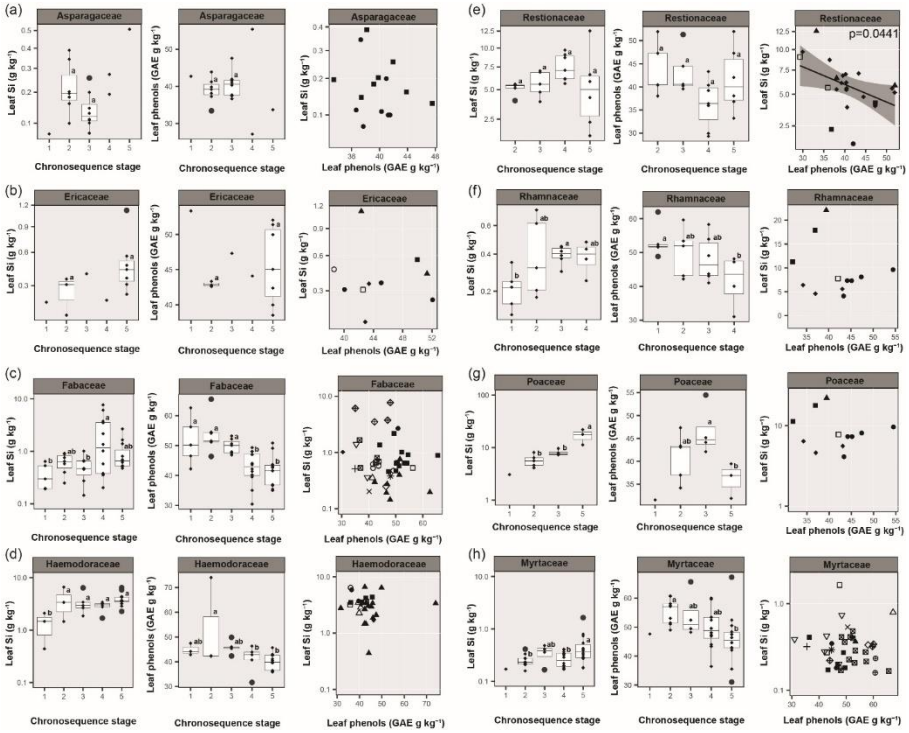

Figure G-4 : Leaf concentrations of silicon (Si) and total phenols across the chronosequence stages and relationship between both for Asparagaceae (a), Ericaceae (b), Fabaceae (c), Haemodoraceae (d), Restionaceae (e), Rhamnaceae (f), Poaceae (g) and Myrtaceae (h). In the box-plots, the black diamonds indicate the species and large black dots represent outliers (outside 1.5*inter-quartile range). Box-plots and means were not shown when n<3. For leaf [Si], Fisher LSD groupings ($p<0.05$) were performed on log-transformed data in (c), (d), (g), (h) and square-root-transformed data in (a), (b), (e), (f), as the scales of the axes. In the third panels, different symbols represent different species, black lines indicate the regression lines between both variables and shaded areas represent 95% confidence intervals of the regressions. The p-values of the corresponding linear mixed-effect models are indicated if < 0.05. Regression lines were removed if the model p-values were > 0.05.

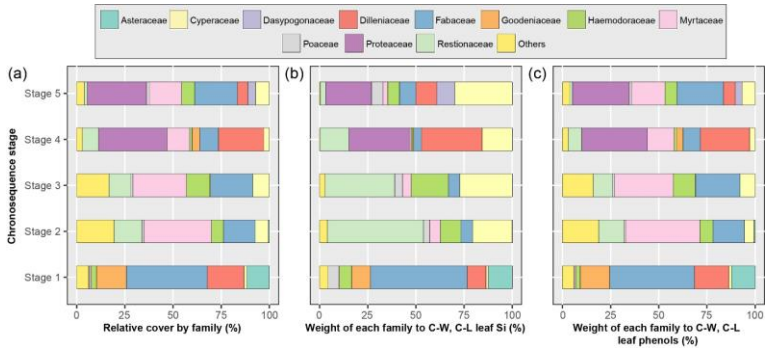

Figure G-5 : Relative cover of each plant family considered in this study (a). Weight of each family to the cover-weighted (C-W), community-level (C-L) leaf silicon concentration (Si), part (b), and leaf total phenols concentration (phenols), part (c).

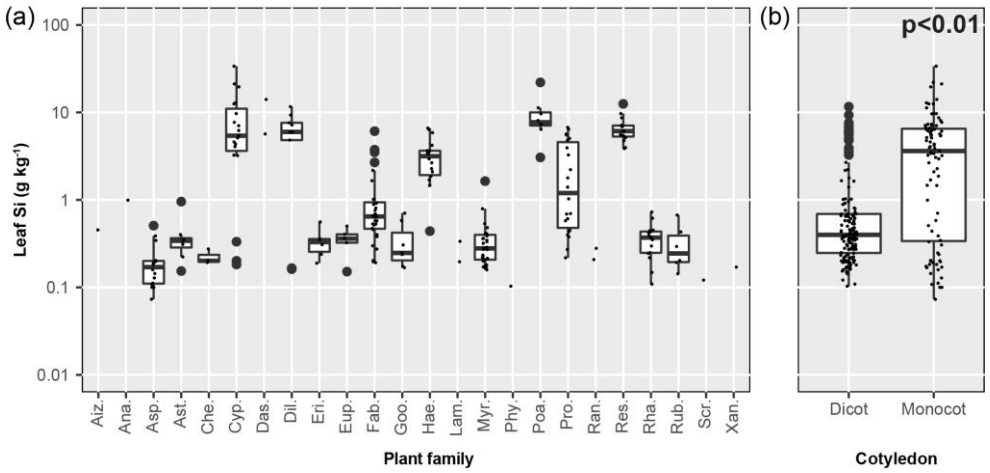

Figure G-6 : Box-plots showing leaf silicon (Si) concentrations in different plant families (a) and as in monocot/dicot species (b) for all individuals. Small black dots represent each species and large black dots represent outliers (outside 1.5*inter-quartile range). Scales are logarithmic. In (a), box-plots were not shown when n<3 and plant families were abbreviated by the first three letters along the x-axis. In (b), a t-test was performed to examine the differences in leaf Si concentration between dicots and monocots.

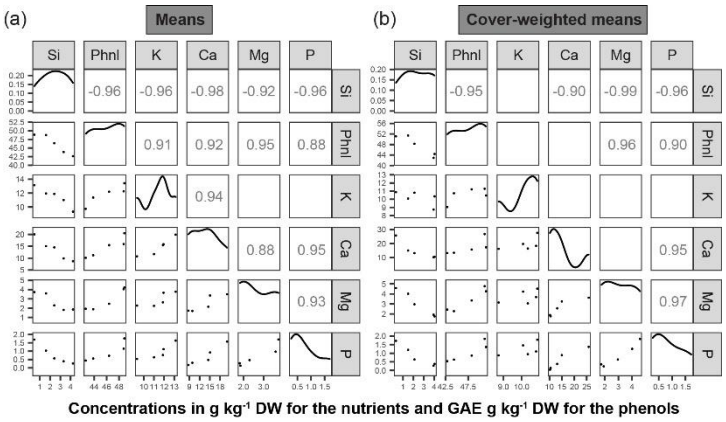

Figure G-7 : Scatterplot correlation matrices of leaf concentrations of silicon (Si), total phenols (Phnl), potassium (K), calcium (Ca), magnesium (Mg) and phosphorus (P) considering the means per chronosequence stage (a) or the cover-weighted means (b). The Pearson correlation coefficient is listed when its p-value < 0.05. Plots on the diagonal represent the distributions of each variable. Concentrations are in gram per kilogram of dry weight for the nutrients, and gallic acid equivalent (GAE) gram per kilogram of dry weight for the total phenols.

Table G-1 – Results of the mixed-effect models considering the seven species for which intraspecific variation in foliar concentrations of silicon and total phenols with respect to chronosequence stage were estimated.

Foliar concentration	Slope (Chronosequence stage)	DF	p-value
Silicon	0.60	77	0.0230
Total phenols	-2.19	77	0.0051

Table G-2 – Plant-available silicon (Si) concentrations across five chronosequence stages (n= 15; mean ± 95% confidence intervals). Fisher LSD groupings (bold letters; $p<0.05$) were performed on square-root-transformed data.

Stage	Plant-available Si (mg kg^{-1})
Stage 1	1.5 ± 0.4**c**
Stage 2	1.5 ± 0.2**c**
Stage 3	4.0 ± 0.3**b**
Stage 4	9.4 ± 1.0**a**
Stage 5	4.3 ± 0.2**b**

Table G-3 – Relationship between leaf silicon (Si) and plant-available Si concentration for the seven species considered for intra-specific variation. The p-values of the corresponding linear mixed-effect models are indicated.

Species	**Number of samples**	**Range of leaf Si (g kg^{-1})**	**Slope (plant-available Si)**	**DF**	**p-value**
Lepidosperma calcicola **(Cyperaceae)**	9	3.2-9.7	1.025	5	0.0190
Conostylis candicans **subsp.** ***Calcicola*** **(Haemodoraceae)**	14	0.4-6.6	0.096	9	0.5805
Desmocladus asper **(Restionaceae)**	15	3.9-9.7	0.295	11	0.0083
Stenanthemum notiale **subsp.** ***Notiale*** **(Rhamnaceae)**	12	0.2-0.5	0.022	8	0.0790
Acanthocarpus preissii **(Asparagaceae)**	10	0.1-0.4	0.005	5	0.6449
Acacia lasiocarpa **var.** ***lasiocarpa*** **(Fabaceae)**	12	0.5-2.2	0.150	7	0.0104
Melaleuca systena **(Myrtaceae)**	13	0.2-0.5	0.004	8	0.7506

Appendix H : Supplementary Material of Chapter 10

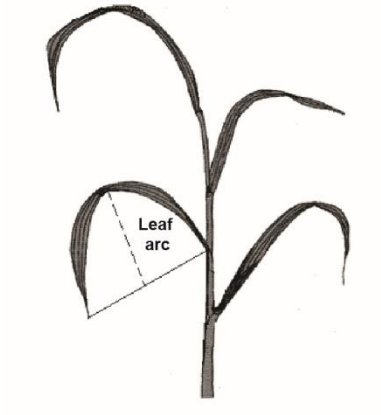

Figure H-1 : Schematic representation of the leaf arc measurement adapted from Zanão Júnior *et al.* (2010). The leaf arc is the distance between the midpoint of the line joining the apex to the point of blade insertion-sheath and the midpoint on the adaxial surface of the leaf.

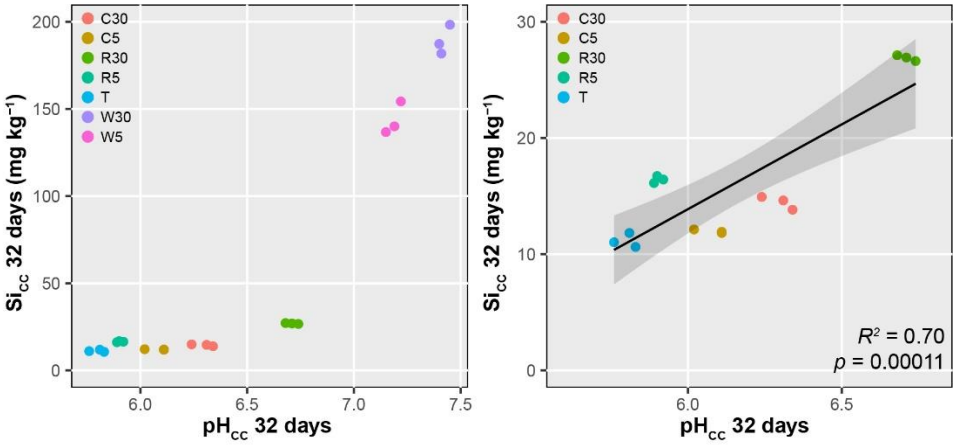

Figure H-2 : Plots of pH versus Si in the $CaCl_2$ 0.01M extract after 32 days. The second plot is a zoom of the first plot. The colors indicate the different treatments. In the second plot, the coefficient of determination (R^2) and p-value of the regressions are shown, and the shaded areas represent 95% confidence intervals.

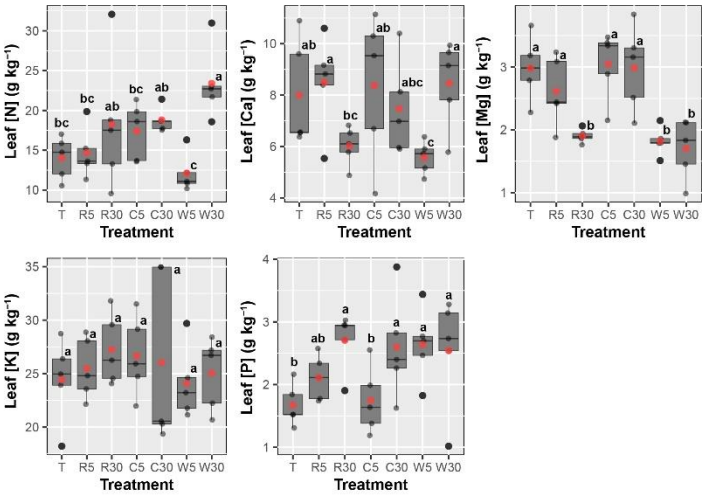

Figure H-3 : Boxplot of leaf N, Ca, Mg, K and P concentrations for the different amendments. The central horizontal bar in each box shows the median, the box represents the interquartile range (IQR), the whiskers show the location of the most extreme data points that are still within a factor of 1.5 of the upper or lower quartiles, and the large black points are values that fall outside the whiskers. The small opaque black points represent the data (n = 5), and red points indicate the overall mean. The letters represent Fisher HSD groupings ($p \leq 0.05$).

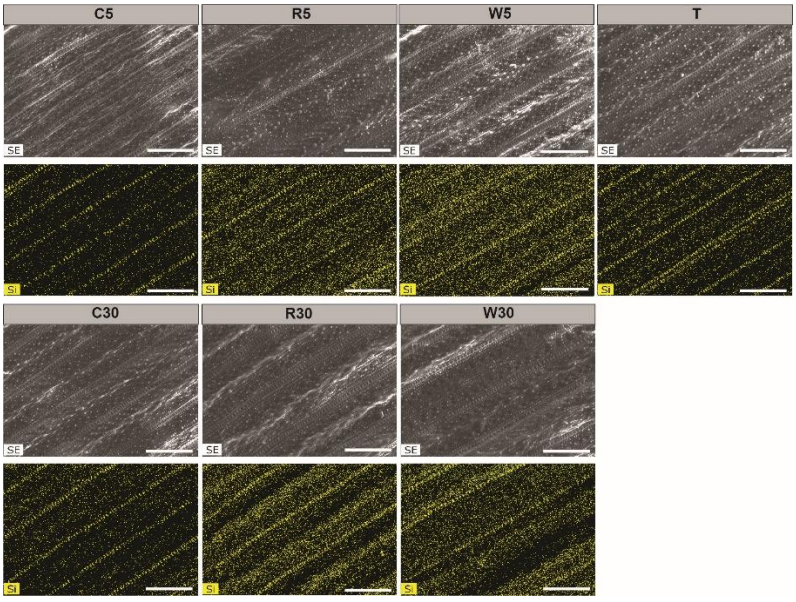

Figure H-4 : Images and Si mapping of leaf abaxial sides of rice plants from the different amendments. All scale bars are equivalent to 200 µm.

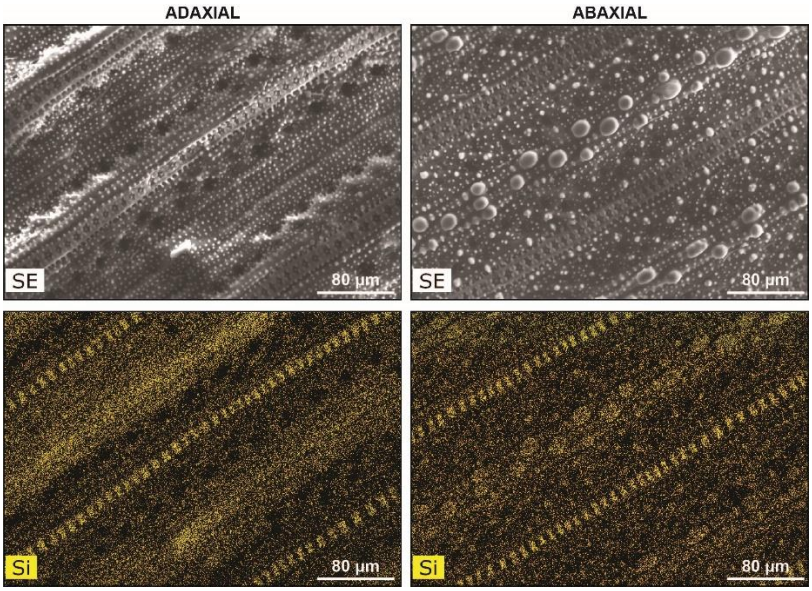

Figure H-5 : Examples of SEM-derived images and Si mappings (EDX) of leaf adaxial and abaxial sides of rice plants (amendment W5).

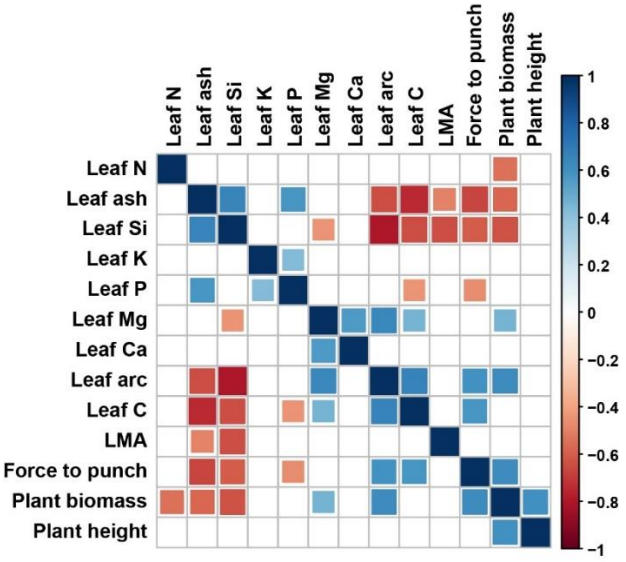

Figure H-6 : Correlation matrix of leaf traits and nutrient concentrations for all individuals (n=35). The color and size of the squares represents Pearson's correlation coefficient. All coefficient having a p-values superior to 0.01 are represented by a blank square.

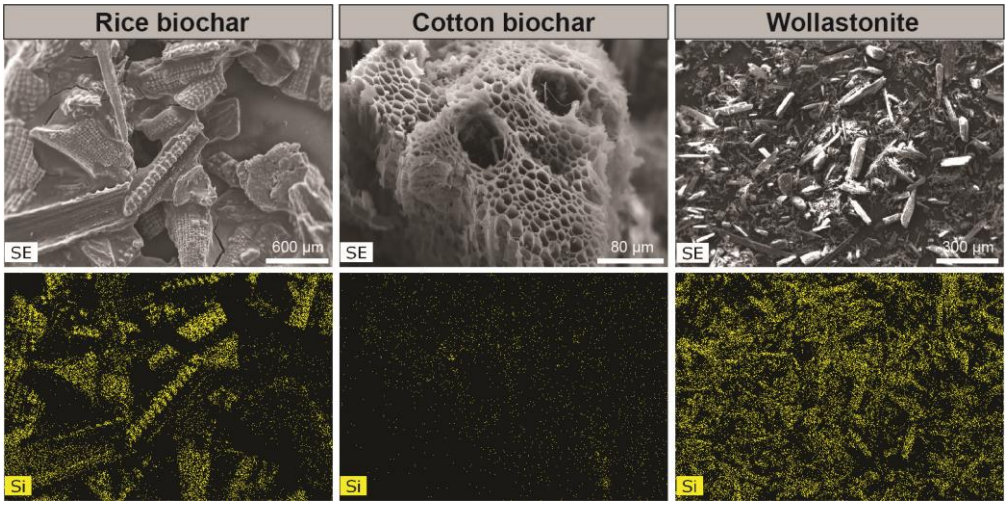

Figure H-7 : SEM-derived images and Si mappings (EDX) of the Si amendments used in this study.

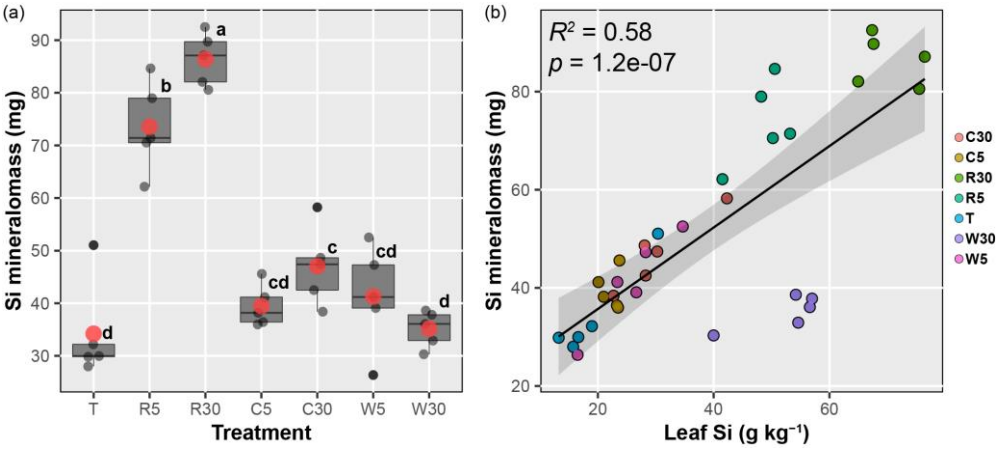

Figure H-8 : In (a), boxplot of rice leaf silicon mineralomass (leaf [Si] multiplied by plant biomass) for the different amendments. The central horizontal bar in each box shows the median, the box represents the interquartile range (IQR), the whiskers show the location of the most extreme data points that are still within a factor of 1.5 of the upper or lower quartiles, and the large black points are values that fall outside the whiskers. The small opaque black points represent the data (n = 5), and red points indicate the overall mean. The letters represent Fisher HSD groupings ($p \leq 0.05$). In (b), plots of rice leaf Si concentrations versus Si mineralomass (n = 35). The coefficient of determination (R2) and p-value of the regressions are shown. Shaded areas represent 95% confidence intervals. The colors of the dots indicate the treatment.

Table H-1 – pH measured in the 32-day $CaCl_2$ extractions. The standard-errors are indicated in brackets (n=3). The letters represent Fisher HSD groupings ($p \leq 0.05$).

Amendment	Input rate (t ha^{-1})	pH_{CC} – 32 days
Control (T)	-	5.8(0.0)g
Rice-biochar	5	5.9(0.0)f
Rice-biochar	30	6.7(0.0)c
Cotton-biochar	5	6.1(0.0)e
Cotton-biochar	30	6.3(0.0)d
Wollastonite	5	7.2(0.0)b
Wollastonite	30	7.4(0.0)a

References

Abbas, T., Rizwan, M., Ali, S., Zia-ur-Rehman, M., Farooq Qayyum, M., Abbas, F., *et al.* (2017). Effect of biochar on cadmium bioavailability and uptake in wheat (*Triticum aestivum* L.) grown in a soil with aged contamination. *Ecotoxicol. Environ. Saf.*, 140, 37–47.

Abbott, L.K., Robson, A.D. & De Boer, G. (1984). The effect of phosphorus on the formation of hyphae in soil by the vesicular-arbuscular mycorrhizal fungus, Glomus Fasciculatum. *New Phytol.*, 97, 437–446.

Abdalla, M., Hastings, A., Cheng, K., Yue, Q., Chadwick, D., Espenberg, M., *et al.* (2019). A critical review of the impacts of cover crops on nitrogen leaching, net greenhouse gas balance and crop productivity. *Glob. Chang. Biol.*, 25, 2530–2543.

Abrahão, A., Lambers, H., Sawaya, A.C.H.F., Mazzafera, P. & Oliveira, R.S. (2014). Convergence of a specialized root trait in plants from nutrient-impoverished soils: phosphorus-acquisition strategy in a nonmycorrhizal cactus. *Oecologia*, 176, 345–355.

Abrahão, A., Ryan, M.H., Laliberté, E., Oliveira, R.S. & Lambers, H. (2018). Phosphorus- and nitrogen-acquisition strategies in two *Bossiaea* species (Fabaceae) along retrogressive soil chronosequences in south-western Australia. *Physiol. Plant.*, 163, 323–343.

Acevedo, F.E., Peiffer, M., Ray, S., Tan, C. & Felton, G.W. (2021). Silicon-mediated enhancement of herbivore resistance in agricultural crops. *Front. Plant Sci.*, 12, 631824.

Adetunji, A.T., Ncube, B., Mulidzi, R. & Lewu, F.B. (2020). Management impact and benefit of cover crops on soil quality: A review. *Soil Tillage Res.*, 204, 104717.

Adrees, M., Ali, S., Rizwan, M., Zia-ur-rehman, M., Ibrahim, M., Abbas, F., *et al.* (2015). Ecotoxicology and Environmental Safety Mechanisms of silicon-mediated alleviation of heavy metal toxicity in plants : A review. *Ecotoxicol. Environ. Saf.*, 119, 186–197.

Aerts, R. & Chapin, F.S. (2000). The mineral nutrition of wild plants revisited: a re-evaluation of processes and patterns. *Adv. Ecol. Res.*, 30, 1–67.

Ahmed, E. & Holmström, S.J.M. (2014). Siderophores in environmental research: Roles and applications. *Microb. Biotechnol.*, 7, 196–208.

Alabouvette, C. (1999). Fusarium wilt suppressive soils: an example of disease-suppressive soils. *Australas. Plant Pathol.*, 28, 57–64.

Alabouvette, C., Olivain, C. & Steinberg, C. (2006). Biological control of plant diseases: the European situation. *Eur. J. Plant Pathol.*, 114, 329–341.

Aleman, J.C., Saint-Jean, A., Leys, B., Carcaillet, C., Favier, C. & Bremond, L. (2013). Estimating phytolith influx in lake sediments. *Quat. Res.*, 80, 341–347.

Alexandre, A., Basile-Doelsch, I., Delhaye, T., Borshneck, D., Mazur, J.C., Reyerson, P., *et al.* (2015). New highlights of phytolith structure and occluded carbon location: 3-D X-ray microscopy and NanoSIMS results. *Biogeosciences*, 12, 863–873.

Alexandre, A., Bouvet, M. & Abbadie, L. (2011). The role of savannas in the terrestrial Si cycle: A case-study from Lamto, Ivory Coast. *Glob. Planet. Change*, 78, 162–169.

Alexandre, A., Meunier, J.-D., Colin, F. & Koud, J.-M. (1997). Plant impact on the biogeochemical cycle of silicon and related weathering processes. *Geochim. Cosmochim. Acta*, 61, 677–682.

Alexandre, A., Webb, E., Landais, A., Piel, C., Devidal, S., Sonzogni, C., *et al.* (2019). Effects of grass leaf anatomy, development and light/dark alternation on the triple oxygen isotope signature of leaf water and phytoliths: insights for a new proxy of continental atmospheric humidity. *Biogeosciences Discuss.*

Altieri, M.A. (2002). Agroecology: the science of natural resource management for poor farmers in marginal environments. *Agric. Ecosyst. Environ.*, 93, 1–24.

Alvarez-Campos, O., Lang, T.A., Bhadha, J.H., McCray, J.M., Glaz, B. & Daroub, S.H. (2018). Biochar and mill ash improve yields of sugarcane on a sand soil in Florida. *Agric. Ecosyst. Environ.*, 253, 122–130.

Alves, L.A., Denardin, L.G. de O., Martins, A.P., Anghinoni, I., Carvalho, P.C. de F. & Tiecher, T. (2019). Soil acidification and P, K, Ca and Mg budget as affected by sheep grazing and crop rotation in a long-term integrated crop-livestock system in southern Brazil. *Geoderma*, 351, 197–208.

Amiotte Suchet, P., Probst, J.-L. & Ludwig, W. (2003). Worldwide distribution of continental rock lithology: Implications for the atmospheric/soil CO2 uptake by continental weathering and alkalinity river transport to the oceans. *Global Biogeochem. Cycles*, 17.

Ando, H., Kakuda, K.I., Fujii, H., Suzuki, K. & Ajiki, T. (2002). Growth and canopy structure of rice plants grown under field conditions as affected by si application. *Soil Sci. Plant Nutr.*, 48, 429–432.

Aplin, T.E.. & Cannon, J.R. (1971). Distribution of alkaloids in some Western Australian plants. *Econ. Bot.*, 25, 366–380.

Armani, M., Goodale, U.M., Charles-Dominique, T., Barton, K.E., Yao, X. & Tomlinson, K.W. (2020). Structural defence is coupled with the leaf economic spectrum across saplings of spiny species. *Oikos*.

Armbrust, E.V. (2009). The life of diatoms in the world's oceans. *Nature*, 459, 185–192.

Autin, A.T. (2002). Differential Effects of Precipitation on Production and Decomposition along a Rainfall Gradient in Hawaii. *Ecology*, 83, 328–338.

Ávila-Valdés, A., Piper, F.I. & Zúñiga-Feest, A. (2019). Cluster root formation and function vary in two species with contrasting geographic ranges. *Plant Soil*, 440, 25–38.

Ba, N.M., Dakouo, D., Nacro, S. & Karamage, F. (2008). Seasonal abundance of lepidopteran stemborers and diopsid flies in irrigated fields of cultivated (*Oryza sativa*) and wild rice (*Oryza longistaminata*) in western Burkina Faso. *Int. J. Trop. Insect Sci.*, 28, 30–36.

Babechuk, M.G., Widdowson, M. & Kamber, B.S. (2014). Quantifying chemical weathering intensity and trace element release from two contrasting basalt profiles, Deccan Traps, India. *Chem. Geol.*, 363, 56–75.

Babu, T., Tubana, B., Paye, W., Kanke, Y. & Datnoff, L. (2016). Establishing soil silicon test procedure and critical silicon level for rice in Louisiana soils. *Commun. Soil Sci. Plant Anal.*, 47, 1578–1597.

Banfield, J.F., Barker, W.W., Welch, S.A. & Taunton, A. (1999). Biological impact on mineral dissolution: Application of the lichen model to understanding mineral weathering in the rhizosphere. *Proc. Natl. Acad. Sci. U. S. A.*, 96, 3404–3411.

Barão, L., Clymans, W., Vandevenne, F., Meire, P., Conley, D.J. & Struyf, E. (2014). Pedogenic and biogenic alkaline-extracted silicon distributions along a temperate land-use gradient. *Eur. J. Soil Sci.*, 65, 693–705.

Bardgett, R.D. & Wardle, D.A. (2003). Herbivore-mediated linkages between aboveground and belowground communities. *Ecology*, 84, 2258–2268.

Barker, W.W., Welch, S.A., Chu, S. & Banfield, J.F. (1998). Experimental observations of the effects of bacteria on aluminosilicate weathering. *Am. Mineral.*, 83, 1551–1563.

Bartoli, F. (1983). The biogeochemical cycle of silicon in two temperate forest ecosystems. *Ecol. Bull.*, 35, 469–476.

Bartoli, F. & Souchier, B. (1978). Cycle et rôle du silicium d'origine végétale dans les écosystèmes forestiers tempérés. *Ann. des Sci. For.*, 35, 187–202.

Bastian, L. V. (1996). Residual soil mineralogy and dune subdivision, swan coastal plain, Western Australia. *Aust. J. Earth Sci.*, 43, 31–44.

Bateman, J.B., Chadwick, O.A. & Vitousek, P.M. (2019). Quantitative Analysis of Pedogenic Thresholds and Domains in Volcanic Soils. *Ecosystems*.

Bauer, P., Elbaum, R. & Weiss, I.M. (2011). Calcium and silicon mineralization in land plants: Transport, structure and function. *Plant Sci.*, 180, 746–756.

Baxter, I.R., Vitek, O., Lahner, B., Muthukumar, B., Borghi, M., Morrissey, J., *et al.* (2008). The leaf ionome as a multivariable system to detect a plant's physiological status. *Proc. Natl. Acad. Sci. U. S. A.*, 105, 12081–12086.

Beasley, D.E., Koltz, A.M., Lambert, J.E., Fierer, N. & Dunn, R.R. (2015). The evolution of stomach acidity and its relevance to the human microbiome. *PLoS One*, 10, 1–12.

Beckwith, R.S. & Reeve, R. (1964). Studies on soluble silica in soils. II. The release of monosilicic acid from soils. *Aust. J. Soil Res.*, 2, 33–45.

Bennett, P.C., Melcer, M.E., Siegel, D.. & Hassett, J.P. (1988). The dissolution of quartz in dilute aqueous solutions of organic acids at 25°C. *Geochim. Cosmochim. Acta*, 52, 1521–1530.

Bennett, P.C., Rogers, J.R., Choi, W.J. & Hiebert, F.K. (2001). Silicates, silicate weathering, and microbial ecology. *Geomicrobiol. J.*, 18, 3–19.

Berner, R.A., Lasaga, A.C. & Garrels, R.M. (1983). The carbonate- silicate geochemical cycle and its effect on atmospheric carbon dioxide over the past 100 million years. *Am. J. Sci.*, 283, 641–683.

Bettaieb Rebey, I., Bourgou, S., Ben Kaab, S., Aidi Wannes, W., Ksouri, R., Saidani Tounsi, M., *et al.* (2020). On the effect of initial drying techniques on essential oil composition, phenolic compound and antioxidant properties of anise (*Pimpinella anisum* L.) seeds. *J. Food Meas. Charact.*, 14, 220–228.

Bhat, J.A., Kundu, M.C., Hazra, G.C., Santra, G.H. & Mandal, B. (2010). Rehabilitating acid soils for increasing crop productivity through low-cost liming material. *Sci. Total Environ.*, 408, 4346–4353.

Bidle, K.D. & Azam, F. (1999). Accelerated dissolution of diatom silica by marine bacterial assemblages. *Nature*, 397, 508–512.

Biederman, L.A. & Stanley Harpole, W. (2013). Biochar and its effects on plant productivity and nutrient cycling: A meta-analysis. *GCB Bioenergy*, 5, 202–214.

Bist, V., Niranjan, A., Ranjan, M., Lehri, A., Seem, K. & Srivastava, S. (2020). Silicon-solubilizing media and its implication for characterization of bacteria to mitigate biotic stress. *Front. Plant Sci.*, 11, 28.

Bityutskii, N., Kaidun, P. & Yakkonen, K. (2016). Earthworms can increase mobility and bioavailability of silicon in soil. *Soil Biol. Biochem.*, 99, 47–53.

Blackman, E. & Bailey, C.B. (1971). Dissolution of silica from dried grass in nylon bags placed in the rumen of a cow. *Can. J. Anim. Sci.*, 51, 327–332.

Blake, R.E. & Walter, L.M. (1999). Kinetics of feldspar and quartz dissolution at 70-80°C and near-neutral pH: Effects of organic acids and NaCl. *Geochim. Cosmochim. Acta*, 63, 2043–2059.

Blamey, F.P.C., McKenna, B.A., Li, C., Cheng, M., Tang, C., Jiang, H., *et al.* (2018). Manganese distribution and speciation help to explain the effects of silicate and phosphate on manganese toxicity in four crop species. *New Phytol.*, 217, 1146–1160.

Blecker, S.W., McCulley, R.L., Chadwick, O.A. & Kelly, E.F. (2006). Biologic cycling of silica across a grassland bioclimosequence. *Global Biogeochem. Cycles*, 20, 1–11.

Blouin, M., Hodson, M.E., Delgado, E.A., Baker, G., Brussaard, L., Butt, K.R., *et al.* (2013). A review of earthworm impact on soil function and ecosystem services. *Eur. J. Soil Sci.*, 64, 161–182.

Bonilla, P.S. (2001). Variation in the cellulose, lignin and silica contents of various parts of difference rice (Oryza sativa L.) cultivars. *Philipp. Agric. Sci.*, 84, 126–137.

Bosecker, K. (1997). Bioleaching: metal solubilization by microorganisms. *FEMS Microbiol. Lett.*, 20, 591–604.

Boudon, G., Dagain, J., Semet, M.P. & Westercamp, D. (1987). Carte géologique 1: 20 000 du massif volcanique de la Soufrière (Département de la Guadeloupe, Petites Antilles). *BRGM, Paris*.

Brantley, S.L. (2008). Kinetics of mineral dissolution. In: *Kinetics of water–rock interaction* (eds. Brantley, S.L., Kubicki, J.D. & White, A.F.). New York: Springer Science & Business Media., pp. 151–210.

Bray, A.W., Oelkers, E.H., Bonneville, S., Wolff-Boenisch, D., Potts, N.J., Fones, G., *et al.* (2015). The effect of pH, grain size, and organic ligands on biotite weathering rates. *Geochim. Cosmochim. Acta*, 164, 127–145.

Van Breemen, N., Finlay, R., Lundström, U., Jongmans, A.G., Giesler, R. & Olsson, M. (2000). Mycorrhizal weathering: A true case of mineral plant nutrition?

Biogeochemistry, 49, 53–67.

Brewer, K.M. & Gaudin, A.C.M. (2020). Potential of crop-livestock integration to enhance carbon sequestration and agroecosystem functioning in semi-arid croplands. *Soil Biol. Biochem.*, 149, 107936.

Brightly, W.H., Hartley, S.E., Osborne, C.P., Simpson, K.J. & Strömberg, C.A.E. (2020). High silicon concentrations in grasses are linked to environmental conditions and not associated with C 4 photosynthesis. *Glob. Chang. Biol.*, 26, 7128–7143.

de Britto Costa, P., Staudinger, C., Veneklaas, E.J., Oliveira, R.S. & Lambers, H. (2021). Root positioning and trait shifts in *Hibbertia racemosa* as dependent on its neighbour's nutrient-acquisition strategy. *Plant Cell Environ.*, In press.

Brizuela, M.A., Detling, J.K. & Cid, M.S. (1986). Silicon Concentration of Grasses Growing in Sites With Different Grazing Histories. *Ecology*, 67, 1098–1101.

Brooke, B.P., Olley, J.M., Pietsch, T., Playford, P.E., Haines, P.W., Murray-Wallace, C. V., *et al.* (2014). Chronology of Quaternary coastal aeolianite deposition and the drowned shorelines of southwestern Western Australia - a reappraisal. *Quat. Sci. Rev.*, 93, 106–124.

Brooker, R.W., Bennett, A.E., Cong, W.F., Daniell, T.J., George, T.S., Hallett, P.D., *et al.* (2015). Improving intercropping: A synthesis of research in agronomy, plant physiology and ecology. *New Phytol.*, 206, 107–117.

Brucker, E., Kernchen, S. & Spohn, M. (2020). Release of phosphorus and silicon from minerals by soil microorganisms depends on the availability of organic carbon. *Soil Biol. Biochem.*, 143, 107737.

Brundrett, M.C. (2002). Coevolution of roots and mycorrhizas of land plants. *New Phytol.*, 154, 275–304.

Bryant, J.P., Chapin, F.S. & Klein, D.R. (1983). Carbon/nutrient balance of boreal plants in relation to vertebrate herbivory. *Oikos*, 40, 357–368.

Burghelea, C., Zaharescu, D.G., Dontsova, K., Maier, R., Huxman, T. & Chorover, J. (2015). Mineral nutrient mobilization by plants from rock: influence of rock type and arbuscular mycorrhiza. *Biogeochemistry*, 124, 187–203.

Búrquez, A. (1987). Leaf thickness and water deficit in plants: A tool for field studies. *J. Exp. Bot.*, 38, 109–114.

Buss, H.L., Lüttge, A. & Brantley, S.L. (2007). Etch pit formation on iron silicate surfaces during siderophore-promoted dissolution. *Chem. Geol.*, 240, 326–342.

Cai, K., Gao, D., Luo, S., Zeng, R., Yang, J. & Zhu, X. (2008). Physiological and cytological mechanisms of silicon-induced resistance in rice against blast

disease. *Physiol. Plant.*, 134, 324–333.

Cakmak, I., Sari, N., Marschner, H., Ekiz, H., Kalayci, M., Yilmaz, A., *et al.* (1996). Phytosiderophore release in bread and durum wheat genotypes differing in zinc efficiency. *Plant Soil*, 180, 183–189.

Calvaruso, C., Turpault, M.P. & Frey-Klett, P. (2006). Root-associated bacteria contribute to mineral weathering and to mineral nutrition in trees: A budgeting analysis. *Appl. Environ. Microbiol.*, 72, 1258–1266.

Cama, J. & Ganor, J. (2006). The effects of organic acids on the dissolution of silicate minerals: A case study of oxalate catalysis of kaolinite dissolution. *Geochim. Cosmochim. Acta*, 70, 2191–2209.

Camargo, M.S. de, Amorim, L. & Gomes Junior, A.R. (2013). Silicon fertilisation decreases brown rust incidence in sugarcane. *Crop Prot.*, 53, 72–79.

Cappelli, S.L., Pichon, N.A., Kempel, A. & Allan, E. (2020). Sick plants in grassland communities: a growth-defense trade-off is the main driver of fungal pathogen abundance. *Ecol. Lett.*, 23, 1349–1359.

Carey, J.C., Abbott, B.W. & Rocha, A. V. (2019). Plant uptake offsets silica release from a large Arctic tundra wildfire. *Earth's Futur.*

Carey, J.C. & Fulweiler, R.W. (2012). The Terrestrial Silica Pump. *PLoS One*, 7.

Carey, J.C. & Fulweiler, R.W. (2016). Human appropriation of biogenic silicon – the increasing role of agriculture. *Funct. Ecol.*, 30, 1331–1339.

Carey, J.C., Parker, T.C., Fetcher, N. & Tang, J. (2017). Biogenic silica accumulation varies across tussock tundra plant functional type. *Funct. Ecol.*, 1–11.

Carlos, F.S., Oliveira Denardin, L.G., Martins, A.P., Anghinoni, I., Faccio Carvalho, P.C., Rossi, I., *et al.* (2020). Integrated crop–livestock systems in lowlands increase the availability of nutrients to irrigated rice. *L. Degrad. Dev.*, 31, 2962–2972.

Carpenter, D., Hodson, M.E., Eggleton, P. & Kirk, C. (2007). Earthworm induced mineral weathering: Preliminary results. *Eur. J. Soil Biol.*, 43, 176–183.

Castro, G.S.A. & Crusciol, C.A.C. (2013). Yield and mineral nutrition of soybean, maize, and congo signal grass as affected by limestone and slag. *Pesqui. Agropecu. Bras.*, 48, 673–681.

Caubet, M., Cornu, S., Saby, N.P.A. & Meunier, J.-D. (2020). Agriculture increases the bioavailability of silicon, a beneficial element for crop, in temperate soils. *Sci. Rep.*, 10, 19999.

Chadwick, O.A. & Chorover, J. (2001). The chemistry of pedogenic thresholds. *Geoderma*, 100, 321–353.

Chadwick, O.A., Derry, L.A., Vitousek, P.M., Huebert, B.J. & Hedin, L.O. (1999). Changing sources of nutrients during four million years ofecosystem development. *Nature*, 397, 1–7.

Chadwick, O.A., Gavenda, R.T., Kelly, E.F., Ziegler, K., Olson, C.G., Crawford Elliott, W., *et al.* (2003). The impact of climate on the biogeochemical functioning of volcanic soils. *Chem. Geol.*, 202, 195–223.

Chandrakala, C., Voleti, S.R., Bandeppa, S., Sunil Kumar, N. & Latha, P.C. (2019). Silicate solubilization and plant growth promoting potential of *Rhizobium* Sp. isolated from rice rhizosphere. *Silicon*, 11, 2895–2906.

Chang, C.C. & Turner, B.L. (2019). Ecological succession in a changing world. *J. Ecol.*, 107, 503–509.

Chao, T.T. & Sanzolone, R.F. (1992). Decomposition techniques. *J. Geochemical Explor.*, 44, 65–106.

Chen, C.R., Hou, E.Q., Condron, L.M., Bacon, G., Esfandbod, M., Olley, J., *et al.* (2015). Soil phosphorus fractionation and nutrient dynamics along the Cooloola coastal dune chronosequence, southern Queensland, Australia. *Geoderma*, 257–258, 4–13.

Chiba, Y., Mitani, N., Yamaji, N. & Ma, J.F. (2009). HvLsi1 is a silicon influx transporter in barley. *Plant J.*, 57, 810–818.

Christl, I., Brechbühl, Y., Graf, M. & Kretzschmar, R. (2012). Polymerization of silicate on hematite surfaces and its influence on arsenic sorption. *Environ. Sci. Technol.*, 46, 13235–13243.

Churchman, G.J. & Lowe, D.. (2012). Alteration, formation, and occurrence of minerals in soils. *Handb. Soil Sci. Prop. Process.*, 1, 20–72.

Cid, M.S., Detling, J.K., Brizuela, M.A. & Whicker, A.D. (1989). Patterns in grass silicifieation: response to grazing history and defoliation. *Oecologia*, 80, 268–271.

Ciesielski, H., Proix, N. & Sterckeman, T. (1997). Détermination des incertitudes liées à une méthode de mise en solution des sols et sédiments par étude interlaboratoire. *Analusis*, 25, 188–192.

Clark, R.B. & Zeto, S.K. (1996). Mineral acquisition by mycorrhizal maize grown on acid and alkaline soil. *Soil Biol. Biochem.*, 28, 1495–1503.

Clark, R.B. & Zeto, S.K. (2000). Mineral acquisition by arbuscular mycorrhizal plants. *J. Plant Nutr.*, 23, 867–902.

Clymans, W., Struyf, E., Govers, G., Vandevenne, F. & Conley, D.J. (2011). Anthropogenic impact on amorphous silica pools in temperate soils. *Biogeosciences*, 8, 2281–2293.

Coley, P.D., Bryant, J.P. & Chapin, F.S. (1985). Resource availability and plant antiherbivore defense. *Science (80-.).*, 230, 895–899.

Colmet-Daage, F. & Lagache, P. (1965). Caratéristiques de quelques groupes de sols dérivés de roches volcaniques aux antilles françaises. *Cah. ORSTOM. Série Pédologie*, 3, 91–121.

Colombo, C., Palumbo, G., He, J.Z., Pinton, R. & Cesco, S. (2014). Review on iron availability in soil: Interaction of Fe minerals, plants, and microbes. *J. Soils Sediments*, 14, 538–548.

Cong, W.F., Hoffland, E., Li, L., Six, J., Sun, J.H., Bao, X.G., *et al.* (2015). Intercropping enhances soil carbon and nitrogen. *Glob. Chang. Biol.*, 21, 1715–1726.

Conley, D.J. & Carey, J.C. (2015). Biogeochemistry: Silica cycling over geologic time. *Nat. Geosci.*, 8, 431–432.

Cook, R.J. & Baker, K.F. (1983). *The nature and practice of biological control of plant pathogens.* American Phytopathological Society, St Paul, Minnesota, USA.

Cooke, J., DeGabriel, J.L. & Hartley, S.E. (2016). The functional ecology of plant silicon: geoscience to genes. *Funct. Ecol.*, 30, 1270–1276.

Cooke, J. & Leishman, M.R. (2011a). Is plant ecology more siliceous than we realise? *Trends Plant Sci.*, 16, 61–68.

Cooke, J. & Leishman, M.R. (2011b). Silicon concentration and leaf longevity: Is silicon a player in the leaf dry mass spectrum? *Funct. Ecol.*, 25, 1181–1188.

Cooke, J. & Leishman, M.R. (2012). Tradeoffs between foliar silicon and carbon-based defences: Evidence from vegetation communities of contrasting soil types. *Oikos*, 121, 2052–2060.

Cooke, J. & Leishman, M.R. (2016). Consistent alleviation of abiotic stress with silicon addition: a meta-analysis. *Funct. Ecol.*, 30, 1340–1357.

Corbineau, R., Reyerson, P.E., Alexandre, A. & Santos, G.M. (2013). Towards producing pure phytolith concentrates from plants that are suitable for carbon isotopic analysis. *Rev. Palaeobot. Palynol.*, 197, 179–185.

Cornelis, J.-T. & Delvaux, B. (2016). Soil processes drive the biological silicon feedback loop. *Funct. Ecol.*, 30, 1298–1310.

Cornelis, J.-T., Delvaux, B., Georg, R.B., Lucas, Y., Ranger, J. & Opfergelt, S. (2011a). Tracing the origin of dissolved silicon transferred from various soil-plant systems towards rivers: A review. *Biogeosciences*, 8, 89–112.

Cornelis, J.-T., Dumon, M., Tolossa, A.R., Delvaux, B., Deckers, J. & Van Ranst, E. (2014). The effect of pedological conditions on the sources and sinks of silicon in the vertic planosols in south-western ethiopia. *Catena*, 112, 131–138.

Cornelis, J.-T., Ranger, J., Iserentant, A. & Delvaux, B. (2010). Tree species impact the terrestrial cycle of silicon through various uptakes. *Biogeochemistry*, 97, 231–245.

Cornelis, J.-T., Titeux, H., Ranger, J. & Delvaux, B. (2011b). Identification and distribution of the readily soluble silicon pool in a temperate forest soil below three distinct tree species. *Plant Soil*, 342, 369–378.

Cornu, S., Lucas, Y., Ambrosi, J.P. & Desjardins, T. (1998). Transfer of dissolved Al, Fe and Si in two Amazonian forest environments in Brazil. *Eur. J. Soil Sci.*

Cornu, S., Montagne, D., Hubert, F., Barré, P. & Caner, L. (2012). Evidence of short-term clay evolution in soils under human impact. *Comptes Rendus - Geosci.*, 344, 747–757.

Coskun, D., Britto, D.T., Huynh, W.Q. & Kronzucker, H.J. (2016). The role of silicon in higher plants under salinity and drought stress. *Front. Plant Sci.*, 7, 1–7.

Coskun, D., Deshmukh, R., Sonah, H., Menzies, J.G., Reynolds, O., Ma, J.F., *et al.* (2019). The controversies of silicon's role in plant biology. *New Phytol.*, 221, 67–85.

Coughenour, M.B. (1985). Graminoid responses to grazing by large herbivores: adaptations, exaptations, and interacting processes. *Ann. Missouri Bot. Gard.*, 72, 852–863.

Covacevich, F., Echeverría, H.E. & Aguirrezabal, L.A.N. (2007). Soil available phosphorus status determines indigenous mycorrhizal colonization of field and glasshouse-grown spring wheat from Argentina. *Appl. Soil Ecol.*, 35, 1–9.

Crews, T.E., Kitayama, K., Fownes, J.H., Riley, R.H., Herbert, D.A., Mueller-Dombois, D., *et al.* (1995). Changes in soil phosphorus fractions and ecosystem dynamics across a long chronosequence in Hawaii. *Ecology*, 76, 1407–1424.

Crutzen, P.J. (2002). Geology of mankind. *Nature*, 415, 23.

Dakora, F.D. & Phillips, D.A. (2002). Root exudates as mediators of mineral acquisition in low-nutrient environments. *Plant Soil*, 245, 35–47.

Datnoff, L.E., Snyder, G.H. & Korndörfer, G.H. (2001a). *Silicon in Agriculture, Volume 8*.

Datnoff, L.E., Snyder, G.H. & Korndörfer, G.H. (2001b). The relationship between silicon and soil physical and chemical properties. In: *Silicon in Agriculture*. pp. 209–219.

Debona, D., Rodrigues, F.A. & Datnoff, L.E. (2017). Silicon's role in abiotic and biotic plant stresses. *Annu. Rev. Phytopathol.*, 55, 85–107.

Delgado-Baquerizo, M., Maestre, F.T., Gallardo, A., Bowker, M.A., Wallenstein, M.D., Quero, J.L., *et al.* (2013). Decoupling of soil nutrient cycles as a function of aridity in global drylands. *Nature*, 502, 672–676.

DeMaster, D.J. (1981). The supply and accumulation of silica in the marine environments. *Geochim. Cosmochim. Acta*, 45, 1715–1732.

Derry, L.A., Kurtz, A.C., Ziegler, K. & Chadwick, O.A. (2005). Biological control of terrestrial silica cycling and export fluxes to watersheds. *Nature*, 433, 728–731.

Deshmukh, R. & Bélanger, R.R. (2016). Molecular evolution of aquaporins and silicon influx in plants. *Funct. Ecol.*, 30, 1277–1285.

Deshmukh, R., Sonah, H. & Belanger, R.R. (2020). New evidence defining the evolutionary path of aquaporins regulating silicon uptake in land plants. *J. Exp. Bot.*, 71, 6775–6788.

Deshmukh, R.K., Vivancos, J., Guérin, V., Sonah, H., Labbé, C., Belzile, F., *et al.* (2013). Identification and functional characterization of silicon transporters in soybean using comparative genomics of major intrinsic proteins in Arabidopsis and rice. *Plant Mol. Biol.*, 83, 303–315.

Desplanques, V., Cary, L., Mouret, J.C., Trolard, F., Bourrié, G., Grauby, O., *et al.* (2006). Silicon transfers in a rice field in Camargue (France). *J. Geochemical Explor.*, 88, 190–193.

Deveau, A., Bonito, G., Uehling, J., Paoletti, M., Becker, M., Bindschedler, S., *et al.* (2018). Bacterial-fungal interactions: Ecology, mechanisms and challenges. *FEMS Microbiol. Rev.*, 42, 335–352.

Díaz, S., Kattge, J., Cornelissen, J.H.C., Wright, I.J., Lavorel, S., Dray, S., *et al.* (2016). The global spectrum of plant form and function. *Nature*, 529, 167–171.

Dincher, M., Calvaruso, C. & Turpault, M.-P. (2019). Major element residence times in humus from a beech forest: The role of element forms and recycling. *Soil Biol. Biochem.*, 141, 107674.

Dong, H., Kostka, J.E. & Kim, J. (2003). Microscopic evidence for microbial

dissolution of smectite. *Clays Clay Miner.*, 51, 502–512.

Dontsova, K., Balogh-Brunstad, Z. & Le Roux, G. (2020). *Biogeochemical Cycles: Ecological Drivers and Environmental Impact*. Geophysical Monograph Series. Wiley.

Dove, P.M. (1995). Kinetic and thermodynamic controls on silica reactivity in weathering environments. In: *Chemical Weathering Rates of Silicate Minerals*. pp. 235–290.

Drees, L.R., Wilding, L.P., Smeck, N.E. & Senkeyi, A.L. (1989). Silica in Soils: Quartz and Disordered Silica Polymorphs. In: *Minerals in Soil Environments*. pp. 913–974.

Drever, J.I. (1994). The effect of land plants on weathering rates of silicate minerals. *Geochim. Cosmochim. Acta*, 58, 2325–2332.

Drever, J.I. & Stillings, L.L. (1997). The role of organic acids in mineral weathering. *Colloids Surfaces A Physicochem. Eng. Asp.*, 120, 167–181.

Du, E., Terrer, C., Pellegrini, A.F.A., Ahlström, A., van Lissa, C.J., Zhao, X., *et al.* (2020). Global patterns of terrestrial nitrogen and phosphorus limitation. *Nat. Geosci.*, 13, 221–226.

Duchaufour, P. & Souchier, B. (1966). Note sur une méthode d'extraction combinée de l'aluminium et du fer libre dans les sols. *Bull. A.F.E.S*, 3, 161–175.

Ehrlich, H., Demadis, K.D., Pokrovsky, O.S. & Koutsoukos, P.G. (2010). Modern views on desilicification: Biosilica and abiotic silica dissolution in natural and artificial environments. *Chem. Rev.*, 110, 4656–4689.

Elliott, E.T., Palm, C.A., Reuss, D.E. & Monz, C.A. (1991). Organic matter contained in soil aggregates from a tropical chronosequence: Correction for sand and light fraction. *Agric. Ecosyst. Environ.*, 34, 443–451.

Elser, J.J., Bracken, M.E.S., Cleland, E.E., Gruner, D.S., Harpole, W.S., Hillebrand, H., *et al.* (2007). Global analysis of nitrogen and phosphorus limitation of primary producers in freshwater, marine and terrestrial ecosystems. *Ecol. Lett.*, 10, 1135–1142.

Endara, M.J. & Coley, P.D. (2011). The resource availability hypothesis revisited: A meta-analysis. *Funct. Ecol.*, 25, 389–398.

de Endredy, A.S. (1963). Estimation of free iron oxides in soils and clays by a photolytic method. *Clay Mineral. Bull.*, 5, 209–217.

Eneji, A.E., Inanaga, S., Muranaka, S., Li, J., Hattori, T., An, P., *et al.* (2008). Growth and nutrient use in four grasses under drought stress as mediated by silicon fertilizers. *J. Plant Nutr.*, 31, 355–365.

van der Ent, A., Casey, L.W., C. Blamey, C.P. & Kopittke, P.M. (2020). Time-resolved laboratory micro-X-ray fluorescence reveals silicon distribution in relation to manganese toxicity in soybean and sunflower. *Ann. Bot.*, 126, 331–341.

Epstein, E. (1994). The anomaly of silicon in plant biology. *Proc. Natl. Acad. Sci.*, 91, 11–17.

Epstein, E. (1999). Silicon. *Annu. Rev.Plant Physiol. Plant Mol. Biol.*, 50, 641–664.

Epstein, E. (2009). Silicon: Its manifold roles in plants. *Ann. Appl. Biol.*, 155, 155–160.

Euliss, K.W., Dorsey, B.L., Benke, K.C., Banks, M.K. & Schwab, A.P. (2005). The use of plant tissue silica content for estimating transpiration. *Ecol. Eng.*, 25, 343–348.

Euteneuer, P., Wagentristl, H., Steinkellner, S., Fuchs, M., Zaller, J.G., Piepho, H.P., *et al.* (2020). Contrasting effects of cover crops on earthworms: Results from field monitoring and laboratory experiments on growth, reproduction and food choice. *Eur. J. Soil Biol.*, 100, 103225.

Exley, C. (2015). A possible mechanism of biological silicification in plants. *Front. Plant Sci.*, 6, 1–7.

Exley, C. & Guerriero, G. (2019). A reappraisal of biological silicification in plants? *New Phytol.*, 1–3.

FAO. (2014). *Résidus agricoles et sous-produits agro-industriels en Afrique de l'Ouest*.

Farmer, V.C., Delbos, E. & Miller, J.D. (2005). The role of phytolith formation and dissolution in controlling concentrations of silica in soil solutions and streams. *Geoderma*, 127, 71–79.

Faucon, M.P., Houben, D. & Lambers, H. (2017). Plant Functional Traits : Soil and Ecosystem Services. *Trends Plant Sci.*

Fauteux, F., Chain, F., Belzile, F., Menzies, J.G. & Bélanger, R.R. (2006). The protective role of Si in the Arabidopsis-powdery mildew pathosystem. *Proc. Natl. Acad. Sci.*, 103, 17554–17559.

Fauteux, F., Rémus-Borel, W., Menzies, J.G. & Bélanger, R.R. (2005). Silicon and plant disease resistance against pathogenic fungi. *FEMS Microbiol. Lett.*, 249, 1–6.

Finlay, R.D., Mahmood, S., Rosenstock, N., Bolou-Bi, E.B., Köhler, S.J., Fahad, Z., *et al.* (2020). Reviews and syntheses: Biological weathering and its consequences at different spatial levels - From nanoscale to global scale.

Biogeosciences, 17, 1507–1533.

Fisher, R.A. (1929). A preliminary note on the effect of sodium silicate in increasing the yield of barley. *J. Agric. Sci.*, 19, 132–139.

Fishkis, O., Ingwersen, J. & Streck, T. (2009). Phytolith transport in sandy sediment: Experiments and modeling. *Geoderma*, 151, 168–178.

Fitzpatrick, R.W. & Chittleborough, D.J. (2002). Titanium and zirconium minerals. In: *Soil Mineralogy with Environmental Applications, Volume 7*. pp. 667–690.

Flemming, H.C. & Wingender, J. (2010). The biofilm matrix. *Nat. Rev. Microbiol.*, 8, 623–633.

Fonte, S.J., Nesper, M., Hegglin, D., Velásquez, J.E., Ramirez, B., Rao, I.M., *et al.* (2014). Pasture degradation impacts soil phosphorus storage via changes to aggregate-associated soil organic matter in highly weathered tropical soils. *Soil Biol. Biochem.*, 68, 150–157.

Forbes, E.S., Cushman, J.H., Burkepile, D.E., Young, T.P., Klope, M. & Young, H.S. (2019). Synthesizing the effects of large, wild herbivore exclusion on ecosystem function. *Funct. Ecol.*, 33, 1597–1610.

Fraysse, F., Cantais, F., Pokrovsky, O.S., Schott, J. & Meunier, J.D. (2006a). Aqueous reactivity of phytoliths and plant litter: Physico-chemical constraints on terrestrial biogeochemical cycle of silicon. *J. Geochemical Explor.*, 88, 202–205.

Fraysse, F., Pokrovsky, O.S. & Meunier, J.D. (2010). Experimental study of terrestrial plant litter interaction with aqueous solutions. *Geochim. Cosmochim. Acta*, 74, 70–84.

Fraysse, F., Pokrovsky, O.S., Schott, J. & Meunier, J.D. (2006b). Surface properties, solubility and dissolution kinetics of bamboo phytoliths. *Geochim. Cosmochim. Acta*, 70, 1939–1951.

Fraysse, F., Pokrovsky, O.S., Schott, J. & Meunier, J.D. (2009). Surface chemistry and reactivity of plant phytoliths in aqueous solutions. *Chem. Geol.*, 258, 197–206.

Freschet, G.T., Cornelissen, J.H.C., van Logtestijn, R.S.P. & Aerts, R. (2010). Evidence of the “plant economics spectrum” in a subarctic flora. *J. Ecol.*, 98, 362–373.

Frew, A., Powell, J.R., Allsopp, P.G., Sallam, N. & Johnson, S.N. (2017a). Arbuscular mycorrhizal fungi promote silicon accumulation in plant roots, reducing the impacts of root herbivory. *Plant Soil*, 419, 423–433.

Frew, A., Powell, J.R., Hiltpold, I., Allsopp, P.G., Sallam, N. & Johnson, S.N.

(2017b). Host plant colonisation by arbuscular mycorrhizal fungi stimulates immune function whereas high root silicon concentrations diminish growth in a soil-dwelling herbivore. *Soil Biol. Biochem.*, 112, 117–126.

Frew, A., Powell, J.R. & Johnson, S.N. (2020). Aboveground resource allocation in response to root herbivory as affected by the arbuscular mycorrhizal symbiosis. *Plant Soil*, 447, 463–473.

Frew, A., Powell, J.R., Sallam, N., Allsopp, P.G. & Johnson, S.N. (2016). Trade-offs between silicon and phenolic defenses may explain enhanced performance of root herbivores on phenolic-rich plants. *J. Chem. Ecol.*, 42, 768–771.

Frew, A., Weston, L.A., Reynolds, O.L. & Gurr, G.M. (2018). The role of silicon in plant biology: a paradigm shift in research approach. *Ann. Bot.*, 121, 1265–1273.

Gadd, G.M. (2017). Fungi, rocks, and minerals. *Elements*, 13, 171–176.

Gaillardet, J., Dupré, B., Louvat, P. & Allègre, C.J. (1999). Global silicate weathering and CO2 consumption rates deduced from the chemistry of large rivers. *Chem. Geol.*, 159, 3–30.

Gao, J., Wang, F., Ranathunge, K., Arruda, A.J., Cawthray, G.R., Clode, P.L., *et al.* (2020). Edaphic niche characterization of four Proteaceae reveals unique calcicole physiology linked to hyper-endemism of *Grevillea thelemanniana*. *New Phytol.*, 228, 869–883.

Garg, N. & Bhandari, P. (2016). Silicon nutrition and mycorrhizal inoculations improve growth, nutrient status, K+/Na+ ratio and yield of *Cicer arietinum* L. genotypes under salinity stress. *Plant Growth Regul.*, 78, 371–387.

Garg, N. & Singh, S. (2018). Mycorrhizal inoculations and silicon fortifications improve rhizobial symbiosis, antioxidant defense, trehalose turnover in pigeon pea genotypes under cadmium and zinc stress. *Plant Growth Regul.*, 86, 105–119.

Garnier, E., Cortez, J., Billès, G., Navas, M.-L., Roumet, C., Debussche, M., *et al.* (2004). Plant functional markers capture ecosystem properties during secondary succession. *Ecology*, 85, 2630–2637.

Garnier, E. & Navas, M.-L. (2013). Caractérisation fonctionnelle des végétaux. In: *Diversité fonctionnelle des plantes* (ed. Boeck, D.). p. 353.

Gattullo, C.E., Allegretta, I., Medici, L., Fijan, R., Pii, Y., Cesco, S., *et al.* (2016). Silicon dynamics in the rhizosphere: Connections with iron mobilization. *J. Plant Nutr. Soil Sci.*, 179, 409–417.

Gbongue, L.R., Lalaymia, I., Zeze, A., Delvaux, B. & Declerck, S. (2019). Increased

silicon acquisition in bananas colonized by *Rhizophagus irregularis* MUCL 41833 reduces the incidence of *Pseudocercospora fijiensis*. *Front. Plant Sci.*, 9, 1977.

Geng, Y., Baumann, F., Song, C., Zhang, M., Shi, Y., Kühn, P., *et al.* (2017). Increasing temperature reduces the coupling between available nitrogen and phosphorus in soils of Chinese grasslands. *Sci. Rep.*, 7, 1–10.

Georgiadis, A., Marhan, S., Lattacher, A., Mäder, P. & Rennert, T. (2019). Do earthworms affect the fractionation of silicon in soil? *Pedobiologia (Jena).*, 75, 1–7.

Georgiadis, A., Sauer, D., Herrmann, L., Breuer, J., Zarei, M. & Stahr, K. (2013). Development of a method for sequential Si extraction from soils. *Geoderma*, 209–210, 251–261.

Gérard, F., Mayer, K.U., Hodson, M.J. & Ranger, J. (2008). Modelling the biogeochemical cycle of silicon in soils: Application to a temperate forest ecosystem. *Geochim. Cosmochim. Acta*, 72, 741–758.

Gerke, J., Römer, W. & Jungk, A. (1994). The excretion of citric and malic acid by proteoid roots of *Lupinus albus* L.; effects on soil solution concentrations of phosphate, iron, and aluminum in the proteoid rhizosphere in samples of an oxisol and a luvisol. *J. Plant Nutr. Soil Sci.*, 157, 289–294.

Gewirtzman, J., Tang, J., Melillo, J.M., Werner, W.J., Kurtz, A.C., Fulweiler, R.W., *et al.* (2019). Soil Warming Accelerates Biogeochemical Silica Cycling in a Temperate Forest. *Front. Plant Sci.*, 10, 1–15.

Godin, B., Agneessens, R., Gerin, P. & Delcarte, J. (2014). Structural carbohydrates in plant biomasses: correlations between the detergent fiber and the dietary fiber methods. *J. Agric. Food Chem.*, 62, 5609–5616.

Godin, B., Agneessens, R., Gerin, P. & Delcarte, J. (2015). Lignin in plant biomasses: comparative metrological assessment of the detergent fiber and the insoluble dietary fiber methods. *Cellulose*, 22, 2235–2340.

Godin, B., Agneessens, R., Gofflot, S., Lamaudière, S., Sinnaeve, G., Gerin, P.A., *et al.* (2011). Revue bibliographique sur les méthodes analyse des polysaccharides structuraux des biomasses lignocellulosiques. *Biotechnol. Agron. Société Environ.*, 15, 165–182.

Goldich, S.S. (1938). A Study in Rock-Weathering. *J. Geol.*, 46, 17–58.

Golubev, S. V., Pokrovsky, O.S. & Schott, J. (2005). Experimental determination of the effect of dissolved CO2 on the dissolution kinetics of Mg and Ca silicates at 25 °C. *Chem. Geol.*, 217, 227–238.

Gong, H.J., Chen, K.M., Chen, G.C., Wang, S.M. & Zhang, C.L. (2003). Effects of silicon on growth of wheat under drought. *J. Plant Nutr.*, 26, 1055–1063.

Gong, H.J., Randall, D.P. & Flowers, T.J. (2006). Silicon deposition in the root reduces sodium uptake in rice (*Oryza sativa* L.) seedlings by reducing bypass flow. *Plant, Cell Environ.*, 29, 1970–1979.

Gould, S.J. & Lewontin, R.C. (1979). The Spandrels of San Marco and the Panglossian Paradigm : A Critique of the Adaptationist Programme. *Proc. R. Soc. London. Ser. B, Biol. Sci.*, 205, 581–598.

Guennoc, C.M., Rose, C., Labbé, J. & Deveau, A. (2018). Bacterial biofilm formation on the hyphae of ectomycorrhizal fungi: A widespread ability under controls? *FEMS Microbiol. Ecol.*, 94, 1–14.

Güereña, D., Lehmann, J., Hanley, K., Enders, A., Hyland, C. & Riha, S. (2013). Nitrogen dynamics following field application of biochar in a temperate North American maize-based production system. *Plant Soil*, 365, 239–254.

Guerriero, G., Hausman, J.-F. & Legay, S. (2016). Silicon and the Plant Extracellular Matrix. *Front. Plant Sci.*, 7, 1–8.

Guerriero, G., Law, C., Stokes, I., Moore, K.L. & Exley, C. (2018). Rough and tough. How does silicic acid protect horsetail from fungal infection? *J. Trace Elem. Med. Biol.*, 47, 45–52.

Guerriero, G., Stokes, I., Valle, N., Hausman, J. & Exley, C. (2020). Visualising Silicon in Plants : Histochemistry , Silica Sculptures and Elemental Imaging. *Cells*, 1–18.

Guilherme Pereira, C., Hayes, P.E., O'Sullivan, O.S., Weerasinghe, L.K., Clode, P.L., Atkin, O.K., *et al.* (2019). Trait convergence in photosynthetic nutrient-use efficiency along a 2-million year dune chronosequence in a global biodiversity hotspot. *J. Ecol.*, 107, 2006–2023.

Gul, S., Whalen, J.K., Thomas, B.W., Sachdeva, V. & Deng, H. (2015). Physico-chemical properties and microbial responses in biochar-amended soils: Mechanisms and future directions. *Agric. Ecosyst. Environ.*, 206, 46–59.

Guntzer, F., Keller, C. & Meunier, J.D. (2012a). Benefits of plant silicon for crops: A review. *Agron. Sustain. Dev.*, 32, 201–213.

Guntzer, F., Keller, C., Poulton, P.R., McGrath, S.P. & Meunier, J.D. (2012b). Long-term removal of wheat straw decreases soil amorphous silica at Broadbalk, Rothamsted. *Plant Soil*, 352, 173–184.

Haefele, S.M., Konboon, Y., Wongboon, W., Amarante, S., Maarifat, A.A., Pfeiffer, E.M., *et al.* (2011). Effects and fate of biochar from rice residues in rice-based

systems. *F. Crop. Res.*, 121, 430–440.

Hall, A.D. & Morison, C.G.T. (1906). On the function of silica in the nutrition of cereals.—Part I. *Proc. R. Soc. London. Ser. B*, 77, 455–477.

Hall, C.R., Dagg, V., Waterman, J.M. & Johnson, S.N. (2020). Silicon Alters Leaf Surface Morphology and Suppresses Insect Herbivory in a Model Grass Species.

Hall, C.R., Waterman, J.M., Vandegeer, R.K., Hartley, S.E. & Johnson, S.N. (2019). The Role of Silicon in Antiherbivore Phytohormonal Signalling. *Front. Plant Sci.*, 10, 1–7.

Hallama, M., Pekrun, C., Lambers, H. & Kandeler, E. (2019). Hidden miners – the roles of cover crops and soil microorganisms in phosphorus cycling through agroecosystems. *Plant Soil*, 434, 7–45.

Harrison, K.G. (2000). The role of increased silica input on Paleo-CO2 levels. *Paleoceanography*, 15, 292–298.

Hartley, S.E. & DeGabriel, J.L. (2016). The ecology of herbivore-induced silicon defences in grasses. *Funct. Ecol.*, 30, 1311–1322.

Hartley, S.E., Fitt, R.N., McLarnon, E.L. & Wade, R.N. (2015). Defending the leaf surface: intra- and inter-specific differences in silicon deposition in grasses in response to damage and silicon supply. *Front. Plant Sci.*, 6, 35.

Hasan, K.A., Soliman, H., Baka, Z. & Shabana, Y.M. (2020). Efficacy of nano-silicon in the control of chocolate spot disease of *Vicia faba* L. caused by *Botrytis fabae*. *Egypt. J. Basic Appl. Sci.*, 7, 53–66.

Hättenschwiller, S., Hagerman, A.E. & Vitousek, P.M. (2003). Polyphenols in litter from tropical montane forests across a wide range in soil fertility. *Biogeochemistry*, 64, 129–148.

Haukioja, E., Ossipov, V., Koricheva, J., Honkanen, T., Larsson, S. & Lempa, K. (1998). Biosynthetic origin of carbon-based secondary compounds: Cause of variable responses of woody plants to fertilization? *Chemoecology*, 8, 133–139.

Hayes, P., Turner, B.L., Lambers, H. & Laliberté, E. (2014). Foliar nutrient concentrations and resorption efficiency in plants of contrasting nutrient-acquisition strategies along a 2-million-year dune chronosequence. *J. Ecol.*, 102, 396–410.

Haymsom, M. & Chapman, L. (1975). Some aspects of the calcium silicate trials at Mackay. *Proc. Queensl. Soc. Sugar Cane Technol.*, 42, 117–122.

Haynes, R.J. (2014). A contemporary overview of silicon availability in agricultural

soils. *J. Plant Nutr. Soil Sci.*, 177, 831–844.

Haynes, R.J. (2017). The nature of biogenic Si and its potential role in Si supply in agricultural soils. *Agric. Ecosyst. Environ.*, 245, 100–111.

Haynes, R.J. (2019). What effect does liming have on silicon availability in agricultural soils? *Geoderma*, 337, 375–383.

Haynes, R.J., Belyaeva, O.N. & Kingston, G. (2013). Evaluation of industrial wastes as sources of fertilizer silicon using chemical extractions and plant uptake. *J. Plant Nutr. Soil Sci.*, 176, 238–248.

Haynes, R.J. & Zhou, Y.F. (2018). Effect of pH and added slag on the extractability of Si in two Si-deficient sugarcane soils. *Chemosphere*, 193, 431–437.

Haynes, R.J. & Zhou, Y.F. (2020). Silicate sorption and desorption by a Si-deficient soil – Effects of pH and period of contact. *Geoderma*, 365, 3–8.

He, H., Wu, M., Guo, L., Fan, C., Zhang, Z., Su, R., *et al.* (2020). Release of tartrate as a major carboxylate by alfalfa (*Medicago sativa* L.) under phosphorus deficiency and the effect of soil nitrogen supply. *Plant Soil*, 449, 169–178.

van Hees, P.A.W., Lundström, U.S. & Mörth, C.M. (2002). Dissolution of microcline and labradorite in a forest O horizon extract: The effect of naturally occurring organic acids. *Chem. Geol.*, 189, 199–211.

van Hees, P.A.W., Rosling, A., Lundström, U.S. & Finlay, R.D. (2006). The biogeochemical impact of ectomycorrhizal conifers on major soil elements (Al, Fe, K and Si). *Geoderma*, 136, 364–377.

Van Der Heijden, M.G.A., Bardgett, R.D. & Van Straalen, N.M. (2008). The unseen majority: Soil microbes as drivers of plant diversity and productivity in terrestrial ecosystems. *Ecol. Lett.*, 11, 296–310.

Van Der Heijden, M.G.A., Klironomos, J.N., Ursic, M., Moutoglis, P., Streitwolf-Engel, R., Boller, T., *et al.* (1998). Mycorrhizal fungal diversity determines plant biodiversity, ecosystem variability and productivity. *Nature*, 396, 69–72.

Henriet, C., Bodarwé, L., Dorel, M., Draye, X. & Delvaux, B. (2008a). Leaf silicon content in banana (*Musa* spp.) reveals the weathering stage of volcanic ash soils in Guadeloupe. *Plant Soil*, 313, 71–82.

Henriet, C., Draye, X., Oppitz, I., Swennen, R. & Delvaux, B. (2006). Effects, distribution and uptake of silicon in banana (*Musa* spp.) under controlled conditions. *Plant Soil*, 287, 359–374.

Henriet, C., De Jaeger, N., Dorel, M., Opfergelt, S. & Delvaux, B. (2008b). The reserve of weatherable primary silicates impacts the accumulation of biogenic silicon in volcanic ash soils. *Biogeochemistry*, 90, 209–223.

Herbillon, A.J. (1986). Chemical estimation of weatherable minerals present in the diagnostic horizons of low activity clay soils. In: *Proc. 8th Intern. Soil Classif. Workshop: Classification, Characterization and Utilization of Oxisols.* (eds. Beinroth, F., Camargo, M. & Eswaran). Embrapa, Rio de Janeiro, pp. 39–48.

Herrero, M., Thronton, P.K., Notenbaert, A.M., Wood, S., Msangi, S., Freeman, H.A., *et al.* (2010). Smart investments in sustainable production: Revisiting mixed crop-livestock systems. *Science (80-.).*, 327, 822–825.

Hilbrandt, I., Lehmann, V., Zietzschmann, F., Ruhl, A.S. & Jekel, M. (2019). Quantification and isotherm modelling of competitive phosphate and silicate adsorption onto micro-sized granular ferric hydroxide. *RSC Adv.*, 9, 23642–23651.

Hingston, F.J., Posner, A.M. & Quirk, J.P. (1972). Anion adsoprtion by goethite and gibbsite. I. The role of the proton in determining adsorption envelopes. *J. Soil Sci.*, 23, 177–192.

Hingston, F.J. & Raupach, M. (1967). The reaction between monosilicic acid and aluminium hydroxide. *Aust. J. Soil Res.*, 5, 295–309.

Hinsinger, P., Betencourt, E., Bernard, L., Brauman, A., Plassard, C., Shen, J., *et al.* (2011). P for two, sharing a scarce resource: Soil phosphorus acquisition in the rhizosphere of intercropped species. *Plant Physiol.*, 156, 1078–1086.

Hinsinger, P., Fernandes Barros, O.N., Benedetti, M.F., Noack, Y. & Callot, G. (2001). Plant-induced weathering of a basaltic rock: Experimental evidence. *Geochim. Cosmochim. Acta*, 65, 137–152.

Hodson, M.J. (2019). The relative importance of cell wall and lumen phytoliths in carbon sequestration in soil: A hypothesis. *Front. Earth Sci.*, 7, 167.

Hodson, M.J. & Evans, D.E. (2020). Aluminium–silicon interactions in higher plants: an update. *J. Exp. Bot.*, 71, 6719–6729.

Hodson, M.J., Sangster, A.G. & Parry, D.W. (1985). An ultrastructural study on the developmental phases and silicification of the glumes of *Phalaris canariensis* L. *Ann. Bot.*, 55, 649–665.

Hodson, M.J., White, P.J., Mead, A. & Broadley, M.R. (2005). Phylogenetic variation in the silicon composition of plants. *Ann. Bot.*, 96, 1027–1046.

Högberg, P., Nordgren, A., Buchmann, N., Taylor, A.F.S., Ekblad, A., Högberg, M.N., *et al.* (2001). Large-scale forest girdling shows that current photosynthesis drives soil respiration. *Nature*, 411, 789–792.

Höhn, A., Sommer, M., Kaczorek, D., Schalitz, G. & Breuer, J. (2008). Silicon fractions in Histosols and Gleysols of a temperate grassland site. *J. Plant Nutr.*

Soil Sci., 171, 409–418.

Hömberg, A., Obst, M., Knorr, K.H., Kalbitz, K. & Schaller, J. (2020). Increased silicon concentration in fen peat leads to a release of iron and phosphate and changes in the composition of dissolved organic matter. *Geoderma*, 374, 114422.

Hopper, S.D. & Gioia, P. (2004). The Southwest Australian floristic region: Evolution and conservation of a global hot spot of biodiversity. *Annu. Rev. Ecol. Evol. Syst.*, 35, 623–650.

Horrigan, L., Lawrence, R.S. & Walker, P. (2002). How Sustainable Agriculture Can Address the Environmental and Human Health Harms of Industrial Agriculture. *Environ. Health Perspect.*, 110, 445–456.

Horst, W.J. & Marschner, H. (1978). Effect of silicon on manganese tolerance of bean plants (*Phaseolus vulgaris* L.). *Plant Soil*, 50, 287–303.

Hossain, K.A., Horiuchi, T. & Miyagawa, S. (2001). Effects of silicate materials on growth and grain yield of rice plants grown in clay loam and sandy loam soils. *J. Plant Nutr.*, 24, 1–13.

Hothorn, T., Bretz, F. & Westfall, P. (2008). Simultaneous Inference in General Parametric Models. *Biometrical J.*, 50, 346–363.

Hou, E., Chen, C., Luo, Y., Zhou, G., Kuang, Y., Zhang, Y., *et al.* (2018). Effects of climate on soil phosphorus cycle and availability in natural terrestrial ecosystems. *Glob. Chang. Biol.*, 24, 3344–3356.

Houben, D. & Sonnet, P. (2012). Zinc mineral weathering as affected by plant roots. *Appl. Geochemistry*, 27, 1587–1592.

Houben, D., Sonnet, P. & Cornelis, J.T. (2014). Biochar from *Miscanthus*: A potential silicon fertilizer. *Plant Soil*, 374, 871–882.

Hu, L., Xia, M., Lin, X., Xu, C., Li, W., Wang, J., *et al.* (2018). Earthworm gut bacteria increase silicon bioavailability and acquisition by maize. *Soil Biol. Biochem.*, 125, 215–221.

Hu, L., Xu, C.C., Wang, J., Chen, D.Q., Zeng, R.S., Song, Y.Y., *et al.* (2019). Application of bryophyte rhizoid-associated bacteria increases silicon accumulation and growth in maize (*Zea mays* L.) seedlings. *Appl. Ecol. Environ. Res.*, 17, 13423–13433.

Huang, F., Gao, L.Y., Wu, R.R., Wang, H. & Xiao, R.B. (2020). Qualitative and quantitative characterization of adsorption mechanisms for Cd2+ by silicon-rich biochar. *Sci. Total Environ.*, 731, 139163.

Hughes, H.J., Hung, D.T. & Sauer, D. (2020). Silicon recycling through rice residue

management does not prevent silicon depletion in paddy rice cultivation. *Nutr. Cycl. Agroecosystems*, 118, 75–89.

Huitu, O., Forbes, K.M., Helander, M., Julkunen-Tiitto, R., Lambin, X., Saikkonen, K., *et al.* (2014). Silicon, endophytes and secondary metabolites as grass defenses against mammalian herbivores. *Front. Plant Sci.*, 5, 1–10.

Hummel, J., Findeisen, E., Südekum, K.H., Ruf, I., Kaiser, T.M., Bucher, M., *et al.* (2011). Another one bites the dust: Faecal silica levels in large herbivores correlate with high-crowned teeth. *Proc. R. Soc. B Biol. Sci.*, 278, 1742–1747.

Hwang, B.C. & Metcalfe, D.B. (2021). Reviews and syntheses: Impacts of plant-silica–herbivore interactions on terrestrial biogeochemical cycling. *Biogeosciences*, 18, 1259–1268.

Ibrahim, M., Khan, S., Hao, X. & Li, G. (2016). Biochar effects on metal bioaccumulation and arsenic speciation in alfalfa (*Medicago sativa* L.) grown in contaminated soil. *Int. J. Environ. Sci. Technol.*, 13, 2467–2474.

Ingham, R.E., Trofymow, J.A., Ingham, E.R. & Coleman, D.C. (1985). Interactions of bacteria, fungi, and their nematode grazers: Effects on nutrient cycling and plant growth. *Ecol. Monogr.*, 55, 119–140.

Ishizawa, H., Niiyama, K., Iida, Y., Shari, N.H.Z., Ripin, A. & Kitajima, K. (2019). Spatial variations of soil silicon availability and biogenic silicon flux in a lowland tropical forest in Malaysia. *Ecol. Res.*, 34, 548–559.

Issaharou-Matchi, I., Barboni, D., Meunier, J.D., Saadou, M., Dussouillez, P., Contoux, C., *et al.* (2016). Intraspecific biogenic silica variations in the grass species Pennisetum pedicellatum along an evapotranspiration gradient in South Niger. *Flora Morphol. Distrib. Funct. Ecol. Plants*, 220, 84–93.

IUSS. (2014). World reference base for soil classification 2014. *Food Agric. Organ. United Nations, Rome*.

Jackson, T.A. (1971). Biochemical weathering of calcium-bearing minerals by rhizosphere micro-organisms, and its influence on calcium accumulation in trees. *Plant Soil*, 35, 655–658.

Jenny, H. (1941). *Factors of Soil Formation.* McGraw Hill Co., New York.

Jia, G., Shevliakova, E., Artaxo, P., De Noblet-Ducoudré, N., R., H., House, J., *et al.* (2019). Land-climate interactions. In: *Climate Change and Land: an IPCC special report on climate change, desertification, land degradation, sustainable land management, food security, and greenhouse gas fluxes in terrestrial ecosystems*.

Jiang, Y., Wang, W., Xie, Q., Liu, N., Liu, L., Wang, D., *et al.* (2017). Plants

transfer lipids to sustain colonization by mutualistic mycorrhizal and parasitic fungi. *Science (80-.).*, 356, 1172–1173.

Johnson, S.N. & Hartley, S.E. (2018). Elevated carbon dioxide and warming impact silicon and phenolic-based defences differently in native and exotic grasses. *Glob. Chang. Biol.*, 24, 3886–3896.

Johnson, S.N., Hartley, S.E. & Moore, B.D. (2021). Silicon defence in plants: Does herbivore identity matter? *Trends Plant Sci.*, 26, 99–101.

Johnson, S.N., Hartley, S.E., Ryalls, J.M.W., Frew, A. & Hall, C.R. (2020). Targeted plant defense: silicon conserves hormonal defense signaling impacting chewing but not fluid-feeding herbivores. *Ecology*, In press.

Johnson, S.N., Lopaticki, G., Aslam, T.J., Barnett, K., Frew, A., Hartley, S.E., *et al.* (2018). Dryland management regimes alter forest habitats and understory arthropod communities. *Ann. Appl. Biol.*, 172, 282–294.

Johnson, S.N., Rowe, R.C. & Hall, C.R. (2019a). Silicon is an inducible and effective herbivore defence against *Helicoverpa punctigera* (Lepidoptera: Noctuidae) in soybean. *Bull. Entomol. Res.*, 1–6.

Johnson, S.N., Tjoelker, M.G., Ryalls, J.M.W., Wright, I.J., Barton, C.V.M. & Moore, B.D. (2019b). Climate warming and plant biomechanical defences : Silicon addition contributes to herbivore suppression in a pasture grass. *Funct. Ecol.*, 33, 587–596.

Jones, C.G. & Hartley, S.E. (1999). A protein competition model of phenolic allocation. *Oikos*, 86, 27–44.

Jones, L.H.P. & Handreck, K.A. (1963). Effects of iron and aluminium oxides on silica in solution in soils. *Nature*, 198, 852–853.

Jones, L.H.P. & Handreck, K.A. (1967). Silica in soils, plants, and animals. *Adv. Agron.*, 19, 107–149.

Jónsson, J.Ö.G. & Davídsdóttir, B. (2016). Classification and valuation of soil ecosystem services. *Agric. Syst.*, 145, 24–38.

Jordan, N., Marmier, N., Lomenech, C., Giffaut, E. & Ehrhardt, J.J. (2009). Competition between selenium (IV) and silicic acid on the hematite surface. *Chemosphere*, 75, 129–134.

Jouquet, P., Jamoteau, F., Majumdar, S., Podwojewski, P., Nagabovanalli, P., Caner, L., *et al.* (2020). The distribution of Silicon in soil is influenced by termite bioturbation in South Indian forest soils. *Geoderma*, 372, 114362.

Jouquet, P., Mamou, L., Lepage, M. & Velde, B. (2002). Effect of termites on clay minerals in tropical soils: Fungus-growing termites as weathering agents. *Eur.*

J. Soil Sci., 53, 521–528.

Jouquet, P., Traoré, S., Choosai, C., Hartmann, C. & Bignell, D. (2011). Influence of termites on ecosystem functioning. Ecosystem services provided by termites. *Eur. J. Soil Biol.*, 47, 215–222.

Kabas, S., Saavedra-Mella, F., Huynh, T., Kopittke, P.M., Carter, S. & Huang, L. (2017). Metal uptake and organic acid exudation of native *Acacia* species in mine tailings. *Aust. J. Bot.*, 65, 357–367.

Kameník, J., Mizera, J. & Řanda, Z. (2013). Chemical composition of plant silica phytoliths. *Environ. Chem. Lett.*, 11, 189–195.

Kang, J., Zhao, W. & Zhu, X. (2016). Silicon improves photosynthesis and strengthens enzyme activities in the C3 succulent xerophyte Zygophyllum xanthoxylum under drought stress. *J. Plant Physiol.*, 199, 76–86.

Kang, S.M., Waqas, M., Shahzad, R., You, Y.H., Asaf, S., Khan, M.A., *et al.* (2017). Isolation and characterization of a novel silicate-solubilizing bacterial strain *Burkholderia eburnea* CS4-2 that promotes growth of japonica rice (*Oryza sativa* L. cv. Dongjin). *Soil Sci. Plant Nutr.*, 63, 233–241.

Katz, O. (2014). Beyond grasses: the potential benefits of studying silicon accumulation in non-grass species. *Front. Plant Sci.*, 376, 1–3.

Katz, O. (2015). Silica phytoliths in angiosperms: Phylogeny and early evolutionary history. *New Phytol.*, 208, 642–646.

Katz, O. (2019). Silicon content is a plant functional trait: implications in a changing world. *Flora*, 254, 88–94.

Katz, O. (2020). Silicon and plant–animal interactions: Towards an evolutionary framework. *Plants*, 9.

Kaufman, P.B., Dayanandan, P. & Franklin, C.I. (1985). Structure and function of silica bodies in the epidermal system of grass shoots. *Ann. Bot.*, 55, 487–507.

Keeping, M.G., Kvedaras, O.L. & Bruton, A.G. (2009). Epidermal silicon in sugarcane: Cultivar differences and role in resistance to sugarcane borer Eldana saccharina. *Environ. Exp. Bot.*, 66, 54–60.

Keeping, M.G. & Meyer, J.H. (2006). Silicon-mediated resistance of sugarcane to Eldana saccharina Walker (Lepidoptera: Pyralidae): Effects of silicon source and cultivar. *J. Appl. Entomol.*, 130, 410–420.

Keeping, M.G., Meyer, J.H. & Sewpersad, C. (2013). Soil silicon amendments increase resistance of sugarcane to stalk borer *Eldana saccharina* Walker (Lepidoptera: Pyralidae) under field conditions. *Plant Soil*, 363, 297–318.

Keeping, M.G., Miles, N. & Rutherford, R.S. (2017). Liming an acid soil treated with diverse silicon sources: Effects on silicon uptake by sugarcane (*Saccharum* spp. hybrids). *J. Plant Nutr.*, 40, 1417–1436.

Keller, C., Guntzer, F., Barboni, D., Labreuche, J. & Meunier, J.D. (2012). Impact of agriculture on the Si biogeochemical cycle: Input from phytolith studies. *Comptes Rendus - Geosci.*, 344, 739–746.

Keller, C., Rizwan, M. & Meunier, J.-D. (2021). Are clay minerals a significant source of Si for crops? A comparison of amorphous silica and the roles of the mineral type and pH. *Silicon*, In press.

Kelly, E.F. (1990). Methods for extracting opal phytoliths from soil and plant material. In: *Workshop on biotic indicators of global change, Seattle, Washington.*

Kelly, E.F., Chadwick, O.A. & Hilinski, T.E. (1998). The effect of plants on mineral weathering. *Biogeochemistry*, 42, 21–53.

Kendrick, G.W., Wyrwoll, K.-H. & Szabo, B.J. (1991). Pliocene-Pleistocene coastal events and history along the western margin of Australia. *Quat. Sci. Rev.*, 10, 419–439.

Kido, N., Yokoyama, R., Yamamoto, T., Furukawa, J., Iwai, H., Satoh, S., *et al.* (2015). The matrix polysaccharide (1;3,1;4)-2- d -glucan is involved in silicon-dependent strengthening of rice cell wall. *Plant Cell Physiol.*, 56, 268–276.

Kim, J., Dong, H., Seabaugh, J., Newell, S.W. & Eberl, D.D. (2004). Role of microbes in the smectite-to-illite reaction. *Science (80-.).*, 303, 830–832.

Kim, S.A. & Guerinot, M. Lou. (2007). Mining iron: Iron uptake and transport in plants. *FEBS Lett.*, 581, 2273–2280.

Kitajima, K., Llorens, A.-M., Stefanescu, C., Timchenko, M.-V., Lucas, P.-W. & Wright, S.-J. (2012). How cellulose-based leaf toughness and lamina density contribute to long leaf lifespans of shade-tolerant species. *New Phytol.*, 195, 640–652.

Kitajima, K., Wright, S.J. & Westbrook, J.W. (2016). Leaf cellulose density as the key determinant of inter- and intra-specific variation in leaf fracture toughness in a species-rich tropical forest. *Interface Focus*, 6, 20150100.

Klotzbücher, A., Klotzbücher, T., Jahn, R., Xuan, L.D., Cuong, L.Q., Van Chien, H., *et al.* (2018a). Effects of Si fertilization on Si in soil solution, Si uptake by rice, and resistance of rice to biotic stresses in Southern Vietnam. *Paddy Water Environ.*, 16, 243–252.

Klotzbücher, T., Klotzbücher, A., Kaiser, K., Merbach, I. & Mikutta, R. (2018b).

Impact of agricultural practices on plant-available silicon. *Geoderma*, 331, 15–17.

Klotzbücher, T., Klotzbücher, A., Kaiser, K., Vetterlein, D., Jahn, R. & Mikutta, R. (2018c). Variable silicon accumulation in plants affects terrestrial carbon cycling by controlling lignin synthesis. *Glob. Chang. Biol.*, 24, 183–189.

Klotzbücher, T., Marxen, A., Vetterlein, D., Schneiker, J., Türke, M., van Sinh, N., *et al.* (2015). Plant-available silicon in paddy soils as a key factor for sustainable rice production in Southeast Asia. *Basic Appl. Ecol.*, 16, 665–673.

Klotzbücher, T., Treptow, C., Kaiser, K., Klotzbücher, A. & Mikutta, R. (2020). Sorption competition with natural organic matter as mechanism controlling silicon mobility in soil. *Sci. Rep.*, 1–11.

Kodama, H. & Ross, G.J. (1991). Tiron dissolution method used to remove and characterize inorganic components in soils. *Soil Sci. Soc. Am. J.*, 55, 1180–1187.

Komorowski, J.-C., Boudon, G., Semet, M., Beauducel, F., Anténor-Habazac, C., Bazin, S., *et al.* (2005). Guadeloupe. In: *Volcanic Hazard Atlas of The Lesser Antilles*. Seismic Research Unit, Univesrity of the West Indies, pp. 65–102.

Konhauser, K.O., Lalonde, S. V., Amskold, L. & Holland, H.D. (2007). Was there really an archean phosphate crisis? *Science (80-.).*, 315, 1234.

Koricheva, J., Larsson, S., Haukioja, E. & Keinanen, M. (1998). Regulation of woody plant secondary metabolism by resource availability: hypothesis testing by means of meta-analysis. *Oikos*, 83, 212–226.

Kostic, L., Nikolic, N., Bosnic, D., Samardzic, J. & Nikolic, M. (2017). Silicon increases phosphorus (P) uptake by wheat under low P acid soil conditions. *Plant Soil*, 419, 447–455.

Kothari, S.K., Marschner, H. & Römheld, V. (1990). Direct and indirect effects of VA mycorrhizal fungi and rhizosphere microorganisms on acquisition of mineral nutrients by maize (*Zea mays* L.) in a calcareous soil. *New Phytol.*, 116, 637–645.

Kováčik, J., Klejdus, B., Bačkor, M. & Repčák, M. (2007). Phenylalanine ammonia-lyase activity and phenolic compounds accumulation in nitrogen-deficient *Matricaria chamomilla* leaf rosettes. *Plant Sci.*, 172, 393–399.

Kowalenko, C.G. & Babuin, D. (2014). Use of Lithium Metaborate to Determine Total Phosphorus and Other Element Concentrations in Soil, Plant, and Related Materials. *Commun. Soil Sci. Plant Anal.*, 45, 15–28.

Koyama, S. & Hayashi, H. (2017). Rice yield and soil carbon dynamics over three

years of applying rice husk charcoal to an Andosol paddy field. *Plant Prod. Sci.*, 20, 176–182.

Kraus, T.E.C., Zasoski, R.J. & Dahlgren, R.A. (2004). Fertility and pH effects on polyphenol and condensed tannin concentrations in foliage and roots. *Plant Soil*, 262, 95–109.

Kreyling, J., Schweiger, A.H., Bahn, M., Ineson, P., Migliavacca, M., Morel-Journel, T., *et al.* (2018). To replicate, or not to replicate – that is the question: how to tackle nonlinear responses in ecological experiments. *Ecol. Lett.*, 21, 1629–1638.

Kumar, S. & Elbaum, R. (2018). Interplay between silica deposition and viability during the life span of sorghum silica cells. *New Phytol.*, 217, 1137–1145.

Kumar, S., Milstein, Y., Brami, Y., Elbaum, M. & Elbaum, R. (2017a). Mechanism of silica deposition in sorghum silica cells. *New Phytol.*, 213, 791–798.

Kumar, S., Soukup, M. & Elbaum, R. (2017b). Silicification in grasses: variation between different cell types. *Front. Plant Sci.*, 8, 438.

Kump, L.R., Brantley, S.L. & Arthur, M.A. (2000). Chemical weathering, atmospheric CO2, and climate. *Annu. Rev. Earth Planet. Sci.*, 28, 611–667.

Kundu, S., Kamath, M.B. & Goswami, N.N. (1988). Effect of sulphate, silicate and fluoride anions - I. Phosphate fixation in soils. *J. Indian Soc. Soil Sci.*, 36, 43–47.

Kuzyakov, Y. & Blagodatskaya, E. (2015). Microbial hotspots and hot moments in soil: Concept & review. *Soil Biol. Biochem.*, 83, 184–199.

Lakanen, E. & Erviö, R. (1971). A comparison of eight extractans for the determination of plant available micronutrients in soils. *Acta Agral. Fenn.*, 123, 223–232.

Laliberté, E., Kardol, P., Didham, R.K., Teste, F.P., Turner, B.L. & Wardle, D.A. (2017). Soil fertility shapes belowground food webs across a regional climate gradient. *Ecol. Lett.*, 20, 1273–1284.

Laliberté, E., Turner, B.L., Costes, T., Pearse, S.J., Wyrwoll, K.H., Zemunik, G., *et al.* (2012). Experimental assessment of nutrient limitation along a 2-million-year dune chronosequence in the south-western Australia biodiversity hotspot. *J. Ecol.*, 100, 631–642.

Laliberté, E., Turner, B.L., Zemunik, G., Wyrwoll, K.H., Pearse, S.J. & Lambers, H. (2013). Nutrient limitation along the Jurien Bay dune chronosequence: Response to Uren & Parsons (2013). *J. Ecol.*, 101, 1088–1092.

Laliberté, E., Zemunik, G. & Turner, B.L. (2014). Environmental filtering explains

variation in plant diversity along resource gradients. *Science (80-.).*, 345, 1602–1605.

Lambers, H. (2014). *Plant Life on the Sandplains in Southwest Australia, a Global Biodiversity Hotspot*. 2004th edn. Univerty of Western Australia Publishing, Crawley, Australia.

Lambers, H., Albornoz, F., Kotula, L., Laliberté, E., Ranathunge, K., Teste, F.P., *et al.* (2018). How belowground interactions contribute to the coexistence of mycorrhizal and non-mycorrhizal species in severely phosphorus-impoverished hyperdiverse ecosystems. *Plant Soil*, 424, 11–33.

Lambers, H., Bishop, J.G., Hopper, S.D., Laliberté, E. & Zúñiga-Feest, A. (2012). Phosphorus-mobilization ecosystem engineering: the roles of cluster roots and carboxylate exudation in young P-limited ecosystems. *Ann. Bot.*, 110, 329–348.

Lambers, H., Finnegan, P.M., Laliberté, E., Pearse, S.J., Ryan, M.H., Shane, M.W., *et al.* (2011). Phosphorus nutrition of proteaceae in severely phosphorus-impoverished soils: Are there lessons to be learned for future crops? *Plant Physiol.*, 156, 1058–1066.

Lambers, H., Hayes, P.E., Laliberté, E., Oliveira, R.S. & Turner, B.L. (2015). Leaf manganese accumulation and phosphorus-acquisition efficiency. *Trends Plant Sci.*, 20, 83–90.

Lambers, H. & Oliveira, R.S. (2019). *Plant Physiological Ecology, 3rd edition*. Springer International Publishing.

Lambers, H. & Poorter, H. (1992). Inherent variation in growth rate between higher plants: a search for physiological causes and ecological consequences. *Adv. Ecol. Res.*, 23, 187–261.

Lambers, H., Raven, J.A., Shaver, G.R. & Smith, S.E. (2008). Plant nutrient-acquisition strategies change with soil age. *Trends Ecol. Evol.*, 23, 95–103.

Lambers, H., Shane, M.W., Cramer, M.D., Pearse, S.J. & Veneklaas, E.J. (2006). Root structure and functioning for efficient acquisition of phosphorus: Matching morphological and physiological traits. *Ann. Bot.*, 98, 693–713.

Lambers, H., Wright, I.J., Guilherme Pereira, C., Bellingham, P.J., Bentley, L.P., Boonman, A., *et al.* (2021). Leaf manganese concentrations as a tool to assess belowground plant functioning in phosphorus-impoverished environments. *Plant Soil*, In press.

Lamont, B. (1982). Mechanisms for enhancing nutrient uptake in plants, with particular reference to mediterranean South Africa and Western Australia. *Bot. Rev.*, 48, 597–689.

Lauwers, A.M. & Heinen, W. (1974). Bio-degradation and utilization of silica and quartz. *Arch. Microbiol.*, 95, 67–78.

Lavinsky, A.O., Detmann, K.C., Reis, J. V., Ávila, R.T., Sanglard, M.L., Pereira, L.F., *et al.* (2016). Silicon improves rice grain yield and photosynthesis specifically when supplied during the reproductive growth stage. *J. Plant Physiol.*, 206, 125–132.

Law, C. & Exley, C. (2011). New insight into silica deposition in horsetail (Equisetum arvense). *BMC Plant Biol.*, 11, 112.

Leake, J.R. & Read, D.J. (2017). Mycorrhizal Symbioses and Pedogenesis Throughout Earth's History. In: *Mycorrhizal Mediation of Soil: Fertility, Structure, and Carbon Storage*. Elsevier Inc., pp. 9–33.

Lee, K.E., Adhikari, A., Kang, S.M., You, Y.H., Joo, G.J., Kim, J.H., *et al.* (2019). Isolation and characterization of the high silicate and phosphate solubilizing novel strain enterobacter ludwigii GAK2 that promotes growth in rice plants. *Agronomy*, 9.

Leksungnoen, P., Wisawapipat, W., Ketrot, D., Aramrak, S., Nookabkaew, S., Rangkadilok, N., *et al.* (2019). Biochar and ash derived from silicon-rich rice husk decrease inorganic arsenic species in rice grain. *Sci. Total Environ.*, 684, 360–370.

Lemaire, G., Franzluebbers, A., Carvalho, P.C. de F. & Dedieu, B. (2014). Integrated crop-livestock systems: Strategies to achieve synergy between agricultural production and environmental quality. *Agric. Ecosyst. Environ.*, 190, 4–8.

Leroy, Tombeur, Walgraffe, Cornélis & Verheggen. (2019). Silicon and plant natural defenses against insect pests: Impact on plant volatile organic compounds and cascade effects on multitrophic interactions. *Plants*, 8, 444.

Li, C., Hoffland, E., Kuyper, T.W., Yu, Y., Zhang, C., Li, H., *et al.* (2020a). Syndromes of production in intercropping impact yield gains. *Nat. Plants*, 6, 653–660.

Li, F., Zhang, M., Guo, K., Hu, Z., Zhang, R., Feng, Y., *et al.* (2015). High-level hemicellulosic arabinose predominately affects lignocellulose crystallinity for genetically enhancing both plant lodging resistance and biomass enzymatic digestibility in rice mutants. *Plant Biotechnol. J.*, 13, 514–525.

Li, J., Zheng, L., Wang, S.L., Wu, Z., Wu, W., Niazi, N.K., *et al.* (2019a). Sorption mechanisms of lead on silicon-rich biochar in aqueous solution: Spectroscopic investigation. *Sci. Total Environ.*, 672, 572–582.

Li, L., Tilman, D., Lambers, H. & Zhang, F.S. (2014). Plant diversity and

overyielding: Insights from belowground facilitation of intercropping in agriculture. *New Phytol.*, 203, 63–69.

Li, Z. & Delvaux, B. (2019). Phytolith-rich biochar: A potential Si fertilizer in desilicated soils. *GCB Bioenergy*, 11.

Li, Z., Delvaux, B., Yans, J., Dufour, N., Houben, D. & Cornelis, J.T. (2018). Phytolith-rich biochar increases cotton biomass and silicon-mineralomass in a highly weathered soil. *J. Plant Nutr. Soil Sci.*

Li, Z., de Tombeur, F., Linden, C. Vander, Cornelis, J.T. & Delvaux, B. (2020b). Soil microaggregates store phytoliths in a sandy loam. *Geoderma*, 360, 114037.

Li, Z., Unzué-Belmonte, D., Cornelis, J.-T., Linden, C. Vander, Struyf, E., Ronsse, F., *et al.* (2019b). Effects of phytolithic rice-straw biochar, soil buffering capacity and pH on silicon bioavailability. *Plant Soil*.

Liang, Y., Hua, H., Zhu, Y.G., Zhang, J., Cheng, C. & Römheld, V. (2006). Importance of plant species and external silicon concentration to active silicon uptake and transport. *New Phytol.*, 172, 63–72.

Liang, Y., Nikolic, M., Bélanger, R., Gong, H. & Song, A. (2015a). Silicon biogeochemistry and bioavailability in soil. In: *Silicon in Agriculture*. pp. 45–68.

Liang, Y., Nikolic, M., Bélanger, R.R., Gong, H. & Song, A. (2015b). *Silicon in Agriculture. From theory to practice.*

Liang, Y., Sun, W., Zhu, Y.G. & Christie, P. (2007). Mechanisms of silicon-mediated alleviation of abiotic stresses in higher plants: A review. *Environ. Pollut.*, 147, 422–428.

Liermann, L.J., Kalinowski, B.E., Brantley, S.L. & Ferry, J.G. (2000). Role of bacterial siderophores in dissolution of hornblende. *Geochim. Cosmochim. Acta*, 64, 587–602.

Limmer, M.A., Mann, J., Amaral, D.C., Vargas, R. & Seyfferth, A.L. (2018). Silicon-rich amendments in rice paddies: Effects on arsenic uptake and biogeochemistry. *Sci. Total Environ.*, 624, 1360–1368.

Vander Linden, C. & Delvaux, B. (2019). The weathering stage of tropical soils affects the soil-plant cycle of silicon, but depending on land use. *Geoderma*, 351, 209–220.

Liu, W.-S., Laird, J.S., Ryan, C.G., Tang, Y.-T., Qiu, R.-L., Echevarria, G., *et al.* (2021). Rare earth elements, aluminium and silicon distribution in the fern *Dicranopteries linearis* revealed by µPIXE Maia analysis. *Ann. Bot.*, In press.

Liu, W., Xu, X., Wu, X., Yang, Q., Luo, Y. & Christie, P. (2006). Decomposition of silicate minerals by Bacillus mucilaginosus in liquid culture. *Environ. Geochem. Health*, 28, 133–140.

Liu, X., Li, L., Bian, R., Chen, D., Qu, J., Wanjiru Kibue, G., *et al.* (2014). Effect of biochar amendment on soil-silicon availability and rice uptake. *J. Plant Nutr. Soil Sci.*, 177, 91–96.

de Long, J.R., Sundqvist, M.K., Gundale, M.J., Giesler, R. & Wardle, D.A. (2016). Effects of elevation and nitrogen and phosphorus fertilization on plant defence compounds in subarctic tundra heath vegetation. *Funct. Ecol.*, 30, 314–325.

Lucas, Y. (2001). The role of plants in controlling rates and products of weathering: Importance of biological pumping. *Annu. Rev. Earth Planet. Sci.*, 29, 135–163.

Lucas, Y., Luizão, F.J., Chauvel, A., Rouiller, J. & Nahon, D. (1993). The relation between biological activity of the rain forest and mineral composition of soils. *Science (80-.).*, 260, 521–523.

Ma, J. & Takahashi, E. (1990a). The effect of silicic acid on rice in a P-deficient soil. *Plant Soil*, 126, 121–125.

Ma, J. & Takahashi, E. (1991a). Availability of rice straw Si to rice plants. *Soil Sci. Plant Nutr.*, 37, 111–116.

Ma, J. & Takahashi, E. (1991b). Effect of silicate on phosphate availability for rice in a P-deficient soil. *Plant Soil*, 133, 151–155.

Ma, J.F. (2004). Role of silicon in enhancing the resistance of plants to biotic and abiotic stresses. *Soil Sci. Plant Nutr.*, 50, 11–18.

Ma, J.F. (2005). Plant root responses to three abundant soil minerals: Silicon, aluminum and iron. *CRC. Crit. Rev. Plant Sci.*, 24, 267–281.

Ma, J.F. & Takahashi, E. (1990b). Effect of silicon on the growth and phosphorus uptake of rice. *Plant Soil*, 126, 115–119.

Ma, J.F., Tamai, K., Yamaji, N., Mitani, N., Konishi, S., Katsuhara, M., *et al.* (2006). A silicon transporter in rice. *Nature*, 440, 688–691.

Ma, J.F. & Yamaji, N. (2008). Functions and transport of silicon in plants. *Cell. Mol. Life Sci.*, 65, 3049–3057.

Ma, J.F., Yamaji, N., Mitani, N., Tamai, K., Konishi, S., Fujiwara, T., *et al.* (2007). An efflux transporter of silicon in rice. *Nature*, 448, 209–212.

MAAH. (2020). *Annuaire des statistiques agricoles 2018.* Ouagadougou, Burkina Faso.

Magalhaes, J. V., Piñeros, M.A., Maciel, L.S. & Kochian, L. V. (2018). Emerging pleiotropic mechanisms underlying aluminum resistance and phosphorus acquisition on acidic soils. *Front. Plant Sci.*, 9, 1420.

Maksimović, J.D., Mojović, M., Maksimović, V., Römheld, V. & Nikolic, M. (2012). Silicon ameliorates manganese toxicity in cucumber by decreasing hydroxyl radical accumulation in the leaf apoplast. *J. Exp. Bot.*, 63, 2411–2420.

Malav, J. & Shaikh, M.S. (2015). Evaluation of different extractants for available silicon in ustocrept soils of Gujarat. *Eco. Env. Cons.*, 21, 277–285.

Mariotte, P., Mehrabi, Z., Bezemer, T.M., De Deyn, G.B., Kulmatiski, A., Drigo, B., *et al.* (2018). Plant–Soil Feedback: Bridging Natural and Agricultural Sciences. *Trends Ecol. Evol.*, 33, 129–142.

Marschner, H. & Dell, B. (1994). Nutrient uptake in mycorrhizal symbiosis. *Plant Soil*, 159, 89–102.

Marschner, H., Römheld, V., Horst, W.J. & Martin, P. (1986). Root-induced changes in the rhizosphere: Importance for the mineral nutrition of plants. *Zeitschrift für Pflanzenernährung und Bodenkd.*, 149, 441–456.

Martin-Guay, M.O., Paquette, A., Dupras, J. & Rivest, D. (2018). The new Green Revolution: Sustainable intensification of agriculture by intercropping. *Sci. Total Environ.*, 615, 767–772.

Marxen, A., Klotzbücher, T., Jahn, R., Kaiser, K., Nguyen, V.S., Schmidt, A., *et al.* (2016). Interaction between silicon cycling and straw decomposition in a silicon deficient rice production system. *Plant Soil*, 398, 153–163.

Mason, C.M. & Donovan, L.A. (2015). Does investment in leaf defenses drive changes in leaf economic strategy? A focus on whole-plant ontogeny. *Oecologia*, 177, 1053–1066.

Massey, F. & Hartley, S. (2009). Physical defences wear you down : progressive and irreversible impacts of silica on insect herbivores. *J. Anim. Ecol.*, 78, 281–291.

Massey, F.P., Ennos, A.R. & Hartley, S.E. (2006). Silica in grasses as a defence against insect herbivores: Contrasting effects on folivores and a phloem feeder. *J. Anim. Ecol.*, 75, 595–603.

Massey, F.P., Ennos, A.R. & Hartley, S.E. (2007a). Grasses and the resource availability hypothesis: The importance of silica-based defences. *J. Ecol.*, 95, 414–424.

Massey, F.P. & Hartley, S.E. (2006). Experimental demonstration of the antiherbivore effects of silica in grasses: impacts on foliage digestibility and

vole growth rates. *Proc. R. Soc. B Biol. Sci.*, 273, 2299–2304.

Massey, F.P., Roland Ennos, A. & Hartley, S.E. (2007b). Herbivore specific induction of silica-based plant defences. *Oecologia*, 152, 677–683.

Mathews, B.W., Carpenter, J.R. & Sollenberger, L.E. (2009). In vitro digestibility and chemical composition of kikuyugrass as influenced by soil silicon, liming, and genotype. *Commun. Soil Sci. Plant Anal.*, 40, 2855–2873.

Matychenkov, V.V. & Ammosova, Y.M. (1996). Effect of amorphous silica on some properties of a sod-podzolic soil. *Eurasian Soil Sci.*, 28, 87–99.

McArthur, W.M. & Bettenay, E. (1974). *Development and distribution of soils of the Swan Coastal Plain, Western Australia. Canberra: CSIRO.* CSIRO. Melbourne.

McBurney, T. (1992). The relationship between leaf thickness and plant water potential. *J. Exp. Bot.*, 43, 327–335.

McCray, J.M., Rice, R.W. & Baucum, L.E. (2011). Calcium Silicate Recommendations for Sugarcane on Florida Organic Soils. *Electron. Data Inf. Source (EDIS), Soil Water Sci. Dep. Univ. Florida*, 1–5.

McKeague, J.A. & Cline, M.G. (1963a). Silica in soil solutions. I. The form and concentration of dissolved silica in aqueous extarcts of some soils. *Can. J. Soil Sci.*, 43, 70–82.

McKeague, J.A. & Cline, M.G. (1963b). Silica in soil solutions. II. The adsorption of monosilicic acid by soil and by other substances. *Can. J. Soil Sci.*, 43, 83–96.

McLarnon, E., McQueen-Mason, S., Lenk, I. & Hartley, S.E. (2017). Evidence for active uptake and deposition of Si-based defenses in tall fescue. *Front. Plant Sci.*, 8, 1–11.

McNaughton, S.J. & Tarrants, J.L. (1983). Grass leaf silicification: Natural selection for an inducible defense against herbivores. *Proc. Natl. Acad. Sci. U. S. A.*, 80, 790–791.

McNaughton, S.J., Tarrants, J.L., McNaughton, M.M. & Davis, R.D. (1985). Silica as a defense against herbivory and a growth promotor in african grasses. *Ecology*, 66, 528–535.

Meena, V.D., Dotaniya, M.L., Coumar, V., Rajendiran, S., Ajay, Kundu, S., *et al.* (2014). A case for silicon fertilization to improve crop yields in tropical soils. *Proc. Natl. Acad. Sci. India Sect. B - Biol. Sci.*, 84, 505–518.

Meharg, C. & Meharg, A.A. (2015). Silicon, the silver bullet for mitigating biotic and abiotic stress, and improving grain quality, in rice? *Environ. Exp. Bot.*,

120, 8–17.

Mehra, O.P. & Jackson, M.L. (1960). Iron oxide removal from soils and clays by a dithionite-citrate system buffered with sodium bicarbonate. *Clays Clay Miner.*, 7, 317–327.

Melzer, S.E., Chadwick, O.A., Hartshorn, A.S., Khomo, L.M., Knapp, A.K. & Kelly, E.F. (2012). Lithologic controls on biogenic silica cycling in South African savanna ecosystems. *Biogeochemistry*, 108, 317–334.

Melzer, S.E., Knapp, A.K., Kirkman, K.P., Smith, M.D., Blair, J.M. & Kelly, E.F. (2010). Fire and grazing impacts on silica production and storage in grass dominated ecosystems. *Biogeochemistry*, 97, 263–278.

Metson, A.J. (1956). *Methods of Chemical Analysis for Soil Survey Samples.* Bulletin 1. Wellington.

Meunier, J.D., Barboni, D., Anwar-ul-Haq, M., Levard, C., Chaurand, P., Vidal, V., *et al.* (2017). Effect of phytoliths for mitigating water stress in durum wheat. *New Phytol.*, 215, 229–239.

Meunier, J.D., Colin, F. & Alarcon, C. (1999). Biogenic silica storage in soils. *Geology*, 27, 835–838.

Meunier, J.D., Sandhya, K., Prakash, N.B., Borschneck, D. & Dussouillez, P. (2018). pH as a proxy for estimating plant-available Si? A case study in rice fields in Karnataka (South India). *Plant Soil*, 432, 143–155.

Meyer, J.H. & Keeping, M.G. (2000). Review of Research Into the Role of Silicon for Sugarcane Production. *Proc. South African Sugar Technol. Assoc.*, 74, 29–40.

Mikha, M.M. & Rice, C.W. (2004). Tillage and Manure Effects on Soil and Aggregate-Associated Carbon and Nitrogen. *Soil Sci. Soc. Am. J.*, 68, 809.

Miles, N., Manson, A.D., Rhodes, R., van Antwerpen, R. & Weigel, A. (2014). Extractable Silicon in Soils of the South African Sugar Industry and Relationships with Crop Uptake. *Commun. Soil Sci. Plant Anal.*, 45, 2949–2958.

Minden, V., Schaller, J. & Olde Venterink, H. (2020). Plants increase silicon content as a response to nitrogen or phosphorus limitation: a case study with *Holcus lanatus*. *Plant Soil*, In press.

Mitani, N., Yamaji, N. & Ma, J.F. (2009). Identification of maize silicon influx transporters. *Plant Cell Physiol.*, 50, 5–12.

Moles, A.T., Peco, B., Wallis, I.R., Foley, W.J., Poore, A.G.B., Seabloom, E.W., *et al.* (2013). Correlations between physical and chemical defences in plants:

Tradeoffs, syndromes, or just many different ways to skin a herbivorous cat? *New Phytol.*, 198, 252–263.

Montpetit, J., Vivancos, J., Mitani-Ueno, N., Yamaji, N., Rémus-Borel, W., Belzile, F., *et al.* (2012). Cloning, functional characterization and heterologous expression of TaLsi1, a wheat silicon transporter gene. *Plant Mol. Biol.*, 79, 35–46.

Motomura, H., Fujii, T. & Suzuki, M. (2006). Silica deposition in abaxial epidermis before the opening of leaf blades of *Pleioblastus chino* (Poaceae, Bambusoideae). *Ann. Bot.*, 97, 513–519.

Motomura, H., Mita, N. & Suzuki, M. (2002). Silica accumulation in long-lived leaves of *Sasa veitchii* (Carrière) rehder (Poaceae-Bambusoideae). *Ann. Bot.*, 90, 149–152.

Müller, D.W.H., Caton, J., Codron, D., Schwarm, A., Lentle, R., Streich, W.J., *et al.* (2011). Phylogenetic constraints on digesta separation: Variation in fluid throughput in the digestive tract in mammalian herbivores. *Comp. Biochem. Physiol. Part A Mol. Integr. Physiol.*, 160, 207–220.

Nair, V.D., Nair, P.K.R., Dari, B., Freitas, A.M., Chatterjee, N. & Pinheiro, F.M. (2017). Biochar in the agroecosystem-climate-change-sustainability Nexus. *Front. Plant Sci.*, 8.

Nakamura, R., Cornélis, J.-T., de Tombeur, F., Nakagawa, M. & Kitajima, K. (2020a). Comparative analysis of borate fusion versus sodium carbonate extraction for quantification of silicon contents in plants. *J. Plant Res.*, 133, 271–277.

Nakamura, R., Cornelis, J., de Tombeur, F., Yoshinaga, A., Nakagawa, M. & Kitajima, K. (2020b). Diversity of silicon release rates among tropical tree species during leaf-litter decomposition. *Geoderma*, 368.

Nakamura, R., Ishizawa, H., Wagai, R., Suzuki, S., Kitayama, K. & Kitajima, K. (2019). Silicon cycled by tropical forest trees: effects of species, elevation and parent material on Mount Kinabalu, Malaysia. *Plant Soil*, 443, 155–166.

Narayanaswamy, C. & Prakash, N.B. (2009). Calibration and categorization of plant available silicon in rice soils of South India. *J. Plant Nutr.*, 32, 1237–1254.

Do Nascimento, N.R., Fritsch, E., Bueno, G.T., Bardy, M., Grimaldi, C. & Melfi, A.J. (2008). Podzolization as a deferralitization process: Dynamics and chemistry of ground and surface waters in an Acrisol - Podzol sequence of the upper Amazon Basin. *Eur. J. Soil Sci.*, 59, 911–924.

National Research Council. (2001). *Basic research opportunities in Earth science*. Washington, DC, USA: National Academy Press.

Ndayiragije, S. & Delvaux, B. (2003). Coexistence of allophane, gibbsite, kaolinite and hydroxy-Al-interlayered 2:1 clay minerals in a perudic Andosol. *Geoderma*, 117, 203–214.

Nelson, D.M. & Dortch, Q. (1996). Silicic acid depletion and silicon limitation in the plume of the Mississippi River: evidence from kitenic studies in spring and summer. *Mar. Ecol. Prog. Ser.*, 136, 163–178.

Nelson, D.M., Tréguer, P., Brzezinski, M.A., Leynaert, A. & Quéguiner, B. (1995). Production and dissolution of biogenic silica in the ocean: Revised global estimates, comparison with regional data and relationship to biogenic sedimentation. *Global Biogeochem. Cycles*, 9, 359–372.

Neu, S., Schaller, J. & Dudel, E.G. (2017). Silicon availability modifies nutrient use efficiency and content, C:N:P stoichiometry, and productivity of winter wheat (Triticum aestivum L.). *Sci. Rep.*, 7, 1–8.

Nguyen, M.N., Picardal, F., Dultz, S., Dam, T.T.N., Nguyen, A. V. & Nguyen, K.M. (2017). Silicic acid as a dispersibility enhancer in a Fe-oxide-rich kaolinitic soil clay. *Geoderma*, 286, 8–14.

Ning, C., Qu, J., He, L., Yang, R., Chen, Q., Luo, S., *et al.* (2017). Improvement of yield, pest control and Si nutrition of rice by rice-water spinach intercropping. *F. Crop. Res.*, 208, 34–43.

Northup, R.R., Yu, Z., Dahlgren, R.A. & Vogt, A. (1995). Polyphenol control of nitrogen release from pine litter. *Nature*, 377, 227–229.

Nottingham, A.T., Meir, P., Velasquez, E. & Turner, B.L. (2020). Soil carbon loss by experimental warming in a tropical forest. *Nature*, 584, 234–237.

Nottle, M.C. & Armstrong, J.M. (1966). Urinary excretion of silica by grazing sheep. *Aust. J. Agric. Res.*, 17, 165–173.

Nussaume, L., Kanno, S., Javot, H., Marin, E., Pochon, N., Ayadi, A., *et al.* (2011). Phosphate import in plants: Focus on the PHT1 transporters. *Front. Plant Sci.*, 2, 83.

Obihara, C.H. & Russell, E.W. (1972). Specific adsorption of silicate and phosphate by soils. *J. Soil Sci.*, 23, 105–117.

Olsen, S. & Paasche, E. (1986). Variable kinetics of silicon-limited growth in thalassiosira pseudonana (Bacillariophyceae) in response to changed chemical composition of the growth medium. *Br. Phycol. J.*, 21, 183–190.

Olsen, S.R., Sommers, L.E. & Page, A.L. (1982). Methods of soil analysis. Part 2. Chem. Microbiol. Prop. Phosphorus. *Am. Soc. Agron. Inc. Soil Sci. Soc. Am. Inc.*, 9, 403–430.

Onoda, Y., Westoby, M., Adler, P.B., Choong, A.M.F., Clissold, F.J., Cornelissen, J.H.C., *et al.* (2011). Global patterns of leaf mechanical properties. *Ecol. Lett.*, 14, 301–312.

Or, D., Keller, T. & Schlesinger, W.H. (2021). Natural and managed soil structure: On the fragile scaffolding for soil functioning. *Soil Tillage Res.*, 208, 104912.

Owino-Gerroh, C. & Gascho, G.J. (2004). Effect of silicon on low pH soil phosphorus sorption and on uptake and growth of maize. *Commun. Soil Sci. Plant Anal.*, 35, 2369–2378.

Oye Anda, C.C., Opfergelt, S. & Declerck, S. (2016). Silicon acquisition by bananas (c.V. Grande Naine) is increased in presence of the arbuscular mycorrhizal fungus Rhizophagus irregularis MUCL 41833. *Plant Soil*, 409, 77–85.

Palandri, J.L. & Kharaka, Y.K. (2004). *A compilation of rate parameters of water-mineral interaction kinetics for application to geochemical modeling*. *U.S. Geol. Surv.*

Pang, J., Bansal, R., Zhao, H., Bohuon, E., Lambers, H., Ryan, M.H., *et al.* (2018). The carboxylate-releasing phosphorus-mobilizing strategy can be proxied by foliar manganese concentration in a large set of chickpea germplasm under low phosphorus supply. *New Phytol.*, 219, 518–529.

Panizzo, V., Crespin, J., Crosta, X., Shemesh, A., Massé, G., Yam, R., *et al.* (2014). Sea ice diatom contributions to Holocene nutrient utilization in East Antarctica. *Paleoceanography*, 29, 328–343.

Pawlik, Ł., Phillips, J.D. & Šamonil, P. (2016). Roots, rock, and regolith: Biomechanical and biochemical weathering by trees and its impact on hillslopes—A critical literature review. *Earth-Science Rev.*, 159, 142–159.

Peeters, P.J. (2002). Correlations between leaf structural traits and the densities of herbivorous insect guilds. *Biol. J. Linn. Soc.*, 77, 43–65.

Peltzer, D.A., Wardle, D.A., Allison, V.J., Baisden, W.T., Bardgett, D., Chadwick, O.A., *et al.* (2010). Understanding ecosystem retrogression. *Ecol. Monogr.*, 80, 509–529.

Perry, C.C. & Fraser, M.A. (1991). Silica deposition and ultrastructure in the cell wall of Equisetum arvense: The importance of cell wall structures and flow control in biosilicification? *Philos. Trans. R. Soc. B Biol. Sci.*, 334, 149–157.

Perry, C.C. & Keeling-Tucker, T. (2000). Biosilicification: The role of the organic matrix in structure control. *J. Biol. Inorg. Chem.*, 5, 537–550.

Philippini, V., Naveau, A., Catalette, H. & Leclercq, S. (2006). Sorption of silicon on magnetite and other corrosion products of iron. *J. Nucl. Mater.*, 348, 60–69.

Phillips, J.D. (1989). An evaluation of the state factor model of soil ecosystems. *Ecol. Modell.*, 45, 165–177.

Phonde, D.B., Deshmukh, P.S., Banerjee, K. & Adsule, P.G. (2014). Plant available silicon in sugarcane soils and its relationship with soil properties, leaf silicon and cane yield. *An Asian J. Soil Sci.*, 9, 176–180.

Pillon, Y., Jaffré, T., Birnbaum, P., Bruy, D., Cluzel, D., Ducousso, M., *et al.* (2020). Infertile landscapes on an old oceanic island: the biodiversity hotspot of New Caledonia. *Biol. J. Linn. Soc.*, blaa146.

Pinheiro, J., Bates, D., DebRoy, S., Sarkar, D. & Team, R.C. (2020). nlme: Linear and Nonlinear Mixed Effects Models.

Playford, P.E., Cockbain, A.E. & Lowe, G.H. (1976). *Geology of the Perth Basin, Western Australia*. Perth, W.A.

Porder, S. & Chadwick, O.A. (2009). Climate and soil-age constraints on nutrient uplift and retention by plants. *Ecology*, 90, 623–636.

Prescott, C.E., Grayston, S.J., Helmisaari, H., Ka, E., Körner, C., Lambers, H., *et al.* (2020). Surplus Carbon Drives Allocation and Plant – Soil Interactions, xx, 1–9.

Puppe, D. (2020). Review on protozoic silica and its role in silicon cycling. *Geoderma*, 365, 114224.

Puppe, D., Ehrmann, O., Kaczorek, D., Wanner, M. & Sommer, M. (2015). The protozoic Si pool in temperate forest ecosystems - Quantification, abiotic controls and interactions with earthworms. *Geoderma*, 243–244, 196–204.

Puppe, D., Höhn, A., Kaczorek, D., Wanner, M. & Sommer, M. (2016). As time goes by-Spatiotemporal changes of biogenic Si pools in initial soils of an artificial catchment in NE Germany. *Appl. Soil Ecol.*, 105, 9–16.

Puppe, D., Kaczorek, D., Wanner, M. & Sommer, M. (2014). Dynamics and drivers of the protozoic Si pool along a 10-year chronosequence of initial ecosystem states. *Ecol. Eng.*, 70, 477–482.

Putra, R., Powell, J.R., Hartley, S.E. & Johnson, S.N. (2020). Is it time to include legumes in plant silicon research? *Funct. Ecol.*, 1–16.

Qian, L., Chen, B. & Chen, M. (2016). Novel Alleviation Mechanisms of Aluminum Phytotoxicity via Released Biosilicon from Rice Straw-Derived Biochars. *Sci. Rep.*, 6, 29346.

Quigley, K.M. & Anderson, T.M. (2014). Leaf silica concentration in Serengeti grasses increases with watering but not clipping: insight from a common garden study and literature review. *Front. Plant Sci.*, 5, 568.

Quigley, K.M., Donati, G.L. & Anderson, T.M. (2016). Variation in the soil "silicon landscape" explains plant silica accumulation across environmental gradients in Serengeti. *Plant Soil*, 410, 217–229.

Quigley, K.M., Griffith, D.M., Donati, G.L. & Anderson, T.M. (2020). Soil nutrients and precipitation are major drivers of global patterns of grass leaf silicification. *Ecology*, 101, e03006.

Quinton, J.N., Govers, G., Van Oost, K. & Bardgett, R.D. (2010). The impact of agricultural soil erosion on biogeochemical cycling. *Nat. Geosci.*, 3, 311–314.

Rafferty, C., Lamont, B.B. & Hanley, M.E. (2005). Selective feeding by kangaroos (*Macropus fuliginosus*) on seedlings of Hakea species: Effects of chemical and physical defences. *Plant Ecol.*, 177, 201–208.

Rafferty, C.M., Lamont, B.B. & Hanley, M.E. (2010). Herbivore feeding preferences in captive and wild populations. *Austral Ecol.*, 35, 257–263.

Rai, D. & Kittrick, J.A. (1989). Mineral equilibria and the soil system. In: *Minerals in Soil Environments* (ed. America, S.S.S. of). Madison, USA, pp. 161–198.

Raven, J.A. (1983). The transport and function of silicon in plants. *Biol. Rev.*, 58, 179–207.

Raven, J.A., Lambers, H., Smith, S.E. & Westoby, M. (2018). Costs of acquiring phosphorus by vascular land plants: patterns and implications for plant coexistence. *New Phytol.*, 217, 1420–1427.

Raven, J.A. & Waite, A.M. (2004). The evolution of silicification in diatoms: Inescapable sinking and sinking as escape? *New Phytol.*, 162, 45–61.

Reeves, D.W. (1994). Cover crops and rotations. In: *Crops Residue Management*. pp. 125–172.

Reibe, K., Roß, C.L. & Ellmer, F. (2015). Hydro-/Biochar application to sandy soils: impact on yield components and nutrients of spring wheat in pots. *Arch. Agron. Soil Sci.*, 61, 1055–1060.

Reich, P.B. (2014). The world-wide "fast-slow" plant economics spectrum: A traits manifesto. *J. Ecol.*, 102, 275–301.

Reichard, P.U., Kraemer, S.M., Frazier, S.W. & Kretzschmar, R. (2005). Goethite dissolution in the presence of phytosiderophores: rates, mechanisms, and the synergistic effect of oxalate. *Plant Soil*, 276, 115–132.

Reichard, P.U., Kretzschmar, R. & Kraemer, S.M. (2007). Dissolution mechanisms of goethite in the presence of siderophores and organic acids. *Geochim. Cosmochim. Acta*, 71, 5635–5650.

Reithmaier, G.-M.S., Knorr, K.-H., Arnhold, S., Planer-Friedrich, B. & Schaller, J. (2017). Enhanced silicon availability leads to increased methane production, nutrient and toxicant mobility in peatlands. *Sci. Rep.*, 7, 8728.

Revell, L.J. (2010). Phylogenetic signal and linear regression on species data. *Methods Ecol. Evol.*, 1, 319–329.

Revell, L.J. (2012). phytools: An R package for phylogenetic comparative biology (and other things). *Methods Ecol. Evol.*, 3, 217–223.

Reynolds, O.L., Keeping, M.G. & Meyer, J.H. (2009). Silicon-augmented resistance of plants to herbivorous insects: A review. *Ann. Appl. Biol.*, 155, 171–186.

Rich, M.K., Nouri, E., Courty, P.E. & Reinhardt, D. (2017). Diet of arbuscular mycorrhizal fungi: bread and butter? *Trends Plant Sci.*, 22, 652–660.

Richardson, A.E., Barea, J.M., McNeill, A.M. & Prigent-Combaret, C. (2009). Acquisition of phosphorus and nitrogen in the rhizosphere and plant growth promotion by microorganisms. *Plant Soil*, 321, 305–339.

Richardson, A.E., Lynch, J.P., Ryan, P.R., Delhaize, E., Smith, F.A., Smith, S.E., *et al.* (2011). Plant and microbial strategies to improve the phosphorus efficiency of agriculture. *Plant Soil*, 349, 121–156.

Richardson, S.J., Peltzer, D.A., Allen, R.B., McGlone, M.S. & Parfitt, R.L. (2004). Rapid development of phosphorus limitation in temperate rainforest along the Franz Josef soil chronosequence. *Oecologia*, 139, 267–276.

Richter, D. de B. & Billings, S.A. (2015). "One physical system": Tansley's ecosystem as Earth's critical zone. *New Phytol.*, 206, 900–912.

Ritchie, H. & Roser, M. (2013). *"Crop Yields." Publ. online OurWorldInData.org. Retrieved from "https//ourworldindata.org/crop-yields."*

Roarty, S., Hackett, R.A. & Schmidt, O. (2017). Earthworm populations in twelve cover crop and weed management combinations. *Appl. Soil Ecol.*, 114, 142–151.

Rohatgi, A. (2012). WebPlotDigitalizer: HTML5 based online tool to extract numerical data from plot images. Version 4.2.

Rosen, A.M. & Weiner, S. (1994). Identifying ancient irrigation: a new method using opaline phytoliths from emmer wheat. *J. Archaeol. Sci.*, 21, 125–132.

le Roux, E., van Veenhuisen, L.S., Kerley, G.I.H. & Cromsigt, J.P.G.M. (2020). Animal body size distribution influences the ratios of nutrients supplied to plants. *Proc. Natl. Acad. Sci. U. S. A.*, 117, 22256–22263.

Ruffino, L., Hartley, S.E., DeGabriel, J.L. & Lambin, X. (2018). Population-level

manipulations of field vole densities induce subsequent changes in plant quality but no impacts on vole demography. *Ecol. Evol.*, 8, 7752–7762.

Russelle, M.P., Entz, M.H. & Franzluebbers, A.J. (2007). Reconsidering integrated crop-livestock systems in North America. *Agron. J.*, 99, 325–334.

Ryalls, J.M.W., Moore, B.D. & Johnson, S.N. (2018). Silicon uptake by a pasture grass experiencing simulated grazing is greatest under elevated precipitation. *BMC Ecol.*, 1–8.

Saccone, L., Conley, D.J., Koning, E., Sauer, D., Sommer, M., Kaczorek, D., *et al.* (2007). Assessing the extraction and quantification of amorphous silica in soils of forest and grassland ecosystems. *Eur. J. Soil Sci.*, 58, 1446–1459.

Salminen, J.P. & Karonen, M. (2011). Chemical ecology of tannins and other phenolics: We need a change in approach. *Funct. Ecol.*, 25, 325–338.

Sampedro, L., Moreira, X. & Zas, R. (2011). Costs of constitutive and herbivore-induced chemical defences in pine trees emerge only under low nutrient availability. *J. Ecol.*, 99, 818–827.

Sangster, A.G., Hodson, M.J. & Tubb, H.J. (2001). Silicon deposition in higher plants. In: *Silicon in Agriculture*. The Netherlands, pp. 85–113.

Sanson, G., Read, J., Aranwela, N., Clissold, F. & Peeters, P. (2001). Measurement of leaf biomechanical properties in studies of herbivory: Opportunities., problems and procedures. *Austral Ecol.*, 26, 535–546.

Sauer, D., Saccone, L., Conley, D.J., Herrmann, L. & Sommer, M. (2006). Review of methodologies for extracting plant-available and amorphous Si from soils and aquatic sediments. *Biogeochemistry*, 80, 89–108.

Savant, N.K., Korndörfer, G.H., Datnoff, L.E. & Snyder, G.H. (1999). Silicon nutrition and sugarcane production: A review. *J. Plant Nutr.*, 22, 1853–1903.

Schachtschabel, V.P. & Heinemann, C.G. (1967). Wasserlösliche kieselsäure in lößböden. *Z. Pflanzenern. Bodenk.*, 118, 22–35.

Schaller, J., Brackhage, C. & Dudel, E.G. (2012a). Silicon availability changes structural carbon ratio and phenol content of grasses. *Environ. Exp. Bot.*, 77, 283–287.

Schaller, J., Brackhage, C., Gessner, M.O., Bäuker, E. & Gert Dudel, E. (2012b). Silicon supply modifies C:N:P stoichiometry and growth of *Phragmites australis*. *Plant Biol.*, 14, 392–396.

Schaller, J., Frei, S., Rohn, L. & Gilfedder, B.S. (2020). Amorphous Silica Controls Water Storage Capacity and Phosphorus Mobility in Soils. *Front. Environ. Sci.*, 8.

Schaller, J., Heimes, R., Ma, J.F., Meunier, J.-D., Shao, J.F., Fujii-Kashino, M., *et al.* (2019). Silicon accumulation in rice plant aboveground biomass affects leaf carbon quality. *Plant Soil*, 444, 399–407.

Schaller, J., Hines, J., Brackhage, C., Bäucker, E. & Gessner, M.O. (2014). Silica decouples fungal growth and litter decomposition without changing responses to climate warming and N enrichment. *Ecology*, 95, 3181–3189.

Schaller, J., Hodson, M.J. & Struyf, E. (2017). Is relative Si/Ca availability crucial to the performance of grassland ecosystems? *Ecosphere*, 8.

Schaller, J., Puppe, D., Kaczorek, D., Ellerbrock, R. & Sommer, M. (2021). Silicon cycling in soils revisited. *Plants*, 10, 295.

Schaller, J., Turner, B.L., Weissflog, A., Pino, D., Bielnicka, A.W. & Engelbrecht, B.M.J. (2018). Silicon in tropical forests: large variation across soils and leaves suggests ecological significance. *Biogeochemistry*, 140, 161–174.

Schlatter, D., Kinkel, L., Thomashow, L., Weller, D. & Paulitz, T. (2017). Disease suppressive soils: New insights from the soil microbiome. *Phytopathology*, 107, 1284–1297.

Schmidt, O., Clements, R.O. & Donaldson, G. (2003). Why do cereal-legume intercrops support large earthworm populations? *Appl. Soil Ecol.*, 22, 181–190.

Schmidt, O., Curry, J.P., Hackett, R.A., Purvis, G. & Clements, R.O. (2001). Earthworm communities in conventional wheat monocropping and low-input wheat-clover intercropping systems. *Ann. Appl. Biol.*, 138, 377–388.

Schoelynck, J., Bal, K., Backx, H., Okruszko, T., Meire, P. & Struyf, E. (2010). Silica uptake in aquatic and wetland macrophytes: A strategic choice between silica, lignin and cellulose? *New Phytol.*, 186, 385–391.

Schoelynck, J. & Struyf, E. (2016). Silicon in aquatic vegetation. *Funct. Ecol.*, 30, 1323–1330.

Schoelynck, J., Subalusky, A.L., Struyf, E., Dutton, C.L., Unzué-Belmonte, D., Van de Vijver, B., *et al.* (2019). Hippos (*Hippopotamus amphibius*): The animal silicon pump. *Sci. Adv.*, 5, eaav0395.

van Schöll, L., Hoffland, E. & Van Breemen, N. (2006). Organic anion exudation by ectomycorrhizal fungi and Pinus sylvestris in response to nutrient deficiencies. *New Phytol.*, 170, 153–163.

van Schöll, L., Kuyper, T.W., Smits, M.M., Landeweert, R., Hoffland, E. & Breemen, N. Van. (2008). Rock-eating mycorrhizas: their role in plant nutrition and biogeochemical cycles. *Plant Soil*, 303, 35–47.

Schröer, H.C., Krasko, A., Le Pennec, G., Adell, T., Wiens, M., Hassanein, H., *et al.*

(2003). Silicase, an Enzyme Which Degrades Biogenous Amorphous Silica: Contribution to the Metabolism of Silica Deposition in the Demosponge Suberites domuncula. In: *Silicon Biomineralization. Progress in Molecular and Subcellular Biology* (ed. Springer). Berlin, pp. 249–268.

Schubert, S., Steffens, D. & Ashraf, I. (2020). Is occluded phosphate plant-available? *J. Plant Nutr. Soil Sci.*, 183, 338–344.

Schulmann, O.P. & Tiunov, Alexei, V. (1999). Leaf litter fragmentation by the earthworm *Lumbricus terrestris* L. *Pedobiologia (Jena).*, 43, 453–458.

Seleiman, M.F., Refay, Y., Al-Suhaibani, N., Al-Ashkar, I., El-Hendawy, S. & Hafez, E.M. (2019). Integrative Effects of Rice-Straw Biochar and Silicon on Oil and Seed Quality , Yield and Physiological Traits of Helianthus annuus L . Grown under Water Deficit Stress. *Agronomy*, 9, 1–21.

Seyfferth, A.L., Kocar, B.D., Lee, J.A. & Fendorf, S. (2013). Seasonal dynamics of dissolved silicon in a rice cropping system after straw incorporation. *Geochim. Cosmochim. Acta*, 123, 120–133.

Shewmaker, G.E., Mayland, H.F., Rosenau, R.C. & Asay, K.H. (1989). Silicon in C-3 Grasses: Effects on Forage Quality and Sheep Preference. *J. Range Manag.*, 42, 122.

Simpson, K.J., Wade, R.N., Rees, M., Osborne, C.P. & Hartley, S.E. (2017). Still armed after domestication? Impacts of domestication and agronomic selection on silicon defences in cereals. *Funct. Ecol.*, 31, 2108–2117.

Singh, K.P. & Sarkar, M.C. (1992). Phosphorus availability in soils as affected by fertilizer phosphorus, sodium silicate and farmyeard manure. *J. Indian Soc. Soil Sci.*, 40, 762–767.

Sistani, K.R., Savant, N.K. & Reddy, K.C. (1997). Effect of rice hull ash silicon on rice seedling growth. *J. Plant Nutr.*, 20, 195–201.

Sitters, J., Kimuyu, D.M., Young, T.P., Claeys, P. & Olde Venterink, H. (2020). Negative effects of cattle on soil carbon and nutrient pools reversed by megaherbivores. *Nat. Sustain.*, 3, 360–366.

Six, J., Bossuyt, H., Degryze, S. & Denef, K. (2004). A history of research on the link between (micro)aggregates, soil biota, and soil organic matter dynamics. *Soil Tillage Res.*, 79, 7–31.

Slessarev, E.W., Lin, Y., Bingham, N.L., Johnson, J.E., Dai, Y., Schimel, J.P., *et al.* (2016). Water balance creates a threshold in soil pH at the global scale. *Nature*, 540, 567–569.

Smith, H.A. & McSorley, R. (2000). Intercropping and pest management: A Review

of major concepts. *Am. Entomol.*, 46, 154–161.

Smith, S. & Read, D. (2008). *Mycorrhizal Symbiosis*. Elsevier.

Smits, M.M., Hoffland, E., Jongmans, A.G. & van Breemen, N. (2005). Contribution of mineral tunneling to total feldspar weathering. *Geoderma*, 125, 59–69.

Smits, M.M. & Wallander, H. (2017). Role of Mycorrhizal Symbiosis in Mineral Weathering and Nutrient Mining from Soil Parent Material. In: *Mycorrhizal Mediation of Soil: Fertility, Structure, and Carbon Storage*. Elsevier Inc., pp. 35–46.

Smyth, T.J. & Sanchez, P.A. (1980). Effect of lime, silicate, and phosphorus applications to an Oxisol on phosphorus sorption and ion retention. *Soil Sci. Soc. Am. J.*, 44, 500–505.

Snyder, G.H. (2001). Methods for silicon analyses in plants, soils and fertilizers. In: Datnoff, L.E., Snyder, G.H., Korndörfer, G.H. (Eds.), Silicon in Agriculture. In: (ed. B.V, E.S.). Amsterdam, pp. 185–196.

Van Soest, P.J. (1973). Collaborative study of acid-detergent fiber and lignin. *J. AOAC*, 56, 781–784.

Van Soest, P.J. & Wine, R. (1967). Use of detergents in the analysis of fibrous feeds. IV. Determiantion of plant cell well constituants. *J. AOAC*, 50, 50–55.

Soininen, E.M., Bråthen, K.A., Jusdado, J.G.H., Reidinger, S. & Hartley, S.E. (2013). More than herbivory: Levels of silica-based defences in grasses vary with plant species, genotype and location. *Oikos*, 122, 30–41.

Sommer, M., Jochheim, H., Höhn, A., Breuer, J., Zagorski, Z., Busse, J., *et al.* (2013). Si cycling in a forest biogeosystem-the importance of transient state biogenic Si pools. *Biogeosciences*, 10, 4991–5007.

Sommer, M., Kaczorek, D., Kuzyakov, Y. & Breuer, J. (2006). Silicon pools and fluxes in soils and landscapes—a review. *J. Plant Nutr. Soil Sci.*, 169, 310–329.

Song, A., Li, Z., Zhang, J., Xue, G., Fan, F. & Liang, Y. (2009). Silicon-enhanced resistance to cadmium toxicity in Brassica chinensis L. is attributed to Si-suppressed cadmium uptake and transport and Si-enhanced antioxidant defense capacity. *J. Hazard. Mater.*, 172, 74–83.

Song, W., Ogawa, N., Oguchi, C.T., Hatta, T. & Matsukura, Y. (2007). Effect of *Bacillus subtilis* on granite weathering: A laboratory experiment. *Catena*, 70, 275–281.

Song, Z., Wang, H., Strong, P.J. & Shan, S. (2014). Increase of available soil silicon

by Si-rich manure for sustainable rice production. *Agron. Sustain. Dev.*, 34, 813–819.

Soratto, R.P., Crusciol, C.A.C., Castro, G.S.A., da Costa, C.H.M. & Neto, J.F. (2012). Leaf application of silicic acid to white oat and wheat. *Rev. Bras. Ciência do Solo*, 36, 1538–1544.

Soukup, M., Martinka, M., Bosnić, D., Čaplovičová, M., Elbaum, R. & Lux, A. (2017). Formation of silica aggregates in sorghum root endodermis is predetermined by cell wall architecture and development. *Ann. Bot.*, 120, 739–753.

Steuer, P., Südekum, K.-H., Müller, D.W.H., Franz, R., Kaandorp, J., Clauss, M., *et al.* (2011). Is there an influence of body mass on digesta mean retention time in herbivores? A comparative study on ungulates. *Comp. Biochem. Physiol. Part A Mol. Integr. Physiol.*, 160, 355–364.

Stevens, P.R. & Walker, T.W. (1970). The chronosequence concept and soil formation. *Quaterly Rev. Biol.*, 45, 333–350.

Stillings, L.L., Drever, J.I., Brantley, S.L., Sun, Y. & Oxburgh, R. (1996). Rates of feldspar dissolution at pH 3–7 with 0–8 mM oxalic acid. *Chem. Geol.*, 132, 79–89.

Stirling, C.H., Esat, T.M., Lambeck, K. & McCulloch, M.T. (1998). Timing and duration of the Last Interglacial: Evidence for a restricted interval of widespread coral reef growth. *Earth Planet. Sci. Lett.*, 160, 745–762.

Stitt, M. & Quick, W.P. (1989). Photosynthetic carbon partitioning: its regulation and possibilities for manipulation. *Physiol. Plant.*, 77, 633–641.

Stoate, C., Báldi, A., Beja, P., Boatman, N.D., Herzon, I., van Doorn, A., *et al.* (2009). Ecological impacts of early 21st century agricultural change in Europe - A review. *J. Environ. Manage.*, 91, 22–46.

Stotzky, G. (1986). Influence of soil minerals colloids on metabolic processes, growth, adhesion, and ecology of microbes and viruses. In: *Interactions of soil minerals with natural organisms and microbes.* (eds. Huang, P.M. & Schnitzer, M.). Madison, Wisconsin, pp. 305–428.

Stotzky, G. & Martin, T. (1963). Soil mineralogy in relation to the spread of Fusarium wilt of banana in Central America. *Plant Soil*, 18, 317–337.

Street-Perrott, F.A. & Barker, P.A. (2008). Biogenic silica: a neglected component of the coupled global continental biogeochemical cycles of carbon and silicon. *Earth Surf. Process. Landforms*, 33, 1436–1457.

Ström, L., Owen, A.G., Godbold, D.L. & Jones, D.L. (2005). Organic acid

behaviour in a calcareous soil implications for rhizosphere nutrient cycling. *Soil Biol. Biochem.*, 37, 2046–2054.

Strömberg, C.A.E., Dunn, R.E., Crifò, C. & Harris, E.B. (2018). Phytoliths in Paleoecology: Analytical Considerations, Current Use, and Future Directions. In: *Methods in Paleoecology*. pp. 235–287.

Strömberg, C.A.E., Di Stilio, V.S. & Song, Z. (2016). Functions of phytoliths in vascular plants: an evolutionary perspective. *Funct. Ecol.*, 30, 1286–1297.

Struyf, E., Smis, A., Van Damme, S., Garnier, J., Govers, G., Van Wesemael, B., *et al.* (2010a). Historical land use change has lowered terrestrial silica mobilization. *Nat. Commun.*, 1, 129.

Struyf, E., Smis, A., van Damme, S., Meire, P. & Conley, D.J. (2010b). The global biogeochemical silicon cycle. *Silicon*, 1, 207–213.

Su, C., Harsh, J.B. & Boyle, J.S. (1995). Solubility of hydroxy-aluminum interlayers and imogolite in a Spodosol. *Soil Sci. Soc. Am. J.*, 59, 373.

Sun, H., Duan, Y., Mitani-Ueno, N., Che, J., Jia, J., Liu, J., *et al.* (2020a). Tomato roots have a functional silicon influx transporter but not a functional silicon efflux transporter. *Plant. Cell Environ.*, 43, 732–744.

Sun, T., Liu, Y., Wu, S., Zhang, J., Qu, B. & Xu, J. (2020b). Effects of background fertilization followed by co-application of two kinds of bacteria on soil nutrient content and rice yield in Northeast China. *Int. J. Agric. Biol. Eng.*, 13, 154–162.

Suzuki, S., Ma, J.F., Yamamoto, N., Hattori, T., Sakamoto, M. & Umezawa, T. (2012). Silicon deficiency promotes lignin accumulation in rice. *Plant Biotechnol.*, 29, 391–394.

Suzuki, Y., Matsubara, T. & Hoshino, M. (2003). Breakdown of mineral grains by earthworms and beetle larvae. *Geoderma*, 112, 131–142.

Tamm, O. (1922). Eine method zur bestimmung der anorganishen komponenten des golkomplex in boden. *Medd. Statens skogforsoksanst*, 19, 385–404.

Tammeorg, P., Simojoki, A., Mäkelä, P., Stoddard, F.L., Alakukku, L. & Helenius, J. (2014). Short-term effects of biochar on soil properties and wheat yield formation with meat bone meal and inorganic fertiliser on a boreal loamy sand. *Agric. Ecosyst. Environ.*, 191, 108–116.

Tang, F., White, J.A. & Charvat, I. (2001). The effect of phosphorus availability on arbuscular mycorrhizal colonization of *Typha angustifolia*. *Mycologia*, 93, 1042–1047.

Tang, X., Zhang, C. & Yu, Y. (2020). Intercropping legumes and cereals increases

phosphorus use efficiency ; a meta-analysis. *Plant Soil*, In press.

Tavakkoli, E., Lyons, G., English, P. & Guppy, C.N. (2011). Silicon nutrition of rice is affected by soil pH, weathering and silicon fertilisation. *J. Plant Nutr. Soil Sci.*, 174, 437–446.

Teodoro, G.S., Lambers, H., Nascimento, D.L., de Britto Costa, P., Flores-Borges, D.N.A., Abrahão, A., *et al.* (2019). Specialized roots of Velloziaceae weather quartzite rock while mobilizing phosphorus using carboxylates. *Funct. Ecol.*, 33, 762–773.

de Tombeur, F., Cooke, J., Collard, L., Cisse, D., Saba, F., Lefebvre, D., *et al.* (2021a). Biochar affects silicification patterns and physical traits of rice leaves cultivated in a desilicated soil (Ferric Lixisol). *Plant Soil*, 460, 375–390.

de Tombeur, F., Laliberté, E., Lambers, H., Faucon, M.P., Zemunik, G., Turner, B.L., *et al.* (2021b). A shift from phenol to silica-based leaf defences during long-term soil and ecosystem development. *Ecol. Lett.*, 24, 984–995.

de Tombeur, F., Vander Linden, C., Cornélis, J.-T., Godin, B., Compère, P. & Delvaux, B. (2020a). Soil and climate affect foliar silicification patterns and silica-cellulose balance in sugarcane (*Saccharum officinarum*). *Plant Soil*, 452, 529–546.

de Tombeur, F., Turner, B.L., Laliberté, E., Lambers, H. & Cornelis, J.-T. (2020b). Silicon dynamics during 2 million years of soil development in a coastal dune chronosequence under a Mediterranean climate. *Ecosystems*, 23, 1614–1630.

de Tombeur, F., Turner, B.L., Laliberté, E., Lambers, H., Mahy, G., Faucon, M.-P., *et al.* (2020c). Plants sustain the terrestrial silicon cycle during ecosystem retrogression. *Science (80-.).*, 369, 1245–1248.

Traoré, A., Traoré, K., Traoré, O., Bado, B. V, Nacro, B.H. & Sedogo, M.P. (2015). Caractérisation des systèmes de production à base de riz pluvial strict dans les exploitations agricoles de la zone Sud-soudanienne du Burkina Faso. *Int. J. Biol. Chem. Sci.*, 9, 2685–2697.

Treguer, P., Nelson, D.M., Van Bennekom, A.J., DeMaster, D.J., Leynaert, A. & Queguiner, B. (1995). The Silica Balance in the World Ocean: A Reestimate. *Science (80-.).*, 268, 375–379.

Tréguer, P. & Pondaven, P. (2000). Silica control of carbon dioxide. *Nature*, 406, 358–359.

Tréguer, P.J. & De La Rocha, C.L. (2013). The World Ocean Silica Cycle. *Ann. Rev. Mar. Sci.*, 5, 477–501.

Trembath-Reichert, E., Wilson, J.P., McGlynn, S.E. & Fischer, W.W. (2015). Four

hundred million years of silica biomineralization in land plants. *Proc. Natl. Acad. Sci. U. S. A.*, 112, 5449–54.

Trinh, T.K., Nguyen, T.T.H., Nguyen, T.N., Wu, T.Y., Meharg, A.A. & Nguyen, M.N. (2017). Characterization and dissolution properties of phytolith occluded phosphorus in rice straw. *Soil Tillage Res.*, 171, 19–24.

Tripathi, A.D., Mishra, R., Maurya, K.K., Singh, R.B. & Wilson, D.W. (2018). *Estimates for world population and global food availability for global health. Role Funct. Food Secur. Glob. Heal.* Elsevier Inc.

Tubana, B.S., Babu, T. & Datnoff, L.E. (2016). A Review of Silicon in Soils and Plants and Its Role in US Agriculture. *Soil Sci.*, 181, 1.

Turner, B.L., Condron, L.M., Richardson, S.J., Peltzer, D.A. & Allison, V.J. (2007). Soil organic phosphorus transformations during pedogenesis. *Ecosystems*, 10, 1166–1181.

Turner, B.L., Hayes, P.E. & Laliberté, E. (2018). A climosequence of chronosequences in southwestern Australia. *Eur. J. Soil Sci.*, 69, 69–85.

Turner, B.L. & Laliberté, E. (2015). Soil development and nutrient availability along a 2 million-year coastal dune chronosequence under species-rich mediterranean shrubland in Southwestern Australia. *Ecosystems*, 18, 287–309.

Turner, B.L., Wells, A., Andersen, K.M. & Condron, L.M. (2012). Patterns of tree community composition along a coastal dune chronosequence in lowland temperate rain forest in New Zealand. *Plant Ecol.*, 213, 1525–1541.

Turpault, M.P., Calvaruso, C., Kirchen, G., Redon, P.O. & Cochet, C. (2018). Contribution of fine tree roots to the silicon cycle in a temperate forest ecosystem developed on three soil types. *Biogeosciences*, 15, 2231–2249.

Uroz, S., Calvaruso, C., Turpault, M.P. & Frey-Klett, P. (2009). Mineral weathering by bacteria: ecology, actors and mechanisms. *Trends Microbiol.*, 17, 378–387.

USDA's Soil Survey Laboratory Staff. (2017). *Soil survey manual. USDA Handbook 18. Government Printing Office, Washinton, D. C.* USDA Handb. Washington, D. C.

Vandenkoornhuyse, P., Quaiser, A., Duhamel, M., Le Van, A. & Dufresne, A. (2015). The importance of the microbiome of the plant holobiont. *New Phytol.*, 206, 1196–1206.

Vandevenne, F.I., Barão, A.L., Schoelynck, J., Smis, A., Ryken, N., Van Damme, S., *et al.* (2013). Grazers: Biocatalysts of terrestrial silica cycling. *Proc. R. Soc. B Biol. Sci.*, 280, 1–9.

Vandevenne, F.I., Barão, L., Ronchi, B., Govers, G., Meire, P., Kelly, E.F., *et al.*

(2015). Silicon pools in human impacted soils of temperate zones. *Global Biogeochem. Cycles*, 29, 1439–1450.

Veldhuis, M.P., Gommers, M.I., Olff, H. & Berg, M.P. (2018). Spatial redistribution of nutrients by large herbivores and dung beetles in a savanna ecosystem. *J. Ecol.*, 106, 422–433.

Vernavá, M.N., Phillips-Aalten, P.M., Hughes, L.A., Rowcliffe, H., Wiltshire, C.W. & Glen, D.M. (2004). Influences of preceding cover crops on slug damage and biological control using *Phasmarhabditis hermaphrodita*. *Ann. Appl. Biol.*, 145, 279–284.

Vessey, J.K. (2003). Plant growth promoting rhizobacteria as biofertilizers. *Plant Soil*, 255, 571–586.

Violle, C., Navas, M.L., Vile, D., Kazakou, E., Fortunel, C., Hummel, I., *et al.* (2007). Let the concept of trait be functional! *Oikos*, 116, 882–892.

Vitousek, P. (2004). *Nutrient Cycling and Limitation - Hawai'i as Model System*. Princeton University Press, New Jersey.

Vitousek, P.M. & Chadwick, O.A. (2013). Pedogenic thresholds and soil process domains in basalt-derived soils. *Ecosystems*, 16, 1379–1395.

Vitousek, P.M. & Farrington, H. (1997). Nutrient limitation and soil development: Experimental test of a biogeochemical theory. *Biogeochemistry*, 37, 63–75.

Vitousek, P.M. & Howarth, R.W. (1991). Nitrogen limitation on land and in the sea: How can it occur? *Biogeochemistry*, 13, 87–115.

Vitousek, P.M., Porder, S., Houlton, B.Z. & Chadwick, O.A. (2010). Terrestrial phosphorus limitation: Mechanisms, implications, and nitrogen-phosphorus interactions. *Ecol. Appl.*, 20, 5–15.

Vitousek, P.M., Walker, L.R., Whiteaker, L.D. & Matson, P.A. (1993). Nutrient limitations to plant growth during primary succession in Hawaii Volcanoes National Park. *Biogeochemistry*, 23, 197–215.

Voinovitch, I.A., Debras-Guedon, J. & Louvrier, J. (1962). L'analyse des silicates. Hermann, Paris, pp. 145–158.

Wada, K. (1989). Allophane and imogolite. In: *Minerals in Soil Environments* (ed. America, S.S.S. of). Madison, USA, pp. 1051–1087.

Walder, F., Niemann, H., Natarajan, M., Lehmann, M.F., Boller, T. & Wiemken, A. (2012). Mycorrhizal networks: Common goods of plants shared under unequal terms of trade. *Plant Physiol.*, 159, 789–797.

Walker, L.R., Wardle, D.A., Bardgett, R.D. & Clarkson, B.D. (2010). The use of

chronosequences in studies of ecological succession and soil development. *J. Ecol.*, 98, 725–736.

Walker, T.W. & Syers, J.K. (1976). The fate of phosphorous during pedogenesis. *Geoderma*, 15, 1–19.

Wang, H.Y., Shen, Q.H., Zhou, J.M., Wang, J., Du, C.W. & Chen, X.Q. (2011). Plants use alternative strategies to utilize nonexchangeable potassium in minerals. *Plant Soil*, 343, 209–220.

Wang, M., Wang, J.J., Tafti, N.D., Hollier, C.A., Myers, G. & Wang, X. (2019a). Effect of alkali-enhanced biochar on silicon uptake and suppression of gray leaf spot development in perennial ryegrass. *Crop Prot.*, 119, 9–16.

Wang, R.R., Wang, Q., He, L.Y., Qiu, G. & Sheng, X.F. (2015). Isolation and the interaction between a mineral-weathering Rhizobium tropici Q34 and silicate minerals. *World J. Microbiol. Biotechnol.*, 31, 747–753.

Wang, Y., Krogstad, T., Clarke, J.L., Hallama, M., Øgaard, A.F., Eich-Greatorex, S., *et al.* (2016). Rhizosphere organic anions play a minor role in improving crop species' ability to take up residual phosphorus (P) in agricultural soils low in P availability. *Front. Plant Sci.*, 7, 1664.

Wang, Y., Xiao, X. & Chen, B. (2018). Biochar Impacts on Soil Silicon Dissolution Kinetics and their Interaction Mechanisms. *Sci. Rep.*, 1–11.

Wang, Y., Xiao, X., Xu, Y. & Chen, B. (2019b). Environmental Effects of Silicon within Biochar (Sichar) and Carbon-Silicon Coupling Mechanisms: A Critical Review. *Environ. Sci. Technol.*, 53, 13570–13582.

Wang, Y., Zhang, K., Lu, L., Xiao, X. & Chen, B. (2020). Novel insights into effects of silicon-rich biochar (Sichar) amendment on cadmium uptake, translocation and accumulation in rice plants. *Environ. Pollut.*, 265, 114772.

Wardle, D.A., Bardgett, R.D., Walker, L.R., Peltzer, D.A. & Lagerström, A. (2008). The response of plant diversity to ecosystem retrogression: Evidence from contrasting long-term chronosequences. *Oikos*, 117, 93–103.

Wardle, D.A., Walker, Lawrence, R. & Bardgett, R.D. (2004). Ecosystem properties and forest decline in constrasting long-term chronosequences. *Science (80-.).*, 305, 509–513.

Watanabe, T., Luu, H.M. & Inubushi, K. (2017). Effects of the continuous application of rice straw compost and chemical fertilizer on soil carbon and available silicon under a double rice cropping system in the Mekong Delta, Vietnam. *Japan Agric. Res. Q.*, 51, 233–239.

Waterman, J.M., Hall, C.R., Mikhael, M., Cazzonelli, C.I., Hartley, S.E. & Johnson,

S.N. (2021). Short-term resistance that persists: Rapidly induced silicon anti-herbivore defence affects carbon-based plant defences. *Funct. Ecol.*, 35, 82–92.

Wedepohl, K.H. (1995). The composition of the continental crust. *Geochim. Cosmochim. Acta*, 59, 1217–1232.

Welch, S.A. & Ullman, W.J. (1999). The effect of microbial glucose metabolism on bytownite feldspar dissolution rates between 5°and 35°C. *Geochim. Cosmochim. Acta*, 63, 3247–3259.

Wen, Z., Pang, J., Tueux, G., Liu, Y., Shen, J., Ryan, M.H., *et al.* (2020). Contrasting patterns in biomass allocation, root morphology and mycorrhizal symbiosis for phosphorus acquisition among 20 chickpea genotypes with different amounts of rhizosheath carboxylates. *Funct. Ecol.*, 34, 1311–1324.

Westoby, M. & Falster, D.S. (2021). The conservative low-phosphorus niche in Proteaceae. *Plant Soil*, 462, 89–93.

White, A.F., Vivit, D. V., Schulz, M.S., Bullen, T.D., Evett, R.R. & Aagarwal, J. (2012). Biogenic and pedogenic controls on Si distributions and cycling in grasslands of the Santa Cruz soil chronosequence, California. *Geochim. Cosmochim. Acta*, 94, 72–94.

Wickramasinghe, D.B. & Rowell, D.L. (2006). The release of silicon from amorphous silica and rice straw in Sri Lankan soils. *Biol. Fertil. Soils*, 42, 231–240.

Wieczorek, M., Zub, K., Szafrańska, P.A., Ksiazek, A. & Konarzewski, M. (2015). Plant-herbivore interactions: Silicon concentration in tussock sedges and population dynamics of root voles. *Funct. Ecol.*, 29, 187–194.

Wilson, M.J. (2004). Weathering of the primary rock-forming minerals: processes, products and rates. *Clay Miner.*, 39, 233–266.

Wouterlood, M., Cawthray, G.R., Scanlon, T.T., Lambers, H. & Veneklaas, E.J. (2004). Carboxylate concentrations in the rhizosphere of lateral roots of chickpea (*Cicer arietinum*) increase during plant development, but are not correlated with phosphorus status of soil or plants. *New Phytol.*, 162, 745–753.

WRB. (2015). *World reference base for soil resources 2014 International soil classification system for naming soils and creating legends for soil maps*. FAO, Rome, Italy.

Wright, A.L. & Hons, F.M. (2005). Soil Carbon and Nitrogen Storage in Aggregates from Different Tillage and Crop Regimes. *Soil Sci. Soc. Am. J.*, 69, 141–147.

Wright, D.M., Jordan, G.J., Lee, W.G., Duncan, R.P., Forsyth, D.M. & Coomes,

D.A. (2010). Do leaves of plants on phosphorus-impoverished soils contain high concentrations of phenolic defence compounds? *Funct. Ecol.*, 24, 52–61.

Wright, I.J., Reich, P.B., Cornelissen, J.H.C., Falster, D.S., Garnier, E., Hikosaka, K., *et al.* (2005). Assessing the generality of global leaf trait relationships. *New Phytol.*, 166, 485–496.

Wright, I.J., Westoby, M., Reich, P.B., Oleksyn, J., Ackerly, D.D., Baruch, Z., *et al.* (2004). The worldwide leaf economics spectrum. *Nature*, 428, 821–827.

Wu, J.W., Shi, Y., Zhu, Y.X., Wang, Y.C. & Gong, H.J. (2013). Mechanisms of Enhanced Heavy Metal Tolerance in Plants by Silicon: A Review. *Pedosphere*, 23, 815–825.

Wu, L., Jacobson, A.D. & Hausner, M. (2008). Characterization of elemental release during microbe-granite interactions at T = 28 °C. *Geochim. Cosmochim. Acta*, 72, 1076–1095.

Wu, W., Limmer, M.A. & Seyfferth, A.L. (2020). Quantitative assessment of plant-available silicon extraction methods in rice paddy soils under different management. *Soil Sci. Soc. Am. J.*, 84, 618–626.

Wyrwoll, K.-H., Turner, B.L. & Findlater, P. (2014). On The Origins, Geomorphology And Soils Of The Sandplains Of South-Western Australia. In: *Lambers H, Ed. Plant life on the sandplains in Southwest Australia, a global biodiversity hotspot*. University of Western Australia Publishing, Crawley, pp. 3–23.

Xiao, W., Yuqiao, L., Qiang, Z., Matichenkov, V., Bocharnikova, E. & Dåstøl, M. (2016). Efficacy of Si fertilization to modulate the heavy metals absorption by barley (*Hordeum vulgare* L.) and pea (*Pisum sativum* L.). *Environ. Sci. Pollut. Res.*, 23, 20402–20407.

Xiao, X., Chen, B. & Zhu, L. (2014). Transformation, morphology, and dissolution of silicon and carbon in rice straw-derived biochars under different pyrolytic temperatures. *Environ. Sci. Technol.*, 48, 3411–3419.

Xu, D., Gao, T., Fang, X., Bu, H., Li, Q., Wang, X., *et al.* (2020). Silicon addition improves plant productivity and soil nutrient availability without changing the grass:legume ratio response to N fertilization. *Sci. Rep.*, 10, 1–9.

Xue, Y., Xia, H., Christie, P., Zhang, Z., Li, L. & Tang, C. (2016). Crop acquisition of phosphorus, iron and zinc from soil in cereal/legume intercropping systems: a critical review. *Ann. Bot.*, 117, 363–377.

Yamaji, N. & Ma, J.F. (2011). Further characterization of a rice silicon efflux transporter, Lsi2. *Soil Sci. Plant Nutr.*, 57, 259–264.

Yamamoto, T., Nakamura, A., Iwai, H., Ishii, T., Ma, J.F., Yokoyama, R., *et al.* (2012). Effect of silicon deficiency on secondary cell wall synthesis in rice leaf. *J. Plant Res.*, 125, 771–779.

Yang, X., Song, Z., Qin, Z., Wu, L., Yin, L., Van Zwieten, L., *et al.* (2020). Phytolith-rich straw application and groundwater table management over 36 years affect the soil-plant silicon cycle of a paddy field. *Plant Soil*, 454, 343–358.

Yoshida, S., Onishi, Y. & Kitagishi, K. (1959). The chemical nature of silicon in rice plant. *Soil Sci. Plant Nutr.*, 5, 23–27.

Yost, R.S. & Fox, R.L. (1982). Influence of mycorrhizae on the mineral contents of cowpea and soybean grown in an Oxisol. *Agron. J.*, 74, 475–481.

Yu, R.P., Li, X.X., Xiao, Z.H., Lambers, H. & Li, L. (2020a). Phosphorus facilitation and covariation of root traits in steppe species. *New Phytol.*, 226, 1285–1298.

Yu, R.P., Zhang, W.P., Yu, Y.C., Yu, S.B., Lambers, H. & Li, L. (2020b). Linking shifts in species composition induced by grazing with root traits for phosphorus acquisition in a typical steppe in Inner Mongolia. *Sci. Total Environ.*, 712, 136495.

Yuan, Z., Jiang, S., Sheng, H., Liu, X., Hua, H., Liu, X., *et al.* (2018). Human perturbation of the global phosphorus cycle: Changes and consequences. *Environ. Sci. Technol.*, 52, 2438–2450.

Zaharescu, D.G., Burghelea, C.I., Dontsova, K., Presler, J.K., Hunt, E.A., Domanik, K.J., *et al.* (2019). Ecosystem-bedrock interaction changes nutrient compartmentalization during early oxidative weathering. *Sci. Rep.*, 9, 15006.

Zahra, M.K., Monib, M., Abdel-Al, S.I. & Heggo, A. (1984). Significance of Soil Inoculation with Silicate Bacteria. *Zentralbl. Mikrobiol.*, 139, 349–357.

Zalasiewicz, J., Williams, M., Fortey, R., Smith, A., Barry, T.L., Coe, A.L., *et al.* (2011). Stratigraphy of the anthropocene. *Philos. Trans. R. Soc. A Math. Phys. Eng. Sci.*, 369, 1036–1055.

Zama, E.F., Reid, B.J., Sun, G.X., Yuan, H.Y., Li, X.M. & Zhu, Y.G. (2018). Silicon (Si) biochar for the mitigation of arsenic (As) bioaccumulation in spinach (Spinacia oleracean) and improvement in the plant growth. *J. Clean. Prod.*, 189, 386–395.

Zanão Júnior, L.A., Ávila, V.T. de, Neves, J.C.L., Fontes, R.L.F. & Korndörfer, G.H. (2010). Rice grown in nutrient solution with doses of manganese and silicon. *Rev. Bras. Ciência do Solo*, 34, 1629–1639.

Zanin, L., Venuti, S., Zamboni, A., Varanini, Z., Tomasi, N. & Pinton, R. (2017). Transcriptional and physiological analyses of Fe deficiency response in maize reveal the presence of *Strategy I* components and Fe/P interactions. *BMC Genomics*, 18, 1–15.

Zemunik, G., Turner, B.L., Lambers, H. & Laliberté, E. (2015). Diversity of plant nutrient-acquisition strategies increases during long-term ecosystem development. *Nat. Plants*, 1, 1–4.

Zemunik, G., Turner, B.L., Lambers, H. & Laliberté, E. (2016). Increasing plant species diversity and extreme species turnover accompany declining soil fertility along a long-term chronosequence in a biodiversity hotspot. *J. Ecol.*, 104, 792–805.

Zhang, F.S. (1993). Mobilisation of iron and manganese by plant-borne and synthetic metal chelators. *Plant Soil*, 155–156, 111–114.

Zhang, L.H., Shao, H.B., Ye, G.F. & Lin, Y.M. (2012). Effects of fertilization and drought stress on tannin biosynthesis of *Casuarina equisetifolia* seedlings branchlets. *Acta Physiol. Plant.*, 34, 1639–1649.

Zhong, H., Zhou, J., Azmi, A., Arruda, A.J., Doolette, A.L., Smernik, R.J., *et al.* (2021). *Xylomelum occidentale* (Proteaceae) accesses relatively mobile soil organic phosphorus without releasing carboxylates. *J. Ecol.*, 109, 246–259.

Zhu, Y. & Gong, H. (2014). Beneficial effects of silicon on salt and drought tolerance in plants. *Agron. Sustain. Dev.*, 34, 455–472.

Zuo, Y., Zhang, F., Li, X. & Cao, Y. (2000). Studies on the improvement in iron nutrition of peanut by intercropping with maize on a calcareous soil. *Plant Soil*, 220, 13–25.

Züst, T. & Agrawal, A.A. (2017). Trade-Offs Between Plant Growth and Defense Against Insect Herbivory: An Emerging Mechanistic Synthesis. *Annu. Rev. Plant Biol.*, 68, 513–534.

Zuur, A.F., Ieno, E.N., Walker, N., Saveliev, A.A. & Smith, G.M. (2009). *Mixed Effects Models and Extensions in Ecology with R.* Springer-Verlag New York, New York, USA.

List of publications

de Tombeur F, Turner BL, Laliberté E, Lambers H, Cornelis JT (2020) Silicon dynamics during 2 million years of soil development in a coastal dune chronosequence under a Mediterranean climate. *Ecosystems*. 23, 1614-1630.

de Tombeur F, Turner BL, Laliberté E, Lambers H, Mahy G, Faucon MP, Zemunik G, Cornelis JT (2020) Plants sustain the terrestrial silicon cycle during ecosystem retrogression. *Science*. 369, 1245-1248.

de Tombeur F, Cornelis JT, Laliberté E, Lambers H, Mahy G, Faucon MP, Turner BL, Impact of ecosystem water balance and soil parent material on the terrestrial silicon cycle: insights from three long-term chronosequences. *Under review in Biogeochemistry*.

de Tombeur F, Laliberté E, Lambers H, Faucon MP, Zemunik G, Turner BL, Cornelis JT, Mahy G, A shift from phenol to silica-based leaf defenses during long-term soil and ecosystem development. *Ecology Letters.* 24, 984-995.

de Tombeur F, Cornelis JT, Lambers H, Silicon mobilization by root-released carboxylates. *Under review in Trends in Plant Science.*

de Tombeur F, Roux, P, Cornelis JT, Silicon dynamics through the lens of soil-plant feedback interactions: perspectives for agricultural practices. *'Marschner review' under review in Plant and Soil.*

de Tombeur F, Vander Linden C, Cornelis JT, Godin B, Compere P, Delvaux B, Soil and climate affect foliar silicification patterns and silica-cellulose balance in sugarcane (*Saccharum officinarum*). *Plant and Soil*. 452, 529-546.

de Tombeur F, Cooke J, Collard L, Cisse D, Saba F, Burgeon V, Hassan N, Cornelis JT, Rice-husk biochar affects silicification patterns and physical traits of rice leaves cultivated in desilicated soils (Ferric Lixisol). *Plant and Soil.* 460, 375-390.

Li Z, **de Tombeur F**, Vander Linden C, Cornelis JT, Delvaux B (2020) Soil microaggregates store phytoliths in a sandy loam. *Geoderma*. 360, 114037.

Leroy N, **de Tombeur F**, Walgraffe Y, Cornelis JT, Verheggen F (2019) Silicon and plant natural defenses against insect pests: impact on plant volatile organic compounds and cascade effects on multitrophic interactions. *Plants*. 8, 444.

Nakamura R, Cornelis JT, **de Tombeur F**, Yoshinaga A, Nakagawa M, Kitajima K (2020) Diversity of silicon release rates among tropical tree species during leaf-litter decomposition. *Geoderma*. 368, 114288.

Nakamura R, Cornelis JT, **de Tombeur F**, Nakagawa M, Kitajima K (2020) Comparative analysis of borate fusion versus sodium carbonate extraction for quantification of silicon contents in plants. *Journal of Plant Research*. 133, 271–277.

Vander Linden C, Li Z, Iserentant A, Van Ranst E, **de Tombeur F**, Delvaux B, Rainfall is the major driver of plant Si availability in perudic gibbsitic Andosols. *Under review in Geoderma*.

de Tombeur F, Cornu S, Bourlès D, Duvivier A, Pupier J, ASTER Team, Brossard M, Evrard O (2020) Retention of ^{10}Be, ^{137}Cs and $^{210}Pb_{xs}$ in soils: Impact of physico-chemical characteristics. *Geoderma*. 367, 114242.

de Tombeur F, Sohy V, Chenu C, Colinet G, Cornelis JT (2018) Effects of permaculture practices on soil physicochemical properties and organic matter distribution in aggregates: a case study of the Bec-Hellouin Farm (France). *Frontiers in Environmental Science*. 6, 116.

Falster, D, *et al.* (2021) AusTraits – a curated plant trait database for the Australian flora. *Under review in Scientific Data.*